

Fall 9-2014

DEVELOPMENT OF SIMULATION-BASED FRAGILITY RELATIONSHIPS FOR THE SEISMIC RISK ASSESSMENT OF BUILDINGS

Anas Salem (Mohammad Ghaleb) Issa

Follow this and additional works at: https://scholarworks.uaeu.ac.ae/all_theses

Part of the [Civil Engineering Commons](#)

Recommended Citation

Issa, Anas Salem (Mohammad Ghaleb), "DEVELOPMENT OF SIMULATION-BASED FRAGILITY RELATIONSHIPS FOR THE SEISMIC RISK ASSESSMENT OF BUILDINGS" (2014). *Theses*. 2.

https://scholarworks.uaeu.ac.ae/all_theses/2

This Thesis is brought to you for free and open access by the Electronic Theses and Dissertations at Scholarworks@UAEU. It has been accepted for inclusion in Theses by an authorized administrator of Scholarworks@UAEU. For more information, please contact fadl.musa@uaeu.ac.ae.

United Arab Emirates University

College of Engineering

Department of Civil and Environmental Engineering

DEVELOPMENT OF SIMULATION-BASED FRAGILITY
RELATIONSHIPS FOR THE SEISMIC RISK ASSESSMENT OF
BUILDINGS

Anas Salem (Mohammad Ghaleb) Issa

This thesis is submitted in partial fulfillment of the requirements for the degree of
Master of Science in Civil Engineering

Under the supervision of Dr. Aman Mwafy

September 2014

DECLARATION OF ORIGINAL WORK

I, Anas Salem (Mohammad Ghaleb) Issa, the undersigned, a graduate student at the United Arab Emirates University (UAEU), and the author of the thesis entitled “*Development of Simulation-based Fragility Relationships for the Seismic Risk Assessment of Buildings*” hereby, solemnly declare that this thesis is an original research work done and prepared by me under the supervision of Dr. Aman Mwafy, in the College of Engineering at UAEU. This work has not been previously formed as the basis for the award of any academic degree, diploma or similar title at this or any other university. The materials borrowed from other sources and included in my thesis have been properly cited and acknowledged.

Student’s Signature

Date

Copyright © 2014 by Anas Salem (Mohammad Ghaleb) Issa
All Rights Reserved

This Master Thesis is approved by the following Examining Committee Members:

1) Advisor (Committee Chair): Dr. Aman Mwafy

Title: Associate Professor

Department of Civil and Environmental Engineering

College of Engineering

Signature _____

Date _____

2) Member: Prof. Khaled El-Sawy

Title: Professor

Department of Civil and Environmental Engineering

College of Engineering

Signature _____

Date _____

3) Member (External Examiner): Prof. Ahmed Elghazouli

Title: Professor of Structural Engineering - Section Head

Department of Civil and Environmental Engineering

Institution: Imperial College London

Signature _____

Date _____

This Master Thesis is accepted by:

Dean of the College of Engineering: Prof. Mohsen Sherif

Signature _____ Date _____

Dean of the College of Graduate Studies: Prof. Nagi Wakim

Signature _____ Date _____

Copy ___ of ___

ABSTRACT

A number of driving engines are required for earthquake loss estimation and mitigation, including an inventory of exposed systems, seismic hazards of the study area and fragility relationships. The number of existing buildings in the UAE that may be at risk because of insufficient seismic design provisions cannot be underestimated. A crucial role in the recovery period following an earthquake is also played by emergency facilities. Therefore, a systematic seismic vulnerability assessment of a diverse range of reference structures representing pre-seismic code buildings and emergency facilities, in a highly populated and seismically active area in the UAE, has been conducted in this study. Detailed structural design and fiber-based modeling were carried out for nine reference structures. Forty earthquake records were selected to represent potential earthquake scenarios in the study area. Three limit states, namely Immediate Occupancy, Life Safety and Collapse Prevention, were selected based on inelastic analysis results as well as the values recommended in previous studies and code provisions. Over 8000 inelastic pushover and incremental dynamic analyses are performed to assess the lateral capacity and to derive a wide range of fragility relationships for the reference structures. Vulnerability functions were also developed for the buildings that proved to have unsatisfactory performance, and hence proposed to be retrofitted using different mitigation techniques. It was concluded that pre-code structures were significantly more vulnerable than emergency facilities. This is particularly true for low-rise buildings due to their inefficient lateral force resisting systems. Far-field records have much higher impact compared with near-source ground motions. The results reflect the pressing need for the seismic retrofit of pre-code structures to reduce the probability of collapse, and for certain emergency facilities to ensure their continued

service. Four retrofit approaches are therefore assessed, namely reinforced concrete jacketing, fiber reinforced polymers wrapping, adding buckling restrained braces and installing externally unbonded steel plates. The highest positive impact of retrofit are observed on the pre-code buildings, especially frame structures, since they were only designed to resist gravity and wind loads. The reductions achieved in the vulnerability of the retrofitted structures confirmed the effectiveness of the techniques selected for upgrading the seismic performance of buildings and mitigating earthquake losses in the study area.

Keywords: vulnerability assessment, pre-code buildings, emergency facilities, inelastic dynamic simulations, seismic retrofit, UAE

تطوير علاقات معتمدة على المحاكاة لتقييم مخاطر الزلازل على المباني

ملخص الرسالة

تتطلب دراسات تقدير الخسائر المحتملة للزلازل والتخفيف من أضرارها عدة عناصر أساسية، والتي تشمل المنشآت المعرضة للزلازل والمخاطر الزلزالية لمنطقة الدراسة وأخيراً علاقات الهشاشة (Fragility Relationships). لا يمكن الانتقاص من عدد المباني القديمة التي قد تكون معرضة لمخاطر الزلازل في دولة الإمارات العربية المتحدة نتيجة لعدم كفاية احتياطات التصميم الحديثة لمقاومة الزلازل، كما تلعب منشآت الطوارئ دوراً حاسماً في فترة ما بعد حدوث الزلازل، وبناء على ذلك فقد أجريت هذه الدراسة المنهجية لمجموعة متنوعة من المباني التي تمثل المنشآت القديمة ومرافق الطوارئ في منطقة نشطة زلزالياً وكثيفة السكان في دولة الإمارات وذلك لتقييم مدى مقاومتها للزلازل. وقد تم عمل تصميم انشائي مفصل ونمذجة على الحاسب الآلي باستخدام طريقة الألياف لتسعة مباني مرجعية، كما تم اختيار أربعين سجلاً زلزالياً من قواعد البيانات لتمثيل سيناريوهات محتملة للزلازل في منطقة الدراسة، كما أجريت العديد من التحليلات الاستاتيكية الغير مرنة (inelastic pushover analysis) والديناميكية متزايدة الشدة (incremental dynamic analysis) لتقييم الخصائص الاستاتيكية والديناميكية والأداء الزلزالي للمباني المرجعية. كذلك تم اختيار ثلاثة معايير لتقييم الأداء الإنشائي بناءً على نتائج التحليلات الغير مرنة فضلاً عن القيم الموصى بها في الدراسات السابقة واحتياطات التصميم. وقد تم إجراء أكثر من ثمانية آلاف من التحليلات الغير مرنة وذلك لاشتقاق مجموعة واسعة من علاقات الهشاشة للمباني المرجعية، كما تم اشتقاق علاقات هشاشة إضافية للمباني التي وجد بها قصور في الأداء وبالتالي تم تقويمها باستخدام تقنيات تقويم مختلفة. خلصت الدراسة إلى أن المباني القديمة أكثر عرضة لمخاطر الزلازل من مرافق الطوارئ، وعلى وجه الخصوص المباني القديمة المنخفضة الارتفاع ويرجع ذلك إلى قلة فعالية أنظمتها الإنشائية لمقاومة القوى العرضية. كما ثبت أن الزلازل الناشئة من صدوع بعيدة لها تأثيرات أكبر بكثير على المباني من الزلازل المتولدة من صدوع زلزالية قريبة. كذلك عكست النتائج الحاجة الملحة لتحسين أداء المباني القديمة لتقليل الأضرار بها نتيجة الزلازل، وذلك بالإضافة لضرورة تحسين أداء بعض مرافق الطوارئ لضمان جاهزيتها التامة عن حدوث الزلازل. وقد تم تقييم أربعة اساليب لتقويم المباني وتشمل زيادة القطاع الخرساني للأعمدة (RC jacketing) ولفائف البوليمرات المقواة بالألياف

(Buckling Restrained Fiber Reinforced Polymers) وإضافة دعائم معدنية غير قابلة للالتواء (Externally Unbonded Steel Braces) واخيراً تركيب شرائح معدنية خارجية مثبتة بحوائط القص (Plates). ولقد تم تسجيل أفضل نتائج لأساليب التقويم المختلفة بالمباني القديمة وذلك نظراً لضعف هيكلها الإنشائي قبل التقويم نتيجة تصميمها لمقاومة الأحمال الرأسية وأحمال الرياح فقط، كما أثبتت نتائج تقويم المباني المرجعية فعالية التقنيات المستخدمة لرفع مستوى الأداء الإنشائي والحد من الخسائر المحتملة للزلازل في منطقة الدراسة.

كلمات البحث: تقييم تأثير الزلازل على المباني، المحاكاة الديناميكية الغير مرنة، المباني القديمة، مرافق الطوارئ، تعزيز كفاءة المباني، دولة الإمارات العربية المتحدة

ACKNOWLEDGEMENTS

I would like to thank God for giving me the faith and strength to successfully complete this work. I would also like to express my sincere thanks to my family who have provided me with all the support and strength to complete this work. I would like to express my deepest thanks to all individuals who helped me during this significant period of my life. In the first place, I would like to deliver my deepest respect and appreciation to my thesis supervisor Dr. Aman Mwafy for his continuous support, inestimable guidance, and the valuable knowledge he provided me throughout the project. I would like to thank him for the friendly environment he has created for me and the brotherly advice I received from him.

Special recognition also goes to my colleagues and friends and all faculty members of the Civil and Environmental Engineering Department at the UAEU for their help and support. This work was supported by the United Arab Emirates University under research grants no. 31N007 and 31N132.

DEDICATION

To my beloved parents and family

TABLE OF CONTENTS

TITLE.....	I
DECLARATION OF ORIGINAL WORK.....	II
COPYRIGHT.....	III
SIGNATURES.....	IV
ABSTRACT.....	VI
ACKNOWLEDGEMENTS.....	X
DEDICATION.....	XI
TABLE OF CONTENTS.....	XII
LIST OF TABLES.....	XV
LIST OF FIGURES.....	XVII
LIST OF NOTATIONS.....	XXI
CHAPTER 1: INTRODUCTION.....	1
1.1 Introduction.....	1
1.2 Scope and Objective.....	3
1.3 Report Organization.....	3
CHAPTER 2: LITERATURE REVIEW.....	6
2.1 Seismic Risk Assessment Framework.....	6
2.2 Building Inventory.....	8
2.2.1 Pre-Seismic Code Buildings.....	8
2.2.2 Emergency Facilities.....	11
2.3 Seismic Hazard Studies in the UAE.....	15
2.3.1 Tectonic Settings of the UAE.....	15
2.3.2 Previous Hazard Assessment Studies.....	18
2.4 Vulnerability Relationships.....	21
2.4.1 Vulnerability Assessment of Buildings.....	21
2.4.2 Previous Vulnerability Assessment Studies for the UAE.....	25
2.5 Seismic Design Loads and Wind Effects.....	28
2.5.1 Seismic Loads.....	28
2.5.2 Wind Effects.....	30
2.6 Seismic Rehabilitation of Structures.....	31
2.6.1 FEMA-547 Seismic Rehabilitation Provisions.....	32

2.6.2 Previous Seismic Rehabilitation Studies	33
2.6.3 Comparative Evaluation of Retrofit Techniques	39
2.7 Concluding Remarks	39
CHAPTER 3: SELECTION AND DESIGN OF REFERENCE STRUCTURES	43
3.1 Selection of Representative Buildings	43
3.1.1 Selection Based on Construction Date	44
3.1.2 Selection Based on Risk Category.....	45
3.2 Design Approach.....	53
3.3 Design Results	56
3.4 Comments on the Design Results.....	68
CHAPTER 4: MODELING AND INPUT GROUND MOTIONS	70
4.1 Fiber Based Modeling	70
4.1.1 Material Modeling	70
4.1.2 Member and Section Modeling	71
4.1.3 Structural Modeling	75
4.2 Selection of Ground Motions	77
4.3 Concluding Remarks	87
CHAPTER 5: PERFORMANCE ASSESSMENT OF EXISTING STRUCTURES	88
5.1 Introduction	88
5.2 Free Vibration Analysis	89
5.3 Inelastic Static Pushover Analysis	92
5.3.1 Estimation of Lateral Capacity	93
5.3.2 Monitoring of Member Yielding and Failure	99
5.4 Incremental Dynamic Analysis	105
5.5 Performance Criteria	109
5.5.1 First Yield and Crushing using IPA	110
5.5.2 Strength Degradation using IPA.....	110
5.5.3 Shear Response using Time History Analysis (THA).....	111
5.5.4 First Yield and Crushing using THA.....	113
5.5.5 Global Yield and Collapse using IDA Curves.....	115
5.5.6 Selection of Limit States.....	117
5.6 Derivation of Fragility Relationships using IDA	119

5.7 Concluding Remarks	129
CHAPTER 6: PERFORMANCE ASSESSMENT OF RETROFITTED STRUCTURES	131
6.1 Introduction	131
6.2 Design of Strengthening Techniques	133
6.2.1 RC Jacketing	133
6.2.2 FRP Wrapping	135
6.2.3 Buckling Restrained Braces	136
6.2.4 Steel Plates	138
6.3 Modeling of Strengthening Techniques	139
6.3.1 RC Jacketing	139
6.3.2 FRP Wrapping	139
6.3.3 Buckling Restrained Braces	140
6.3.4 Steel Plates	144
6.4 Impact of Retrofit on Lateral Capacity	144
6.5 Impact of Retrofit on Seismic Performance	147
6.6 Concluding Remarks	153
CHAPTER 7: CONCLUSIONS AND RECOMMENDATIONS	156
7.1 Synopsis	156
7.2 Summary of Conclusions	158
7.3 Recommendations for Future Research	161
REFERENCES	163
APPENDIX A: SAMPLE IDA RESULTS	172

LIST OF TABLES

Table 2.1: Summary of IDRs for different limit states and structural systems.....	24
Table 2.2: Advantages and disadvantages of retrofit techniques.....	39
Table 3.1: Summary of the selected buildings (Mwafy, 2013).....	49
Table 3.2: Vertical members design summary of the 2-story building.....	57
Table 3.3: Floor slabs reinforcement of the 2-story building.....	57
Table 3.4: Vertical members design summary of the 8-story building.....	58
Table 3.5: Floor slabs reinforcement of the 8-story building.....	58
Table 3.6: Vertical members design summary of the 18-story building.....	60
Table 3.7: Vertical members design summary of the 26-story building.....	60
Table 3.8: Floor slabs reinforcement of the 18-story building.....	60
Table 3.9: Floor slabs reinforcement of the 26-story building.....	61
Table 3.10: Coupling beams reinforcement of the 18-story building.....	61
Table 3.11: Coupling beams reinforcement of the 26-story building.....	61
Table 3.12: Floor slabs reinforcement of the 40-story building.....	63
Table 3.13: Coupling beams reinforcement of the 40-story building.....	63
Table 3.14: Vertical structural members design summary of the 40-story building.....	64
Table 3.15: Vertical members design summary of the fire station.....	65
Table 3.16: Floor slabs reinforcement of the fire station.....	65
Table 3.17: Vertical members design summary of the police station.....	66
Table 3.18: Floor slabs reinforcement of the police station.....	66
Table 3.19: Vertical members design summary of the hospital.....	67
Table 3.20: Floor slabs reinforcement of the hospital.....	67
Table 3.21: Vertical members design summary of the school.....	68
Table 3.22: Floor slabs reinforcement of the school building.....	68
Table 4.1: Summary of near-source earthquake records.....	81
Table 4.2: Summary of far-field earthquake records.....	82
Table 5.1: Summary of buildings fundamental periods (T1) from fibre-based and design models.....	90

Table 5.2: First steel yielding in three representative reference structures using THA and 20 input ground motions representing far-field seismic scenario.....	114
Table 5.3: First confined concrete crushing in vertical elements in three representative reference structures using THA and 20 input ground motions representing far-field seismic scenario	114
Table 5.4: Equivalent periods for nine reference structures	115
Table 5.5: Summary of IDRs corresponding to different limit states	118
Table 6.1: Design summary of RC jacketing for three reference structures	135
Table 6.2: Parameters used for modeling the BRB trilinear asymmetric joint element	141
Table 6.3: Summary of IPA results for existing and retrofitted structures	145
Table A.1: Incremental dynamic analysis results showing inter-story drift ratios of reference buildings at different PGA levels for 20 far-field records.....	172
Table A.2: Incremental dynamic analysis results showing inter-story drift ratios of reference buildings at different PGA levels for 20 near-source records	177

LIST OF FIGURES

Figure 2.1: Primary modules of HAZUS Earthquake (Kircher et al., 2006)	7
Figure 2.2: Framework for earthquake loss estimation in the UAE (Mwafy, 2012a).....	7
Figure 2.3: Tectonic setting of the Arabian plate (Aldama-Bustos et al., 2009)	16
Figure 2.4: Plate tectonic setting of the Oman Sea (Jamali et al., 2006)	18
Figure 2.5: Typical fragility curve (Mwafy, 2012a)	25
Figure 3.1: Study area	43
Figure 3.2: Buildings classification according to their construction date (Mwafy, 2013).....	45
Figure 3.3: Building classification according to risk category (Mwafy, 2013)	46
Figure 3.4: Selected real buildings from the study area to represent pre-seismic code structures (Mwafy, 2013).....	47
Figure 3.5: Selected real buildings from the study area to represent emergency facilities (Mwafy, 2013).....	48
Figure 3.6: Layout of the 2-story building showing different structural members	49
Figure 3.7: Layout of the 8-story building showing different structural members	49
Figure 3.8: Layout of the 18 and 26-story building showing different structural members	50
Figure 3.9: Layout of the 40-story building showing different structural members	50
Figure 3.10: Layout of the fire station showing different structural members	51
Figure 3.11: Layout of the police station showing different structural members	51
Figure 3.12: Layout of the school showing different structural members	51
Figure 3.13: Layout of the hospital showing different structural members.....	52
Figure 3.14: Layouts and three-dimensional design models of the reference structures	54
Figure 3.15: Typical reinforcement details for the floor slabs of the 2-story building.....	56
Figure 3.16: RC cross-sections used in the design of the 2-story building.....	56

Figure 3.17: Typical reinforcement details for the floor slabs of the 8-story building.....	57
Figure 3.18: RC cross-sections used in the design of the 8-story building.....	57
Figure 3.19: Typical reinforcement details for the floor slabs of the 18-story and 26-story buildings	58
Figure 3.20: RC cross-sections used in the design of the 18-story building.....	59
Figure 3.21: RC cross-sections used in the design of the 26-story building.....	59
Figure 3.22: Typical reinforcement details for the floor slabs of the 40-story buildings	61
Figure 3.23: RC cross-sections used in the design of the 40-story building.....	62
Figure 3.24: Typical reinforcement details for the floor slabs of the fire station	65
Figure 3.25: RC cross-sections used in the design of the fire station	65
Figure 3.26: Typical reinforcement details for the floor slabs of the police station	65
Figure 3.27: RC cross-sections used in the design of the police station	66
Figure 3.28: Typical reinforcement details for the floor slabs of the hospital.....	66
Figure 3.29: RC cross-sections used in the design of the hospital.....	67
Figure 3.30: Typical reinforcement details for the floor slabs of the school	67
Figure 3.31: RC cross-sections used in the design of the school.....	67
Figure 4.1: Material models used in the reference structures idealization (Elnashai et al., 2012).....	71
Figure 4.2: Cubic elasto-plastic 3D frame element (Elnashai et al., 2012)	72
Figure 4.3: Different cross-sections used to model the reference buildings for inelastic analysis (Elnashai et al., 2012)	73
Figure 4.4: Fiber-based numerical models developed for two set of reference buildings	74
Figure 4.5: LFRSs of shear wall supported structures	76
Figure 4.6: Developed finite element and fiber based models for reference structures	77
Figure 4.7: Stage two, matching design code spectra	80
Figure 4.8: Response spectra of near-source earthquake records	80
Figure 4.9: Response spectra of far-field records	80
Figure 4.10: Selected near-source records	83
Figure 4.11: Selected far-field records.....	85

Figure 5.1: First three mode shapes of pre-code structures	91
Figure 5.2: First three mode shapes of emergency facilities.....	92
Figure 5.3: The capacity curves of the pre-code frame structures	95
Figure 5.4: The capacity curves of the pre-code wall structures	96
Figure 5.5: The capacity curves of the emergency structures.....	97
Figure 5.6: Distribution of inter-story drift ratios of the pre-code structures at the ultimate strength	98
Figure 5.7: Distribution of inter-story drift ratios of the emergency structures at the ultimate strength	99
Figure 5.8: Plastic hinge distributions of the pre-code structures.....	101
Figure 5.9: Distributions of concrete crushing in the vertical elements of the pre-code structures	102
Figure 5.10: Plastic hinge distributions in the vertical structural elements of the emergency structures.....	103
Figure 5.11: Distributions of concrete crushing in the vertical structural elements of the emergency structures	104
Figure 5.12: Distributions of maximum IDRs for the five pre-code structures from IDA under forty earthquake records scaled to twice the design (0.32g for near-source records) and half the design (0.08 for far- field records) earthquake intensity.	107
Figure 5.13: Distributions of maximum IDRs for the four emergency facilities from IDA under forty earthquake records scaled to twice the design (0.32g for near-source records) and half the design (0.08 for far- field records) earthquake intensity.	108
Figure 5.14: 10% reduction in strength for the 8-story building	111
Figure 5.15: Shear response of an internal column in the 2 story building ('Chi- Chi-TAP010' input ground motion and a PGA of 1.5 the design value).....	112
Figure 5.16: Shear response of an internal column in the 8 story building (‘Loma Prieta-ggb’ input ground motion and a PGA of 2.5 the design value)	113
Figure 5.17: CP limit states for three representative buildings using 20 far-field records	116

Figure 5.18: IDA results of the nine reference structures obtained from forty input ground motions along with the power law equations	122
Figure 5.19: Fragility relationships of the nine reference structures obtained from IDAs	124
Figure 5.20: Limit state exceedance probabilities of the pre-code reference buildings	126
Figure 5.21: Limit state exceedance probabilities of the emergency facilities reference buildings	127
Figure 5.22: Developed fragility curves for comparable 2 and 8-story frame pre-code structures (Borzi et al., 2008)	128
Figure 6.1: Proposed retrofit approach.....	132
Figure 6.2: Typical retrofit of rectangular columns (FEMA-547, 2006).....	134
Figure 6.3: Retrofitted RC columns of the 2-story building	135
Figure 6.4: Retrofitted RC columns of the 8-story building	135
Figure 6.5: Retrofitted RC columns of the hospital	135
Figure 6.6: Typical BRB specimen (left) (Tremblay et al., 2004), adopted BRB test result (right) (Tremblay et al., 2008)	137
Figure 6.7: Retrofitted RC cross-sections of the wall buildings	138
Figure 6.8: RC jacket with a rectangular section (Elnashai et al., 2012).....	139
Figure 6.9: Trilinear FRP model (Elnashai et al., 2012).....	140
Figure 6.10: Trilinear asymmetric elasto-plastic curve (Elnashai et al., 2012)	140
Figure 6.11: BRB modeling concept.....	142
Figure 6.12: BRB load-displacement relationships obtained from IPA at three different story levels.....	143
Figure 6.13: BRB load-displacement relationships at the design PGA (top) and five times the design (bottom) PGA.....	143
Figure 6.14: The capacity curves for existing and retrofitted structures	146
Figure 6.15: Regression analysis of retrofitted structures using 20 long period records	149
Figure 6.16: Fragility curves of retrofitted structures using 20 long period records	150
Figure 6.17: Fragility curves before and after retrofit using 20 long period records	151

Figure 6.18: Limit state exceedance probabilities of the eight buildings before and after retrofit.....	152
Figure A.1: Base shear response histories of the 8-story building under twenty short-period records scaled to twice the design (0.32g) earthquake intensity.....	182
Figure A.2: Top displacement response histories of the 8-story building under twenty short-period records scaled to twice the design (0.32g) earthquake intensity	183
Figure A.3: Base shear response histories of the 8-story building under twenty long-period records scaled to the design (0.16g) earthquake intensity.....	184
Figure A.4: Top displacement response histories of the 8-story building under twenty long-period records scaled to the design (0.16g) earthquake intensity.....	185
Figure A.5: Base shear response histories of the 26-story building under twenty short-period records scaled to twice the design (0.32g) earthquake intensity.....	186
Figure A.6: Top displacement response histories of the 26-story building under twenty short-period records scaled to twice the design (0.32g) earthquake intensity.....	187
Figure A.7: Base shear response histories of the 26-story building under twenty long-period records scaled to the design (0.16g) earthquake intensity.....	188
Figure A.8: Top displacement response histories of the 26-story building under twenty long-period records scaled to the design (0.16g) earthquake intensity.....	189
Figure A.9: Base shear response histories of the hospital building under twenty short-period records scaled to twice the design (0.32g) earthquake intensity.....	190
Figure A.10: Top displacement response histories of the hospital building under twenty short-period records scaled to twice the design (0.32g) earthquake intensity.....	191

Figure A.11: Base shear response histories of the hospital building under twenty long-period records scaled to the design (0.16g) earthquake intensity.....	192
Figure A.12: Top displacement response histories of the hospital building under twenty long-period records scaled to the design (0.16g) earthquake intensity.....	193

LIST OF NOTATIONS

2D: Two-dimensional

3D: Three-dimensional

ASD: Allowable Strength Design

A_{sc} : cross-sectional area of the yielding segment of the steel core,

a/v : ratio of peak ground acceleration-to-velocity

BRB: Buckling Restrained Brace

CBF: Conventional Braced Frames

CEPF: Cubic Elasto-Plastic Frame

CFRP: Carbon Fiber Reinforced Polymer

CFT: Concrete Filled steel Tubular

CP: Collapse Prevention limit state

C_a : size effect factor of standard method

C_p : front or rear net pressure coefficient

C_r : dynamic augmentation factor

d_1^+ : Positive displacement where the stiffness changes from K_0^+ to K_1^+

d_2^+ : Positive displacement where the stiffness changes from K_1^+ to K_2^+

d_1^- : Negative displacement where the stiffness changes from K_0^- to K_1^-

d_2^- : Negative displacement where the stiffness changes from K_1^- to K_2^-

D/C: Demand over Capacity

DOF: Degrees Of Freedom

ELFP: Equivalent Lateral Force Procedure

EPA: Effective Peak ground Acceleration

EURB: External Unbonded Reinforcing Bars

EUSP: Externally Unbonded Steel Plates

FE: Finite Element

FRP: Fiber Reinforced Polymer

f_c : unconfined concrete strength

f_c^i : concrete cylindrical strength

F_{ysc} : specified minimum yield stress of the steel core, or actual yield stress of the steel core as determined from a coupon test,

g : gravitational acceleration

GMI: Ground Motion Intensity

H_e : building effective height

I : importance factor

IAEM: Improved Applied Element Method

IDA: Incremental Dynamic Analysis

IDR: Inter-Story Drift Ratio

IO: Immediate Occupancy limit state

IPA: Inelastic Pushover Analysis

K_0^+ : Initial stiffness (positive displacement region)

K_1^+ : Stiffness of second branch (positive displacement region)

K_2^+ : Stiffness of third branch (positive displacement region)

K_0^- : Initial stiffness (negative displacement region)

K_1^- : Stiffness of second branch (negative displacement region)

K_2^- : Stiffness of third branch (negative displacement region)

LFRS: Lateral Force Resisting System

LRFD: Load and Resistance Factor Design

LS: Life Safety limit state

Mb: body-wave magnitude

ML: local magnitude, commonly referred to as "Richter magnitude"

Ms: surface-wave magnitude

Mw: moment magnitude

MCE: Maximum Considered Earthquake

MP: Mass Participation

N: average standard penetration resistance

OP: Operational Performance criterion

PGA: Peak Ground Acceleration

PU: uniform load distribution

PT: inverted triangular load distribution

P_{ysc} : Brace axial strength

R: response modification coefficient

RC: Reinforced Concrete

S_{MS} : maximum considered earthquake spectral response accelerations at short period

S_{M1} : maximum considered earthquake spectral response accelerations at 1-second period

S_{DS} : design spectral response accelerations at short period

S_{D1} : design spectral response accelerations at 1-second period

S_a : Spectral acceleration

S_s : Spectral response acceleration at 0.2 sec

S_1 : Spectral response acceleration at 1 sec

S_u : average undrained shear strength

THA: Time History Analysis

T_{eq} : building equivalent period

V : base shear

V_e : effective wind speed

V_d : design base shear

V_u : base shear at ultimate capacity

V_y : base shear at global yield

v_s : average shear wave velocity

$\beta_{D|GMI}$: demand uncertainty

β_{CL} : drift capacity uncertainty

β_M : modeling uncertainty

Δ : displacement

Δ_y : displacement at global yield

Δ_{max} : maximum deformation

Φ : standard normal cumulative distribution function

λ_{CL} : ln (median of drift capacity for a particular limit state)

$\lambda_{D|GMI}$: ln (calculated median demand drift given the ground motion intensity)

φ : wind direction angle

Ω_0 : overstrength factor

CHAPTER 1: INTRODUCTION

1.1 Introduction

The main components of earthquake loss estimation and mitigation systems are the inventory, seismic hazard and vulnerability. Concerning the inventory of the exposed systems, pre-seismic code buildings may experience a high risk of damage, and hence their vulnerability should be thoroughly assessed. This category of buildings usually undergoes low levels of strength and ductility as they were designed and constructed without proper seismic design provisions. A vital role in the recovery period following an earthquake is also played by emergency facilities such as hospitals and fire stations. In spite of being constructed according to seismic design provisions, they should receive considerable attention to ensure their readiness and continued operation following earthquakes. Recent studies emphasized the significance of assessing the vulnerability of pre-seismic code buildings and emergency facilities, and the pressing need to reduce their seismic losses (e.g. Bruneau & Reinhorn, 2007; Bruno et al., 2000; Ghobarah et al., 1998; Liel et al., 2010; Ramamoorthy et al., 2008; Ray-Chaudhuri & Shinozuka, 2010)

Earthquake loss mitigation of substandard and critical structures represented in the building inventory may require the adoption of efficient retrofit techniques. Seismic retrofit of structures has been experimentally and numerically investigated in several previous studies. The mitigation measures include for instance: Reinforced Concrete (RC) jacketing, Fiber Reinforced Polymers (FRP) wrapping, adding new shear walls, use of Externally Unbonded Steel Plates (EUSP), and installing Buckling Restrained Braces (BRBs), (e.g. Elnashai & Pinho, 1998; Fahnestock et al., 2007; Moehle, 2000; Saadatmanesh et al., 1997). Such mitigation measures can upgrade the seismic response of structures to higher performance levels. This

emphasizes the importance of selecting the proper retrofit techniques, particularly for buildings of high importance and those with poor seismic performance.

As for the seismic hazard, although the United Arab Emirates is generally known to be a region of stable seismic activity, recent events indicated that the region may be prone to damaging earthquakes (e.g. Al Marzooqi et al., 2008; NCMS, 2014; USGS, 2014). Seismic hazard studies Available for the UAE concluded that seismic activities are attributed to the Zagros fold and thrust belt, Makran subduction zone, Oman Mountains and local fault lines and the Zendan-Minab faulting system (e.g. Abdalla & Al-Homoud, 2004; Aldama-Bustos et al., 2009; Malkawi et al., 2007; Shama, 2011; Sigbjornsson & Elnashai, 2006). Even though no human or monetary losses were reported from recent events, the repeated reports of earthquakes have raised concerns regarding the vulnerability of the existing building stock in the region and the associated risk. Non-negligible consequences are expected if the seismic risk of the building stock is overlooked, particularly for substandard and emergency facilities. This highlights the significance of reliable loss estimation and hazard mitigation strategies for the built environment in the UAE.

Finally, few vulnerability and seismic loss assessment studies have been carried out recently for the UAE (Abu-Dagga et al., 2010; Al Shamsi, 2013; Mwafy, 2012a). None of the available studies have been carried out based on reliable inventory data; wide range of reference structures with different characteristics representing the building stock; detailed design and modeling approaches; a diverse range of input ground motions representing different seismic scenarios in the study area; reliable limit states or systematic approaches for developing fragility relationships. The above-mentioned discussion underlines the pressing need for

comprehensive loss estimation and hazard mitigation studies for this region, particularly for pre-code buildings and emergency facilities.

1.2 Scope and Objective

A systematic seismic vulnerability assessment of a diverse range of buildings representing the pre-seismic code and emergency structures in a highly populated and seismically active area in the UAE, was conducted in this study. This enables the direct implementation of a wide range of fragility relationships representing different structures and earthquake scenarios in a loss estimation and hazard mitigation system for the UAE. The main objectives of the present study are as follows:

1. Derive the fragility relationships of a wide range of reference structures by performing Inelastic Pushover Analyses (IPAs) and Incremental Dynamic Analyses (IDAs) using detailed numerical models and diverse seismic scenarios.
2. Propose suitable retrofit techniques for the reference structures that proved to have unsatisfactory performance, and reassess their seismic performance after retrofit through newly developed fragility functions.

1.3 Report Organization

The organization of this work follows the sequence of the research carried out and presented herein. This thesis consists of seven chapters starting with an introduction, going through a literature review, the design, modeling, performance assessment and ending with conclusions and recommendations. The focus of different chapters is as follows:

Chapter 1: Introduction

Discusses the background and motivation for this research, defines the problem and states the main objectives.

Chapter 2: Literature Review

This chapter reviews the current state of knowledge related to UAE seismicity, to select seismic scenarios and representative ground motions for the study region. Previous vulnerability assessment studies related to pre-seismic code buildings and emergency facilities, hazard mitigation techniques for medium seismicity regions and approaches for deriving fragility relationships are also critically reviewed.

Chapter 3: Selection and Design of Reference Structures

This chapter discusses the selection and design of a diverse set of reference structures representing pre-seismic code buildings and emergency facilities according to the building codes that were implemented at the time of construction. The design information is used in the numerical modeling phase discussed in Chapter 4.

Chapter 4: Modeling and Input Ground Motions

The approach adopted for modeling the reference structures for the multi-degree-of-freedom IPA and IDA using the fiber modeling technique is covered in this chapter. The wide range of earthquake records selected to represent the tectonic settings of the study area are also presented.

Chapter 5: Performance Assessment of Existing Structures

This chapter discusses the vulnerability assessment approach of the reference structures using fiber-based numerical models, IPAs and IDAs. It provides insights into the performance criteria and explains the approach of developing a diverse set of simulation-based fragility relationships for the reference structures using different earthquake scenarios.

Chapter 6: Performance Assessment of Retrofitted Structures

The chapter focuses on the assessment of the retrofitted structures using IPAs and IDAs, and the development of their fragility relationships. This chapter also compares between the limit state exceedance probabilities before and after retrofit to understand the impact of retrofit on reducing seismic losses.

Chapter 7: Conclusions and Recommendations

The main findings of this study as well as recommendations for future work are discussed in this chapter.

CHAPTER 2: LITERATURE REVIEW

2.1 Seismic Risk Assessment Framework

One of the early frameworks for the seismic risk assessment includes, for instance, the six primary components shown in Figure 2.1 (Kircher et al., 2006). Each of these components is required for a comprehensive loss estimation study. However, the degree of sophistication required and the associated cost varies greatly. The modular approach of the methodology permits estimates based on simplified models and limited inventory data, as well as refined estimates based on more extensive inventory data and detailed analyses.

The above-mentioned modular methodology is implemented in the loss estimation platform HAZUS, which enables users to limit their studies to selected losses. For example, a user may wish to ignore induced damage when computing direct losses or to study the effect of proposed code changes upon losses to buildings without having to consider lifelines. This would eliminate a portion of the flow diagram shown in Figure 2.1. A limited study may be desirable for a variety of reasons including budget and inventory constraints, or the need for answers to very specific questions. For the UAE, Mwafy (2012a) discussed a framework for developing a loss estimation system in this region. The study utilized three main driving engines for the earthquake loss estimation systems, including: (a) seismic hazard; (b) inventory of the exposed systems; and (c) vulnerability relationships. The framework presented in the latter study for seismic loss estimation in the UAE is portrayed in Figure 2.2.

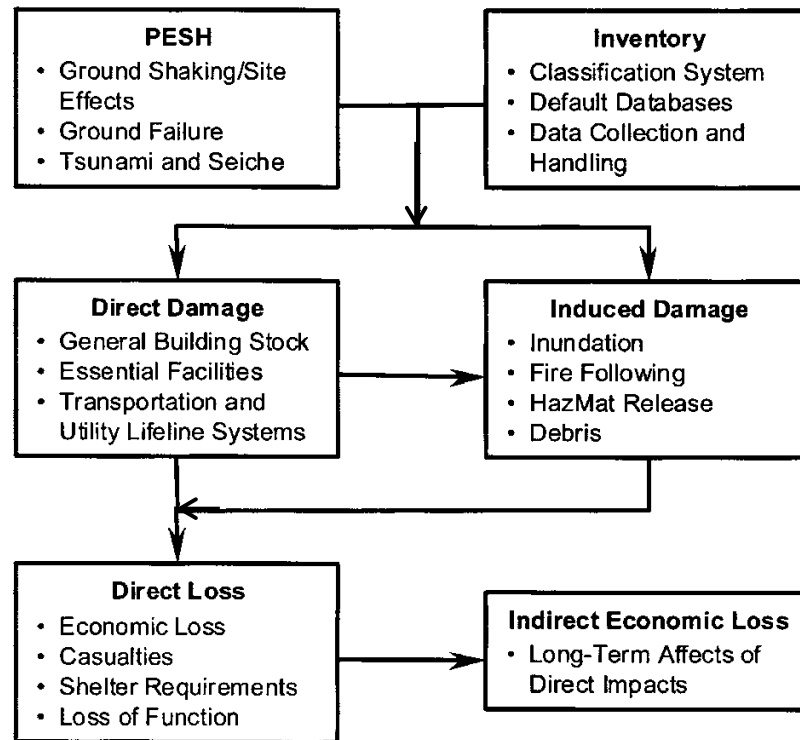


Figure 2.1: Primary modules of HAZUS Earthquake (Kircher et al., 2006)

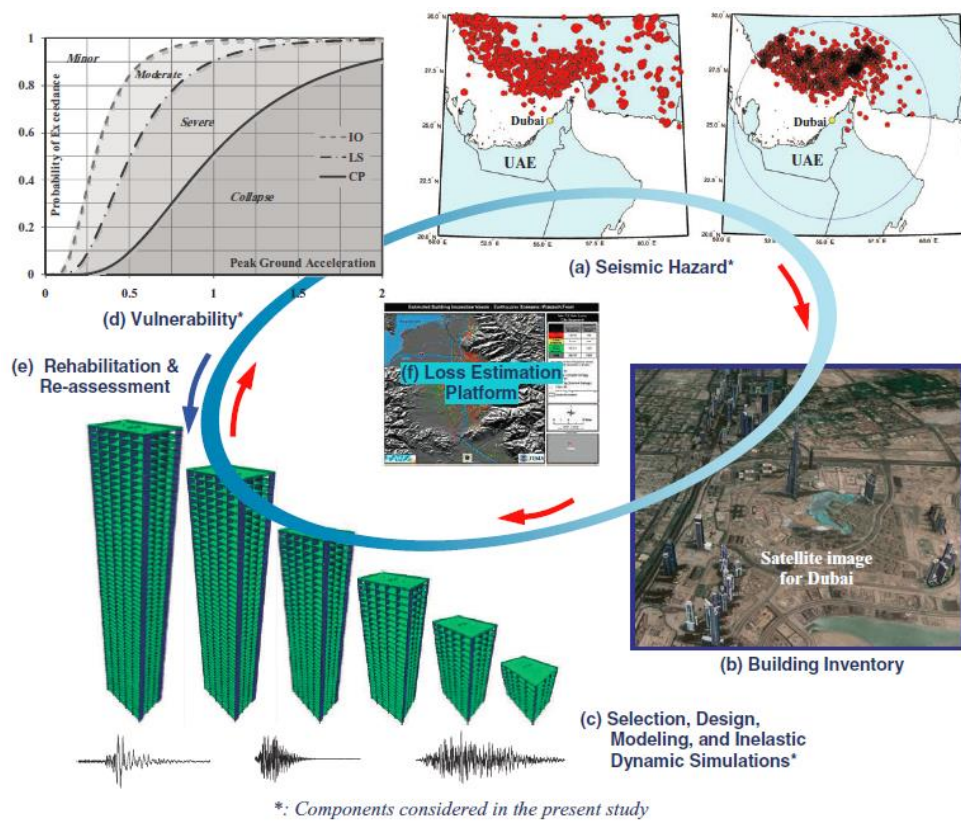


Figure 2.2: Framework for earthquake loss estimation in the UAE (Mwafy, 2012a)

2.2 Building Inventory

2.2.1 Pre-Seismic Code Buildings

The building stock in the UAE, an area with relatively low-to-medium seismicity, includes many old RC buildings. The earthquake risk of these buildings is particularly significant as most were designed without adequate seismic design provisions. In order to assess the seismic risk associated with these buildings and propose retrofit strategies that reduce the possible losses, it is necessary to accurately predict the response of pre-seismic code buildings under different earthquake scenarios representing the UAE seismicity.

Recent reports of seismic events in regions of low-to-moderate seismicity, such as the UAE, have led to concerns regarding safety and the vulnerability of RC buildings, in which ductile detailing was not explicitly provided in the design process. In some cases such as relatively tall buildings, although the design may have considered lateral forces due to wind loads, it is still important to carry out a complete seismic evaluation since higher vibration mode effects may increase the seismic demands in the mid to upper levels of the structure. Seismic vulnerability assessment of existing concrete buildings in which the non-seismic detailing is explicitly included in the evaluation procedure is of immense value to structural engineers. A brief review of previous studies related to the performance assessment of pre-code structures is presented below.

Ghobarah and his co-workers (1998; 1999b) evaluated the performance of an existing non-ductile structure designed according to the ACI-318 (1963) code and compared it to the performance of the same structure when designed according to a recent version of the code. Different performance levels were defined for the

structure in terms of the level of damage. The results obtained from dynamic analysis and static pushover analysis provided the probability of various degrees of damage expected when the existing structure is subjected to different ground motion levels. The comparison with the current code-designed building provided a reference case for the expected damage in a well-designed and detailed ductile structure. The study concluded that the existing non-ductile structure was more vulnerable compared to the well-designed and ductile one.

Bruno et al. (2000) carried out an analytical study on a pre-code reference structure. It was concluded that: a) the seismic performance of pre-code buildings without masonry panels was very poor, and the Effective Peak ground Acceleration (EPA) corresponding to collapse did not exceed 0.1g; b) the presence of masonry infill increased the EPA corresponding to collapse to 0.2g; c) inadequately distributed and located masonry panels may result in concentrated inelastic strain. Retrofit solutions suggested in the above-mentioned study included the introduction of shear walls and dissipative bracings.

Ramamoorthy et al. (2006; 2008) derived vulnerability functions to assess the seismic response of RC frame buildings designed mainly for gravity loads. Five buildings of various heights (one-, two-, three-, six-, and ten-stories) were used to represent RC frame buildings. Seismic structural capacity values were chosen to match the performance levels as specified in FEMA-356 (2000), or as calculated by pushover analyses. For each building, fragility estimates were obtained by assessing the conditional probability that the drift demand reaches or exceeds the drift capacity for a given earthquake spectral acceleration. Fragility estimates, formulated as a function of the fundamental building period and spectral acceleration, were generated to measure the seismic vulnerability of gravity load designed RC frame buildings.

Liel (2008), Haselton et al. (2010) and Liel et al. (2010) evaluated the collapse safety of RC frames in seismic areas by assessing two sets of archetype structures, including modern (ductile) and old (non-ductile) RC frame buildings. Archetype structures varied in height (from 2 to 12 stories) and framing systems (perimeter and space frames), and were designed according to the UBC (1967) and IBC (2003) building code provisions. The ductile (2003) RC frames demonstrated superior seismic performance for all heights and framing systems when compared to the non-ductile (1967) RC frames. Modern RC frame structures were able to withstand higher intensity ground motions and were capable of undergoing more significant deformations before collapse. Collapse margin ratios for the ductile RC frames were approximately three times larger than those of non-ductile frames. In terms of the mean annual frequency of collapse, non-ductile RC frame structures had significantly higher risk of collapse at a typical California high-seismic site.

The latter studies concluded that reinforcement detailing in beams, columns and joints in modern RC frames improved the element deformation capacity and reduced strength and stiffness deterioration as the structure deforms. Capacity design promoted yielding in beams, spreading damage and energy dissipation more over the height of the structure in the ductile RC frames. These improvements in component and system-level performance lead to the differences in collapse safety quantified in the above-mentioned studies. Among the regular set of structures evaluated, tall perimeter non-ductile RC frame structures were most susceptible to side-sway collapse because of their low lateral overstrength and flexibility. Space-frame structures, which have more axial load levels in columns, may experience column shear failure and subsequent loss of column load-bearing capacity, potentially leading to progressive structural collapse. Modest detailing improvements in beams,

columns and joints, such as those that might have been employed in California design practice in the 1960s, improved the seismic performance of non-ductile RC frames in some cases, but fall significantly short of modern code levels. The collapse performance assessments conducted in the latter studies quantified differences in safety for ductile and non-ductile RC structures.

It has been shown from the above-mentioned brief review that most of the previous studies focused on a few building configurations or systems. Previous studies were also directed to certain regions of high seismicity such as the west coast of the U.S. and Italy. No specific vulnerability assessment studies were carried out for pre-code structures in the UAE. Moreover, some of the previous studies adopted simplified seismic assessment approaches including the limited number of reference structures, modeling approaches, seismic scenarios and definition of limit states.

2.2.2 Emergency Facilities

Proper functioning of critical facilities such as acute care hospitals, fire stations, police station and schools are essential in the aftermath of a severe earthquake. For these facilities to remain operational, not only their structural systems must remain safe for continued occupancy, but also their non-structural components/systems must remain functional. For certain acute care hospitals, non-structural components may include elevators, stairs, HVAC systems, water systems for usable water and fire suppression, communications and utility systems, electric power systems as well as a variety of medical equipment for life support, laboratory testing, operations and other primary and secondary needs for patient care. In a severe earthquake event, critical facilities must remain operational in order to lead the emergency response and assist injured people with immediate medical care. For

hospitals, since the evacuation of seriously ill patients may be very difficult, their proper functioning in the aftermath of a seismic event is of utmost important. Furthermore, replacing or repairing heavily damaged critical facilities may take decades. For example, several hospitals in Los Angeles, U.S.A., were non-functional even a decade after the 1994 Northridge Earthquake and, thus deprived regional communities of service.

A number of studies have been carried out to seismically upgrade and retrofit the structural and non-structural components in critical facilities. Developments following the 1971 San Fernando Earthquake, U.S.A., in the seismic design and construction of buildings were significant. For instance, the Olive View Hospital building, which was severely damaged by the San Fernando earthquake and rebuilt conforming to the new design regulations in California, did perform well structure-wise under the 1994 Northridge Earthquake. A brief review of previous studies related to the performance assessment of critical facility structures will be presented below.

Bruneau and Reinhorn (2007) conducted a study that highlighted the concept of seismic resilience and the methodology describing how it can be quantified for acute care facilities. Relationships between seismic performance, fragility curves, and resilience functions were described. The interdependency of structural and non-structural resilience were illustrated for systems having either linear-elastic or nonlinear-inelastic structural behavior. The methods proposed to quantify resilience can be used to provide a comprehensive understanding of damage, response and recovery. The resilience functions explained the time variation of damage and its relationship to response and recovery. The framework proposed by Bruneau and Reinhorn (2007) to quantify resilience can also help the decision process towards

providing seismic mitigation, or the planning process, to guide response and recovery.

Elnashai et al. (2009) presented a comprehensive earthquake impact assessment for the central U.S.A., which employed an analysis methodology comprising three major components: hazard, inventory and fragility. The hazard characterized not only the shaking of the ground but also the consequential transient and permanent deformation of the ground due to strong ground shaking as well as fire and flooding. The inventory comprised all assets in the study region, including the built environment and population data. Vulnerability functions related the severity of shaking to the likelihood of reaching or exceeding damage states. Social impact models were also included and employed physical infrastructure damage results to estimate the effects on exposed communities. Whereas the modeling software packages used, provided default values for all of the above, most of these default values were replaced by components of traceable provenance and higher reliability than the default data.

The inventories in the latter study contained various types of critical infrastructure that are key inventory components for earthquake impact assessment. Transportation and utility inventories were improved while regional natural gas and oil pipelines were added to the inventory, alongside high potential loss facility inventories. New fragility functions were derived for both buildings and bridges to provide more regionally applicable estimations of damage for these infrastructure components. Default fragility values were used to determine damage likelihood for all other infrastructure components.

The results of the Elnashai et al. (2009) study confirmed that three states were heavily affected, namely Tennessee, Arkansas and Missouri. Moreover, the state of Illinois and Kentucky were also affected but to a lesser extent. A large number of buildings were damaged in the study region. Near the rupture zone, damage to critical facilities was considerable in the counties impacted, including 3,500 damaged bridges and hundreds of thousands of disruptions and leakages to both local and regional pipelines. Roughly 2.6 million houses were without electrical power after the earthquake. A large number of hospitals, mostly located near the rupture zone, were damaged. Tens of thousands of injuries and fatalities were reported. Considerable travel delays were also expected and hence obstructed rescue and evacuation. 15 large bridges were also out of service. Millions of people were displaced to temporary shelters. The total estimated direct economic losses were \$300 billion, while indirect losses were double this number.

Ray-Chaudhuri and Shinozuka (2010) developed an approach for the identification of essential components in critical facilities, whose fragility reduction lead to an optimal seismic retrofit of the system. For a hospital building, the procedure represented a systematic approach that integrates component fragilities, seismic response of the hospital structure and system fragilities. Sensitivity analysis was performed to identify the sensitive components within complex systems such as the water and electric power systems. The analysis also reflected that a significant enhancement of fragility at component level is needed in order to reduce the system's annual probability of failure. The conclusions drawn from the numerical results obtained in this study were valid only for the specific examples considered.

2.3 Seismic Hazard Studies in the UAE

Several seismic hazard studies have been published during the past few years for the UAE and its surroundings. These studies were carried out due to raised awareness of the threat posed by earthquakes in the region (Abdalla & Al-Homoud, 2004; Al-Haddad et al., 1994; Al Marzooqi et al., 2008; Aldama-Bustos et al., 2009; Jamali et al., 2006; Khan et al., 2013; Mwafy et al., 2006; Pasucci et al., 2008; Rodgers et al., 2006; Shama, 2011; Sigbjornsson & Elnashai, 2006)

2.3.1 Tectonic Settings of the UAE

Surrounded by a series of definite tectonic boundaries, the UAE is situated on the northeast of the Arabian plate. The regional tectonic setting is shown in Figure 2.3 (Aldama-Bustos et al., 2009). The Dead Sea faults, in the northwest direction, run to the Taurus Mountains through the east of the Turkish plate. The northern edge of the Arabian plate is defined primarily by the Zagros thrust and fold belt. The rest of the north-eastern side of the Arabian plate is defined by the Makran subduction zone where the Arabian plate subducts underneath the Eurasian plate. The Arabian and African plates diverge across the Gulf of Aden in the southeast. The Red Sea boundary outlines the interface between the latter two plates in the southwest direction. The final boundary defining the Arabian plate is the Owen fracture zone which is a transform boundary that separates the Arabian and Indian plates in the east. Aside from these major boundaries, the Arabian plate is a stable zone that does not exhibit any noticeable hint of internal deformation during the late Tertiary. The interior of the Arabian plate has not experienced any noteworthy seismic events over the past twenty decades and may be considered as a stable tectonic region (Reches & Schubert, 1987; Vita-Finzi, 2001).

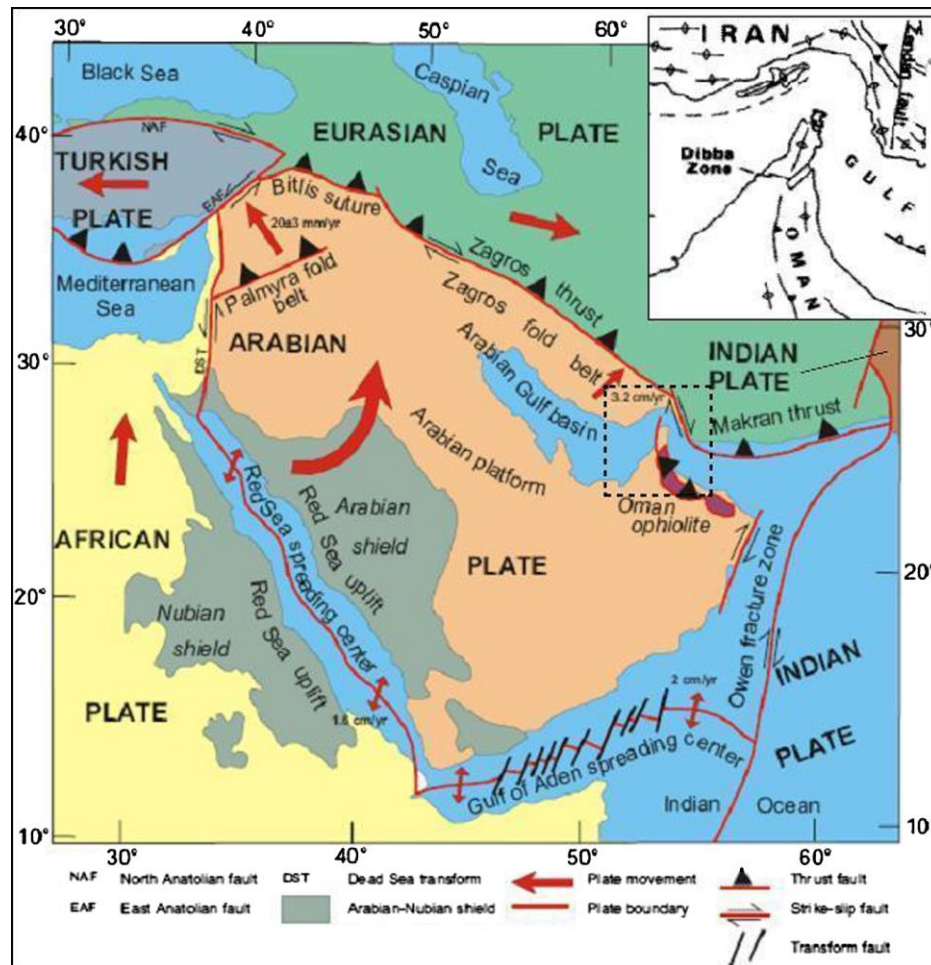


Figure 2.3: Tectonic setting of the Arabian plate (Aldama-Bustos et al., 2009)

At longitudes near the UAE, the Arabian plate is currently moving northwards at a rate of approximately 22 ± 2 mm/year with respect to the Eurasian plate (Vernant et al., 2004). The above-mentioned movement occurs due to a combination of the subduction of the Arabian plate beneath the Eurasian plate and also the intra-continental shortening throughout Iran. Figure 2.4 also shows the presence of some active tectonic structures in the Oman mountains close to the UAE (Aldama-Bustos et al., 2009). The deformation related to this mountain range along with the boundaries of the Zagros fold and thrust belt and the Makran subduction zone, represent the key seismic sources that may affect the seismic hazard for sites within the UAE.

Available seismic hazard studies for the UAE suggest that local seismic activities could be attributed to one of the following geological sources:

- The Zagros fold and thrust belt: is about 200 km wide and is categorized as one of the most active seismic zones in the world. The Zagros region was the source of numerous large earthquakes ($M_b \sim 7$) in the past. The UAE is located at the southeastern end of the Zagros thrust.
- The Makran subduction zone: this seismic source starts from the Gulf of Oman and extends through the Indian Ocean, bordering southern Pakistan. The Makran subduction zone lies approximately 750km away from the UAE. Historical records show that the largest earthquake recorded in this region was an event with a surface-wave magnitude (M_s) of 8.0.
- The Oman Mountains and local fault lines: Many local fault lines are located in the northeastern part of the UAE extending up to the Oman mountains, which are located in northern Oman. Numerous faults lie in this region, which include the Dibba line, Wadi Shimal fault and the Wadi Ham fault. In addition to these faults, the Oman Thrust Front is another seismic source that runs through the Oman mountains (Aldama-Bustos et al., 2009).
- The Zendan-Minab fault system: The region where the Zagros fold and thrust belt join the Makran subduction zone contains diverse complex faults. The linking fault line between these two regions is known as the Zendan-Minab fault.

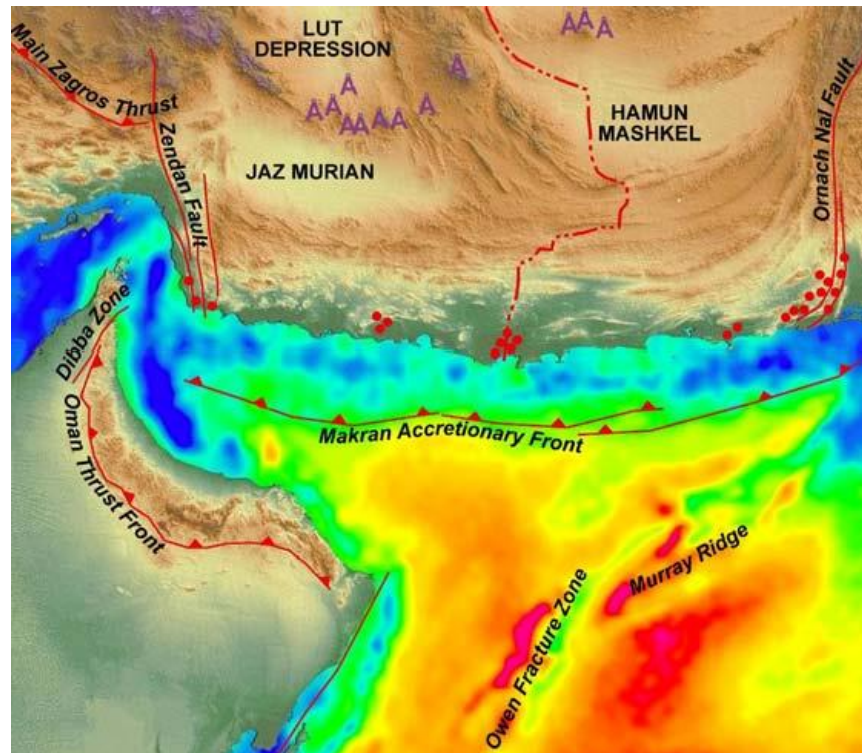


Figure 2.4: Plate tectonic setting of the Oman Sea (Jamali et al., 2006)

2.3.2 Previous Hazard Assessment Studies

Abdalla and Al-Homoud (2004) investigated the seismic hazards of the UAE and its surroundings based on a probabilistic approach. Seismic maps were presented as a guide for determining the design earthquake for different regions of the studied area. The area studied spanned several countries with diverse tectonic and geologic structures as well as various local geotechnical conditions. Although the results indicated that the UAE has low-to-moderate seismic hazard levels, high seismic activities in the north part of UAE deserve attention. The study indicated that the Northern Emirates are the most seismically active part. The recommended design Peak Ground Acceleration (PGA) on bedrock ranged between 0.1g and 0.2g for Dubai and between 0.22g to 0.38g for the Northern Emirates for a return period of 475 years and 1900 years, respectively. It was concluded that this level of PGA on bedrock, together with the amplification of local site effects, can cause structural

damage to key structures and lifeline systems. Therefore, earthquake effects should be taken into consideration when designing major structures in the region.

Sigbjornsson and Elnashai (2006) and Mwafy et al. (2006) presented a site-specific study for Dubai which employed the most recent earthquake data available and modern established procedures for probabilistic seismic hazard assessment. According to the study, the recommended PGA values for Dubai were 0.16g and 0.22g for return periods of 475 and 2475 respectively. Acceleration and displacement spectra suitable for modal analysis were also presented. Generated acceleration records for the two main scenarios of near-moderate and far-severe earthquakes were given for the purposes of a response history analysis of structures. The significance of including both scenarios in the seismic analysis and design was emphasized by presenting results from an advanced dynamic analysis of a high-rise structure. The two scenarios yielded results that were 200% to 500% different, in terms of force and displacement, respectively. The studies concluded that the ground acceleration values, spectra and strong-motion records recommended for design are reliable and should be used with confidence. The approach utilized for assessment of two fundamentally different earthquake scenarios was also recommended for use in regions where near and distant earthquake hazards exist.

Malkawi et al. (2007) carried out a study for the seismic hazard assessment and mitigation of earthquake risk in the UAE. The study concluded that the UAE is located in a region of low-to-moderate seismic activities, and its seismicity increases from southwest to northeast. The northern part of UAE is the most active seismic part due to its location near the causative sources and requires special care in engineering design. The recommended design PGA ranges from 0.0g for a 475 years

return period (50 years life time and 10% probability) in southwest regions to 0.35g for a 3000 years return period in the northeast region. The maximum regional magnitude was determined to be 8.7 ± 0.54 Mb. Although this is a very high value and of low probability, if it occurs in the study region it may cause a significant effect even if its hypocenter is distant.

Pasucci et al. (2008) presented the results of a probabilistic seismic hazard assessment undertaken for the Arabian Peninsula region in terms of ground motions on rock and spectral accelerations at short and long periods for various cities. Uncertainties in seismic sources and ground motion models were incorporated in the seismic hazard model using a logic-tree framework. The study concluded that the seismic hazard level is low with expected bedrock horizontal PGA in the range of 0.04g to 0.06g for a 475 year return period, and 0.06 to 0.11g for a 2475 year return period, with slightly higher values for cities close to the more seismically active regions.

Aldama-Bustos et al. (2009) conducted a probabilistic assessment of seismic hazard in terms of ground motions in rock for three cities in the UAE. The study was performed within a logic-tree framework to account for uncertainties in the models for seismic sources and ground-motion prediction. The results supported the conclusions of previous studies that the hazard levels in the UAE are low except in more northerly areas such as Ras Al Khaimah. The hazard calculations presented in this study demonstrated that the hazard is dominated by local seismicity, particularly at longer return periods. It is important to bear in mind, however, that the study did not consider the effect of surface soil deposits, which significantly amplify long-period motion generated by large-magnitude distant earthquakes in the Zagros and Makran regions. This could affect the high-rise structures dominating the skyline of

Dubai. The latter study concluded that the results should not be treated as definitive regarding the seismic design considerations for Dubai without considering local soil effects.

2.4 Vulnerability Relationships

2.4.1 Vulnerability Assessment of Buildings

Fragility analysis is an important task in seismic risk studies. Researchers have developed methods to perform fragility analysis, motivated by the increasing interest in obtaining accurate estimates of earthquakes losses. Fragility curves, the main output of a fragility analysis, are excellent tools for retrofit decisions, damage estimation, loss estimation and disaster response planning. Fragility functions for buildings are lognormal functions that relate the probability of attaining or exceeding a building damage state to a given intensity measure.

The input ground motions are scaled using Ground Motion Intensity (GMI) such as PGA and spectral acceleration (S_a). Wen et al. (2004) proposed the following expression for deriving the fragility relationships:

$$P(LS|GMI) = 1 - \Phi(\lambda_{CL} - \lambda_{D|GMI} / \sqrt{\beta_{D|GMI}^2 + \beta_{CL}^2 + \beta_M^2}) \quad (2.1)$$

where:

- $P(LS|GMI)$ is the probability of exceeding a limit state given the GMI;
- Φ : is the standard normal cumulative distribution function;
- λ_{CL} : \ln (median of drift capacity for a particular limit state);
- $\lambda_{D|GMI}$: \ln (calculated median demand drift given the ground motion intensity from the fitted power law equation);

- $\beta_{D|GMI}$: demand uncertainty = $\sqrt{\ln(1+s^2)}$, where s^2 is the standard error of the demand drift data;
- β_{CL} : is drift capacity uncertainty;
- β_M : is modeling uncertainty.

Fragility analysis is conducted to evaluate the relative seismic safety margins of structures with varying characteristics and input motion intensities. Uncertainties associated with structural capacity and imposed earthquake demand are accounted for by probabilistically treating structural response and seismic hazards. The most significant uncertainties in vulnerability assessment studies are:

- a) Input ground motions;
- b) Structural systems;
- c) Structural characteristics (e.g., height and period);
- d) Analytical modeling;
- e) Analysis method;
- f) Performance criteria; and
- g) Material properties;

Some of the uncertainties are random, while others are due to the lack of knowledge, as discussed by Wen et al. (2004). In order to account for the abovementioned uncertainties, the typical approach is to conduct Monte Carlo simulations. These simulations require a large number of inelastic response history analyses, which are demanding and expensive particularly when deriving fragility relationships for a wide range of structures with different structural systems. It is, therefore, more practical to focus on the dominant factors that control the probabilistic response, while estimating the impact of other uncertainties based on the conclusions of previous studies. Several studies concluded that material

properties have little impact on the structural response, particularly at high ground motion intensities, compared with the variability of ground motions (Kwon & Elnashai, 2006). Researchers also investigated the sensitivity of structures to major variables. It was found that uncertainties in ground motions are more significant than those in structural properties. Less significant uncertainties may be assumed deterministic such as those related to analytical modeling and analysis method. It is important to note that the reliable modeling approach, such as the fiber-based modeling, and analysis methods, such as the incremental dynamic analysis, are the most suitable for deriving vulnerability curves. The aforementioned approaches significantly contribute in reducing uncertainty compared with other alternatives.

Seismic performance criteria of structures, which are related to the level of damage, have received focused attention. The performance levels considered in seismic provisions and several previous studies include the following (ASCE/SEI-41, 2013; Ashri & Mwafy, 2014; Jeong et al., 2012; Mwafy, 2012b; SEAOC, 1999):

- Collapse Prevention (CP): allows for a small margin of safety against collapse during a severe earthquake.
- Life Safety (LS): indicates a significant damage to the building lateral force resisting system, but maintains a large margin against collapse.
- Immediate Occupancy (IO): where relatively minor damage may occur to the building, and the lateral force-resisting elements retain their initial strength and much of their original ductility.

Other performance levels have been also recommended by seismic provisions such as the Operational Performance (OP) criterion (ASCE/SEI-41, 2013). However, it is impractical to design structures to meet the OP performance level since all

utilities required for normal operation must be available after the earthquake. This is particularly true for standard structures (FEMA, 2009).

The Interstory Drift Ratio (IDR) is usually considered as the primary performance criterion as it is related to performance levels in ASCE/SEI-41 (2013) and in several other provisions (e.g. Eurocode, 2004). ASCE/SEI-41 (2013) adopts IDR corresponding to the IO, LS and CP limit states for ductile concrete wall structures as well as for pre-code frame structures, which are 0.5%, 1.0% and 2.0%. For modern frame structures the latter provisions recommend an IDR of 1%, 2.0% and 4.0% for the same performance criteria, respectively. A thorough review is carried out in the present study to confirm the limit states used for deriving fragility curves. Table 2.1 summarizes recommended values from previous studies, which covered the three categories of buildings considered in the current study, namely pre-seismic frame structures, pre-seismic wall structures and well-designed frame structures. An example of a typical fragility curves is also shown in Figure 2.5.

Table 2.1: Summary of IDRs for different limit states and structural systems

Selection Approach		Reference Structure								
		Pre-code Frames			Pre-code Walls			Modern Frames		
		Limit State - Interstory Drift (%)								
		IO	LS*	CP	IO	LS*	CP	IO	LS*	CP
ASCE/SEI-41, 2013		0.50	1.00	2.00				1.00	2.00	4.00
Experimental studies	Ghobarah, 1998	1.00	2.00	3.28						
	Wood, 1991 - 16%						1.36			
	Wood, 1991 - 50%						1.88			
	Wood, 1991 - 84%						2.60			
	Dymiotis et.al., 1999 - 16%									1.90
	Dymiotis et.al., 1999 - 50%									4.00
	Dymiotis et.al., 1999 - 84%									6.70
Analytical studies	Ghobarah et.al., 1999	0.70	1.10	2.50				0.40	1.80	3.00
	Ramamoorthy et.al., 2008 - 16 %	0.33		0.56						
	Ramamoorthy et.al., 2008 - 50 %	0.50		0.98						
	Ramamoorthy et.al., 2008 - 84 %	0.75		1.71						
	Liel et.al., 2010 - 16 %			3.26						
	Liel et.al., 2010 - 50 %			4.17						
	Liel et.al., 2010 - 84 %			5.34						

IO: Immediate Occupancy, LS: Life Safety, CP: Collapse Prevention
 16%: 16 percentile of the results; 50%: 50 percentile; 84%: 84 percentile

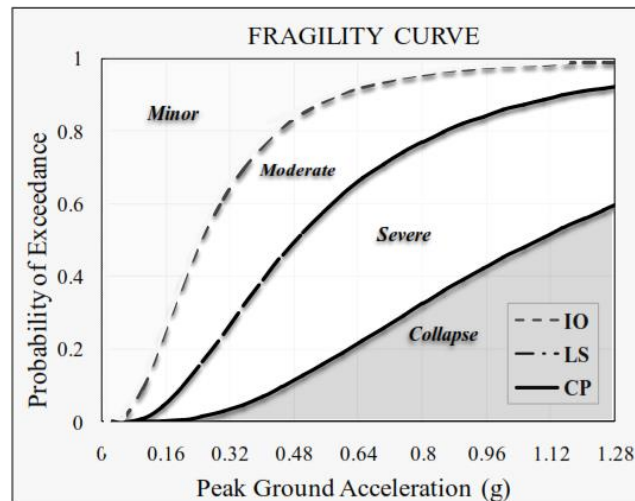


Figure 2.5: Typical fragility curve (Mwafy, 2012a)

2.4.2 Previous Vulnerability Assessment Studies for the UAE

Abu-Dagga et al. (2010) conducted a seismic fragility assessment where the buildings stock in Sharjah, UAE, was represented by 13 model building types according to their height, use and structural systems. Seismic fragility analysis was performed using simple ETABS (CSI, 2011) models for each building type and the associated fragility curves were prepared. The fragility curves were used to estimate the seismic potential losses in Sharjah. It was concluded in this study that the low-rise structures would be responsible for more than half of the human and structural losses in the study area. This result could be due to two main reasons: that these buildings were not designed to resist any lateral load, and that the closeness of the periods of these buildings and the period of the ground motions used in the study. It is worth noting that the study by Abu-Dagga et al. (2010) focused on a limited study area and employed simplified modeling and assessment approaches. This study has already highlighted the need for a more comprehensive and reliable seismic risk assessment for Sharjah.

Mwafy (2012a) conducted a pilot study for the development of fragility relationships, which constitute an essential driving engine in loss assessment systems, in the UAE. The study included the selection, structural design and developed fibre-based simulation models for six reference structures representing a range of modern shear wall buildings in the UAE. The selection and scaling of twenty input ground motions representing long (Set 1) and short (Set 2) source-to-site distance earthquake scenarios anticipated in the study area were discussed. Limit state criteria for deriving fragility curves were selected based on the mapping of local and global response from IPAs and IDAs. The measured seismic response from IDAs was related to ground motion intensity through a statistical model to derive the fragility relationships of the reference structures. The differences between the fragility functions obtained from the two seismic scenarios employed in the study of Mwafy (2012b) were significant for all buildings. The probability of exceeding various limit states was higher and the slopes of the curves were steeper under the effect of the Set 1 earthquake scenario when compared to Set 2. These were attributed to the high spectral amplifications and effective durations of the Set 1 ground motions, which amplified the most significant modes of vibration for high-rise buildings. Under the effect of both Set 1 and 2 events, limit states were exceeded at higher ground motion intensities for taller buildings, which implied that earthquakes have a higher impact on low-rise structures. The study confirmed the vulnerability of shear wall buildings to the severe distant seismic scenario anticipated in earthquake-prone areas of the UAE.

Al Shamsi (2013) assessed the seismic risk for buildings in Dubai. The study area was divided into sectors based on usage, buildings and population distribution data, satellite images and field visits. Only five reference structures, ranging from 2

to 16 stories, representing the building stock of Dubai were modeled using IDARC (Park et al., 1987). Earthquake records representing far-field events were used. The records were adjusted to match a target spectrum representing local seismicity. Dynamic analysis was performed and fragility curves were developed for the reference structures. Performance limit states were adopted from ASCE/SEI (2007). The performance of each building was evaluated at three levels of hazard: the Maximum Considered Earthquake level (MCE); the design level, which corresponded to two-thirds of the MCE level; and twice the MCE level. Human losses and economic losses were estimated in the study by Al Shamsi (2013). It was concluded that the probabilities of exceeding the CP limit state for the reference structures were below 20% at the design and MCE levels. The shorter buildings exhibited better performance than the taller ones. The seismic risk maps illustrated that the estimated number of fatalities at the MCE level were generally low, and that economic and human losses were higher in the commercial zone. Based on the modeling assumptions and analyses performed in this study, there were no major concerns regarding the vulnerability of the representative buildings in Dubai.

More studies focusing on developing vulnerability functions for contemporary buildings in the UAE with varying structural systems and heights are in progress (Ashri & Mwafy, 2014). Al Waile et al. (2014) also proposed a framework for developing fragility relations for high-rise RC buildings based on verified modeling approaches in the UAE. Moreover, Mwafy et al. (2014b) have recently carried out a study on relative safety margins of code-conforming vertically irregular high-rise buildings in the UAE.

It has been observed from the brief review presented above that few seismic hazard assessment studies have been performed for the UAE and the surrounding

region. In addition, none of the available studies were carried out based on reliable inventory data; a wide range of reference structures with different characteristics representing the building stock; detailed design and modeling approaches; selection of input ground motions to represent different seismic scenarios in the study area and the adoption of reliable limit states and approaches for developing fragility curves. The present study takes into consideration the above-mentioned shortcomings, and hence represents a systematic and comprehensive vulnerability assessment study for the UAE.

2.5 Seismic Design Loads and Wind Effects

Structural dynamics is a type of structural analysis which covers the behavior of structures subjected to dynamic loading. Dynamic loads include wind, traffic, earthquake and blast loads. Dynamic analysis is used to determine different response parameters such as displacements, story drifts, story shear forces and building base shear. Dynamic analysis for single degree of freedom structures can be carried out manually, but for complex structures finite element analysis should be used to calculate the mode shapes and frequencies.

2.5.1 Seismic Loads

Earthquake loads consist of the inertia forces of the building mass that result from the shaking of its foundation by a seismic event. Frame buildings, which are light and flexible, are usually less vulnerable to earthquakes than buildings which are heavy and brittle. Although earthquake loads are complex, uncertain and potentially more damaging than wind loads, they do not occur as frequently compared with wind loads. Lateral load resisting systems for earthquake loads are similar to those for

wind loads. The wind load is an external force, the magnitude of which depends upon the height of the building, the velocity of the wind and the amount of surface area that the wind attacks. The earthquake load, on the other hand, depends on the mass, stiffness and strength of the structural system and the acceleration of the earthquake. It is clear that the applications of these two types of loads are different. To estimate the seismic design loads of typical structures, two approaches are used: (i) the Equivalent Lateral Force Procedure (ELFP), and (ii) modal response spectrum analysis, in which the modal frequencies of the structure are analyzed and then used in conjunction with earthquake design spectra to estimate the maximum modal responses.

As outlined in the general procedures and the site-specific procedures of ASCE-7 (2010), the ground motion accelerations, represented by response spectra and coefficients derived from these spectra, shall be determined. Conditions of use of these methods depend on the seismic use group and site characteristics of the structure. The procedure for determining the design spectral response acceleration is as follows:

1. Determine the mapped maximum considered earthquake spectral response accelerations at short periods, S_s , and at 1-second period, S_1 , using the spectral acceleration maps in ASCE-7 (2010). Linear interpolation is allowed for sites inbetween contours. Acceleration values obtained from the maps are given in %g, where g is the gravitational acceleration.
2. Obtain the site class in accordance with ASCE-7 (2010). Site class (A, B, C, D, E or F) is obtained based on the average shear wave velocity, v_s ; average standard penetration resistance, N; or the average undrained shear strength, S_u . These parameters represent average values for the top 100ft (30m) of soil.

3. Calculate the maximum considered earthquake spectral response acceleration, adjusted for site class effects, at short period, S_{MS} , and at 1-second period, S_{M1} , in accordance with ASCE-7 (2010).
4. Estimate the design spectral response accelerations at short period, S_{DS} and 1-second period, S_{D1} in accordance with ASCE-7 (2010).
5. Using the parameters determined in the previous steps, the general response spectrum is obtained in accordance with ASCE-7 (2010).

2.5.2 Wind Effects

Wind is a phenomenon of great complexity because of the many flow situations generated from contact with structures. Wind is measured according to the direction from which the wind is blowing as well as its speed. Winds of shorter durations with higher bursts are called wind gusts. This experience of sudden gusts of rushing air is called gustiness or turbulence. Long-duration winds have various names according to their average strength such as breeze, gale, storm, hurricane and typhoon (Ali, 1994). The Synoptic winds, Shamal winds and thunderstorms are three different wind phenomena, which illustrate the configuration of winds in the UAE (Hubert et al., 1983; Hussain, 2012). Although there have been several important studies done on the structure of wind in the UAE, further research is needed to quantify the profiles of the Shamal winds and thunderstorms, so that they can be incorporated in design codes (Ali, 1994; Hubert et al., 1983; Hussain, 2012).

Calculating wind loads is essential in the design of wind force-resisting systems, including structural members, components and cladding. Wind engineering is concerned with the effect of wind on the natural and built environment and the possible damage which may result from wind. Wind engineering involves analyzing

the wind impact on structural and non-structural components as well as wind comfort near buildings. The structural design of buildings accounts for strong gusts, as well as extreme winds such as in a tornado, hurricane or heavy storm, which may cause extensive destruction. Wind may be the governing load in the analysis and design of a certain class of structures such as tall buildings.

Wind loads are composed of static and dynamic components. Wind forces also increase with building height, as the effect of ground friction decreases. Wind response is quite sensitive to both stiffness and mass, and the lateral response can be reduced by changing these parameters. The detailed procedure described in wind codes is sub-divided into static analysis and dynamic analysis methods. The static approach assumes that the building is a fixed rigid body with its fixed end at the ground. The static method is appropriate for structures with limited height and unsuitable for tall structures of exceptional height, slenderness, or vulnerability to vibration. The dynamic method is recommended for tall, slender or vibration-prone buildings. The design codes not only provide detailed design guidance with respect to dynamic response, but also state specifically that a dynamic analysis is a must to determine the overall force on structures with a large height (length) to breadth ratio, and a first mode frequency less than 1 Hz (e.g. ASCE-7, 2010).

2.6 Seismic Rehabilitation of Structures

There are a number of circumstances where it may become necessary to increase the load-carrying capacity of a structure in service. These include a change of loading or use, and the cases of structures that have been damaged or deteriorated. This concern is more obvious in pre-code structures and emergency facilities as they experience poor seismic performance, and the urgent need to meet stringent

performance criteria for operational readiness, respectively. In the past, the increase in strength was provided by casting additional reinforced concrete, dowelling in additional reinforcement or externally post-tensioning the structure. More recently, attaching steel plates to the surface of the tension zone using adhesives and bolts was used to strengthen concrete structures. Even more recently, the use of FRP sheets, generally using carbon fibres, was developed using the same basic techniques as for steel-plate bonding (Arya et al., 2002). This section highlights general seismic rehabilitation provisions and practices related to the present study, and summarizes the findings of previous studies.

2.6.1 FEMA-547 Seismic Rehabilitation Provisions

FEMA-547 (2006) provides a selected compilation of seismic rehabilitation techniques that are practical and effective. The descriptions of techniques include detailing and constructability tips. The main goals of the document are to:

- Describe rehabilitation techniques commonly used for various building types,
- Incorporate relevant research results;
- Discuss associated details and construction issues; and
- Provide suggestions to engineers on the use of new products and techniques.

Chapter 12 and 13 of FEMA-547 (2006) discuss concrete moment frame and concrete shear wall systems, respectively, which are considered in the current study. The proposed rehabilitation techniques for the concrete moment frame are: (i) add steel braced frame (connected to a concrete diaphragm); (ii) add concrete or masonry shear wall (connected to a concrete diaphragm); (iii) provide collector in a concrete diaphragm; (iv) enhance the column with fiber-reinforced polymer composite overlay; and (v) enhance the column with concrete or steel overlay. The proposed

rehabilitation techniques for the concrete shear wall systems are: (i) enhance shear wall with fiber-reinforced polymer composite overlay; (ii) enhance deficient coupling beam or slab; (iii) enhance connection between slab and walls; and (iv) reduce flexural capacity of shear walls to reduce shear demand. For the sake of brevity, the detailed description of these conventional techniques and general guidelines used for each type of the two systems along with detailed drawings, are to be found in FEMA-547 (2006).

2.6.2 Previous Seismic Rehabilitation Studies

Saadatmanesh et al. (1997) conducted an investigation into the flexural behavior of earthquake-damaged RC columns repaired with FRP wraps. Four column specimens were tested to failure under severe reversed inelastic cyclic loading. The columns were repaired with FRP wraps and retested under simulated earthquake loading. The test specimens were designed to model non-ductile concrete columns in existing highway bridges constructed before modern seismic design provisions. FRP composite wraps were used to repair areas near the column footing joint. The results indicated that the repair technique was effective. Both flexural strength and displacement ductility of the repaired columns were higher than those of the original columns.

Moehle (2000) reviewed different approaches of seismic retrofit for concrete building in the US, in which two general techniques were described. The first technique, involves global modification of the structural system. The structural modifications are designed so that the demands on the existing structural and non-structural components are less than their capacities. This approach includes the addition of structural walls, steel braces or base isolators. Another approach involves

the local modification of isolated components of the structural and non-structural systems. The objective of the latter approach is to increase the deformation capacity of deficient elements. This will prevent such elements from reaching their identified performance criteria. This approach includes the addition of concrete, steel or FRP jackets. It was concluded that global modification schemes are more common in the US than local modification schemes. However, difficulties in developing accurate models of foundation flexibility and conservative acceptance criteria for existing components may require the use of some combination of the two approaches.

Taghdi et al. (2000) conducted an experimental study which indicated that the steel strip system, proposed to retrofit low-rise masonry and concrete walls, is effective in increasing their in-plane strength, ductility and energy dissipation capacity. The details and connections used to ensure continuity between the steel strip system, foundation and top beam also enhanced the sliding friction resistance. It was shown that the anchor bolts along the vertical strips can be placed to provide lateral supports to the end bars of the existing reinforced concrete/masonry walls, helping to eliminate their premature buckling. It was also recommended to pay attention to the wall shear strength since the ultimate strength of walls retrofitted, using only vertical steel strips, can be limited by their less-ductile shear failure.

Ye et al. (2003) tested eight RC column specimens under constant axial load and lateral cyclic load. Two specimens were strengthened using Carbon Fiber Reinforced Polymer (CFRP) sheets after being loaded to imitate strengthening with damage, while one specimen was strengthened under a sustained axial load to imitate strengthening under service conditions. Based on the experimental results, a confinement factor of CFRP and an equivalent transverse reinforcement index were suggested. The study concluded that the ductility of RC columns can be substantially

improved by strengthening using wrapped CFRP sheets due to the confinement from CFRP. The CFRP contribution to confinement can be represented by the confinement factor, which is the ratio of the average CFRP strain in the plastic hinge zone of the column at displacement to the CFRP fracture strain. The amount of CFRP needed for the seismic strengthening of RC columns can be determined using the suggested equivalent transverse reinforcement index.

Ghobarah and Galal (2004) conducted an experimental study which included testing three RC short columns under cyclic lateral loads and constant axial load. The first specimen represented columns designed according to a current code (CSA, 1994). The second specimen was identical to the first one but rehabilitated using anchored carbon fiber sheets. The third specimen represented existing non-ductile short column designed according to pre-1970 codes and rehabilitated using anchored CFRP. The study concluded that short RC columns designed according to the current code failed in brittle shear when subjected to lateral cyclic displacements. The strengthening of a short RC column that contains both a high and low percentage of transverse reinforcement (i.e. designed according to current code and pre-1970 codes, respectively) using anchored CFRP sheets prevented the brittle shear failure of the former and improved the displacement ductility and energy dissipation capacity of both columns. Both steel rods and fiber anchoring techniques were effective in improving the column confinement and in reducing the concrete bulging at column sides. Although there was no test conducted on a column wrapped with FRP without anchors to compare it with, the high strains measured in the steel anchors confirmed the important contribution of the anchors to column confinement.

Tremblay et al. (2004) carried out two sub-assembly tests as well as designing and analyzing a sample three-story building, which showed that the design

forces for capacity protected elements can be reduced considerably when adopting BRB frames compared to Conventional Braced Frames (CBF) structures. Non-linear dynamic analysis of the buildings studied confirmed that low-rise BRB frames designed according to NBCC (2005) provisions with $R = 4.0$ can exhibit reasonable seismic performance. The results indicated, however, that the inelastic demand was concentrated on the bottom floor, resulting in core strain demand exceeding the design values, especially when short brace cores were used.

Fahnestock et al. (2007) conducted an analytical and experimental study on the seismic behavior of BRBs with Concrete Filled steel Tubular (CFT) columns at the ATLSS Center, Lehigh University. They investigated the seismic performance of this type of frame, to evaluate existing design criteria, and to calibrate analytical models. A 4-story prototype building was designed with BRBFs as the lateral load resisting system. Design criteria were taken from the IBC (2000) and the SEAOC (1999) provisions for BRBFs. The analysis program DRAIN-2DX was used to model a one-bay prototype frame including material and geometric nonlinearities. A statistical summary of the analysis results was developed at the design and MCE input levels. The LS performance level was the target level for the design earthquake and the CP performance level was the target level for MCE. The study observed an acceptable BRBF behavior at the above-mentioned seismic input levels.

Di Ludovico et al. (2008) conducted full-scale tests for an under-designed RC structure with and without FRP retrofit. The experimental results provided by the structure in the 'as-built' and FRP-retrofitted configurations highlighted the effectiveness of the FRP technique in improving the global performance of the under-designed RC structure in terms of ductility and energy dissipation capacity. This goal was achieved by confining the column ends and preventing brittle

mechanisms (i.e. exterior joints and column shear failure). The design equations used for shear strengthening of exterior beam-column joints and of the wall-type column were found effective to quantify the FRP laminates needed to enable the structure to fully exploit its improved deformation capacity, given by the increased ductility of the FRP-confined columns. A pushover analysis provided results close to the experimental outcome, confirming the effectiveness of the FRP retrofit in increasing the global deformation capacity of the ‘as-built’ structure by improving its displacement capacity at a significant damage limit state.

Di Sarno and Manfredi (2010) assessed the seismic performance of a typical RC existing building designed for gravity loads only. A fibre-based three-dimensional finite element model was developed to assess the non-linear earthquake response of the non-ductile reference building. The existing two-story framed structure exhibited high vulnerability, and hence an effective strategy scheme for seismic retrofit was employed. Such a scheme comprised BRBs placed along the perimeter frames of the building. The BRBs possess slightly higher compressive strength than tensile strength. Member buckling was prevented and hence the cyclic energy dissipation was large and stable. Non-linear pushover and dynamic response history analyses were carried out for both the ‘as-built’ and retrofitted structures to investigate the efficiency of the adopted intervention strategy. A set of seven code-compliant natural earthquake records were selected and employed to perform inelastic history analyses at serviceability (operational and damageability limit states) and ultimate limit states (life safety and collapse prevention limit states). The comparison between the results obtained from nonlinear analyses demonstrated that both global and local lateral displacements were reduced after the seismic retrofit of the existing system. Lateral drifts of the retrofitted structure were uniformly

distributed along the height, and damage localizations were inhibited, especially at ultimate limit states. The estimated response factor of the retrofitted structure was on average equal to 5.0, which corresponds to the value utilized in seismic codes for ordinary RC moment resisting frames and steel framed structures equipped with BRBs.

Mwafy and Elkholy (2012) carried out a pilot study to select an effective retrofit approach for mitigating the seismic risk of the pre-code school building stock in a medium seismicity region. In this study, a three-story structure was selected to represent the aforementioned category of buildings. The structural elements of the reference structure were rehabilitated through the use of two retrofit techniques, namely RC jackets and FRP wrap of columns. The investigation of two additional alternatives for the applications of these retrofit techniques was included in this study. All columns were retrofitted as the first alternative. However, to reduce the cost, only ground story columns were strengthened in the second one. In addition, to obtain the most effective solution, two different thicknesses of FRP sheets and three types of FRP material properties were also assessed and compared. Models were developed using both the Improved Applied Element Method (IAEM) and the fiber-based modeling approach. Fragility relationships were generated to describe the observed damage before and after the application of retrofit techniques. The retrofitted buildings showed a significant increase in the seismic performance compared with the pre-code counterpart. RC jackets provided the lower probability of damage which supported selecting it over other alternatives.

2.6.3 Comparative Evaluation of Retrofit Techniques

Based on the above-mentioned brief review, a number of retrofit approaches are selected in the present study to enhance the seismic performance of buildings. This section provides a comparative evaluation of different retrofit techniques selected herein. Concrete jacketing is the conventional form of retrofit. Different combinations of constituent materials, fiber structures and methods of application have made FRP composites an attractive alternative for seismic retrofit. Steel plate installment, especially for wall elements, is considered as preferable option in many cases. Finally, BRBs have recently proved to be an excellent solution for seismic retrofit in frame structures. The advantages and disadvantages of various retrofit techniques are summarized in Table 2.2.

Table 2.2: Advantages and disadvantages of retrofit techniques

Technique	Advantage	Disadvantage
RC Jacketing	<ul style="list-style-type: none"> • Increases flexural strength and stiffness, • Durable, • Good fire resistance, and • Low cost. 	<ul style="list-style-type: none"> • High occupant disturbance, and • Labor intensive work.
FRP Wrapping	<ul style="list-style-type: none"> • Easy to handle and apply, • Effective in shear, flexural, and confinement retrofit, and • Low occupant disturbance. 	<ul style="list-style-type: none"> • High material cost, • Needs skilled labor, and • Low fire resistance.
Steel plates	<ul style="list-style-type: none"> • Easy to handle and apply, • Readily available, and • Low occupant disturbance. 	<ul style="list-style-type: none"> • Large amount of welding/bolting required, • Corrosion, • High installation cost, and • Low fire resistance.
BRBs	<ul style="list-style-type: none"> • Low occupant disturbance, • Energy dissipative behavior, • Easy post-earthquake investigation and replacement if needed, and • Fast erection. 	<ul style="list-style-type: none"> • Needs professional skilled labor, and • Ductility properties strongly affected by the material type and geometry of the yielding steel core segment.

2.7 Concluding Remarks

The main driving engines of the earthquake loss estimation systems used are:

(a) seismic hazard; (b) inventory of the exposed systems; and (c) vulnerability

relationships. As they may experience a high risk of damage, pre-seismic code buildings have to be studied thoroughly. A number of peer-reviewed studies that carried out on this category of buildings were reviewed. The literature review concluded that pre-seismic code buildings suffer from low levels of ductility and strength as they were designed and constructed without proper seismic provisions. A crucial role in the recovery period succeeding an earthquake is played by emergency facilities. In spite of being constructed according to modern seismic design provisions, considerable attention should be paid to this type of building. A number of previous studies on critical facilities were reviewed. These studies emphasized the important role of these building and the need to reduce the damage. This may require the application and adoption of mitigation measures in order to achieve the optimum performance during earthquakes. The presented study focuses on the vulnerability assessment of the above-mentioned two categories of buildings and their mitigation measures which emphasize the significance of this study.

Previous seismic hazard studies for the Arabian Peninsula, including the UAE, were reviewed. The UAE is influenced by a number of seismic sources, including the Zagros and Makran sources. The results of previous studies indicated that the design PGA value corresponding to a return period of 475 years for Dubai ranges between 0.05g and 0.32g. Due to the large variation of the recommended design PGA for Dubai in previous studies, the conclusions of three peer-reviewed studies were adopted in the present study. For Dubai, a design PGA of 0.16g, which represents the design PGA for a 10% probability of exceedance in 50 years, was adopted. Dubai and the Northern Emirates are vulnerable to two different seismic scenarios: (i) severe earthquakes with a relatively long epicentral distance; and (ii)

moderate events with short source-to-site distance, typically originating from local seismic faults.

The seismic performance assessment of buildings based on a fragility analysis was also reviewed. Different performance limit states recommended in design provisions were summarized, including Immediate Occupancy (IO), Life Safety (LS) and Collapse Prevention (CP). Uncertainties in fragility analysis were highlighted and methodologies to reduce these uncertainties were studied. The derivation of fragility curves using a detailed fiber modeling approach and inelastic dynamic collapse analyses was implemented in the present study, based on this literature review to reduce the uncertainty. The literature review reflected the pressing need for developing comprehensive fragility relationships for different building classes which is taken care in the current study.

Few seismic hazard assessment studies were carried out for the Arabian Peninsula in general, and for the UAE in particular. In addition, none of the available studies were carried out based on reliable inventory data; a wide range of reference structures with different characteristics representing the building stock, detailed design and modeling approach, selection of input ground motions to represent different seismic scenarios in the study area and the adoption of reliable limit states and approaches for developing fragility curves. The present study takes into consideration the above-mentioned shortcomings, and hence represents a systematic vulnerability assessment study for the UAE.

Extensive research has been directed towards the seismic rehabilitation of structures both experimentally and numerically. Code provisions, as well as several studies regarding this area of research, were reviewed. Several retrofit techniques and

mitigation measures were investigated and recommended in previous studies, including RC jacketing, FRP wrapping, adding new wall elements, the use of steel plates, installing buckling restrained braces, and others. Based on the results of previous studies and the applicability and suitability of the investigated buildings and study region, four techniques were adopted in the present study, namely RC jacketing, FRP wrapping, installing BRBs and the use of EUSP.

CHAPTER 3: SELECTION AND DESIGN OF REFERENCE STRUCTURES

3.1 Selection of Representative Buildings

The selected building inventory in this study includes the building stock in Dubai, Sharjah and Ajman, which represent highly populated earthquake-prone areas in the UAE. One of the major challenges is assembling a database for the existing building stock in the study area (Figure 3.1). This is due to the rapid changes in the exposed inventory and the lack of reliable surveys. Some governmental institutions have partial inventory databases, but the available databases do not contain all the required structural information. Such information is needed to appropriately categorize buildings for seismic risk assessment. Therefore, the building inventory data used in the present study was collected in another study by conducting several site visits and using high resolution satellite images (Mwafy, 2012b; Mwafy, 2013). The area studied is divided into twelve zones; each has common characteristics and features.

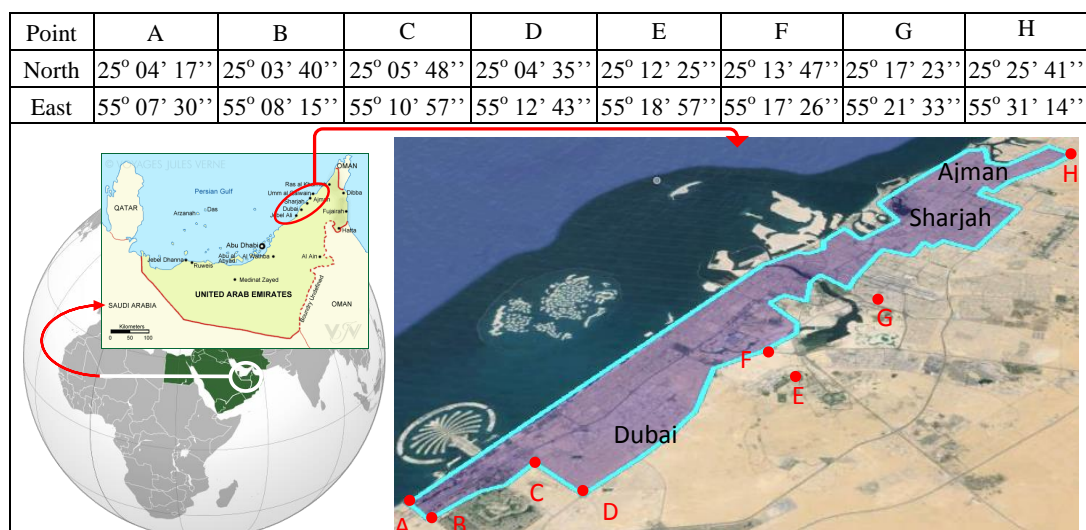


Figure 3.1: Study area

In total 79861 buildings were counted and classified in different categories (Mwafy, 2012b). The building inventory of Dubai, Sharjah and Ajman was classified according to two criteria. This is mainly due to the significance of the classification criteria of the exposed building stock in risk analysis. The classification criteria were: (i) function and (ii) construction date in which various heights have been considered ranging from 2 to 40 stories, as discussed below.

3.1.1 Selection Based on Construction Date

The study area includes a significant amount of the existing inventory that were designed and constructed in accordance with different building codes. The UAE was classified as zone '0' in the Uniform Building Code (UBC, 1997). Therefore, old buildings were not designed to resist seismic loads. Hence, the buildings inventory was categorized into two categories based on their construction date, namely before 1991 (pre-code) and after 1991 (contemporary). The buildings in the contemporary category have adequate structural capacity in terms of strength and ductility since they are designed according to modern design codes. The pre-code structures were only designed to resist gravity and wind loads. This second category of buildings may include design deficiencies. An illustration of the building classification according to their construction date in different zones is shown in Figure 3.2. It is clear that almost half of the building stock represents modern buildings (49 %), while the other half is pre-code (51 %).

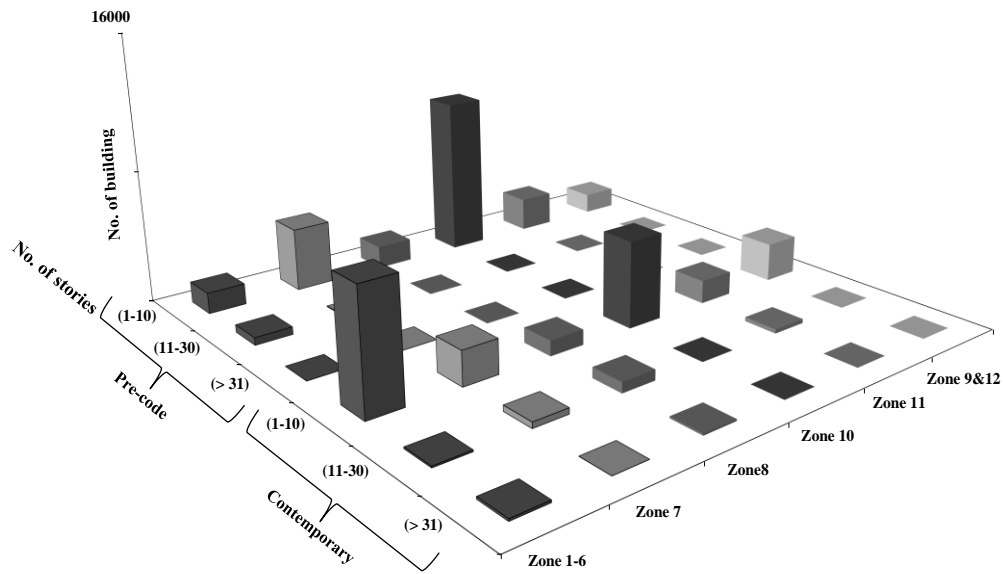


Figure 3.2: Buildings classification according to their construction date (Mwafy, 2013)

3.1.2 Selection Based on Risk Category

Critical facilities play an important role in the recovery period subsequent to an earthquake. Essential and emergency facilities include but are not limited to: hospitals, police stations, fire stations and schools, which may serve as emergency shelters. In any seismic event, in order to guarantee an effective emergency response, the readiness of these buildings after earthquakes is significant. According to ASCE-7 (2010), the building inventory in the present study was classified into four categories, namely risk category I, II, III and IV. Figure 3.3 depicts the distribution of buildings in different zones according to their risk category. It was shown that 80% of the building stock is for buildings with standard occupancy (i.e. risk category II), which is defined as residential and office buildings. The buildings that represent a low risk to human life in the case of failure (i.e. risk category I) are 19% of the inventory. These category I buildings are mainly located in zones 6, 7, 11, and 12. Less than 0.5% of the buildings stock is for buildings with risk categories III and IV, which are located in zones 7, 8, and 11.

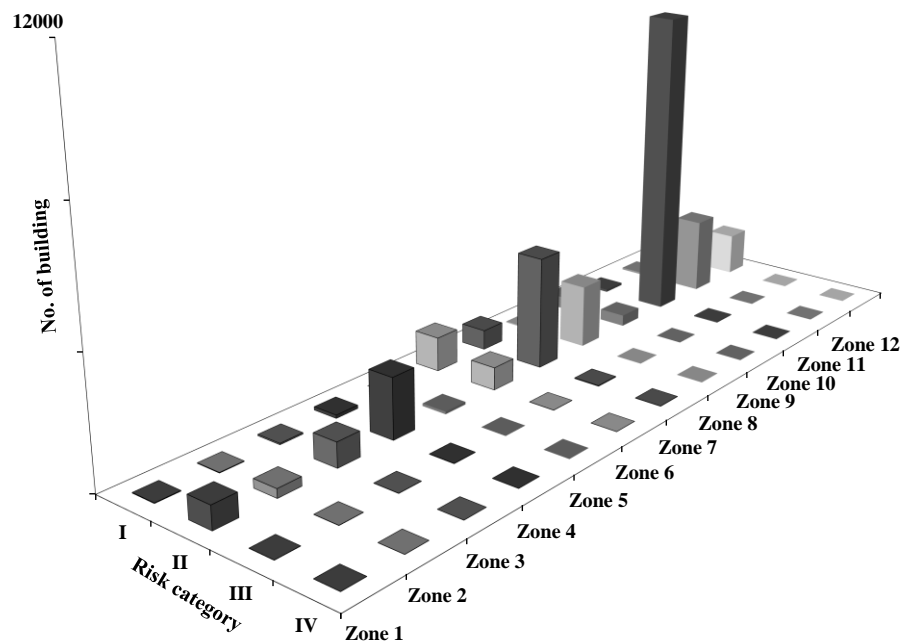


Figure 3.3: Building classification according to risk category (Mwafy, 2013)

Based on the above-mentioned classifications, five pre-code RC buildings of 2, 8, 18, 26, and 40 stories, and four modern essential structures, namely fire station, police station, hospital and school, were selected and fully designed for the purpose of the current study. Figure 3.4 and Figure 3.5 show the selected buildings from the study area that represent pre-code structures and emergency facilities. Table 3.1 summarizes the characteristics of the nine reference structures, while Figure 3.6 to Figure 3.13 show the structural layout of the buildings. It is noteworthy that the 18 and 26-story buildings share the same layout. The selected layouts represent typical architectural layouts from the study area. For the pre-code frame structures, the height of the ground story is 5.0m, while the height of all other stories is 3.5m. For pre-code wall structures, the height of all stories is 3.2m, while the ground story is 4.5m. Emergency structures have a typical story height of 4.0m, while the ground floor is 5m except for the fire station which is 5.5m. The hospital building has one basement of 3.5m height.

				
<p>Building BO-02</p>	<p>Building BO-08</p>	<p>Building BO-18</p>	<p>Building BO-26</p>	<p>Building BO-40</p>

Figure 3.4: Selected real buildings from the study area to represent pre-seismic code structures (Mwafy, 2013)

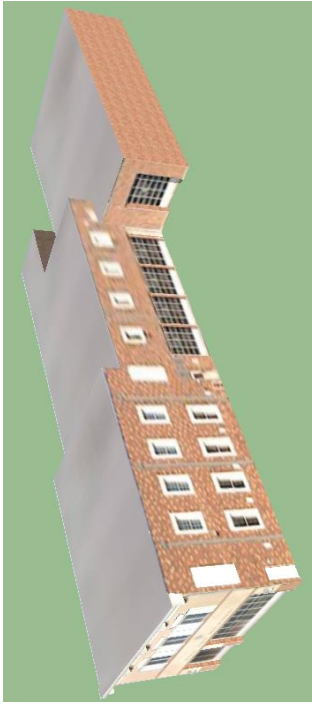



	
<p>3D model of a Fire station</p>	<p>Typical private hospital in Dubai</p>
	
<p>3D model of a police station</p>	<p>Emirates international school in Dubai</p>

Figure 3.5: Selected real buildings from the study area to represent emergency facilities (Mwafy, 2013)

Table 3.1: Summary of the selected buildings (Mwafy, 2013)

Number	Building Reference	Classification criteria	Buildings description	No. of stories	Story height (m)			Total height (m)
					B	GF	TF	
1	BO-02	Based on construction date	Pre-seismic code structures	2	-	5.0	3.5	8.5
2	BO-08			8	-	5.0	3.5	28.5
3	BO-18			18	3.2	4.5	3.2	58.9
4	BO-26			26	3.2	4.5	3.2	84.5
5	BO-40			40	3.2	4.5	3.2	129.3
6	FS	Based on function	Fire station	2	-	5.5	4.0	9.5
7	PS		Police station	2	-	5.0	4.0	9
8	SC		School	3	-	5.0	4.0	13
9	HO		Hospital	6	3.5	5.0	4.0	24.5

B: Basement, GF: Ground Floor, TF: Typical Floor

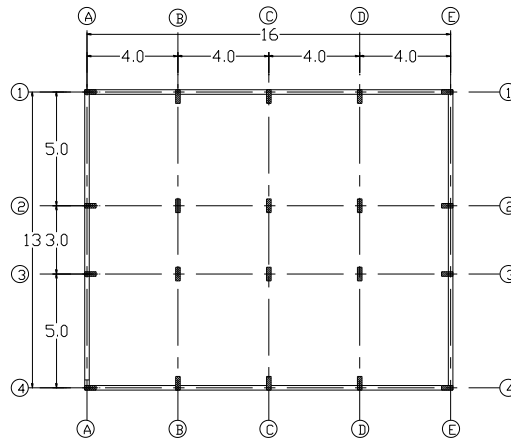


Figure 3.6: Layout of the 2-story building showing different structural members

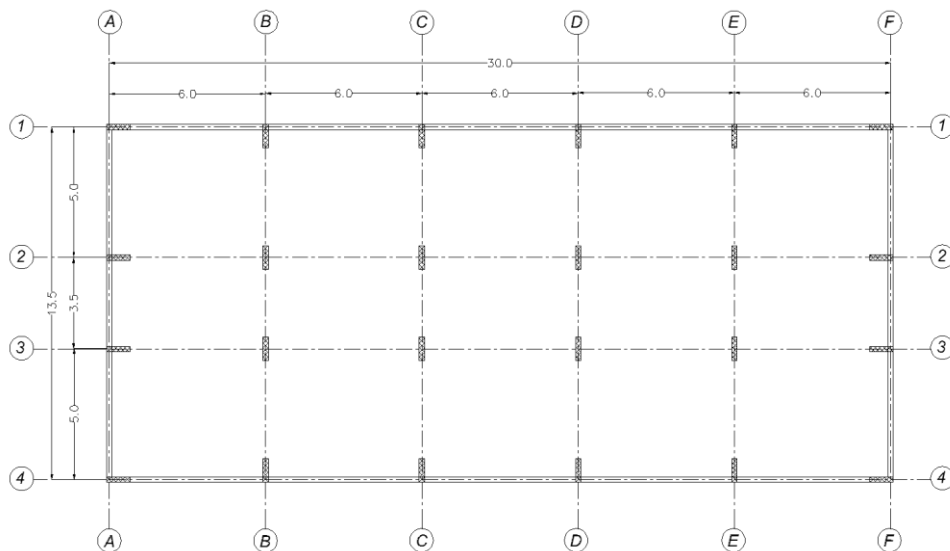


Figure 3.7: Layout of the 8-story building showing different structural members

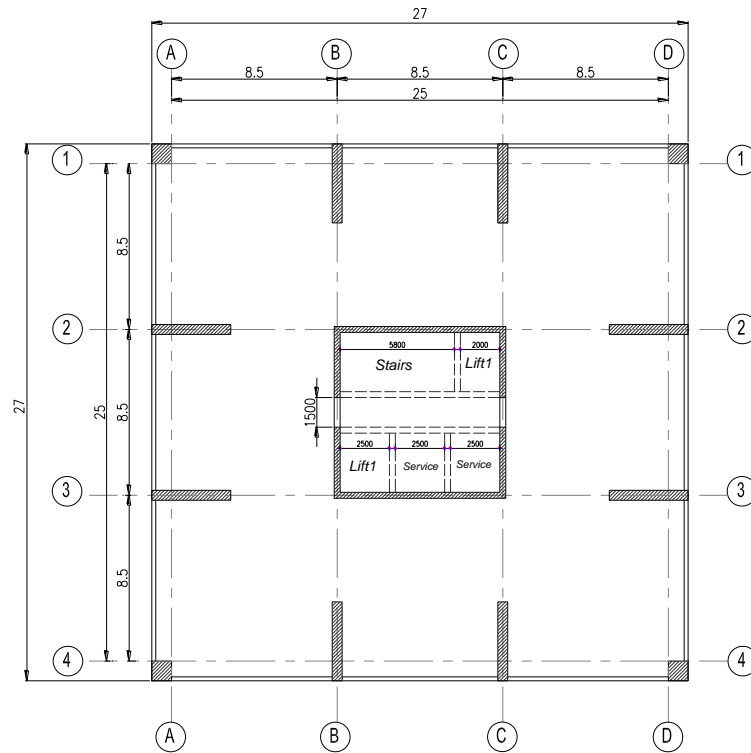


Figure 3.8: Layout of the 18 and 26-story building showing different structural members

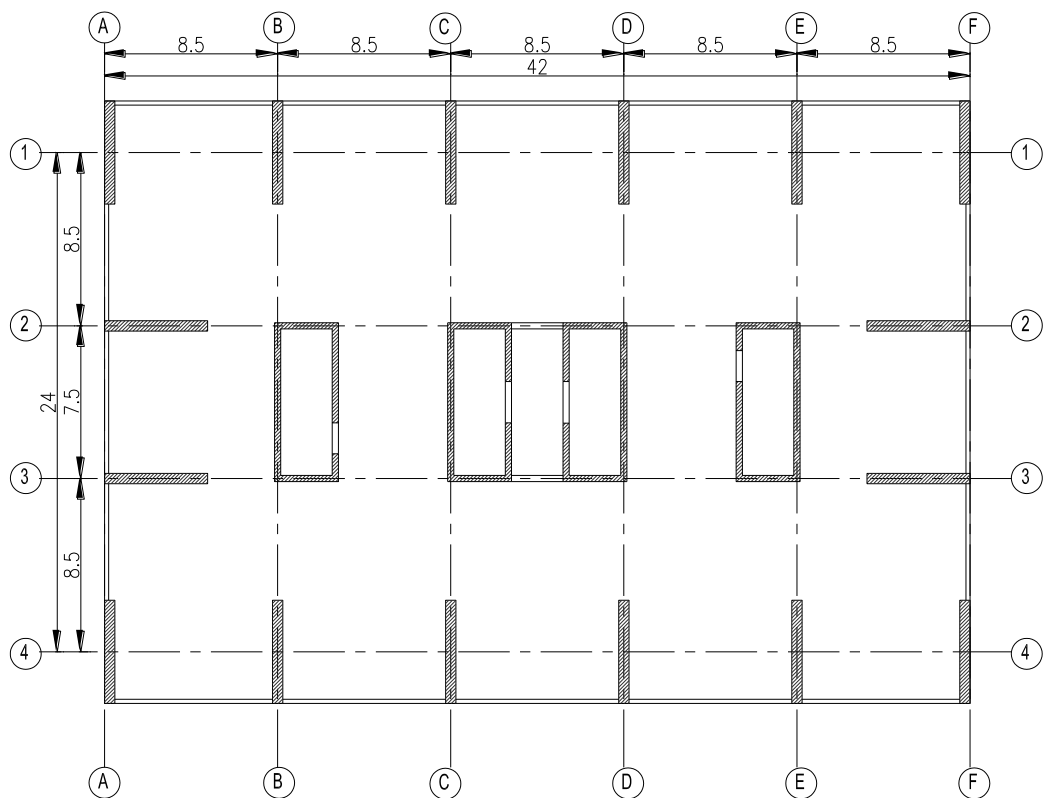


Figure 3.9: Layout of the 40-story building showing different structural members

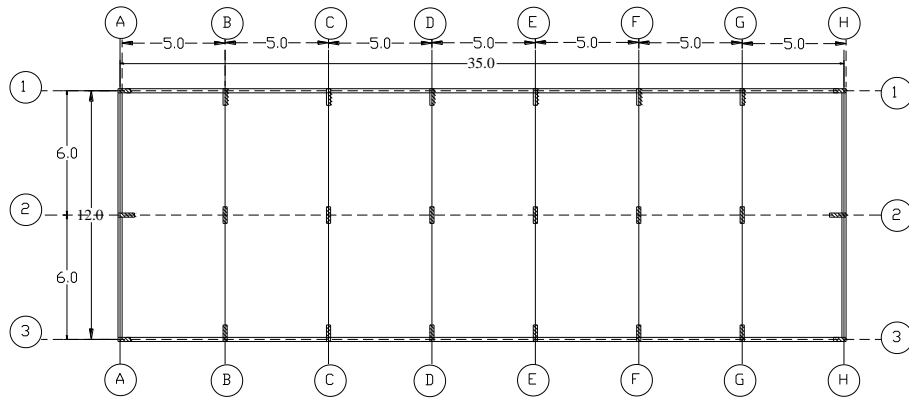


Figure 3.10: Layout of the fire station showing different structural members

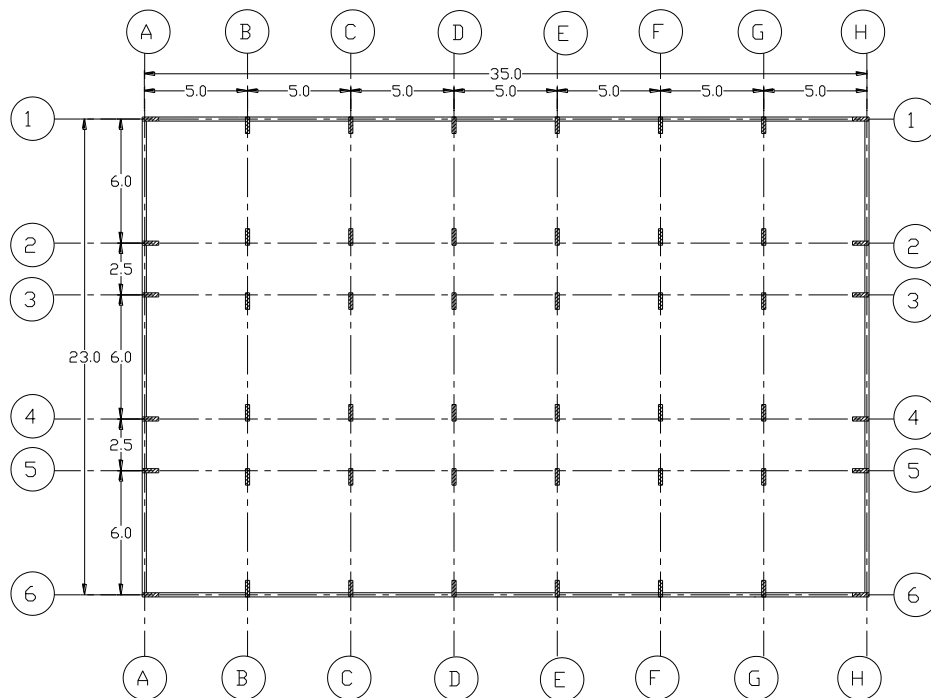


Figure 3.11: Layout of the police station showing different structural members

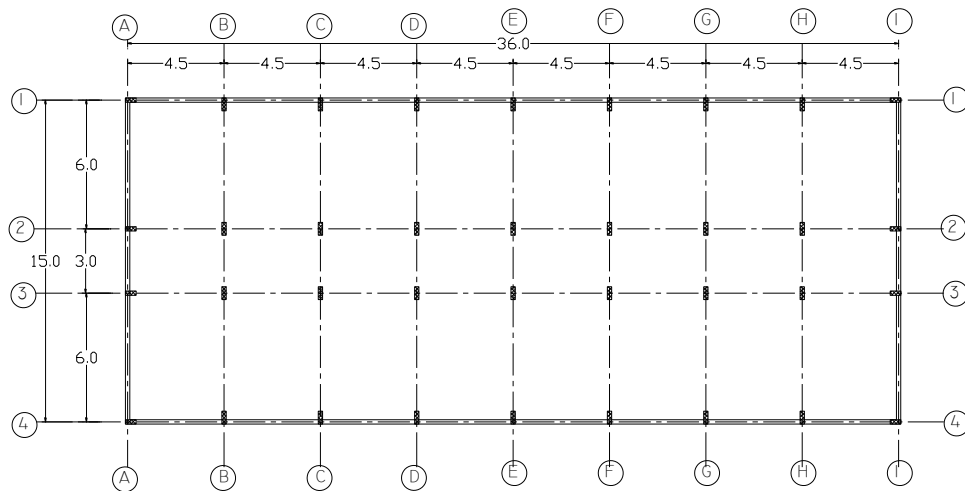


Figure 3.12: Layout of the school showing different structural members

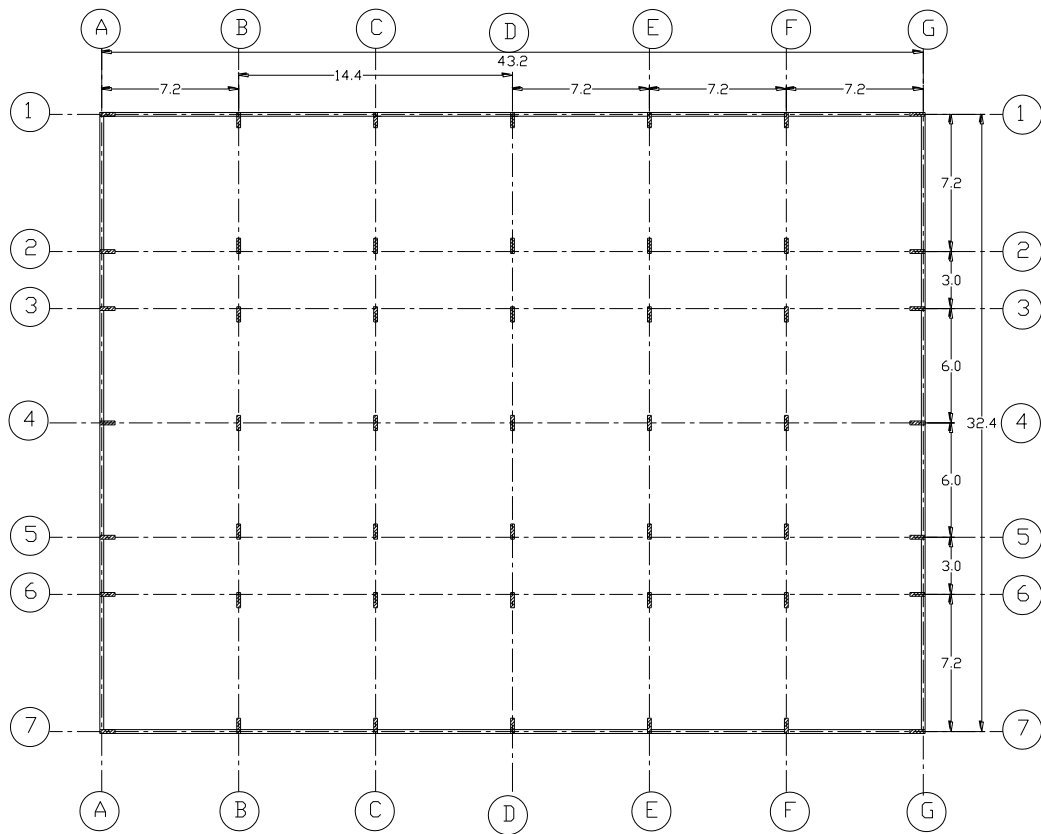


Figure 3.13: Layout of the hospital showing different structural members

3.2 Design Approach

Three-dimensional (3D) finite element (FE) models were developed for the buildings investigated in the present study using the structural analysis and design program ETABS (CSI, 2011). Figure 3.14 depicts the layouts and 3D models of the reference buildings. The five pre-seismic code buildings are designed and detailed specifically for the purpose of the current study according to the building codes that were implemented at the time of construction (BS8110, 1986). Pre-seismic code buildings are defined in this study as those built in the study area before 1991 when seismic design provisions might be disregarded. As discussed earlier, the UBC provisions (1997) recommended the use of Seismic Zone '0' for the cities of Abu Dhabi and Dubai, UAE. Revised seismic design criteria have been adopted in the UAE based on the recommendations of recent seismic hazard studies (e.g. Abdalla & Al-Homoud, 2004; Mwafy et al., 2006). Therefore, wind loads are the only lateral loads considered in design of the pre-code structures to represent the real situation before 1991 (BS8110, 1986). The following parameters are needed to define the wind loads in the study area, including:

- 1- Wind direction angle, φ , depends on the considered direction.
- 2- Front net pressure coefficient, C_p .
- 3- Rear net pressure coefficient C_p .
- 4- Effective height, H_e : Ground story to top story.
- 5- Effective wind speed, V_e : 45 m/s.
- 6- Size effect factor of standard method, C_a .
- 7- Dynamic augmentation factor, C_r .

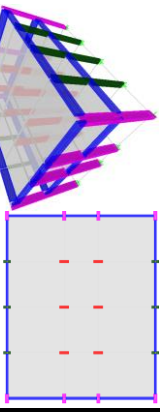
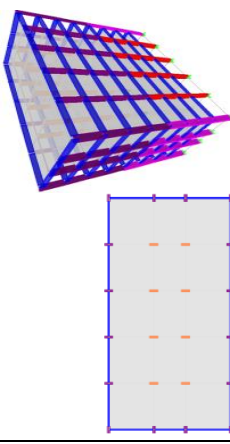
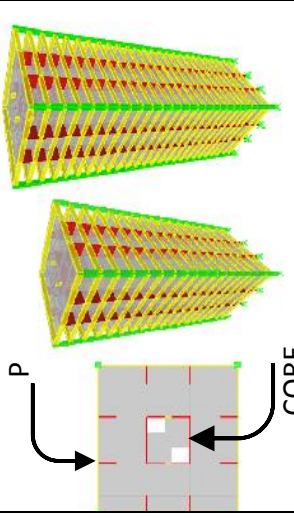
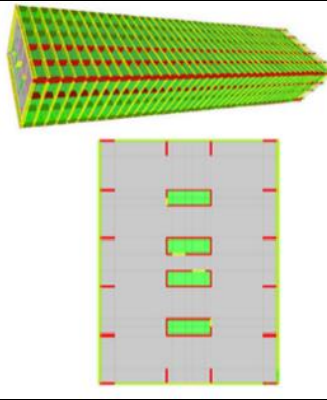
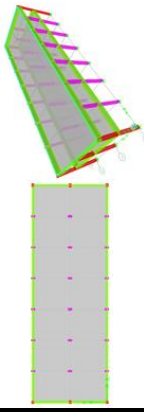
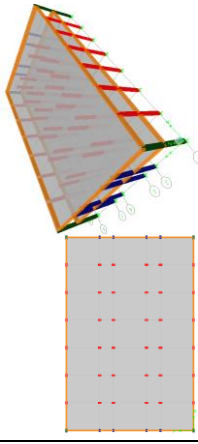
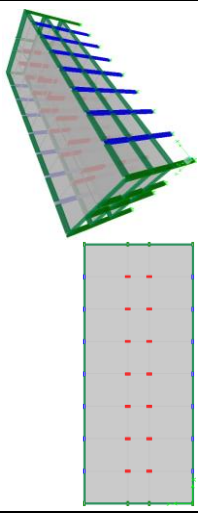
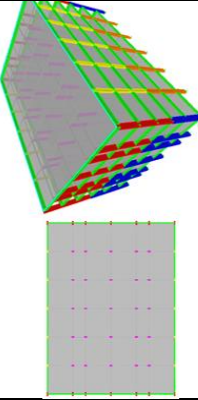
Pre-code Structures		BO-02, 2 story		BO-08, 8 story		BO-18 & BO-26, 18 & 26 story		BO-40, 40 story
Emergency		FS, Fire Station		PS, Police Station		SC, School		HO, Hospital

Figure 3.14: Layouts and three-dimensional design models of the reference structures

The permanent loads used in the design of pre-code buildings include the superimposed dead load of 4.0 kN/m^2 and the self-weight. The live load is 2.0 kN/m^2 , except for staircases and exit ways which are 4.8 kN/m^2 . The design is carried out carefully for each building to obtain the optimum cross sections for different structural elements. To accurately represent the pre-code structures, the material properties that were utilized at the time of construction were considered. The concrete strength ranges from 20 to 40 MPa in vertical elements, while a concrete strength of 20 MPa is used for low-rise buildings and horizontal elements. Mild steel is used in the design with a yield strength of 240 MPa. Pre-code buildings with such material properties are likely to be more vulnerable to earthquake loads due to the large cross sections, heavy mass and inadequate detailing as compared to modern code-designed structures.

The four emergency buildings were designed and detailed in the current study according to modern building codes (ACI-318, 2011; ASCE-7, 2010). Wind loads are estimated using ASCE-7 (2010) based on an exposure category 'C' and basic wind speed of 45m/s. The seismic loads were also estimated using ASCE-7 (2010) with a soil class 'C', as per the recommendations of recent hazard assessment studies and design provisions for the UAE (Abdalla & Al-Homoud, 2004; ADIBC, 2013; Mwafy et al., 2006). The 0.2 sec spectral acceleration, the 1.0 sec spectral acceleration and the Long-period transition period are 0.84g, 0.25g, and 8s, respectively. The response modification coefficient (R) and the importance factor (I) were selected for each of the four buildings as per the structural system and risk category. The live load adopted for emergency facilities is 3.80 kN/m^2 , while the permanent loads include the self-weight of structural elements as well as superimposed dead loads of 4.0 kN/m^2 .

3.3 Design Results

An iterative design process was carried out using ETABS (CSI, 2011) under all load combinations recommended by ACI-318 (2011) and BS8110 (1986). Floor slabs were designed using the design program SAFE (CSI, 2011). Figure 3.15 to Figure 3.31 depict the reinforcement details of floor slabs and the cross sections of the vertical elements used in the nine buildings. Table 3.2 to Table 3.22 summarize the design information of vertical structural members, the reinforcement details for the slabs and the reinforcement schedule of the coupling beams.

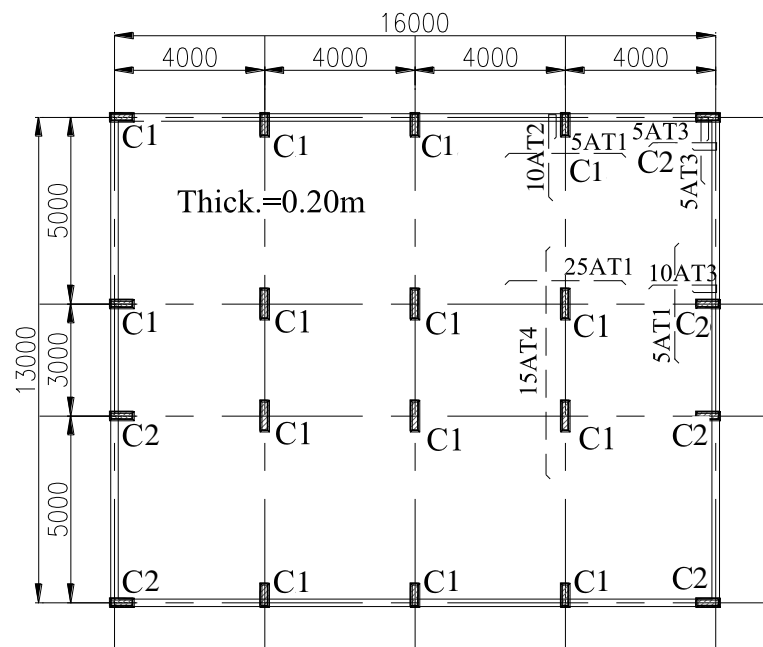


Figure 3.15: Typical reinforcement details for the floor slabs of the 2-story building



Figure 3.16: RC cross-sections used in the design of the 2-story building

Table 3.2: Vertical members design summary of the 2-story building

Section	C1	C2
Location of section	All stories	All stories
Vertical steel ratio ($\mu\%$)	1.15 %	1.13%
VL. Reinforcement	6#14	6#12
HL. Reinforcement	#10@200mm	#10@200mm
Demand/Capacity (D/C) Ratio	0.905	0.659
Column section mm x mm	200x400	200x300
Concrete strength (f_c') MPa	20	20

Table 3.3: Floor slabs reinforcement of the 2-story building

Top and bottom mesh #12@200		
Bar mark	Additional top rebars	Length (m)
AT1	#12@200	2
AT2	#22@200	1.5
AT3	#12@200	1.5
AT4	#22@200	5.5

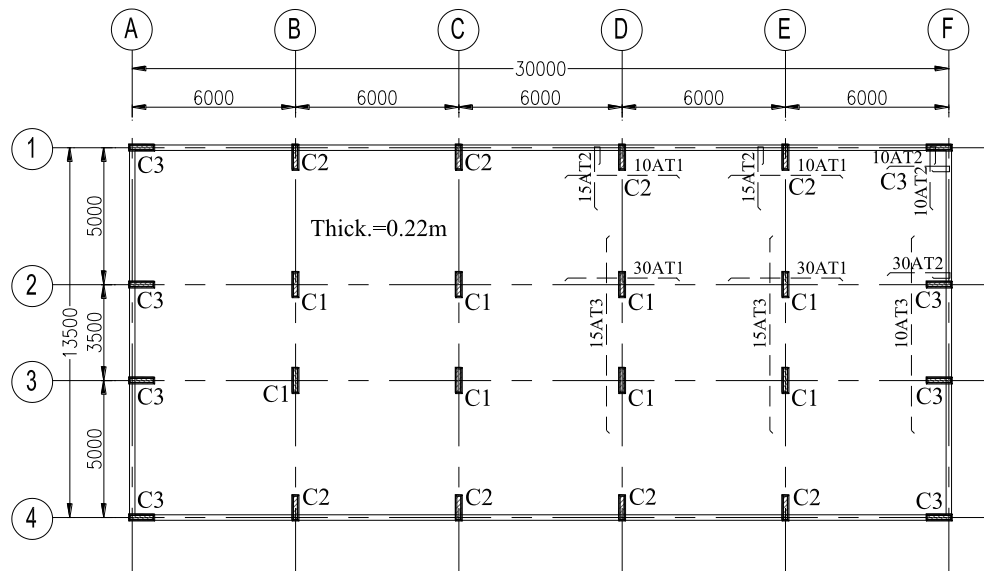


Figure 3.17: Typical reinforcement details for the floor slabs of the 8-story building

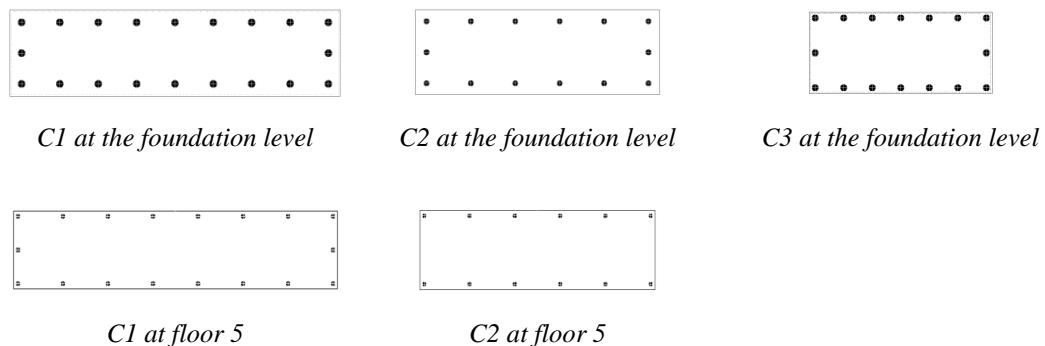


Figure 3.18: RC cross-sections used in the design of the 8-story building

Table 3.4: Vertical members design summary of the 8-story building

Section	C1		C2		C3
	C1A	C1B	C2A	C2B	
Location of section	base	Floor no.5	base	Floor no.5	base
Vertical steel ratio ($\mu\%$)	2.9%	1.00%	1.63%	1.00%	3.74%
VL. Reinforcement	20#26	16#14	14#20	12#14	16#25
HL. Reinforcement	#12@200mm	#10@200mm	#12@200mm	#10@200mm	#10@200mm
(D/C) Ratio	0.967	0.721	0.93	0.645	0.81
Pier section mm x mm	300x1200	250x1200	300x900	250x900	300x700
(f_c') MPa	20	20	20	20	20

Table 3.5: Floor slabs reinforcement of the 8-story building

Top and bottom mesh #12@200		
Bar mark	Additional top rebars	Length (m)
AT1	#25@250	3
AT2	#22@250	1.5
AT3	#22@250	6

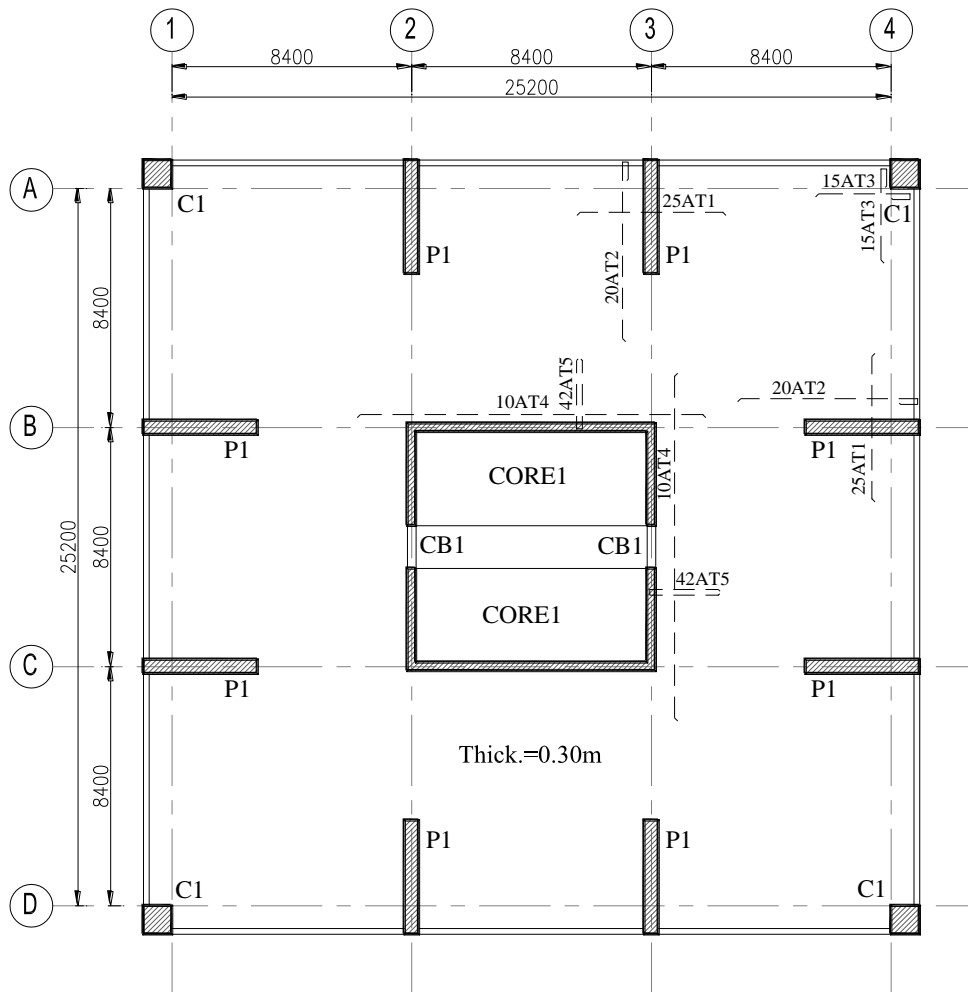


Figure 3.19: Typical reinforcement details for the floor slabs of the 18-story and 26-story buildings

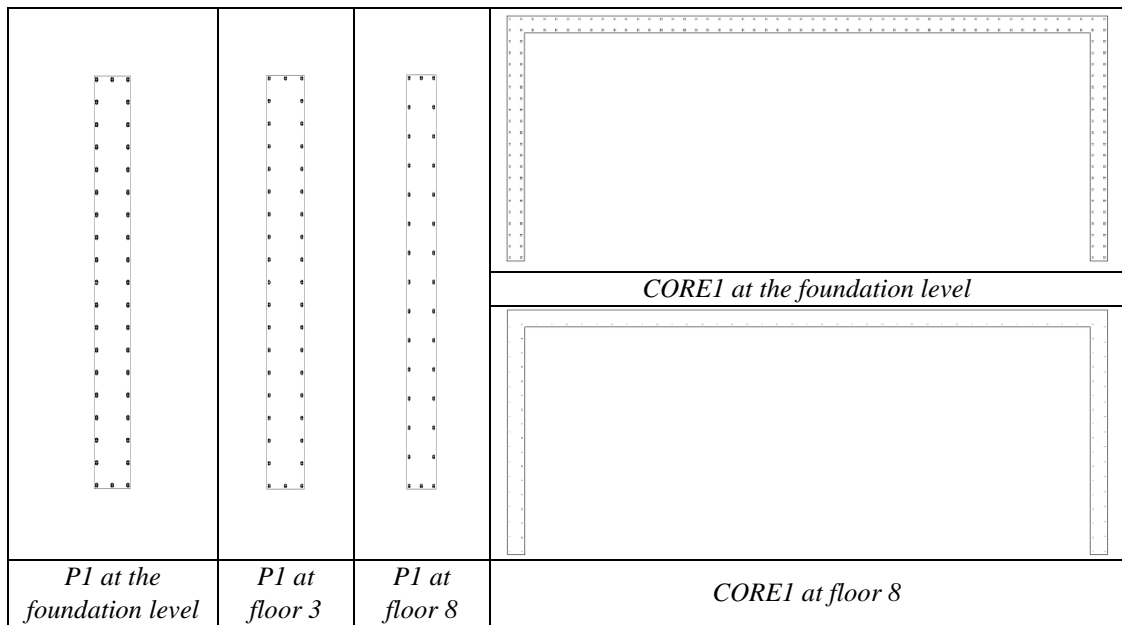


Figure 3.20: RC cross-sections used in the design of the 18-story building

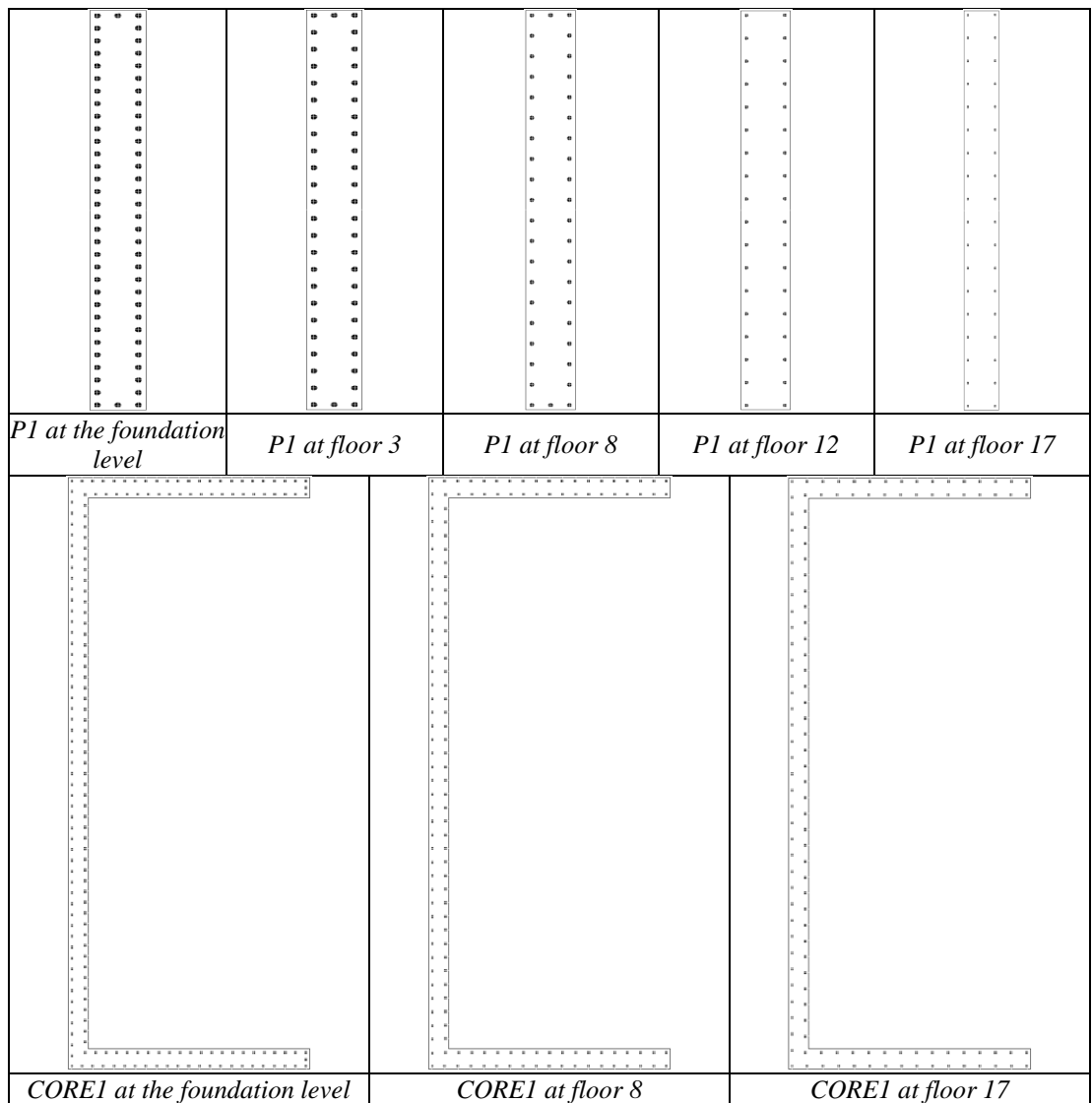


Figure 3.21: RC cross-sections used in the design of the 26-story building

Table 3.6: Vertical members design summary of the 18-story building

Section	P1		
	P1A	P1B	P1C
Location of section	base	Floor no.3	Floor no.8
Vertical steel ratio ($\mu\%$)	3.19 %	2.04%	2.1%
VL. Reinforcement	40#40	40#32	32#32
HL. Reinforcement	#10-200mm	#10-200mm	#10-200mm
Links	#10-430mm	#8-380mm	#8-330mm
Design/Capacity (D/C) Ratio	0.987	0.994	0.987
Pier section mm x mm	450x3500	450x3500	350x3500
Concrete strength (f_c') MPa	28	24	20
Section	Core1		
	Core1A	Core1B	
Location of section	base	Floor no.8	
Vertical steel ratio ($\mu\%$)	1.13%	1.00%	
VL. Reinforcement	140#20	100#20	
HL. Reinforcement	#8-200mm	#8-200mm	
Links	#8-330mm	#8-140mm	
(D/C) Ratio	0.996	0.701	
Core thickness (mm)	250	200	
(f_c') MPa	24	20	

Table 3.7: Vertical members design summary of the 26-story building

Section	P1				
	P1A	P1B	P1C	P1D	P1E
Location of section	base	Floor no.3	Floor no.8	Floor no.12	Floor no.17
Vertical steel ratio ($\mu\%$)	3.9%	3.11%	1.72%	1.34%	1.00%
VL. Reinforcement	66#40	52#40	42#32	36#26	36#20
HL. Reinforcement	#12-200mm	#12-200mm	#8-200mm	#8-200mm	#8-200mm
Links	#12-510mm	#12-510mm	#8-380mm	#8-340mm	#8-260mm
(D/C) Ratio	0.998	1.00	1.00	0.922	0.969
Pier section mm x mm	600x3500	600x3500	550x3500	550x3500	400x3500
(f_c') MPa	28	24	24	24	20
Section	Core1				
	Core1A	Core1B	Core1C		
Location of section	base	Floor no.8	Floor no.17		
Vertical steel ratio ($\mu\%$)	1.1%	1.0%	1.0%		
VL. Reinforcement	160#20	121#20	97#20		
HL. Reinforcement	#10-200mm	#8-200mm	#8-200mm		
links	#10-430mm	#8-300mm	#8-190mm		
(D/C) Ratio	0.999	0.849	0.572		
Core thickness (mm)	300	250	200		
(f_c') MPa	28	24	20		

Table 3.8: Floor slabs reinforcement of the 18-story building

Top & bottom mesh #12@200		
Bar mark	Additional top rebars	Length (m)
AT1	#12@200	4.5
AT2	#12@200	6
AT3	#12@200	2.5
AT4	#16@200	13
AT5	#12@200	2.5

Table 3.9: Floor slabs reinforcement of the 26-story building

Top & bottom mesh #12@200		
Bar mark	Additional top rebars	Length (m)
AT1	#16@200	4.5
AT2	#12@200	6
AT3	#12@200	2.5
AT4	#16@200	13
AT5	#12@200	2.5

Table 3.10: Coupling beams reinforcement of the 18-story building

Beam Model	Beam Location	Dimensions		Reinforcement			
		Width B (mm)	Depth T(mm)	Diagonal bars	Diagonal ties	Horizontal bars	Vertical ties
CB1	Base1	250	1000	25#43	#16@100	14#22@150 (2 layers)	#10@150 (2-legs)
CB1	Floor no.8	200	1000	22#43	#14@150	10#20@150 (2 layers)	#10@200 (2-legs)

Table 3.11: Coupling beams reinforcement of the 26-story building

Beam Model	Beam Location	Dimensions		Reinforcement			
		Width B (mm)	Depth T(mm)	Diagonal bars	Diagonal ties	Horizontal bars	Vertical ties
CB1	Base1	400	1000	28#43	#16@100	14#22@150 (2 layers)	#10@150 (2-legs)
CB1	Floor no.8	300	1000	22#43	#14@150	10#20@150 (2 layers)	#10@200 (2-legs)
CB1	Floor no.17	200	1000	16#43	#12@200	10#16@200 (2 layers)	#10@250 (2-legs)

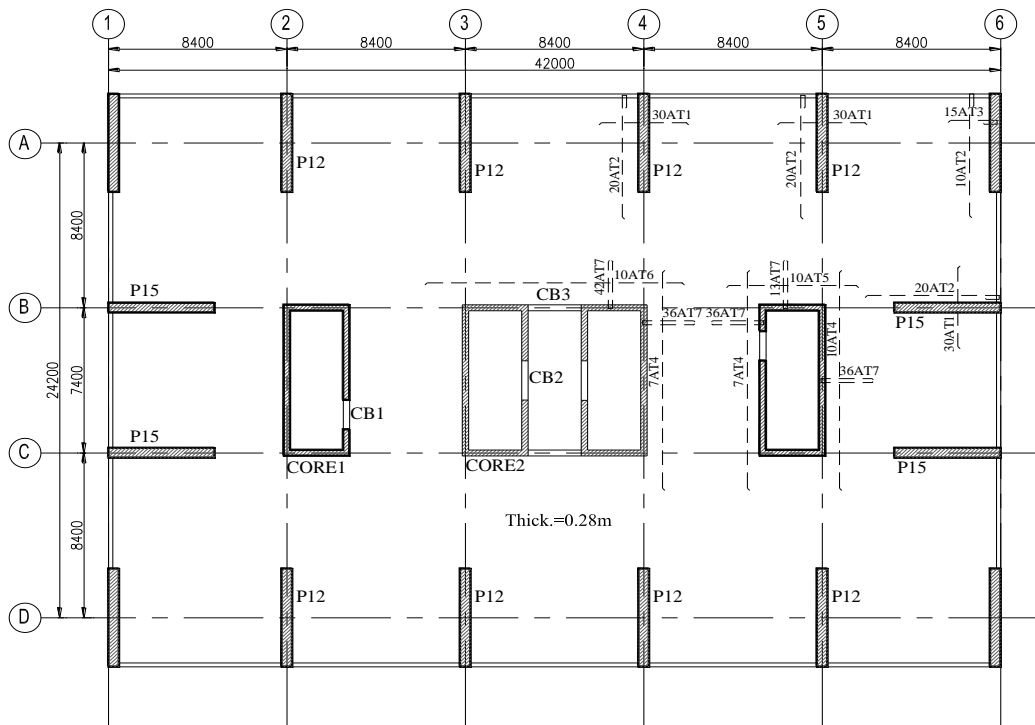


Figure 3.22: Typical reinforcement details for the floor slabs of the 40-story buildings

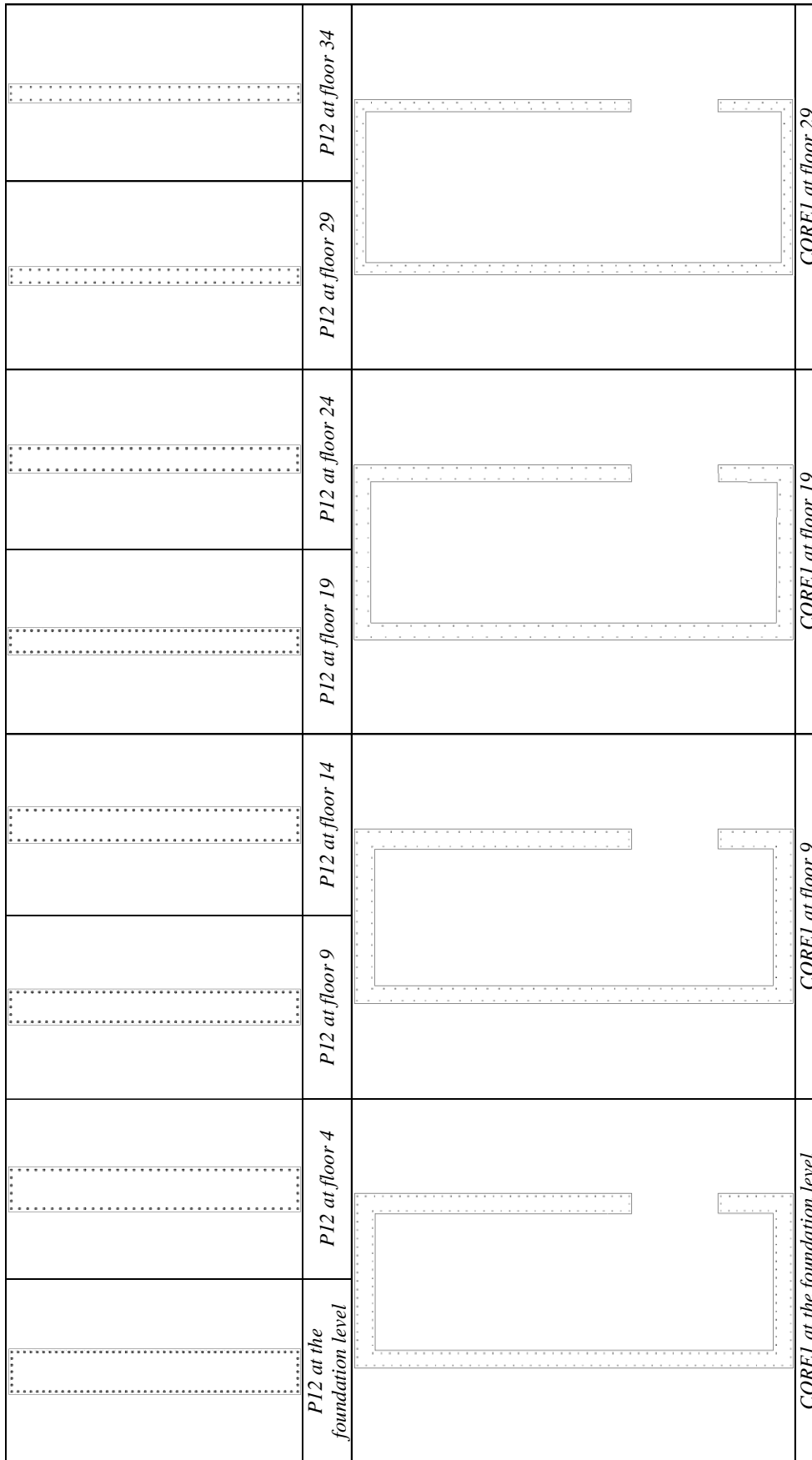


Figure 3.23: RC cross-sections used in the design of the 40-story building.

Table 3.12: Floor slabs reinforcement of the 40-story building

Top & bottom mesh # 12@ 200		
Bar mark	Additional top rebars	Length (m)
AT1	#16@ 200	4.5
AT2	#20@ 200	6.5
AT3	#16@ 200	2.5
AT4	#16@ 200	11.5
AT5	#16@ 200	7
AT6	#16@ 200	13
AT7	#16@ 200	2.5

Table 3.13: Coupling beams reinforcement of the 40-story building

Schedule of coupling beams for 40 floors							
Beam Model	Beam Location	Dimensions		Reinforcement			
		Width B (mm)	Depth T(mm)	Diagonal bars	Diagonal ties	Horizontal bars	Vertical ties
Cb1	Base1	400	1000	28#43	#16@100	14#22@150 (2 layers)	#10@150 (2-legs)
Cb1	Floor no.9	300	1000	22#43	#14@150	10#19@150 (2 layers)	#10@200 (2-legs)
Cb1	Floor no.1	250	1000	16#43	#12@200	10#16@250 (2 layers)	#10@250 (2-legs)
Cb1	Floor no.29	200	1000	14#36	#10@250	8#14@250 (2 layers)	#10@250 (2-legs)

Table 3.14: Vertical structural members design summary of the 40-story building

Section	P1									
	P1A	P1B	P1C	P1D	P1E	P1F	P1G	P1H		
Location of section	base	Floor no.4	Floor no.9	Floor no.14	Floor no.19	Floor no.24	Floor no. 29	Floor no.34		
Vertical steel ratio ($\mu\%$)	3.95%	2.41%	3.76%	1.96%	3.46%	1.47%	2.38%	1.00%		
VL Reinforcement	118#40	72#40	90#40	73#32	97#32	54#28	58#28	48#20		
HL Reinforcement	#12-200mm	#12-200mm	#12-200mm	#8-200mm	#8-200mm	#8-200mm	#8-200mm	#8-200mm		
Links	#12-510mm	#12-510mm	#12-510mm	#8-380mm	#8-380mm	#8-340mm	#8-340mm	#8-220mm		
Design/Capacity (D/C) Ratio	0.996	1	0.985	1	0.995	1	0.995	0.7		
Pier section mm x mm	750x5000	750x5000	600x5000	600x5000	450x5000	450x5000	300x5000	300x5000		
Concrete strength (fc') MPa	28	28	28	24	24	20	20	20		
Section	CORE 1									
	Core1A	Core1B	Core1C	Core1D						
Location of section	Base	Floor no.9	Floor no.19	Floor no.29						
Vertical steel ratio ($\mu\%$)	1.19%	1.05%	1.00%	1.00%						
VL Reinforcement	287#20	215#20	235#16	235#12						
HL Reinforcement	#14-200mm	#14-200mm	#14-200mm	#14-200mm						
Links	#12-100mm	#12-100mm	#12-100mm	#12-100mm						
Design/Capacity (D/C) Ratio	0.977	0.996	0.908	0.585						
Core thickness (mm)	350	300	250	200						
Concrete strength (fc') MPa	28	24	20	20						

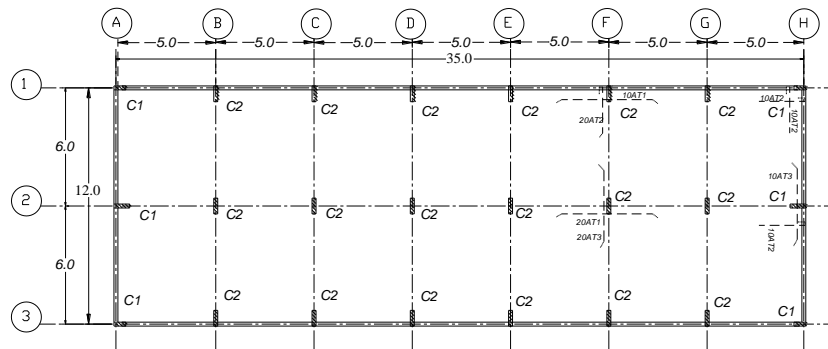
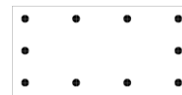


Figure 3.24: Typical reinforcement details for the floor slabs of the fire station



C1 at the foundation level



C2 at the foundation level

Figure 3.25: RC cross-sections used in the design of the fire station

Table 3.15: Vertical members design summary of the fire station

Section	C1	C2
Location of section	base	base
Vertical steel ratio ($\mu\%$)	4.0%	3.67%
VL Reinforcement	10#32	10#29
HL Reinforcement	#12@200mm	#10@200mm
Demand/Capacity (D/C) Ratio	0.95	0.9
Pier section mm x mm	400x500	300x600
Concrete strength (f_c') MPa	40	40

Table 3.16: Floor slabs reinforcement of the fire station

Top and bottom mesh #12@200		
Bar mark	Additional top rebars	Length (m)
AT1	#12@200	2.5
AT2	#12@200	2
AT3	#12@200	3

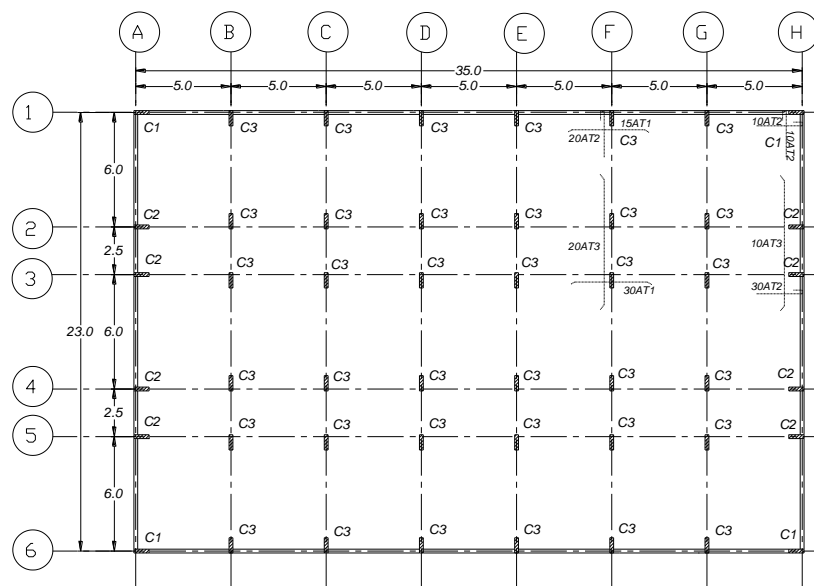


Figure 3.26: Typical reinforcement details for the floor slabs of the police station

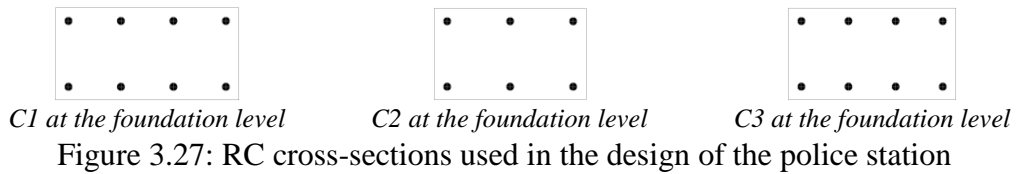


Table 3.17: Vertical members design summary of the police station

Section	C1	C2	C3
Location of section	base	base	base
Vertical steel ratio ($\mu\%$)	2.87 %	3.83%	3.89%
VL. Reinforcement	8#29	6#36	8#32
HL. Reinforcement	#10@200mm	#12@200mm	#12@200mm
Demand/Capacity (D/C) Ratio	0.99	0.95	0.97
Pier section mm x mm	300x600	300x500	300x550
Concrete strength (f_c') MPa	32	32	32

Table 3.18: Floor slabs reinforcement of the police station

Top and bottom mesh #12@200		
Bar mark	Additional top rebars	Length (m)
AT1	#12@200	2.5
AT2	#12@200	2
AT3	#20@200	6

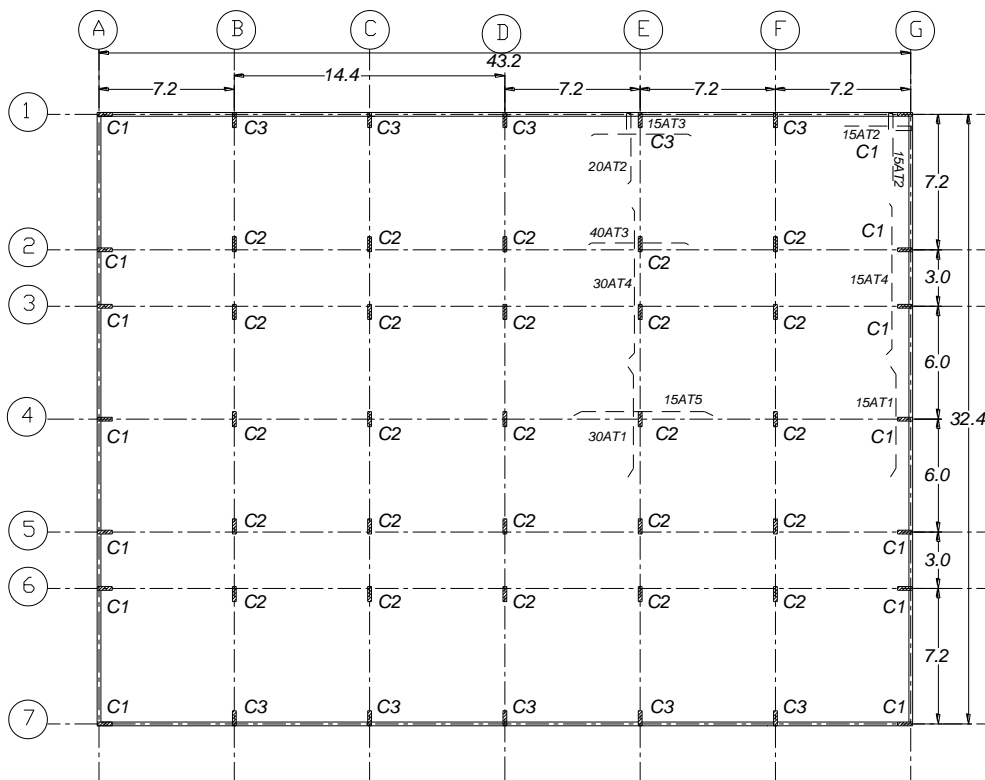


Figure 3.28: Typical reinforcement details for the floor slabs of the hospital

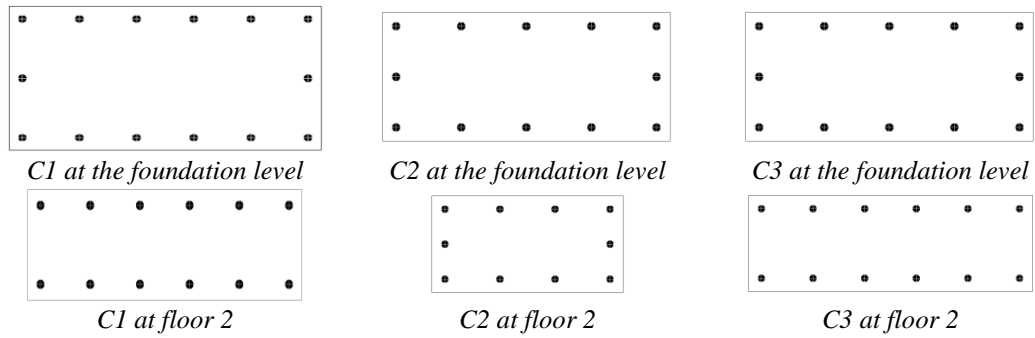


Figure 3.29: RC cross-sections used in the design of the hospital

Table 3.19: Vertical members design summary of the hospital

Section	C1		C2		C3	
	C1A	C1B	C2A	C2B	C3A	C3B
Location of section	base	2nd floor	base	2nd floor	base	2nd floor
Vertical steel ratio ($\mu\%$)	2.17 %	3.49%	2.29%	3.3%	2.56%	3.5%
VL. Reinforcement	14#32	12#32	12#32	10#29	12#32	12#29
HL. Reinforcement	#12@200 mm	#12@200 mm	#12@200 mm	#10@200 mm	#12@200 mm	#10@200 mm
(D/C) Ratio	0.96	0.91	0.85	0.9	0.93	0.89
Pier section mm x mm	500x1000	300x900	400x900	300x600	400x900	300x900
(f_c') MPa	40	40	40	40	40	40

Table 3.20: Floor slabs reinforcement of the hospital

Top and bottom mesh #13@200		
Bar mark	Additional top rebars	Length (m)
AT1	#16@200	4
AT2	#16@200	2
AT3	#12@200	2
AT4	#16@200	7
AT5	#19@200	4

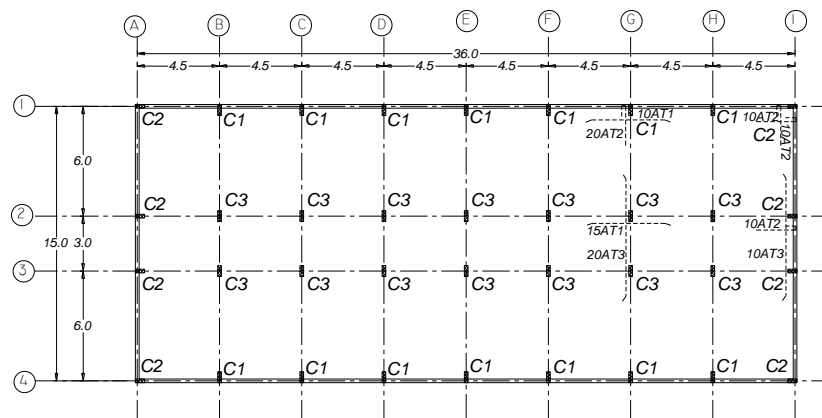


Figure 3.30: Typical reinforcement details for the floor slabs of the school

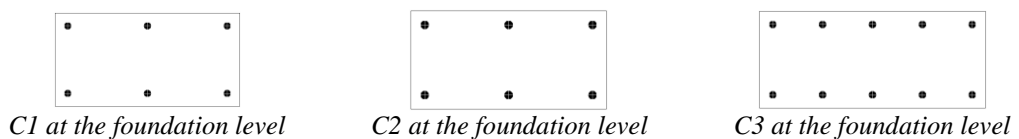


Figure 3.31: RC cross-sections used in the design of the school

Table 3.21: Vertical members design summary of the school

Section	C1	C2	C3
Location of section	base	base	base
Vertical steel ratio ($\mu\%$)	2.20 %	2.64%	3.14%
VL. Reinforcement	6#29	6#32	10#29
HL. Reinforcement	#10@200mm	#12@200mm	#10@200mm
Design/Capacity (D/C) Ratio	0.9	0.95	0.88
Pier section mm x mm	300x600	300x600	300x700
Concrete strength (f_c') MPa	32	32	32

Table 3.22: Floor slabs reinforcement of the school building

Top and bottom mesh #12@200		
Bar mark	Additional top rebars	Length (m)
AT1	#12@200	2.5
AT2	#12@200	2
AT3	#19@200	7

3.4 Comments on the Design Results

An iterative design process was adopted during the design of the reference buildings. This was undertaken by targeting a Demand over Capacity (D/C) ratio as close as 1.0 to guarantee both safety and cost-effective design. It is important to note that the design procedure of this study may not be the typical design practice in everyday applications. In many cases, the overstrength values may be very high and the demand/capacity ratios may be considerably lower than the unity. Such practices will not satisfy the optimum design concept where both satisfactory performance and cost-effective design is achieved. The above-mentioned iterative design process is therefore adopted in the present study due to the high uncertainty related to the real design concepts and the level of overstrength exhibited by the building inventory of the study area.

The design provisions implemented at the construction time of the pre-seismic code buildings were considered to represent the real case scenario. For instance, boundary elements were not considered in shear walls and core walls, unlike the shear walls in modern buildings. This reflects the design provisions and

construction practices for non-seismically designed buildings which were implemented in the study area before 1991.

Although pre-seismic code structures, especially multi-story buildings, were designed to resist gravity and wind loads only, large cross sectional areas were produced for vertical elements due to the low material strength used in the design. These large cross sections would add additional mass and stiffness to pre-code buildings. Along with the lack of efficient reinforcement and detailing, such large mass will attract higher inertia forces. This will undoubtedly increase their vulnerability to earthquake loads. On the other hand, wind loads in pre-code low-rise frame structures were considerably lower than their high-rise counterparts. This resulted in small cross sections in the former buildings which may increase their vulnerability under the effect of strong earthquakes.

The effect of considering the lateral loads (i.e. seismic loads in emergency facilities and wind loads in pre-code structures) in the design of floor slabs was also investigated. The results confirmed that the difference in the top and bottom reinforcement may exceed 100%, particularly at the slab supports (i.e. connection to columns, shear walls and core walls). The difference at the mid-span was marginal. The results confirmed the significance of considering the lateral loads in the design of floor slabs, which may be ignored by practicing engineers. Neglecting the lateral loads in the design of floor slabs may endanger the structure and lead to premature yielding under the design earthquake.

CHAPTER 4: MODELING AND INPUT GROUND MOTIONS

4.1 Fiber Based Modeling

The fibre modeling technique was used to idealize the reference structures for the multi-degree-of-freedom Inelastic Pushover Analysis and Incremental Dynamic Analysis using the inelastic analysis platform ZEUS-NL (Elnashai et al., 2012). ZEUS-NL is a contemporary inelastic analysis software employing the fiber modeling approach. This program was originally developed at Imperial College London during the past two decades, and has been comprehensively verified on member and structure levels against experimental tests carried out in Europe and the U.S.A. (e.g. Abdelnaby et al., 2014; Jeong & Elnashai, 2005; Kwon & Elnashai, 2006).

Reinforcing steel, confined and unconfined concrete are effectively idealized to enable monitoring of stresses and strains during the inelastic simulations. Each structural member is divided into three segments to allow for more accurate representation of longitudinal reinforcement and prediction of steel yielding, concrete crushing and shear capacity of structural members (Elnashai & Mwafy, 2002). The verifications of numerical models were conducted by comparing the periods of vibration of different models used in both design and inelastic analyses.

4.1.1 Material Modeling

A nonlinear constant confinement model was selected to represent the concrete behavior with a crushing strain, ϵ_{cu} , of 0.002 and a confinement factor varying from 1 to 1.2 according to reinforcement detailing. The compressive strength

concrete, f_c' , ranges between 20 to 35 MPa for pre-code structures and between 35 to 40 MPa for emergency facilities. A bilinear elasto-plastic model is used for modeling the reinforcing steel with a strain hardening rate, μE , of 0.005, Young's modulus, E , of 200000 MPa and a yield strength, σ_y , of 240 MPa and 420 MPa for the pre-seismic code and emergency facilities, respectively. The constitutive relationships of materials are illustrated in Figure 4.1.

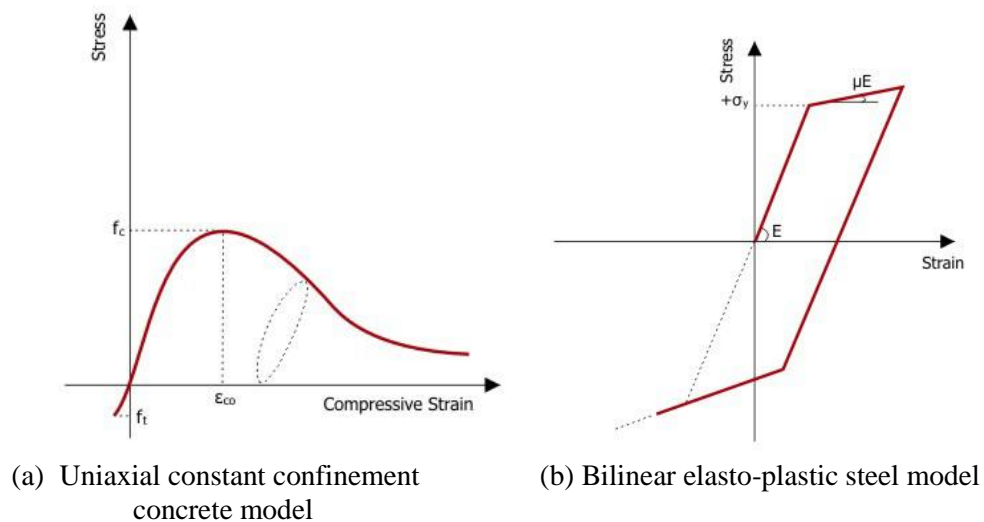


Figure 4.1: Material models used in the reference structures idealization (Elnashai et al., 2012)

4.1.2 Member and Section Modeling

To model each structural member, three Cubic Elasto-Plastic Frame (CEPF) elements capable of representing the cracking and spread of yielding were implemented. The CEPF element can adequately model space frames with geometric and material non-linearities. For the evaluation of element forces, numerical integration was performed at two Gauss sections for each CEPF element. For this purpose, the section at each Gauss point is divided into a number of fibers (monitoring points), the stress-strain relations of which are considered during the integration. For single-material sections such as those used for modeling rigid arms,

50 monitoring points were used. For more complicated sections with several materials such as those used for modeling walls, columns and beams this number was increased to 200 or more, to arrive at a more accurate representation of concrete and steel bars and more reliable response prediction.

The element local x -axis lies on the line defined by the element end nodes (Figure 4.2). This representation of the structural elements enables the monitoring of the steel yielding and concrete crushing throughout the element during the inelastic analysis, with the aid of a post processor in the form of a macro enabled Excel spreadsheets. Two rigid arms (i.e. the length between the center line and the face of the vertical element idealizing the wall) were also employed to attach the slab/beam ends on each side with shear walls. Several cross-sections were used from the ZEUS-NL library to model slabs, connecting beams, shear walls, cores and rigid arms. These include RC rectangular, flexural wall, hollow core and steel rectangular cross-sections, as shown in Figure 4.3. Figure 4.4 depicts a summary of the numerical modeling approach for the nine reference structures investigated in the present study.

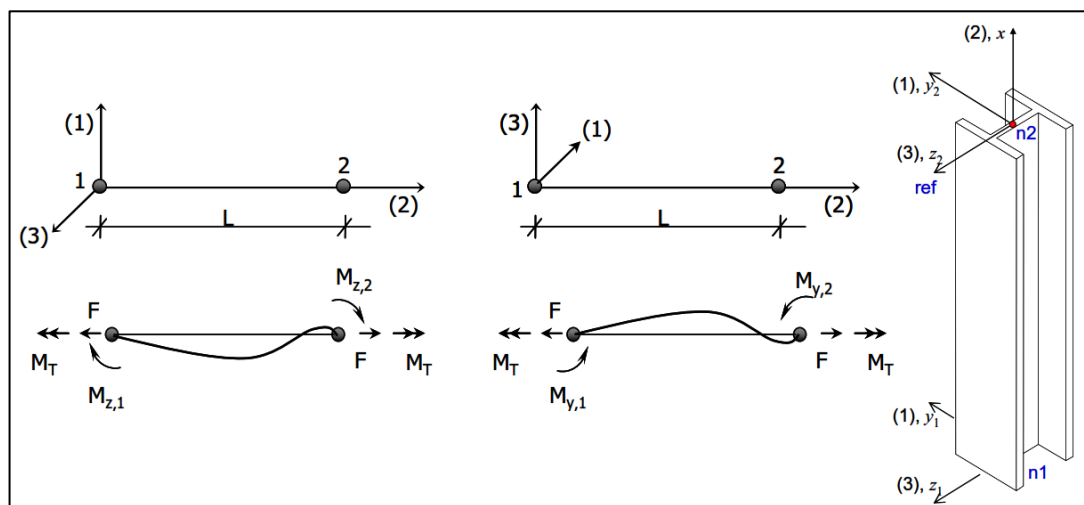


Figure 4.2: Cubic elasto-plastic 3D frame element (Elnashai et al., 2012)

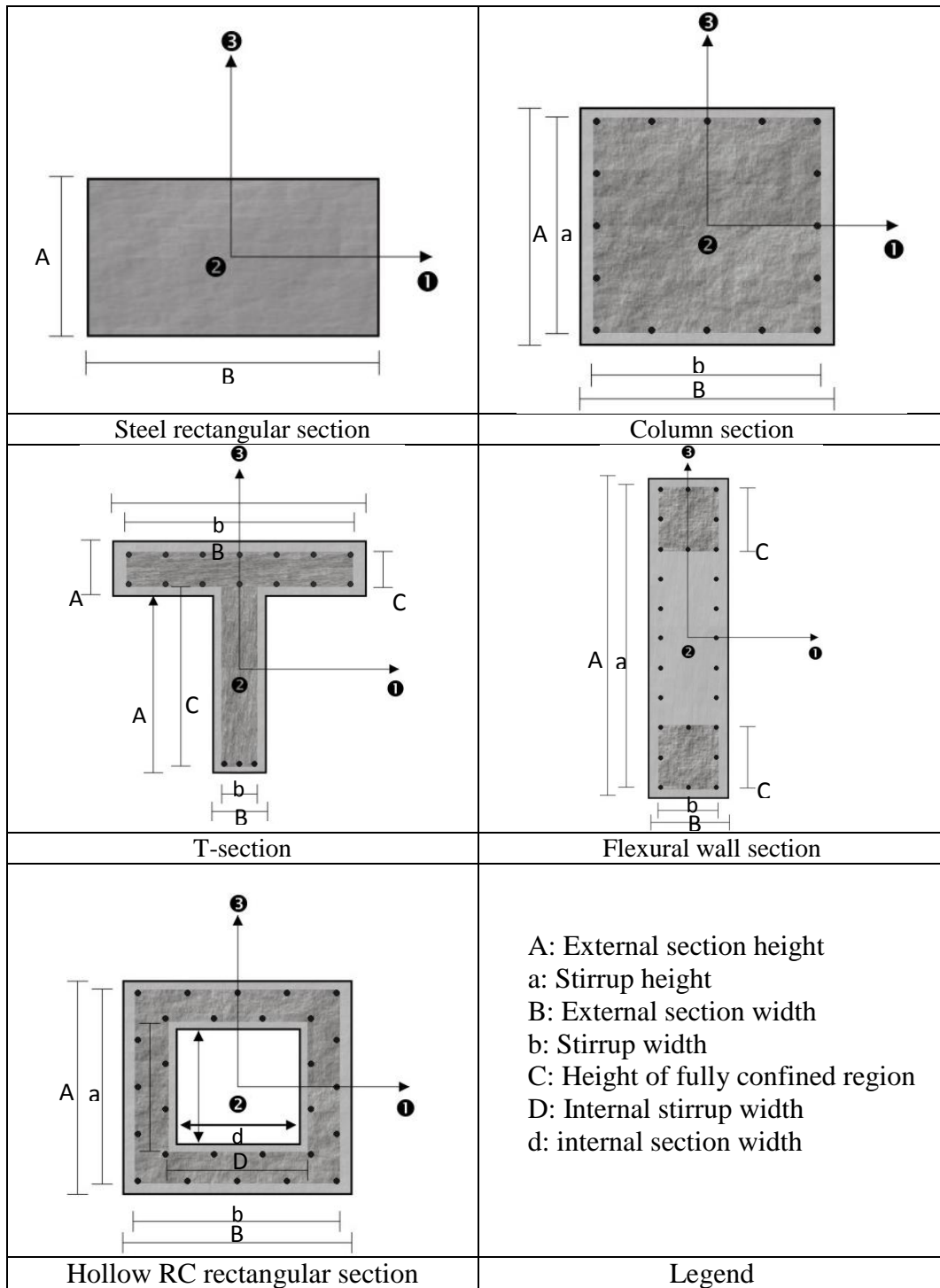


Figure 4.3: Different cross-sections used to model the reference buildings for inelastic analysis (Elnashai et al., 2012)

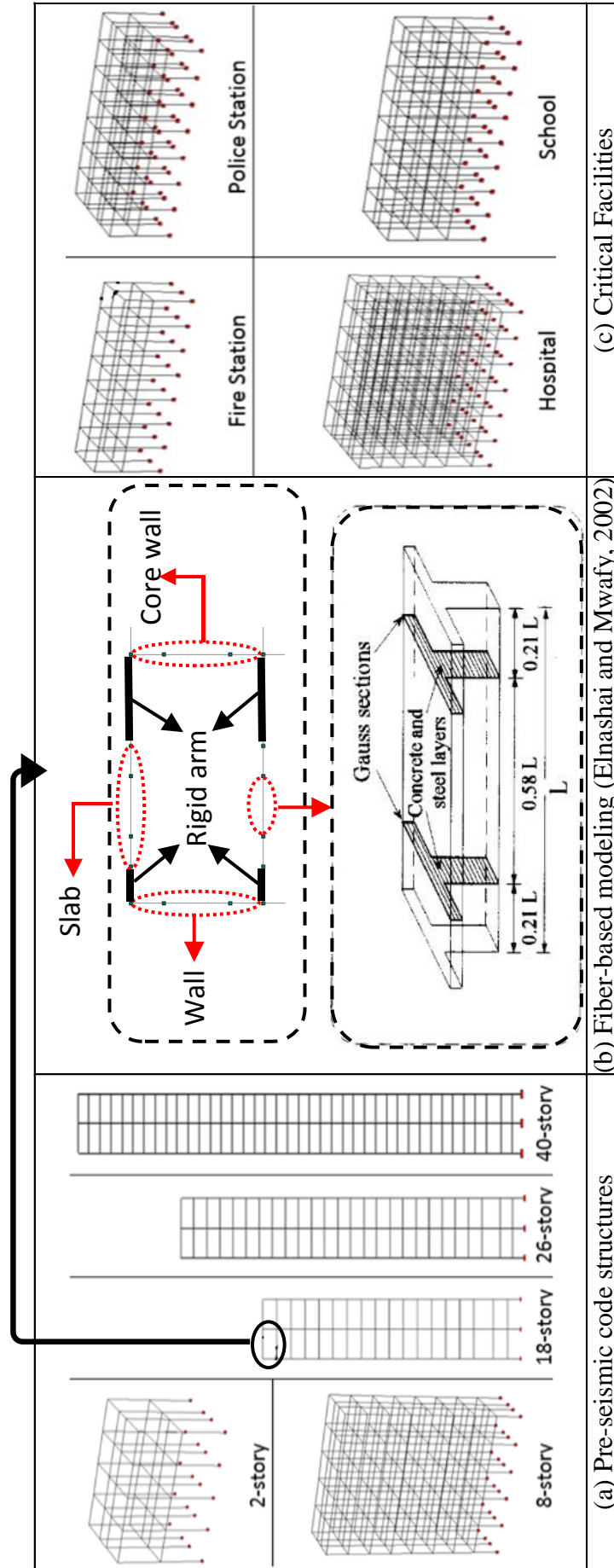


Figure 4.4: Fiber-based numerical models developed for two set of reference buildings

4.1.3 Structural Modeling

ZEUS-NL is capable of effectively performing 3D modeling and inelastic response history analyses of multi-story structures. The 3D dynamic response simulations are computationally demanding, this is particularly true for high-rise structures when assessed using a wide range of input ground motions. Two-dimensional (2D) idealizations have therefore been adopted for the seismic assessment of the high-rise wall structures, while 3D models are developed for the multi-story frame structures, as shown in Figure 4.4. IPAs and IDAs are carried out to assess the seismic response of the nine reference buildings using the ZEUS-NL platform described above.

The wall structures were simplified to 2D framing systems, as described in Figure 4.5. It is assumed that the four Lateral-Force Resisting Systems (LFRSs) resist the seismic forces in the transverse direction of the 40-story structure, while one LFRS resists the entire lateral force of the 26 and 18 story structures, as shown in Figure 4.5 and Figure 4.6. For the 40-story structure, each of the framing systems in the transverse direction, which are loaded with 25% of the total mass of the building, consists of two external shear walls and an internal core. The LFRSs in the transverse direction of the 40-story building is the critical framing system when compared with the longitudinal counterpart, as confirmed from previous studies carried out on comparable layouts (Mwafy et al., 2014a). Therefore, the framing system in the transverse direction is only considered in the IPAs and IDAs discussed hereafter.

The 26 and 18 story structures have symmetric framing systems in both longitudinal and transverse direction. Therefore one LFRS resists the seismic forces in both horizontal orthogonal directions, as shown in Figure 4.5(a). This LFRS is loaded with 100% of the total mass of the building. For the frame structures, since

3D models are developed, the entire mass of the building is implemented in the ZEUS-NL models. Gravity loads are applied as point loads at frame element nodes. The mass is characterized by lumped mass elements and distributed in the same pattern implemented for gravity loads in the IPAs and IDAs.

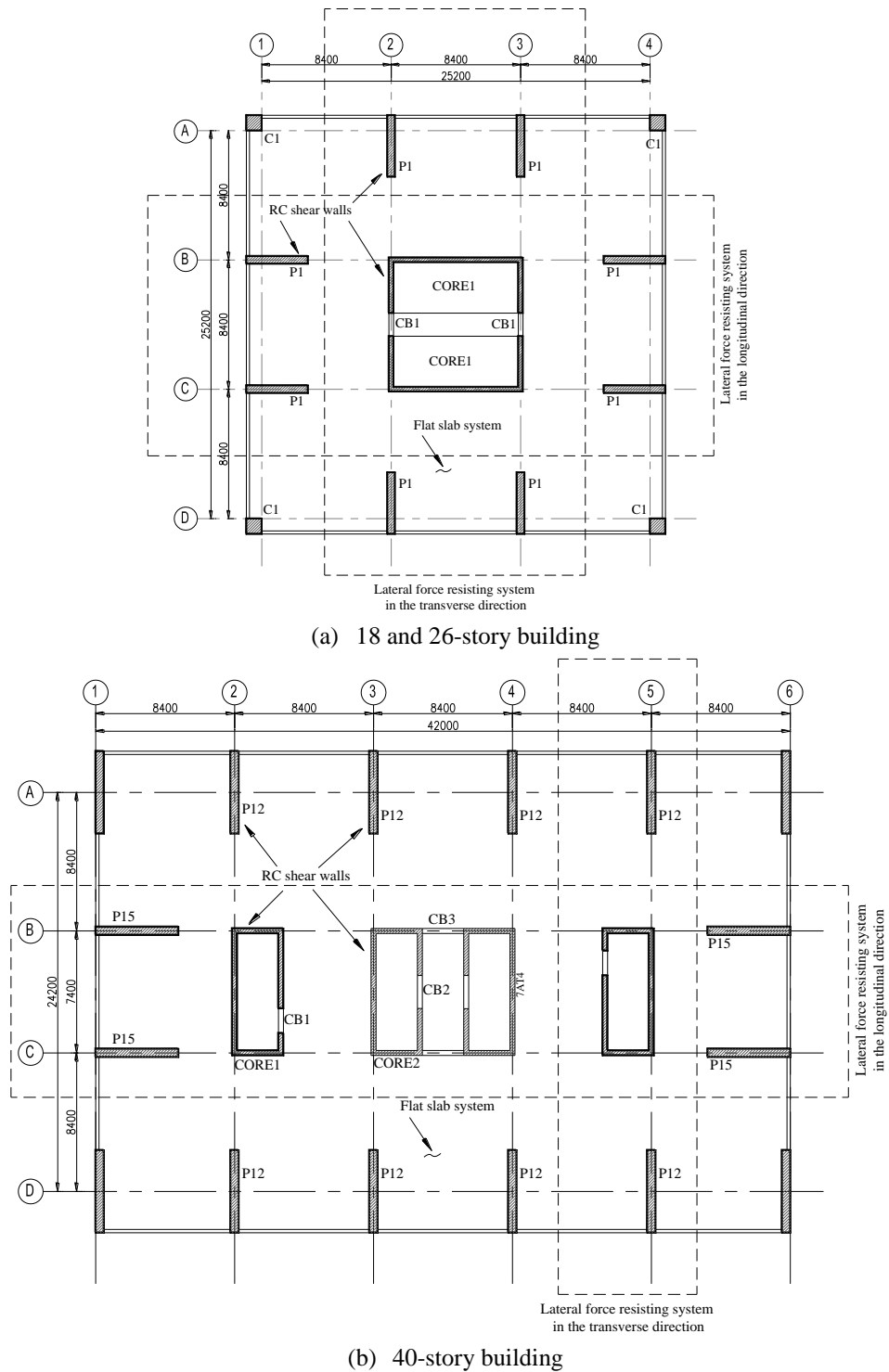


Figure 4.5: LFRSs of shear wall supported structures

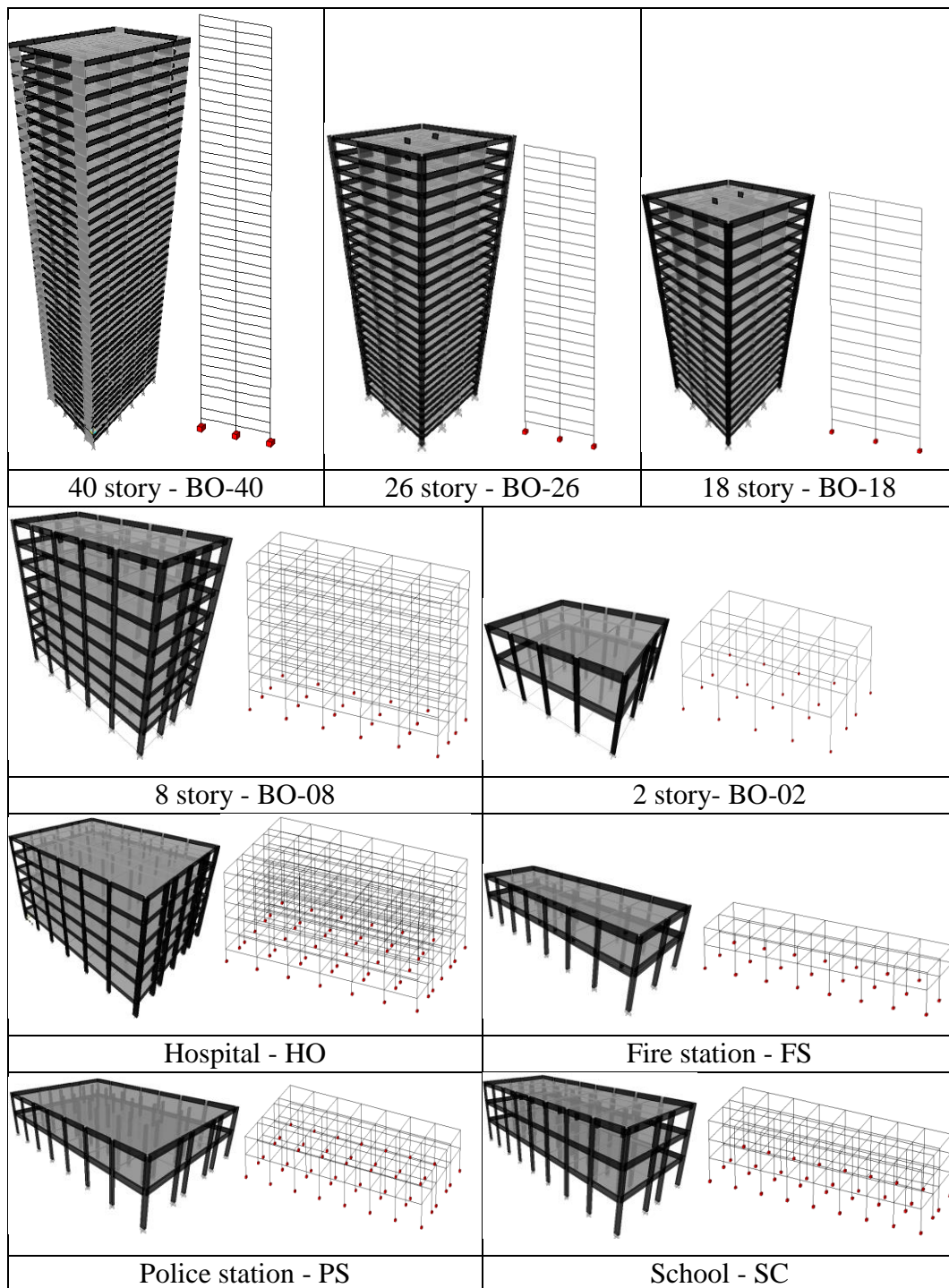


Figure 4.6: Developed finite element and fiber based models for reference structures

4.2 Selection of Ground Motions

The dynamic behavior of a structure during an earthquake depends on the characteristics of the applied earthquake records. Thus, input ground motions are a

key component of seismic risk studies as they significantly affect the output results of the fragility curves. Ground motion parameters that are of interest include PGA, the ratio of peak ground acceleration-to-velocity (a/v), soil condition, magnitude and epicentral distance. There are three types of ground motion records: (i) real records, which are recorded from seismic monitoring stations; (ii) synthetic records, which are generated using seismological models with pre-determined ground motion parameters; and (iii) artificial records, which are generated to match a target spectrum (Yamamoto & Baker, 2013). When performing a seismic risk study, it is preferable to use real ground motions retrieved from local and regional sources in the area of interest.

Based on the results of recent seismic hazard assessment studies by Khan et al. (2013), Shama (2011), Aldama-Bustos et al. (2009), Mwafy et al. (2006), Sigbjornsson and Elnashai (2006) and Abdalla and Al-Homoud (2004), the following conservative design criteria for the study area (Dubai, Sharjah and Ajman, UAE) were adopted:

- A conservative design PGA of 0.16g was adopted for the study area based on the derived hazard curve for Dubai by Sigbjornsson and Elnashai (2006). This value represents the design PGA for a 10% probability of exceedance in 50 years, which represents a mean return period of 475 years.
- Dubai and the Northern Emirates are vulnerable to two different seismic scenarios: (i) severe earthquakes with a relatively long epicentral distance; and (ii) moderate events with short source-to-site distance, typically originating from local seismic faults.

Based on the above-mentioned criteria, two sets of earthquake records representing the study area were selected for inelastic dynamic simulations. Both the PEER Ground Motion Database (PEER, 2013) and the European Strong-Motion Database (Ambraseys et al., 2004) were thoroughly searched to select 40 natural records that represent the aforementioned earthquake scenarios, namely far-field records and near-source events (e.g. Mwafy et al., 2006). Basically, the selection was conducted on two stages. Stage one: initial filtering, and stage two: response spectra matching. For stage one, the filtering of databases was carried out according to pre-defined criteria which represent site specific properties. These criteria are:

- (i) epicentral distance,
- (ii) magnitude,
- (iii) soil condition,
- (iv) PGA, and
- (v) a/v ratio.

The above mentioned criteria however represent the first stage of attaining the natural records, which resulted in about 500 records. Stage two includes plotting the spectral acceleration for each of these records against the design code spectra of the study area (ADIBC, 2013). The response spectra of the selected records was extracted and scaled to the recommended design intensity of the study area (i.e. a PGA of 0.16g). In the latter stage, 20 near-source records matching the short period portion of the code response spectra, and 20 far-field records matching the long period portion, were selected for IDAs, as described in Figure 4.7. The response spectra of the selected 40 input ground motions, that represent the near-source and far-field seismic scenarios with the current design spectra for the study area for soil classes C and D, are illustrated in Figure 4.8 and Figure 4.9. Table 4.1 and Table 4.2

show a summary of the selected near-source and far-field records, respectively. The acceleration time-histories of the selected natural records for the two scenarios are depicted in Figure 4.10 and Figure 4.11.

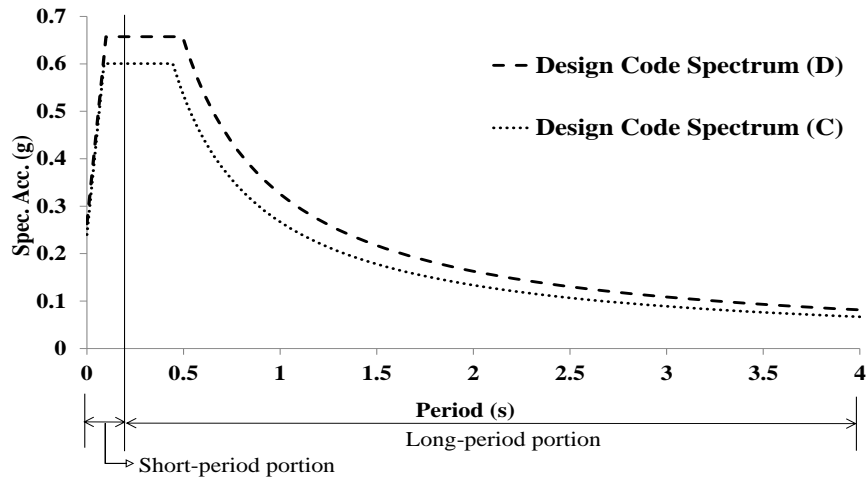


Figure 4.7: Stage two, matching design code spectra

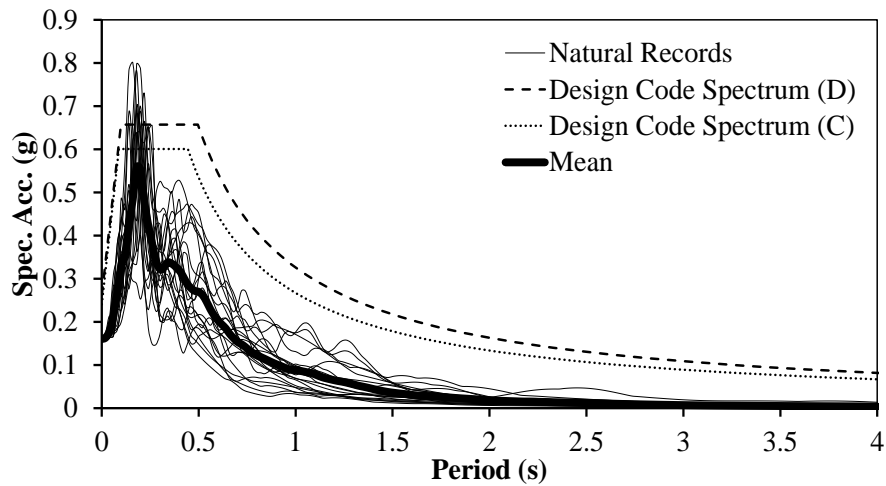


Figure 4.8: Response spectra of near-source earthquake records

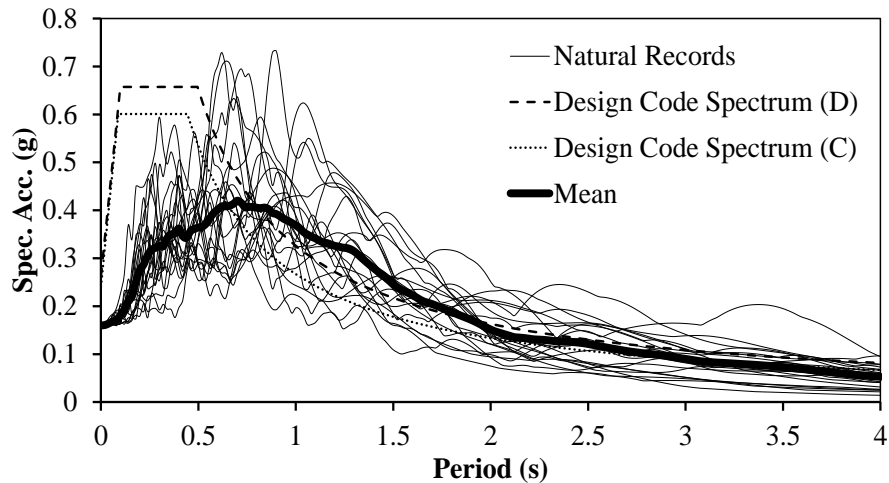


Figure 4.9: Response spectra of far-field records

Table 4.1: Summary of near-source earthquake records

Ref	Earthquake	Station	Component	Date	Mag. (Mw)	Site class	Ep. Dist. (km)	Duration (sec)	PGA (m-s ²)	a/v g-ms ⁻¹	a/v class.
NF01	Coalinga-04	Anticline Ridge Free-Field	270	7-9-1983	5.18	C	6.34	15	3.220	2.048	←
NF02	Coalinga-04	Anticline Ridge Pad	270	7-9-1983	5.18	C	6.34	14	3.246	2.350	
NF03	Coalinga-05	Burnett Construction	360	7-22-1983	5.77	D	12.38	21	2.915	1.988	
NF04	Coyote Lake	San Juan Bautista, 24 polk St	213	8-6-1979	5.74	C	19.7	26	0.991	1.424	
NF05	Friuli	Breginj-Fabrika IGLI	Y	15-9-1976	6	C	21	9.9	4.956	2.333	
NF06	Hollister-04	City Hall	271	28-11-1974	5.14	C	9.8	20	1.651	1.480	
NF07	Lazio Abr. Y	Cassino-Sant Elia	EW	7-5-1984	5.93	C	16	30	1.123	1.590	
NF08	Livermore-02	Livermore-Morgan Terr Park	355	1-27-1980	5.42	C	14.1	15	2.235	2.581	
NF09	Mammoth Lakes-02	Mammoth Lakes H. S.	344	5-25-1980	5.69	C	3.49	12	4.064	1.957	
NF10	Mammoth Lakes-06	Fish & Game (FIS)	0	5-27-1980	5.94	D	12.02	11	3.979	2.753	
NF11	Montenegro	Petrovac-Hotel Oliva	Y	4-15-1979	5.80	C	24.0	28	0.873	1.426	
NF12	Northridge-06	Panorama City-Roscoe	90	3-20-1994	5.28	D	11.8	7.2	1.141	1.916	
NF13	Umbria Ma.	Castelnuovo-Assisi	NE	26-9-1997	6.04	C	22.0	45	1.600	1.254	
NF14	Whittier Narrows-01	Brea Dam (L Abut)	130	10-1-1987	5.99	C	24.0	20	1.299	1.460	
NF15	Whittier Narrows-01	LA-Centry City CC North	90	10-1-1987	5.99	D	29.9	30	0.851	1.788	
NF16	Whittier Narrows-01	LB-Orange Ave	2280	10-1-1987	5.99	D	24.5	21	2.111	1.468	
NF17	Whittier Narrows-01	Alhambra - Fremont School	180	10-1-1987	5.99	C	6.77	26	3.806	1.514	
NF18	Whittier Narrows-01	Garvey Res. - Control Bldg	60	10-1-1987	5.99	C	2.86	38	3.775	2.432	
NF19	Whittier Narrows-01	LA - 116th St School	360	10-1-1987	5.99	D	21.26	25	3.343	1.888	
NF20	Whittier Narrows-01	LA - Obregon Park	360	10-1-1987	5.99	D	9.05	30	4.161	1.748	

* a/v: PGA/PGV, a/v classification (<0.8 Low & >1.2 high), $V_{s,30}$ of very dense soil = 360-760 m/s, and for stiff soil = 180-360 m/s

Table 4.2: Summary of far-field earthquake records

Ref	Earthquake	Station	Component	Date	Mag. (M_w)	Site class	Ep. Dist. (km)	Duration (sec)	PGA ($m-s^{-2}$)	a/v $g-ms^{-1}$	a/v class.
FF1	Bucharest	Building res. Institute	EW	04-03-1977	7.53	stiff	161	18	1.73	0.60	←
FF2	Chi-Chi	CWB 99999 ILA013	EW	20-09-1999	7.62	v. dense	135	117	1.36	0.52	
FF3	Loma Prieta	Emeryville	260	18-10-1989	6.93	v. dense	96.5	39	2.45	0.57	
FF4	Loma Prieta	Golden Gate Bridge	270	18-10-1989	6.93	v. dense	100	38	2.29	0.61	
FF5	Hector Mine	Indio - Coachella Canal	0	16-10-1999	7.13	stiff	99	60	0.90	0.70	
FF6	Izmit	Ambarli-Termik	EW	17-08-1999	7.64	stiff	113	150	1.80	0.60	
FF7	Izmit	Istanbul-Zeytinburnu	NS	17-08-1999	7.64	stiff	96	129.24	1.08	0.77	
FF8	Kocaeli	Bursa Tofas	E	17-08-1999	7.51	stiff	95	139	1.06	0.49	
FF9	Kocaeli	Hava Alani	90	17-08-1999	7.51	v. dense	102	106.615	0.92	0.46	
FF10	Loma Prieta	Alameda Naval Air Stn Hanger	270	18-10-1989	6.93	stiff	91	29	2.39	0.73	
FF11	Loma Prieta	Berkeley LBL	90	18-10-1989	6.93	v. dense	98	39	1.15	0.65	
FF12	Loma Prieta	Oakland-Outer Harbor Wharf	0	18-10-1989	6.93	stiff	94	40	2.75	0.67	
FF13	Manjil	Abhar	N57E	20-06-1990	7.42	stiff	91	29.49	1.30	0.62	
FF14	Manjil	Tonekabun	N132	20-06-1990	7.42	v. dense	131	40	1.22	0.76	
FF15	Chi-Chi	TAP005	E	20-09-1999	7.62	stiff	156	134	1.34	0.49	
FF16	Chi-Chi	TAP010	E	20-09-1999	7.62	stiff	151	144	1.19	0.50	
FF17	Chi-Chi	TAP021	E	20-09-1999	7.62	stiff	151	125	1.15	0.47	
FF18	Chi-Chi	TAP032	N	20-09-1999	7.62	v. dense	144	90	1.13	0.64	
FF19	Chi-Chi	TAP090	E	20-09-1999	7.62	stiff	156	125	1.28	0.41	
FF20	Chi-Chi	TAP095	N	20-09-1999	7.62	stiff	158	123	0.96	0.52	

* a-v: PGA-PGV, a-v classification (<0.8 Low & >1.2 high), V_{s30} of very dense soil = 360-760 m-s, and for stiff soil = 180-360 m-s

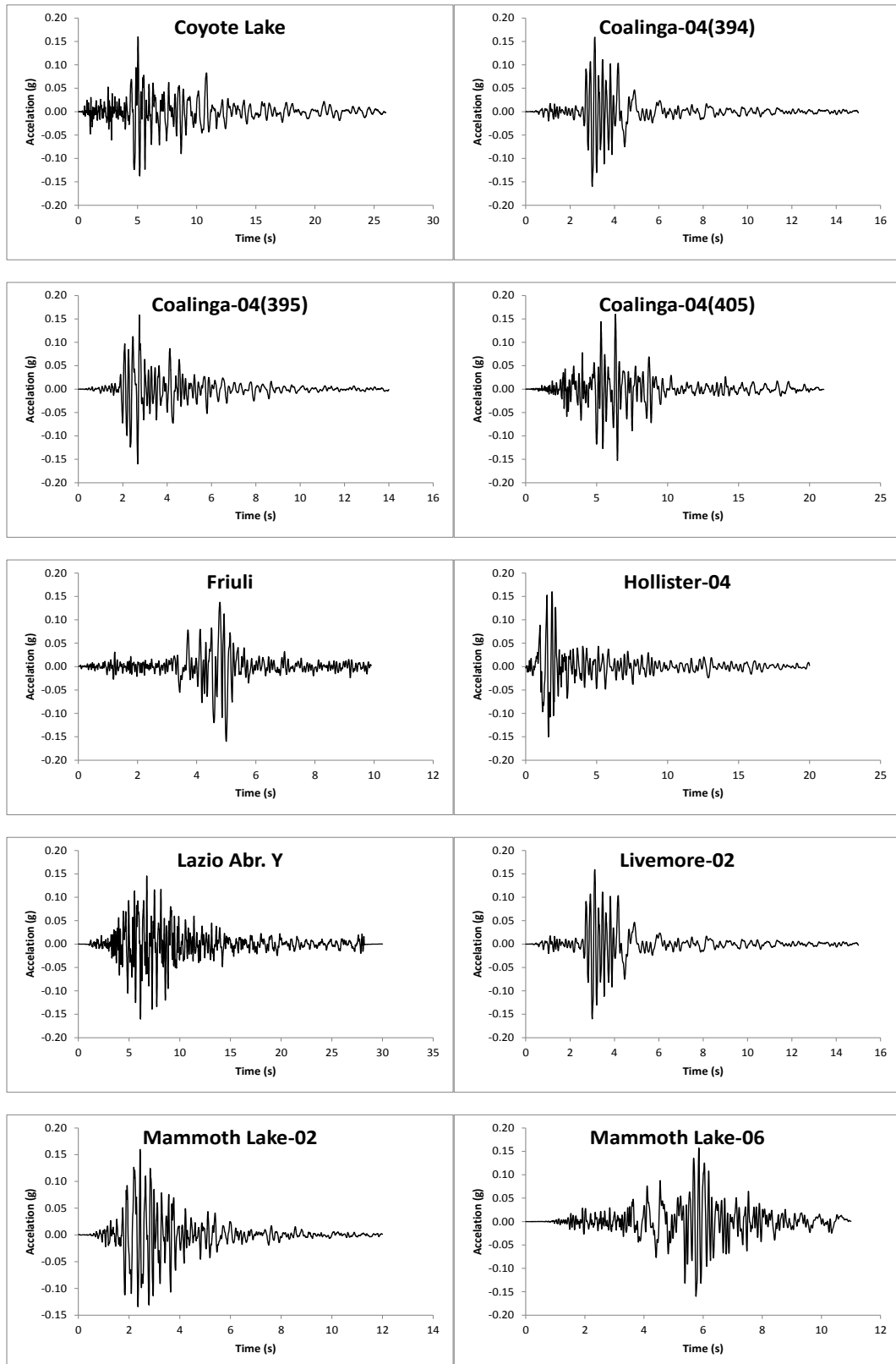


Figure 4.10: Selected near-source records

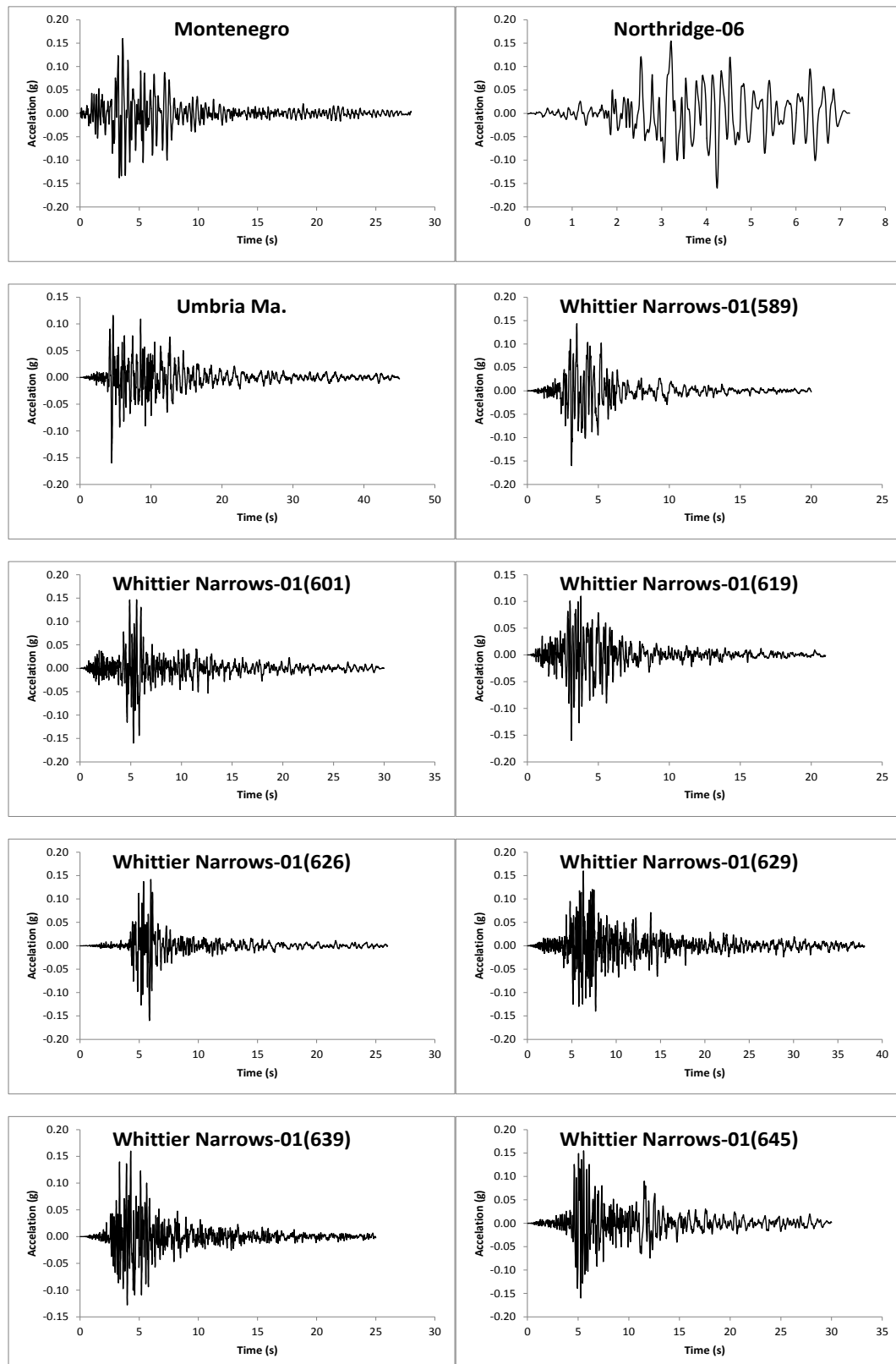


Figure 4.10 (Cont'd): Selected near-source records

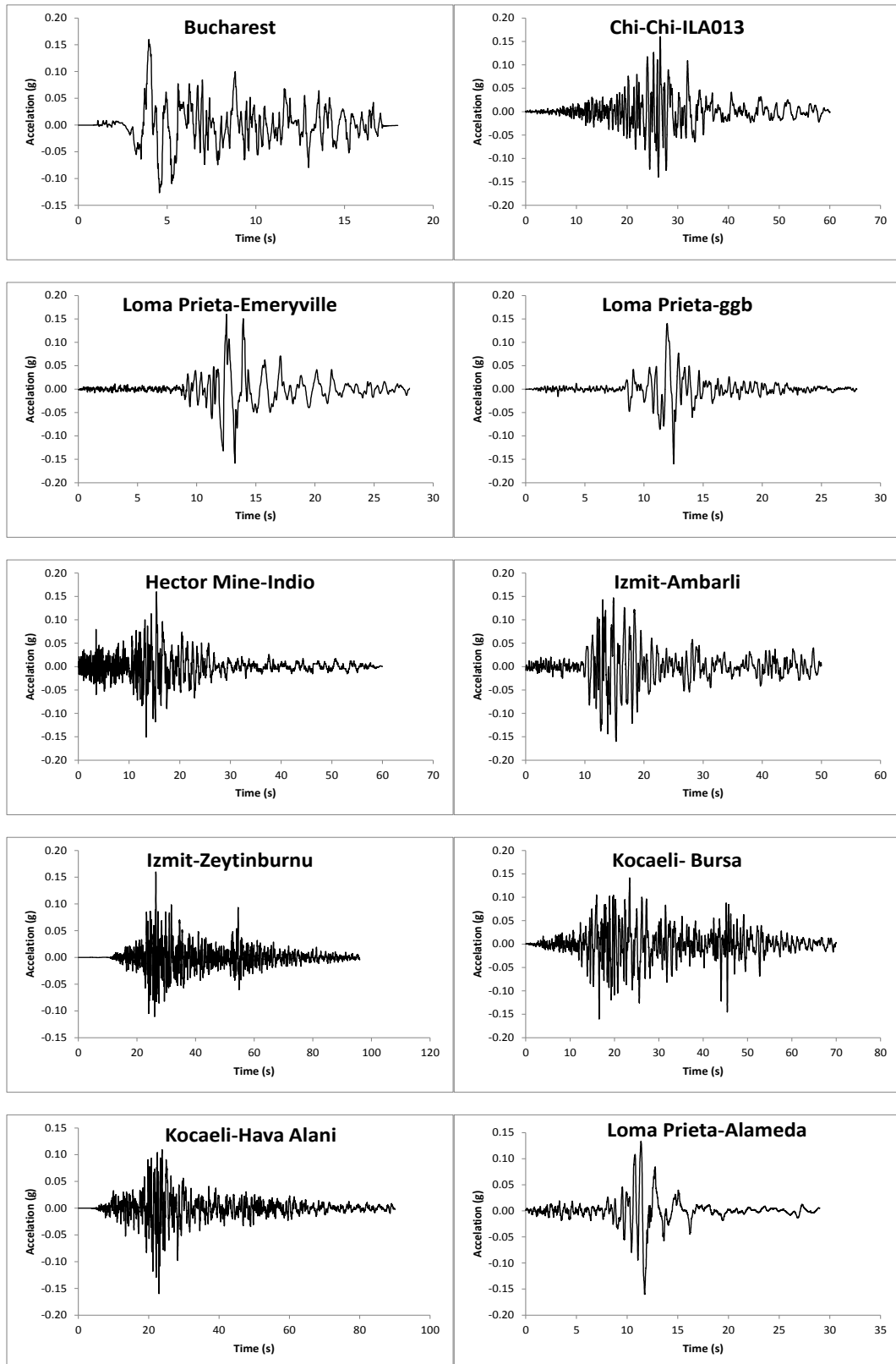


Figure 4.11: Selected far-field records

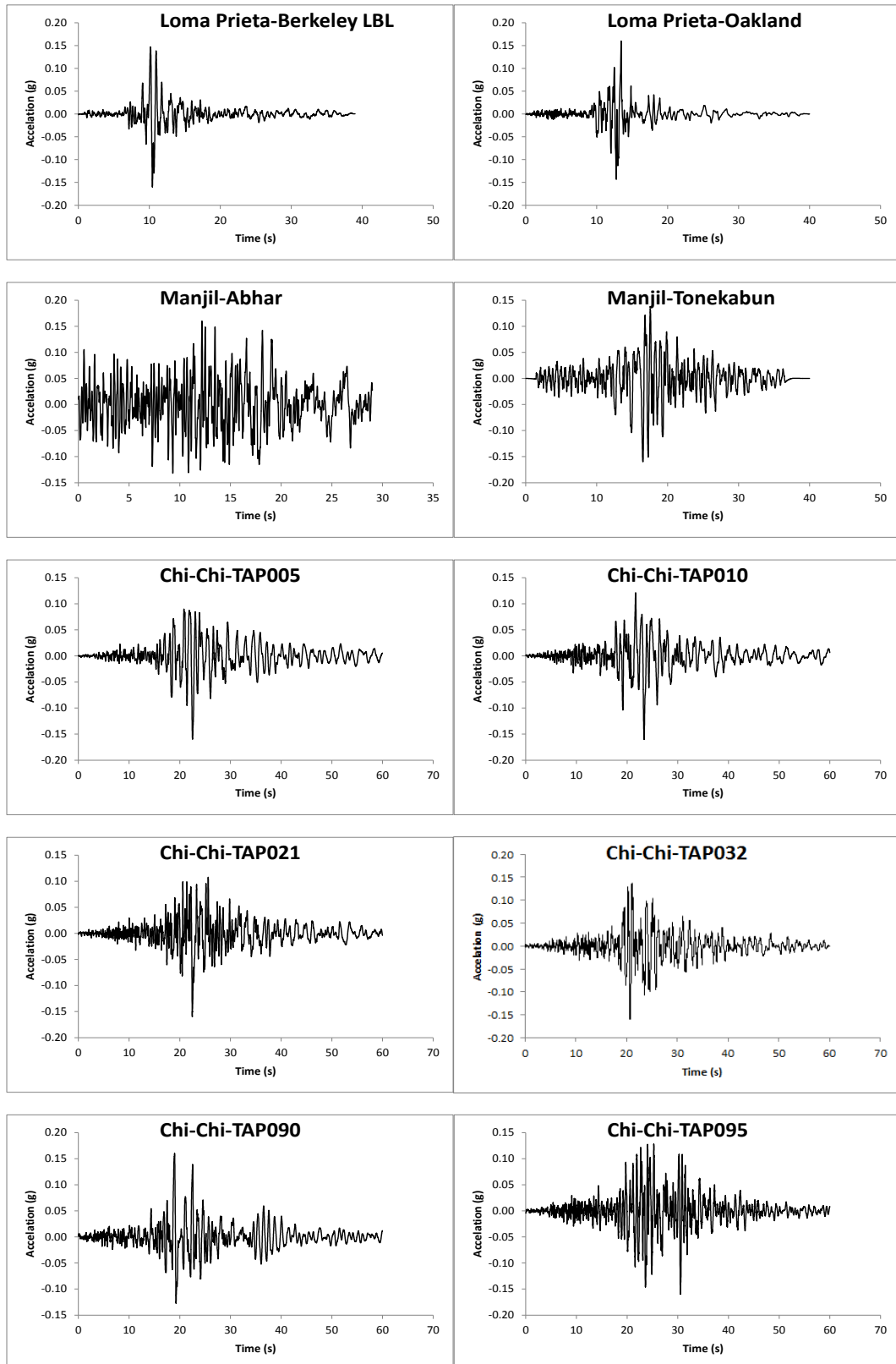


Figure 4.11 (Cont'd): Selected far-field records

4.3 Concluding Remarks

Two and three-dimensional idealizations for wall and frame structures, respectively, were developed using ZEUS-NL to assess the seismic response of the nine reference buildings using IPAs and IDAs. The reference wall buildings were idealized based on the LFRSs in the transverse direction, while 3D models were developed for frame structures. The LFRSs in the transverse direction of the reference structures were considered in the present study as compared to the longitudinal counterpart due to the higher vulnerability in the former direction. In this modeling approach, different structural elements and material properties were represented at the member and the section levels. This enabled monitoring of the stress/strain response in different structural elements throughout the multi-step analysis.

Forty natural input ground motions were carefully chosen and employed in the present study to effectively account for the uncertainty in ground motions. These scenario-based earthquake records were selected based on a number of criteria to represent the study area. The selected records were scaled to the design ground motion intensity based on the recommendations of previous seismic hazard studies before applying to the reference structures. This approach ensures that the reference structures were assessed under input ground motions representing diverse seismic scenarios representing the study area.

CHAPTER 5: PERFORMANCE ASSESSMENT OF EXISTING STRUCTURES

5.1 Introduction

The baseline models of the nine reference structures considered in the present study were subjected to a series of Eigenvalue analyses, IPAs and IDAs to assess their seismic performance. These analyses were entirely performed using detailed fiber-based numerical models (Elnashai et al., 2012). The ZEUS-NL platform accounts for material inelasticity and geometric non-linearity, as discussed in Chapter 4. It is noteworthy that the 3D ETABS models for the reference structures were only used in the design process, as explained in Chapter 3. The following analyses were carried out using ZEUS-NL for the nine reference buildings:

- Free vibration (Eigenvalue) analyses;
- IPAs using different lateral load patterns;
- Extensive IDAs using the 40 natural ground motions representing two seismic scenarios, as discussed in Chapter 4.

In total, over 5000 inelastic multi-step analyses of nine multi-degree-of-freedom systems were performed and their large output files processed and stored in spreadsheets. The results of these analyses were used in the seismic vulnerability assessment of the nine reference buildings using fragility relationships. Moreover, about 3000 additional analyses were performed to assess the vulnerability of the structures that proved to have unsatisfactory performance, and hence retrofitted using different mitigation techniques. The results of the retrofitted structures will be discussed in Chapter 6.

5.2 Free Vibration Analysis

The Eigenvalue analysis was performed to extract the natural frequencies and mode shapes of a structure. This analysis is important as a predecessor to dynamic analysis because knowledge of the natural frequencies and mode shapes helps to provide insights into the dynamic response. In the free vibration analysis, the stiffness and mass distribution of the structure are needed to run the analysis without the application of loads. The results of mode shapes and elastic periods in the transverse directions are only utilized in the present study as it is the most vulnerable direction when compared with the longitudinal direction, as discussed in Chapter 4.

The ETABS 3D models developed for the design of the nine reference buildings were utilized for verifying the ZEUS-NL 2D/3D models before performing the extensive inelastic pushover and time-history analyses. Table 5.1 summarizes the periods of the nine reference buildings from both the fiber-based and design models. It is clear that the periods of the design models are slightly longer (within 13% difference) than the periods of the fiber-based models. This difference is justified by the consideration of actual material strength values and steel reinforcement in the fiber-based models, which increase stiffness and shorten periods. Even though the 2D fiber-based models developed using ZEUS-NL for the wall structures do not account for the vertical elements at boundaries, which have marginal lateral stiffness, the results verify the adopted modeling approach. It is important to note that ZEUS-NL fiber-based models are used for assessing the capacity in the post-elastic range and predicting the inelastic seismic demand of the nine reference buildings, as discussed hereafter.

Figure 5.1 and Figure 5.2 portrays the first three modes of vibration for the five pre-code structures and the four emergency facilities, respectively. These results

are obtained from the ZEUS-NL fiber element models discussed in Chapter 4. The Eigenvalue analysis is also used as a preliminary verification tool of the inelastic analysis models, as discussed in a subsequent section.

It is noteworthy that the reference structures are modeled using ZEUS-NL by employing different idealization approaches. The 40-story building is divided into four framing systems in the transverse direction, while each of the 18 and 26 story buildings are represented by one framing system. Moreover, 3D models are employed in the case of the frame buildings, including the 2 and 8 story buildings and the four emergency facilities. It is interesting to note that despite the different modeling approaches for the nine reference structures, the difference observed between the fundamental periods obtained from the ETABS 3D and the ZEUS-NL 2D/3D models in the transverse direction is less than 13% as shown in Table 5.1. This difference is mainly due to efficiently representing the reinforcement in the ZEUS-NL models in addition to employing the actual/mean material strength values in the ZEUS-NL models instead of the nominal/characteristic strength used in the design. The Eigenvalue results verify the numerical models and lend weight to the results obtained from the present study.

Table 5.1: Summary of buildings fundamental periods (T_1) from fibre-based and design models

Category	Building	T_1 , Fiber-based models	T_1 , Design models	Difference (%)
Pre-code structures	BO-02	0.780	0.880	12.8%
	BO-08	1.344	1.396	3.9%
	BO-18	1.432	1.572	9.8%
	BO-26	2.370	2.457	3.7%
	BO-40	3.901	3.755	3.7%
Emergency Facilities	FS	0.746	0.764	2.4%
	PS	0.656	0.702	7.0%
	SC	0.817	0.891	9.1%
	HO	1.294	1.365	5.5%

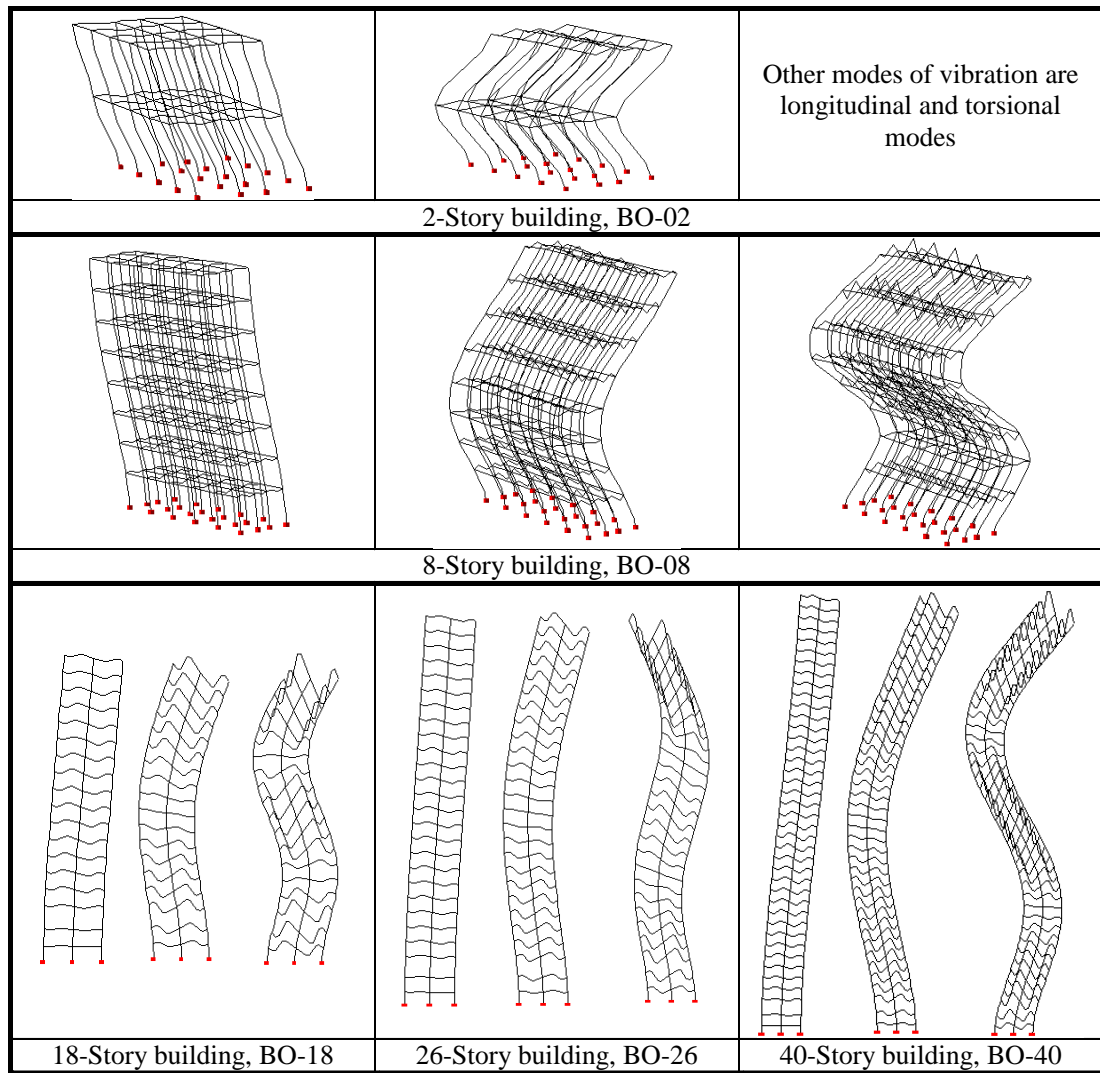


Figure 5.1: First three mode shapes of pre-code structures

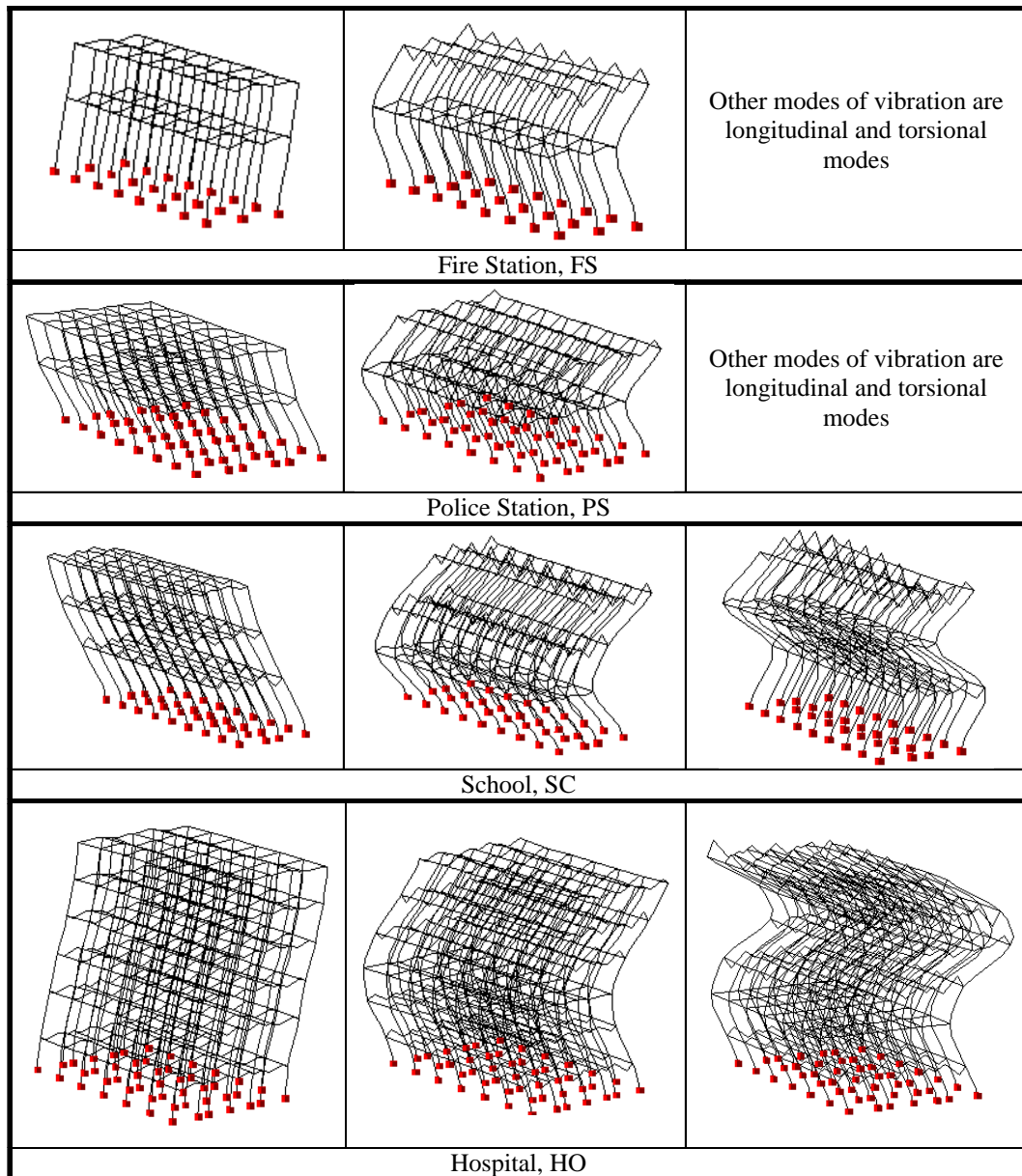


Figure 5.2: First three mode shapes of emergency facilities

5.3 Inelastic Static Pushover Analysis

The inelastic pushover analysis was conducted for the case study buildings to estimate the lateral strength and deformation capacity, and to identify the possible failure mechanisms of the buildings. This analysis procedure reduces the computational effort significantly as compared with IDA, which requires the use of a wide range of input ground motions as well as scaling and applying each record incrementally up to collapse. Displacement-controlled pushover analyses are

conducted for the fiber-based models of the nine case study buildings. This analysis involves applying the distributed gravity load to the structure and then applying an increasing lateral loads. A predefined lateral load pattern such as uniform or inverted triangular loads is distributed along the building height. The analysis is carried out until a predefined limit state or a target displacement of the structure is attained, while controlling the top displacement. With the incremental increase in the magnitude of lateral loading, probable weak areas along with failure modes of the structure can be spotted.

The pushover analysis is used to verify the structural performance of buildings, including for the following purposes: (i) to estimate the lateral capacity of the structure by plotting the total base shear versus top displacement, which helps capturing premature weakness or failure; (ii) to estimate the distribution of inter-story drift that accounts for the lateral strength and stiffness; (iii) to estimate and verify the overstrength values at different strength levels; and (iv) to estimate the expected plastic hinges, damage and failure mechanisms to the structure.

5.3.1 Estimation of Lateral Capacity

The response of the reference structures is examined under two lateral loading patterns, namely a uniform lateral load distribution (PU), which is used for the wall structures, and an inverted triangular lateral load pattern (PT), which is considered in the case of frame structures. The PT load pattern represents the deformed shape of the structure when it vibrates in its fundamental mode. This load distribution is suitable for low-rise structure. The PU load pattern represents the distribution of the mass of the structure, and is more suitable for obtaining conservative estimates of the lateral capacity of multi-story buildings (Mwafy &

Elnashai, 2001). The lateral strength, first yield in structural elements, global yield and first local failure were monitored and mapped on the lateral capacity curves of the reference structures, as shown in Figure 5.3 to Figure 5.5.

The global yield was evaluated from an elastic-perfectly plastic idealization of the capacity envelopes. The initial stiffness was estimated as the secant stiffness passing through the capacity envelope at 75% of the ultimate strength (Park, 1988). In this approach, it is considered that the global yield is the starting point of the post-elastic branch. The ultimate capacity of the structure is calculated at the maximum base shear, as shown in Figure 5.3 to Figure 5.5. It was shown from the results that the steel yielding starts in horizontal structural elements and is followed by vertical elements in all reference structures except the 2, 8 and 18 story buildings, which represent deficiencies in pre-code structures. The large wall sections in the 26 and 40 story buildings prevented the yielding in vertical elements occurring first. Inter-story drift ratios were also studied for any possible strength or stiffness deficiencies, as shown in Figure 5.6 and Figure 5.7. The results indicate that although the pre-code structures have moderate IRDs at their ultimate strength, their deformations increase rapidly afterwards, particularly for frame structures. This is clear from the rapid strength degradation shown in Figure 5.3.

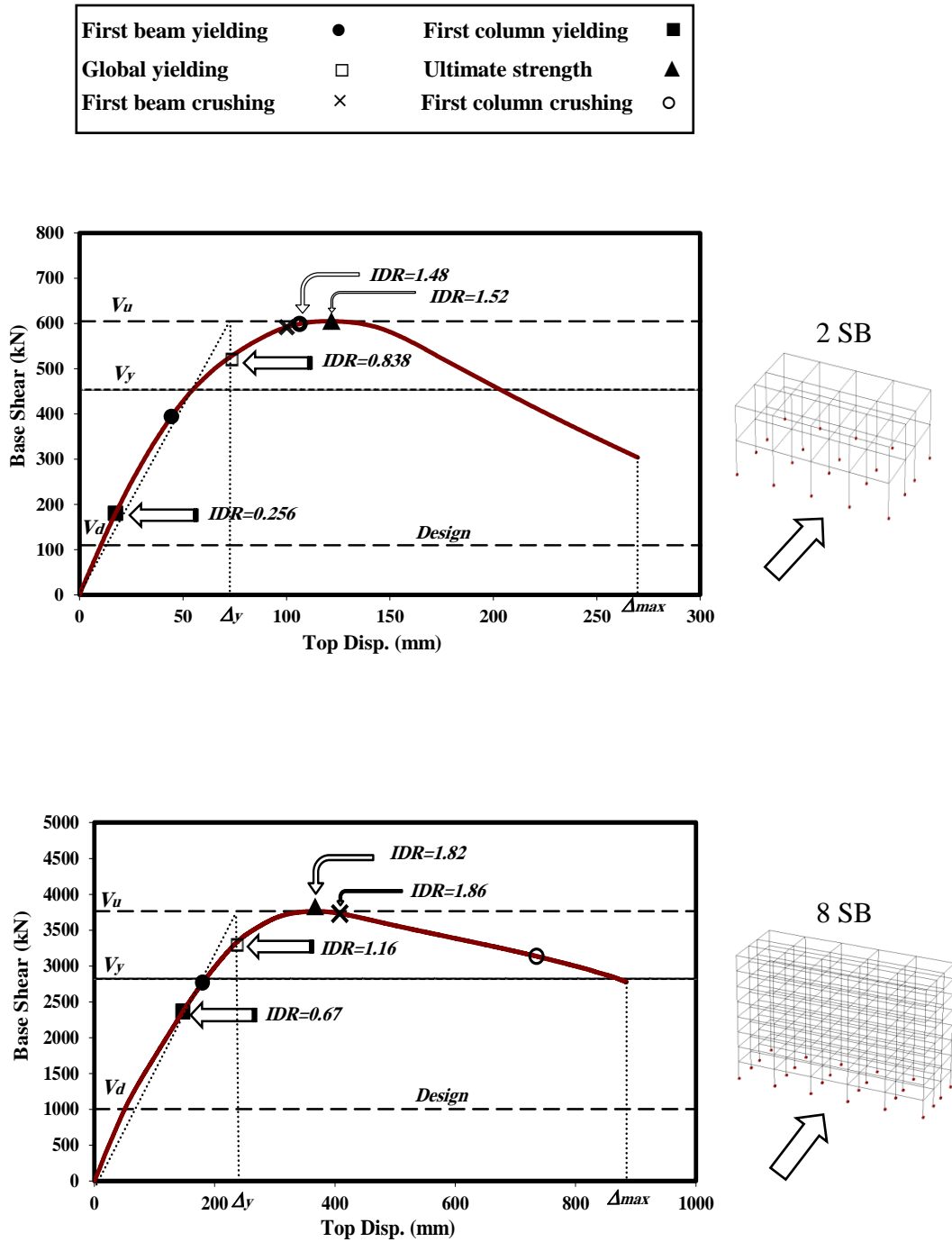


Figure 5.3: The capacity curves of the pre-code frame structures

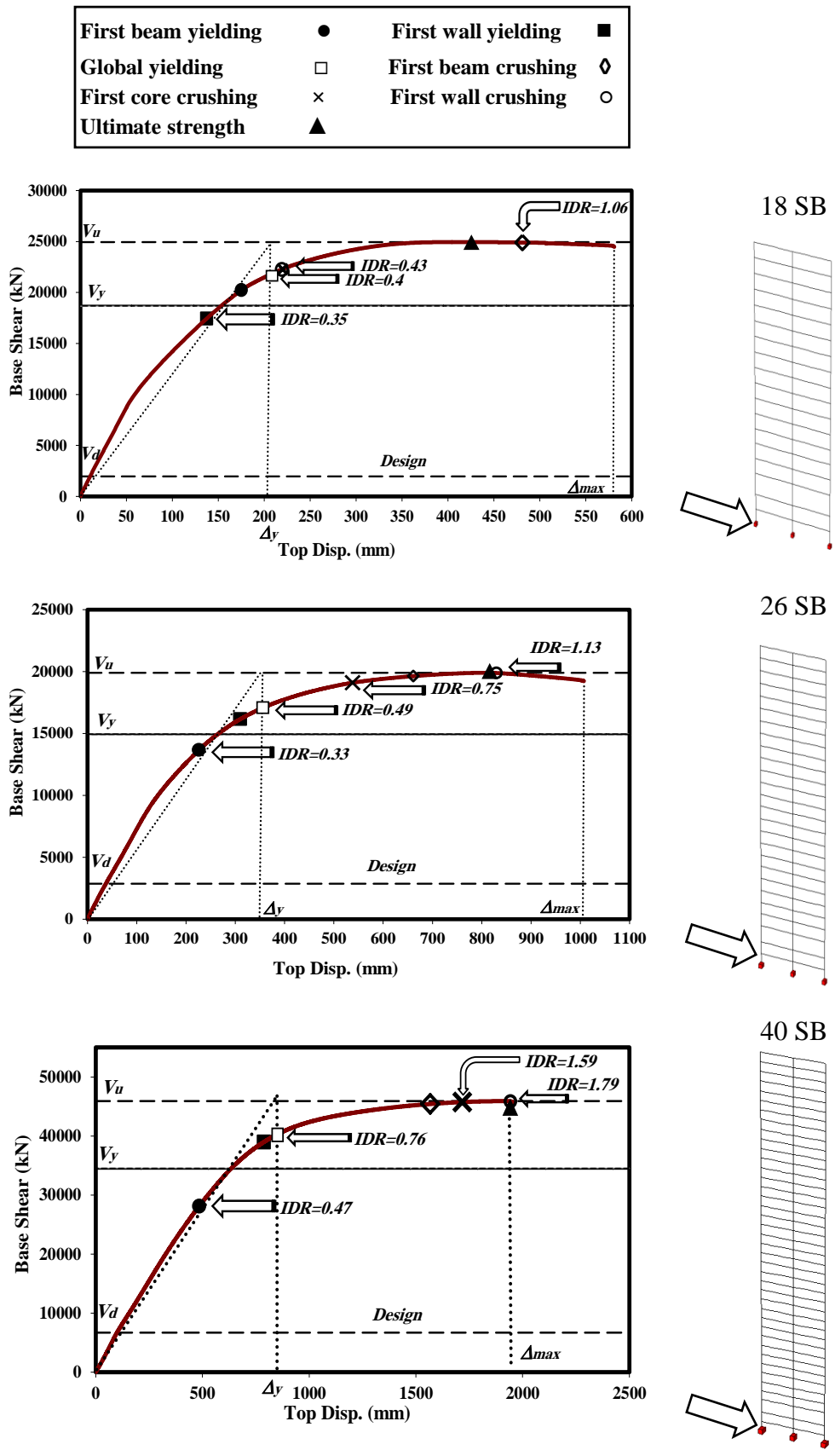


Figure 5.4: The capacity curves of the pre-code wall structures

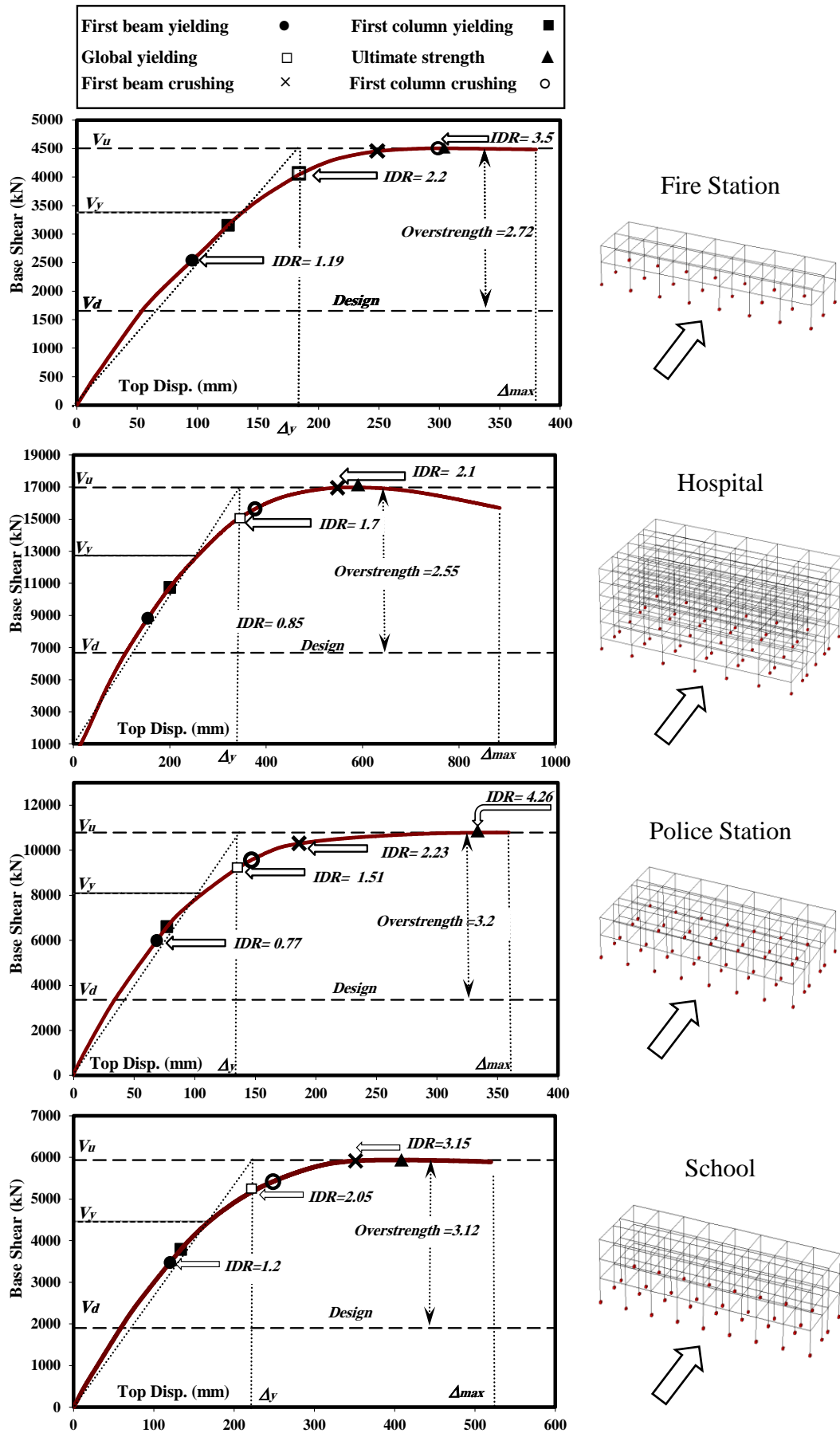


Figure 5.5: The capacity curves of the emergency structures

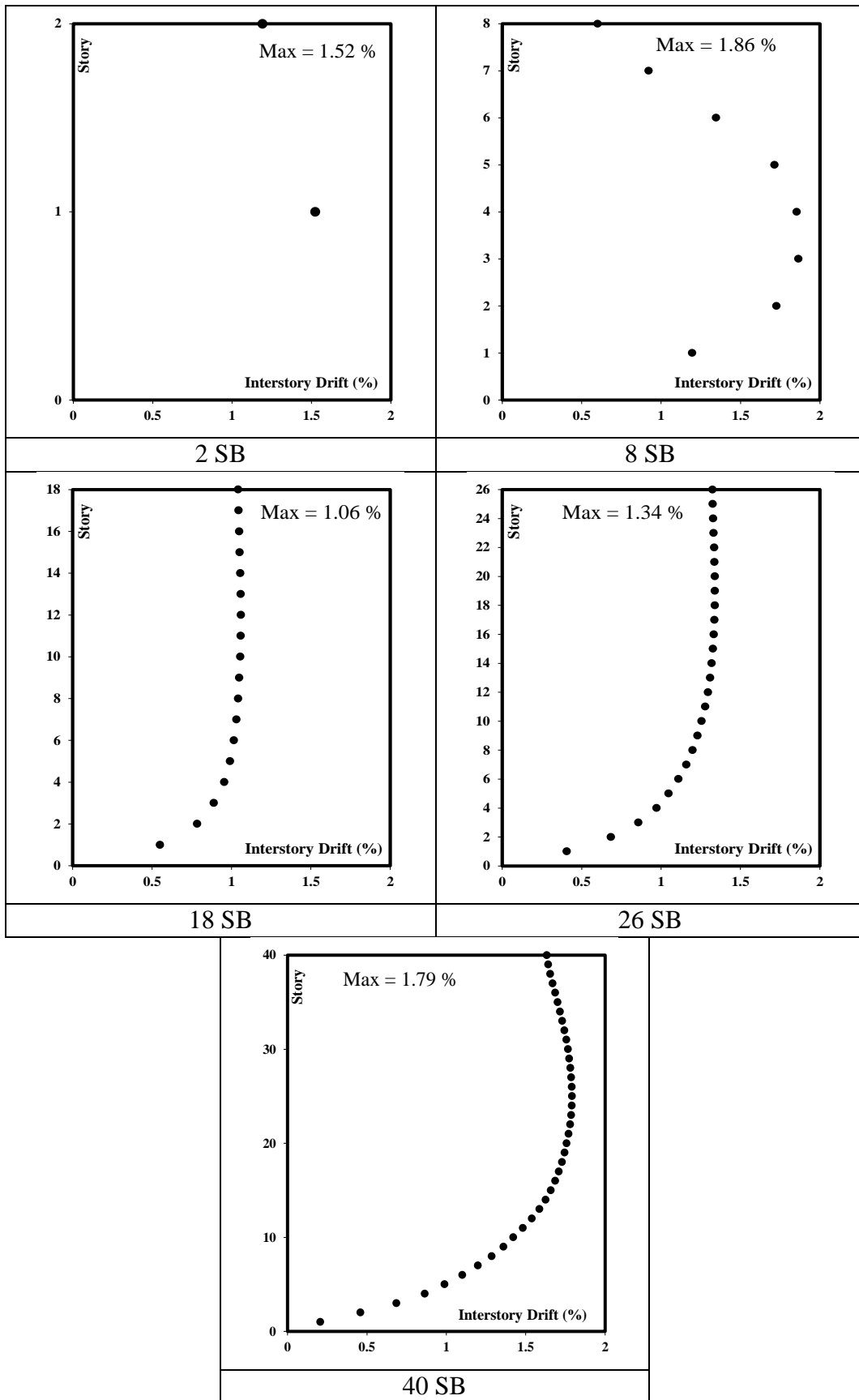


Figure 5.6: Distribution of inter-story drift ratios of the pre-code structures at the ultimate strength

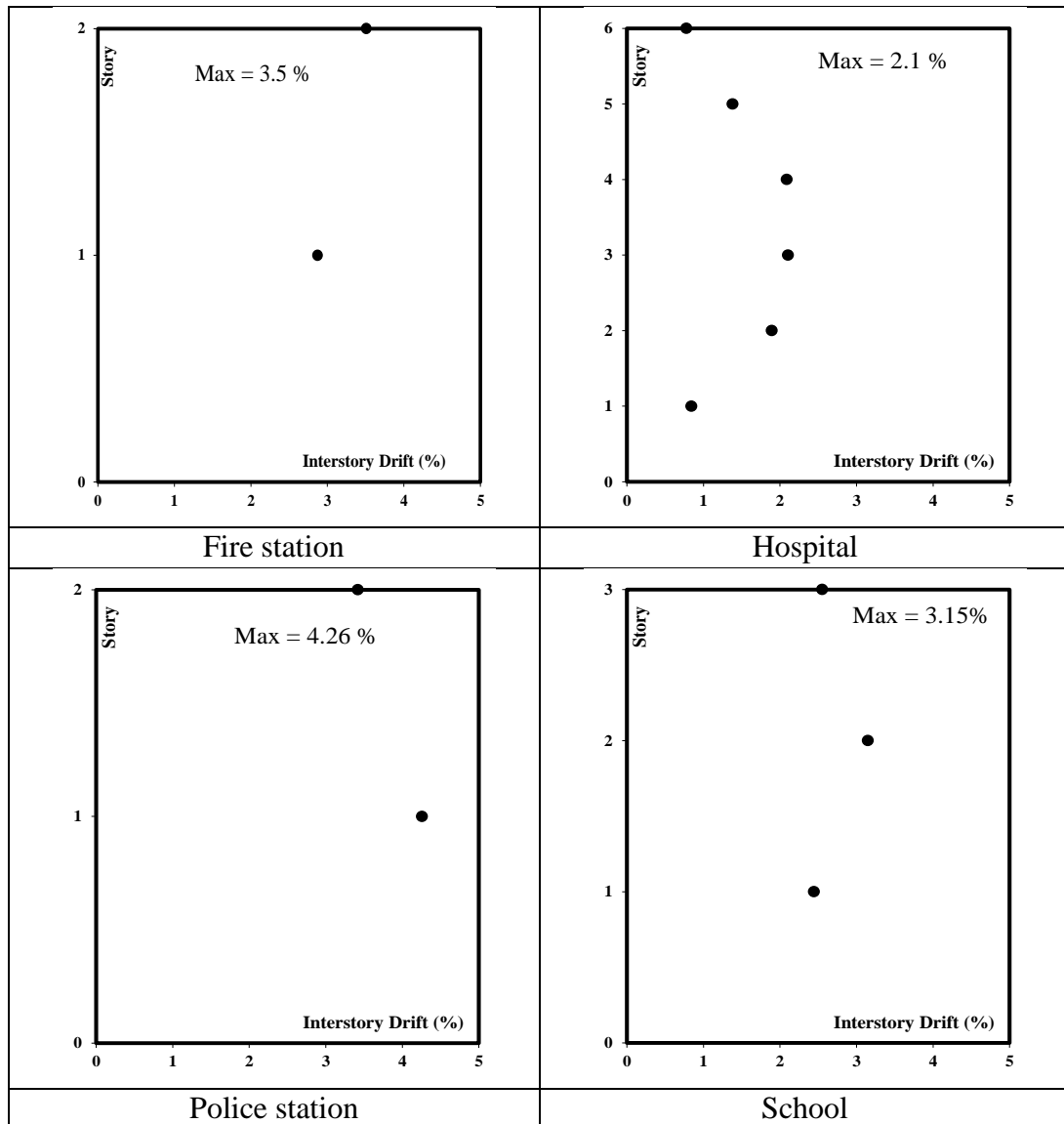


Figure 5.7: Distribution of inter-story drift ratios of the emergency structures at the ultimate strength

5.3.2 Monitoring of Member Yielding and Failure

Predicting the development of plastic hinges caused by excessive loads such as earthquakes plays a significant role in evaluating maximum stable deformation capacities of concrete structures. Plastic hinging is defined in the present study when the strain at the outermost layer of the main steel reinforcement surpasses the yield strain of the steel. The steel yielding development is determined under the uniform and inverted triangular load distributions for the wall and frame structures,

respectively. Figure 5.3 to Figure 5.5 indicate that pre-code structures experience poor performance, especially for the low-rise buildings. Plastic hinges in the 2, 8 and 18-story buildings occur in vertical elements first, then are followed by horizontal elements due to the absence of capacity design. The 26 and 40-story buildings do not experience such poor performance due to vertical element large capacities. For emergency facilities, the first yield always occurs in the horizontal elements before vertical members. This strong-column weak-beam concept is in agreement with the code principle of having energy dissipation concentrated in horizontal elements. The mapping of steel yielding in the reference structures is illustrated in Figure 5.8 and Figure 5.10.

Concrete crushing in vertical elements is defined when the strain of the confined concrete region reaches the crushing strain of concrete, which is estimated as per Mander et al. (1988). Figure 5.9 and Figure 5.11 demonstrates the spread of concrete crushing in walls and columns in the pre-code and emergency structures, respectively. It is noticeable that crushing typically occurs at the base of the vertical elements or where an observable reduction in the section capacity is implemented in the design. Concrete crushing is also observed at higher stories in certain buildings, which is consistent with the results of previous studies (e.g. Di Ludovico et al., 2008).

It was shown from the mapping of plastic hinges all over the framing systems of the reference structures that emergency facilities have a lower number of plastic hinges in vertical structural members than pre-code structures. The latter category represents buildings that lack efficient LFRSs unlike the emergency facilities which characterize well-designed structures. The above-mentioned observations for the

seismic performance of each category of the investigated buildings are emphasized from the incremental dynamic analyses as presented in subsequent sections.

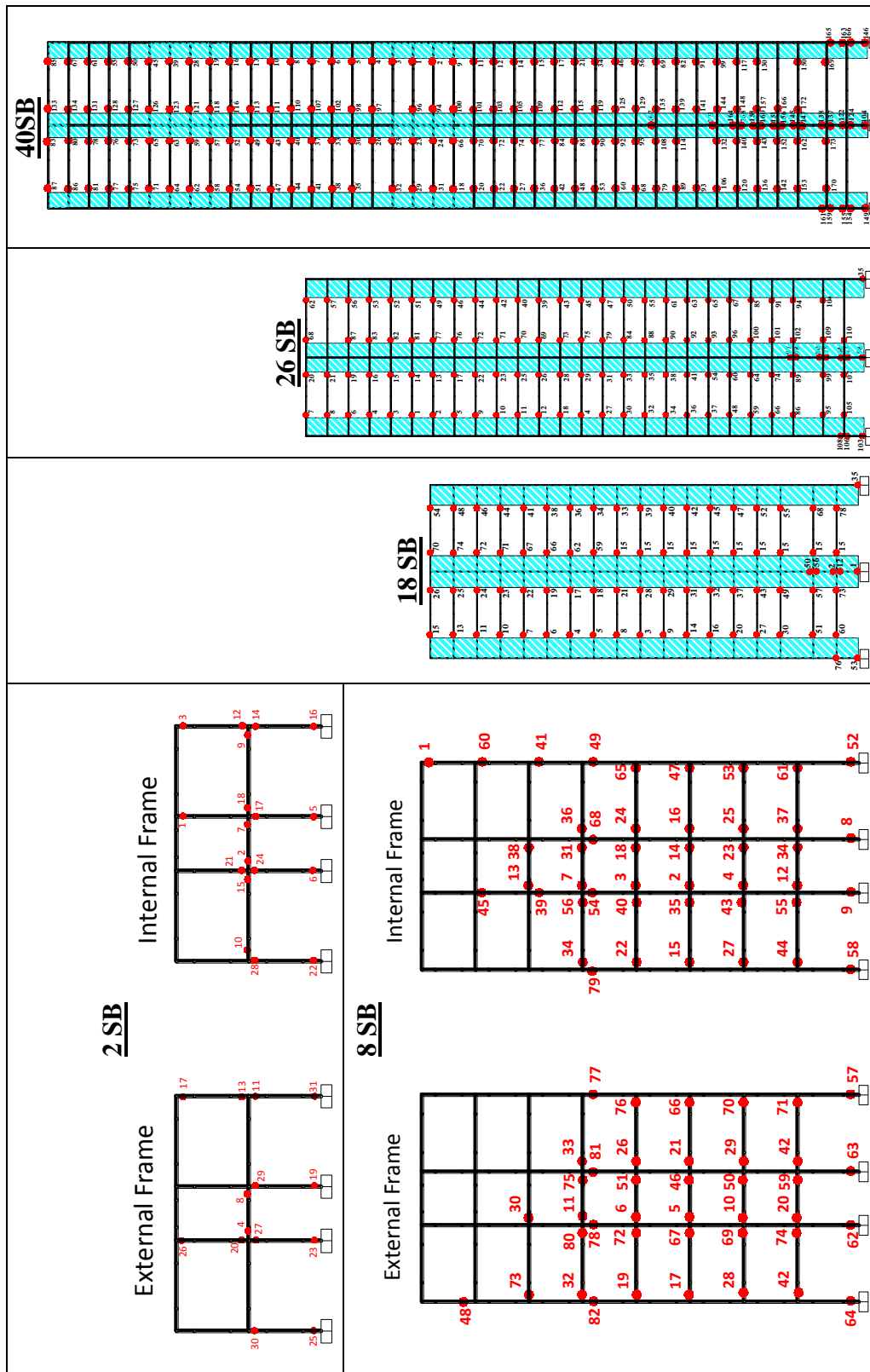


Figure 5.8: Plastic hinge distributions of the pre-code structures

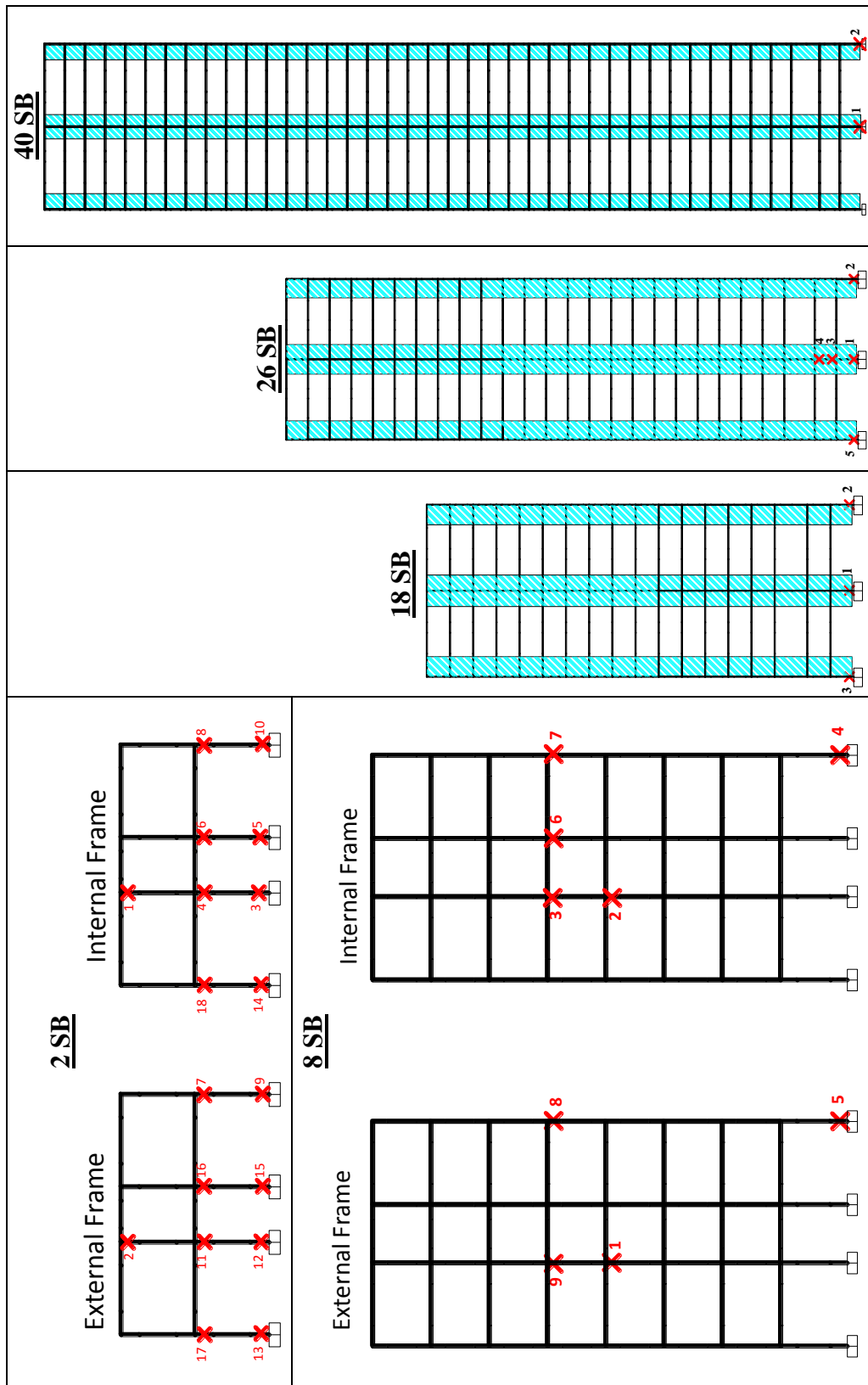


Figure 5.9: Distributions of concrete crushing in the vertical elements of the pre-code structures

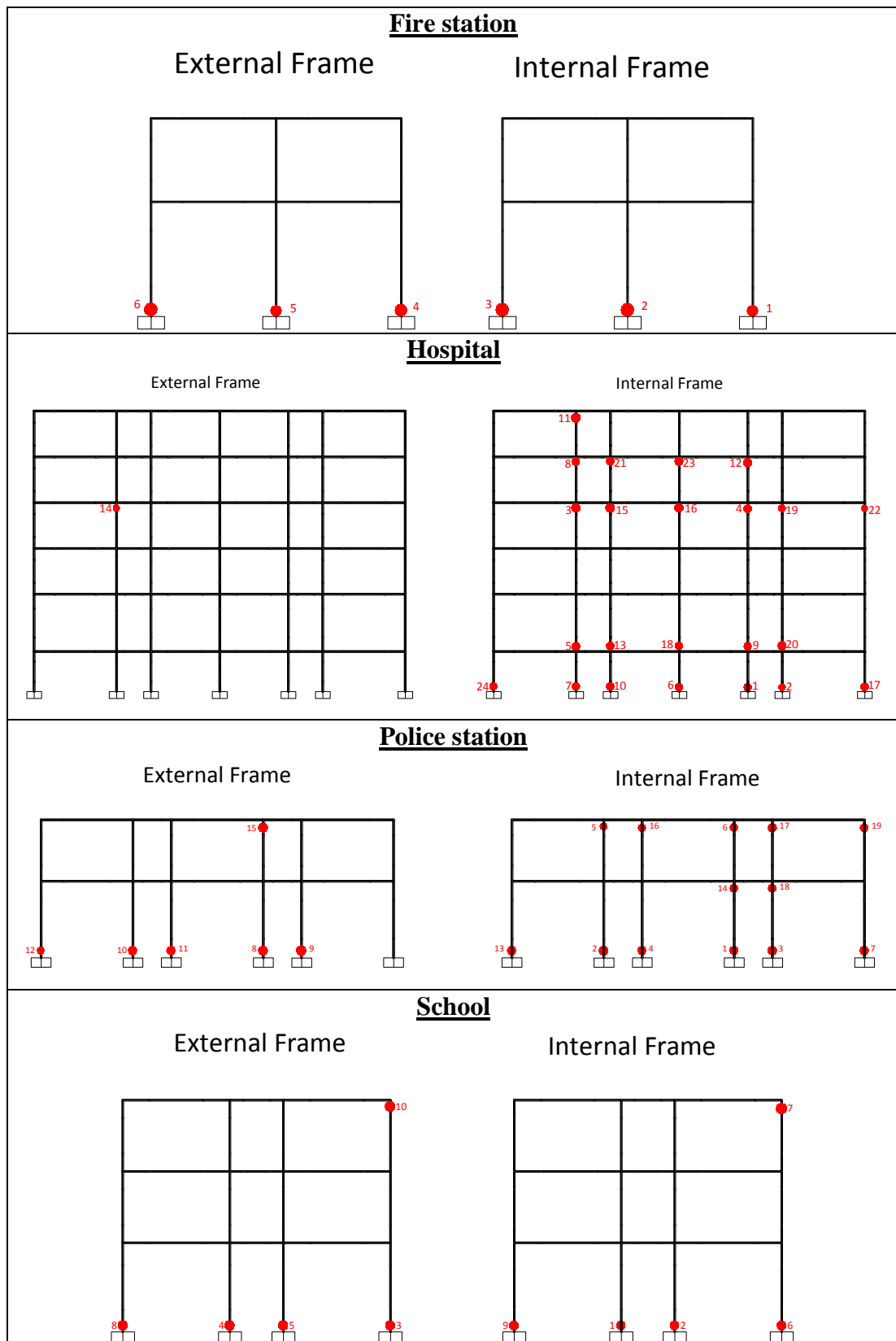


Figure 5.10: Plastic hinge distributions in the vertical structural elements of the emergency structures

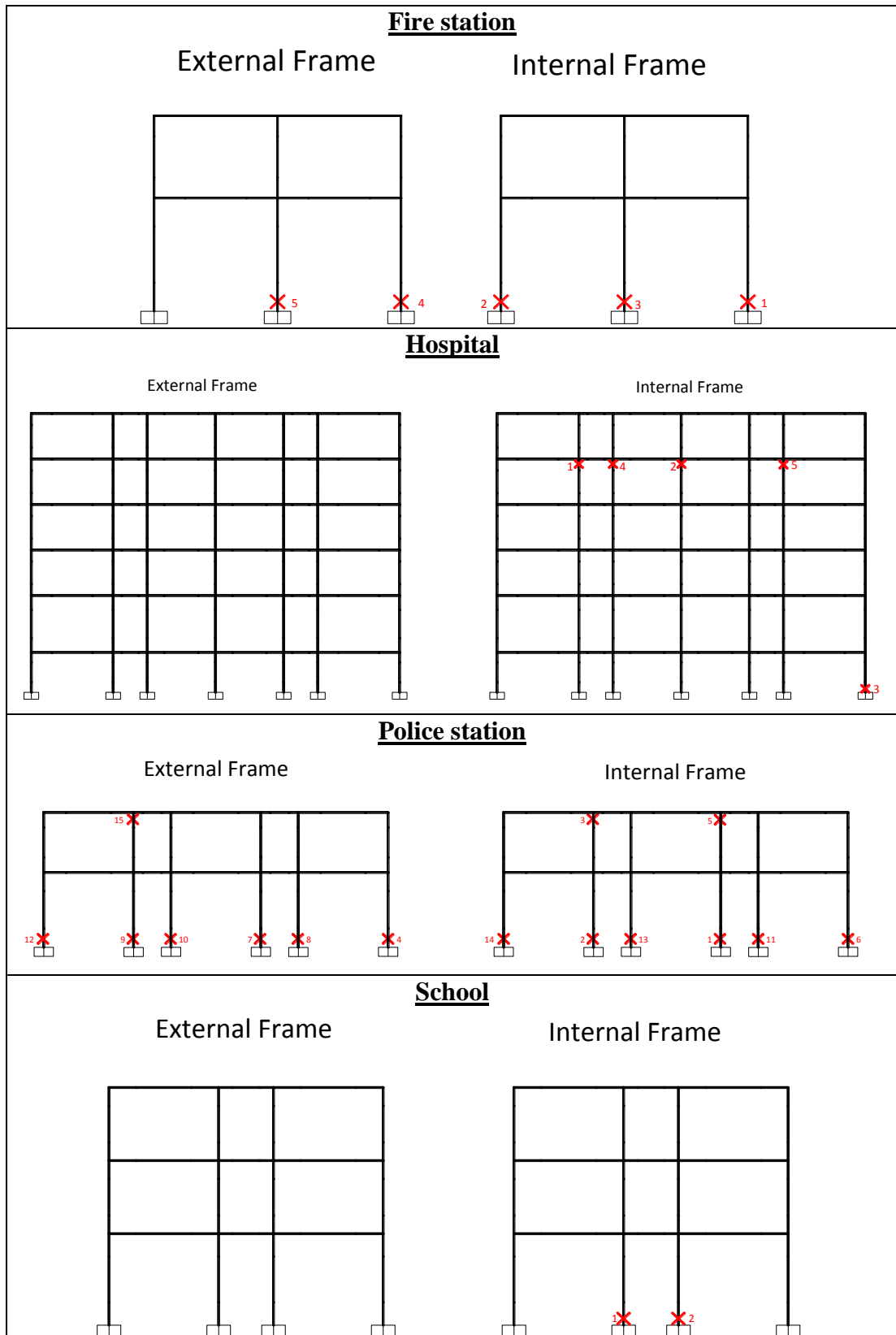


Figure 5.11: Distributions of concrete crushing in the vertical structural elements of the emergency structures

5.4 Incremental Dynamic Analysis

Conventional IPA cannot represent the dynamic behavior of structures with a large degree of precision since it is based on a predefined lateral load distribution. It may not capture some important deformation modes that occur in a structure subjected to severe earthquakes, particularly for long period and irregular structures. To overcome the shortcomings of pushover analysis, extensive IDAs are carried out for the nine reference structures.

In concept, the IDA is a computational analysis method which is used to evaluate precisely the performance of structures under seismic loads with increasing severity. This analysis includes executing multiple non-linear inelastic response history analyses of a structural model under a suite of selected ground motion records (40 in the current study); each is scaled to several levels of seismic intensity (e.g. Mwafy & Elnashai, 2001; Vamvatsikos & Cornell, 2002a). A set of wisely selected ground motion records to outfit the hazard/design spectra of the study area helps to provide a precise evaluation of the seismic performance of structures. The scaling levels are properly selected to force the structure through the entire range of behavior, from elastic to inelastic and lastly to global dynamic instability, where the structure experiences collapse. Suitable post processing can illustrate the results in terms of an IDA curve for each ground motion record. Additional results were obtained for IDA such as the base shear and top displacement histories as well as the distribution of IDR with respect to the building height. The stress-strain response is also processed to assess the formation of plastic hinges of structural elements, which is a method for evaluating limit states.

A significant time and effort is dedicated for conducting the IDAs, which is performed for each of the nine reference structures using the selected forty natural far-field and near-source ground motions, as discussed earlier. For the far-field records, each record is incrementally scaled from a PGA of 0.08g to 1.20g using a scaling factor of 0.08g. For the near-source input ground motions, the records are scaled from a PGA of 0.32g to 4.8g using a scaling factor of 0.32g. This is intended to capture the structural behavior at diverse limit states until the structure reaches collapse. The local and global response parameters of the nine reference structures such as IDR, top displacement, base shear and member yielding and, failure are therefore obtained from over 5000 IDAs.

Figure 5.12 and Figure 5.13 present sample results of the IDR distributions for the nine reference buildings at twice the assumed design PGA (i.e. 0.32g) and half the design PGA (0.08) for near-source and far-field records, respectively. It was observed from the IDA sample results that the IDR distributions vary based on the characteristics of each seismic scenario. The effect of higher modes of vibration is more pronounced under the effect of the near-source records, as compared to the far-field counterpart. Indeed, these results show the higher deformations and vulnerability of the reference structures under the effect of far-field seismic scenario as compared to the near-source counterpart.

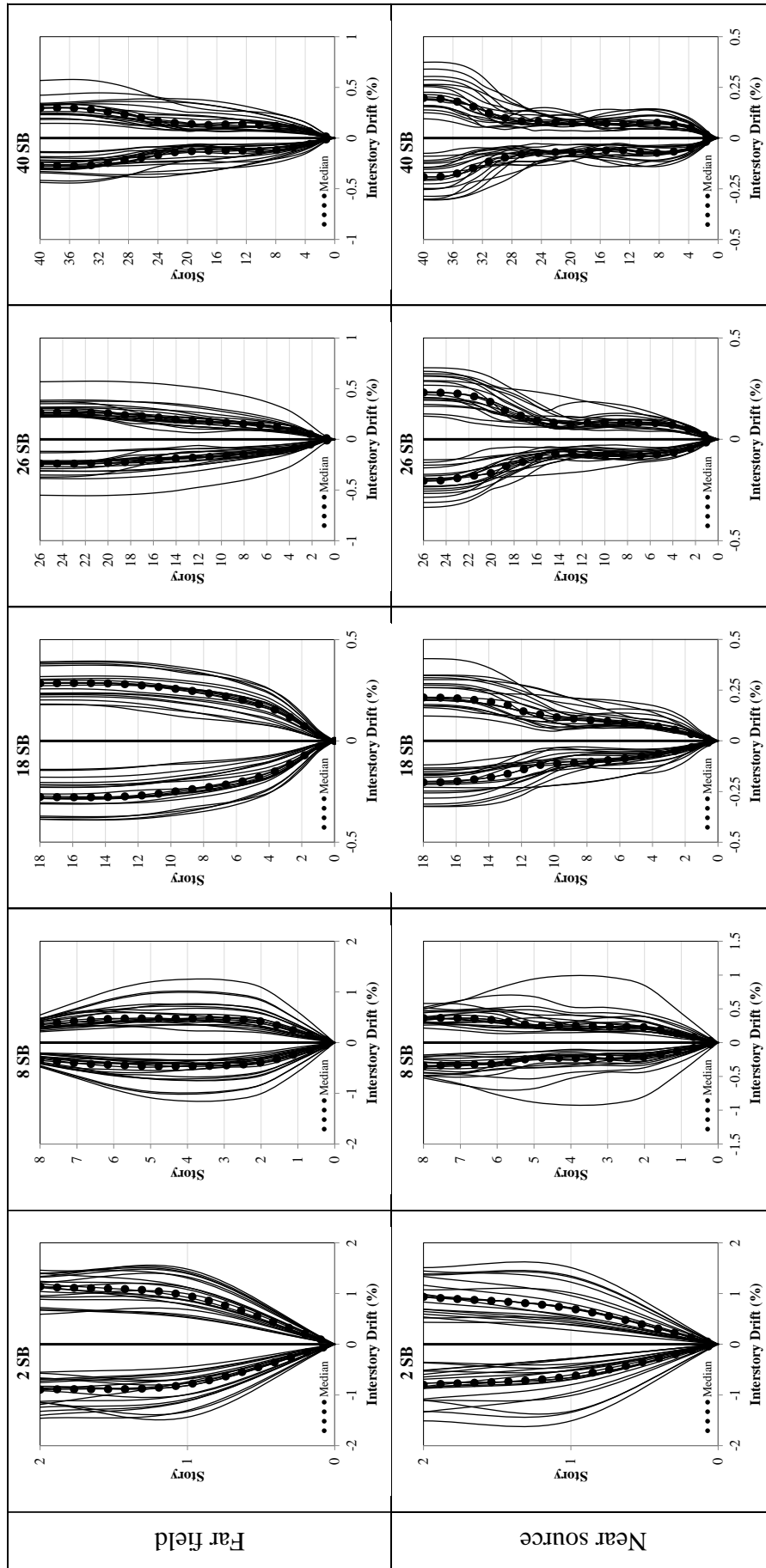


Figure 5.12: Distributions of maximum IDRs for the five pre-code structures from IDA under forty earthquake records scaled to twice the design (0.32g for near-source records) and half the design (0.08 for far-field records) earthquake intensity.

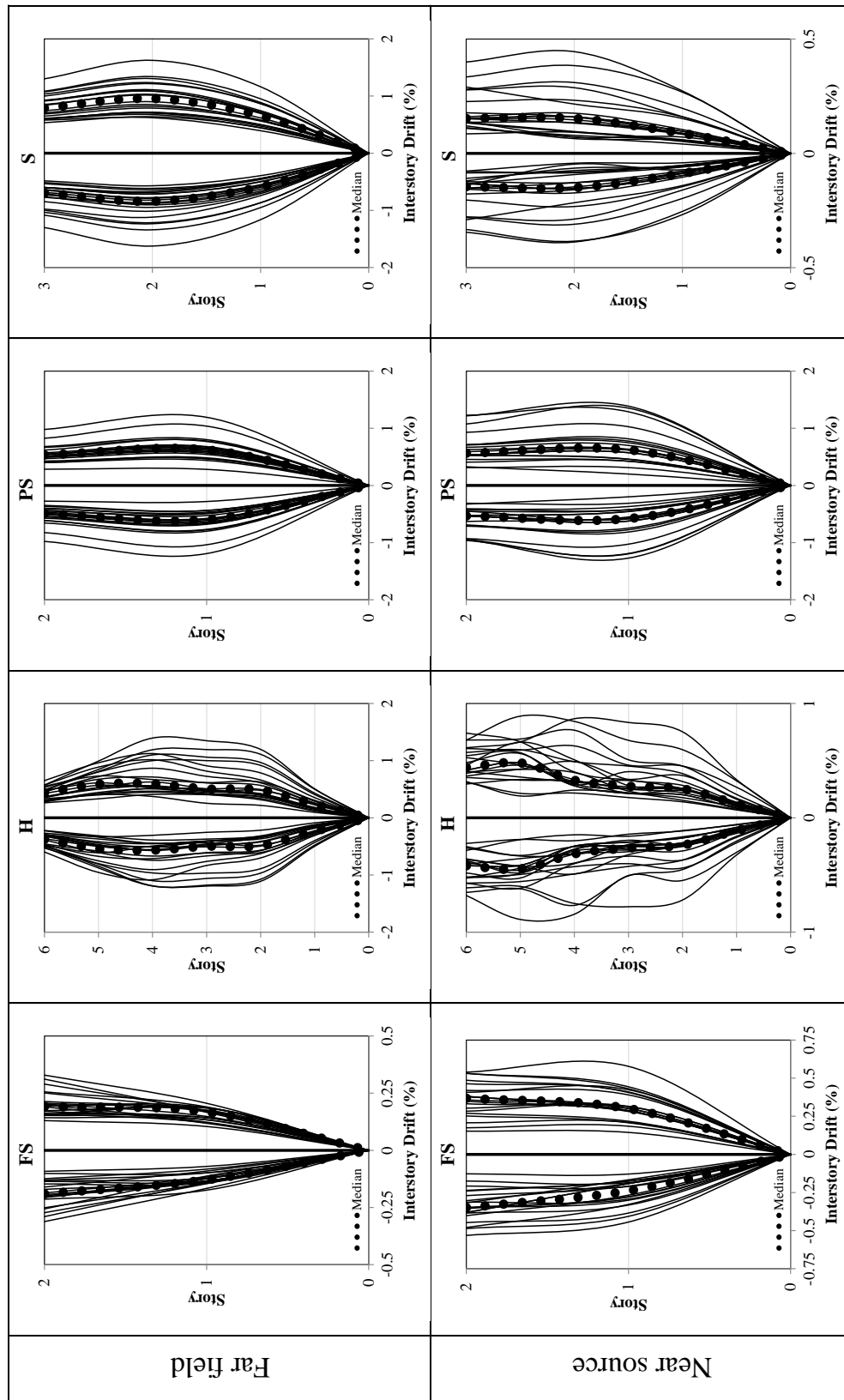


Figure 5.13: Distributions of maximum IDRs for the four emergency facilities from IDA under forty earthquake records scaled to twice the design (0.32g for near-source records) and half the design (0.08 for far-field records) earthquake intensity.

5.5 Performance Criteria

Seismic performance criteria for structures, which are related to the level of non-structural and structural damage, have received attention in recent years. Therefore defining reliable performance criteria is critical when performing a fragility analysis. Recent studies and design guidelines have used IDR for the evaluation of structural damage. Design guidelines provide a detailed description of the expected structural damage at each performance level (e.g. ASCE/SEI-41, 2013). Damage patterns and failure modes are influenced by the relative size and aspect ratio of components that include frames, shear walls and other core systems as well as the overall configuration of the building. The analytical fragility assessment requires a suitable way to track damage patterns for the evaluation of system response. The performance criteria considered in this study are Collapse Prevention, (CP) Life Safety (LS) and Immediate Occupancy (IO), as discussed in Chapter 2 (ASCE/SEI-41, 2013; SEAOC, 1999).

Studying the structural performance at both the global and local response levels provides a clear understanding of the behavior of the structure during an earthquake. The local and global seismic behavior of the reference structures are therefore assessed using IPA and IDA to provide insights into performance limit states. Along with a comprehensive literature review on performance limit states, extensive post processing of the time history analysis results was performed in order to select acceptable values, taking into consideration refined approaches for seismic performance assessment. These assessment methods and approaches are described in detail in subsequent sections.

5.5.1 First Yield and Crushing using IPA

Figure 5.3 to Figure 5.5 depict the IPA results, including mapping the local response with the global capacity envelopes for the nine reference buildings. The global yielding and first concrete crushing are shown in the abovementioned figures. Figure 5.8 to Figure 5.11 show a wide spread of plastic hinges for the nine reference buildings unlike concrete crushing which is limited to certain locations. The concrete crushing is observed at a high level of loading mainly at the foundation levels and at the capacity changes of vertical elements. Despite considering wind loads in the design, the results show the wide spread of plastic hinges of pre-seismic code buildings. On the other hand, emergency facilities show fairly good performance and fewer numbers of plastic hinges, particularly in vertical elements, as a result of adopting design provisions and higher risk category.

5.5.2 Strength Degradation using IPA

A 10% reduction in ultimate strength is considered as an approach to define the CP limit state. This approach was proposed by Park (1988) and implemented in previous studies (e.g. Mwafy & Elnashai, 2001). As shown from Figure 5.3 to Figure 5.5, this condition was not satisfied in the reference structures except for the pre-code frame buildings. Shear wall structures do not reach such degradation in strength due to their lateral force design to wind loads, which result in large wall and core cross section and reinforcement. Moreover, emergency facilities are designed to modern seismic provisions. Hence, this category of buildings does not experience rapid strength degradation. Figure 5.14 illustrates the 10% strength reduction of the 8-story building which is observed at an IDR of 2.96%.

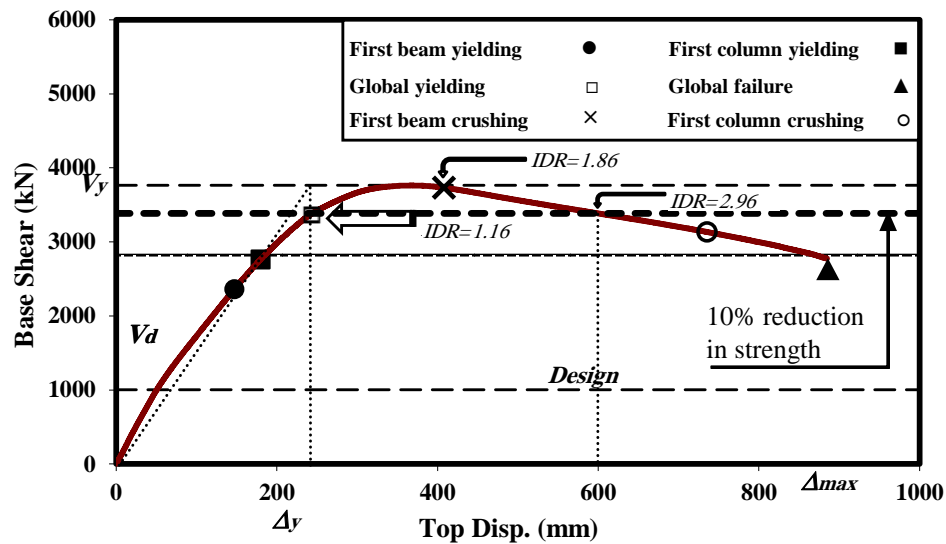


Figure 5.14: 10% reduction in strength for the 8-story building

5.5.3 Shear Response using Time History Analysis (THA)

Acceptable seismic response of RC structures entails that brittle failure modes be prevented. Since it is common practice to depend on the ductile inelastic flexural response of plastic hinges to reduce the strength requirements for structures responding to strong seismic attacks, it is necessary to inhibit the brittle shear failure modes by ensuring that shear strength exceeds the shear corresponding to maximum feasible flexural strength. Exceptional care is needed when plastic hinges form in columns because the shear strength is a function of the flexural ductility. As plastic hinge rotations/curvature increase, the widening of flexure-shear cracks reduces the capacity for shear transfer by aggregate interlock, and the shear strength is reduced (Priestley et al., 1994).

Since pre-code structures lack efficient transverse reinforcement, as they were designed without taking into consideration seismic loads, shear failure may govern the selection of certain limit states. Figure 5.15 and Figure 5.16 present sample results for the shear demand versus capacity of an internal column in the 2 and 8-story buildings, respectively. The results presented are for critical long-period

input ground motions, which are scaled to a high intensity level corresponding to the CP limit state. The experimentally verified shear strength model used to check the shear failure possibility in structural members was proposed by Priestley et al. (1994). The shear strength obtained using the design code is also shown as a reference (BS8110, 1986).

For the 2-story building, the results of the former model clearly show a significant drop in shear strength due to increasing ductility to a level that matches the code shear strength. It is shown from these sample results that the columns of the reference structures are dominated by flexure rather than shear, as the demand does not exceed either of the Priestley or the code shear strength models. It is important to note that to arrive at a final decision regarding the significance, or otherwise, of shear as a controlling failure criterion in seismic loss estimation, a comprehensive shear assessment study using diverse input ground motions and a wide range of buildings with different systems should be undertaken. Such a study is urgently needed for future research.

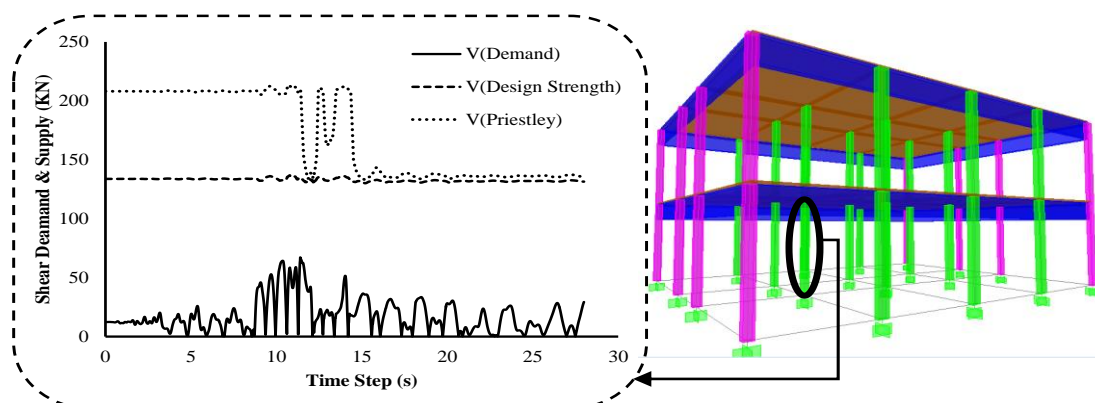


Figure 5.15: Shear response of an internal column in the 2 story building ('Chi-Chi-TAP010' input ground motion and a PGA of 1.5 the design value)

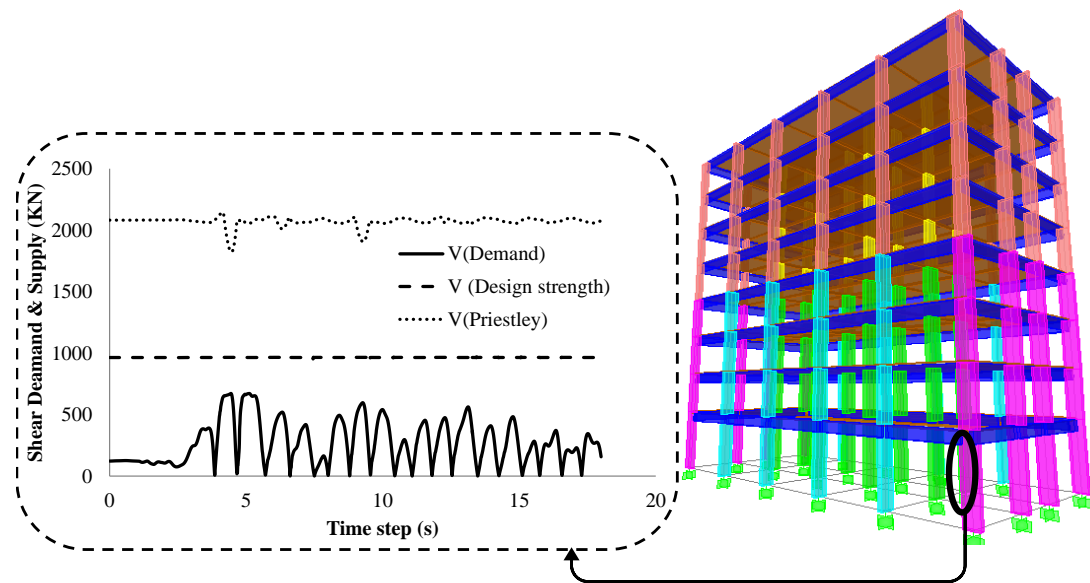


Figure 5.16: Shear response of an internal column in the 8 story building ('Loma Prieta-ggb' input ground motion and a PGA of 2.5 the design value)

5.5.4 First Yield and Crushing using THA

Based on THA, first steel yielding and concrete crushing are monitored and investigated. Post-processors and spread sheets are utilized for monitoring the local and global performance criteria during THA. A representative structure from each building category is investigated as follow: (i) the 8-story building to represent pre-code frame structures, (ii) the 26-story building to represent pre-code shear wall structures, and (iii) the 6-story hospital building to represent emergency facilities. The most critical seismic scenario is considered for obtaining the IDR value associated with the first steel yielding in any structural element, or concrete crushing in confined concrete in vertical elements, which are associated with the IO and CP limit states, respectively. The 16, 50 and 84 percentiles are obtained based on the results of the twenty far-field records. Generally, the 16 percentile is considered in the present study to represent a conservative limit state. Table 5.2 depicts the first steel yielding that occurred in structural elements during THA, which is considered

as the IO limit state, while Table 5.3 illustrates the concrete crushing that occurred in vertical elements which is considered as the CP limit state.

Table 5.2: First steel yielding in three representative reference structures using THA and 20 input ground motions representing far-field seismic scenario

No.	Record ref.	8-story		26-story		Hospital	
		PGA (g)	IDR (%)	PGA (g)	IDR (%)	PGA (g)	IDR (%)
1	FF1	0.08	0.52	0.16	0.31	0.24	0.81
2	FF2	0.08	0.41	0.08	0.34	0.16	1.21
3	FF3	0.16	0.47	0.16	0.34	0.24	1.78
4	FF4	0.16	0.45	0.16	0.33	0.32	0.86
5	FF5	0.16	0.47	0.16	0.33	0.24	0.87
6	FF6	0.16	0.35	0.16	0.33	0.16	0.76
7	FF7	0.16	0.46	0.16	0.35	0.24	0.81
8	FF8	0.16	0.47	0.16	0.28	0.16	0.91
9	FF9	0.16	0.63	0.16	0.37	0.16	1.16
10	FF10	0.08	0.35	0.08	0.17	0.24	1.34
11	FF11	0.16	0.43	0.16	0.34	0.24	0.64
12	FF12	0.16	0.39	0.16	0.31	0.48	1.07
13	FF13	0.16	0.45	0.08	0.32	0.56	1.26
14	FF14	0.08	0.55	0.16	0.31	0.24	0.81
15	FF15	0.08	0.70	0.08	0.33	0.16	0.88
16	FF16	0.08	0.60	0.08	0.33	0.16	1.01
17	FF17	0.08	0.54	0.16	0.32	0.16	1.13
18	FF18	0.08	0.47	0.16	0.31	0.24	0.93
19	FF19	0.08	0.55	0.16	0.35	0.24	0.85
20	FF20	0.08	0.40	0.16	0.30	0.24	1.01
		16 percentile	0.395	16 percentile	0.32	16 percentile	0.773
		50 percentile	0.475	50 percentile	0.39	50 percentile	0.978
		84 percentile	0.571	84 percentile	0.48	84 percentile	1.236

Table 5.3: First confined concrete crushing in vertical elements in three representative reference structures using THA and 20 input ground motions representing far-field seismic scenario

No.	Record ref.	8-story		26-story		Hospital	
		PGA (g)	IDR (%)	PGA (g)	IDR (%)	PGA (g)	IDR (%)
1	FF1	0.24	4.06	0.24	1.044	0.24	3.830
2	FF2	0.16	3.57	0.16	0.565	0.16	2.980
3	FF3	0.24	3.44	0.16	0.495	0.24	1.630
4	FF4	0.32	1.81	0.32	1.015	0.32	3.010
5	FF5	0.24	2.5	0.24	0.626	0.24	3.060
6	FF6	0.16	3.01	0.16	1.261	0.16	2.460
7	FF7	0.24	3.9	0.24	0.880	0.24	3.210
8	FF8	0.16	3.18	0.16	0.688	0.16	3.140
9	FF9	0.16	3.65	0.16	0.536	0.16	2.980
10	FF10	0.24	3.04	0.16	1.008	0.24	3.260
11	FF11	0.24	3.05	0.24	0.747	0.24	3.240
12	FF12	0.48	3.57	0.32	0.880	0.48	3.110
13	FF13	0.56	3.19	0.24	0.588	0.32	2.650
14	FF14	0.24	2.63	0.24	1.218	0.24	3.240
15	FF15	0.16	3.35	0.16	0.565	0.16	3.400
16	FF16	0.16	3.93	0.16	1.037	0.16	3.380
17	FF17	0.16	3.48	0.16	0.956	0.16	2.880
18	FF18	0.24	4.02	0.24	0.846	0.24	3.560
19	FF19	0.24	3.75	0.24	0.495	0.24	2.950
20	FF20	0.24	3.98	0.24	0.956	0.24	2.720
		16 percentile	2.96	16 percentile	1.784	16 percentile	2.91
		50 percentile	3.38	50 percentile	2.271	50 percentile	3.16
		84 percentile	4.00	84 percentile	2.890	84 percentile	3.44

5.5.5 Global Yield and Collapse using IDA Curves

In order to generate the IDA curves, an equivalent time period for each of the nine reference structures is calculated. The equivalent period is used to obtain the corresponding spectral acceleration for the twenty far-field earthquake records. The equivalent periods are calculated from the first three inelastic periods weighted by the mass participation ratios obtained from a Fourier analysis of the top inelastic response (Table 5.4), (Al Waile et al., 2014). Vamvatsikos and Cornell (2002b) proposed an approach for estimating the IO and CP limit states from IDA curves. In this method, the IO limit state is at the first slope change in the linear part of the curve. The CP performance criterion is set at a 20% reduction in slope. Figure 5.17 shows the IDA curves for three representative buildings.

Table 5.4: Equivalent periods for nine reference structures

Building	Elastic period			Mass Participation (MP, %)			ΣMP (%)	Inelastic period at the design earthquake value			T _{eq} *
	T1	T2	T3	Mode1	Mode2	Mode3		T1	T2	T3	
2-St	0.78	0.28	--	96	4	--	100	1.71	0.50	--	1.66
8-St	1.34	0.42	0.22	79	11	5	94.74	2.73	0.86	4.54	2.61
18-St	1.43	0.33	0.13	69	16	5	90.75	2.73	0.71	0.33	2.24
26-St	2.37	0.59	0.25	67	17	6	89.88	3.94	1.04	0.50	3.18
40-St	3.90	1.07	0.48	63	16	7	86.42	6.83	1.79	0.78	5.41
FS	0.75	0.18	--	93	7	--	99.97	0.94	0.23	--	0.89
PS	1.29	0.17	--	93	7	--	99.95	1.15	0.31	--	1.10
SC	0.66	0.23	0.12	86	12	2	99.96	1.53	0.40	0.18	1.36
HO	0.82	0.60	0.22	72	14	4	90.18	2.73	0.76	0.49	2.31

$$*T_{eq} = \sum T_i * MP_i$$

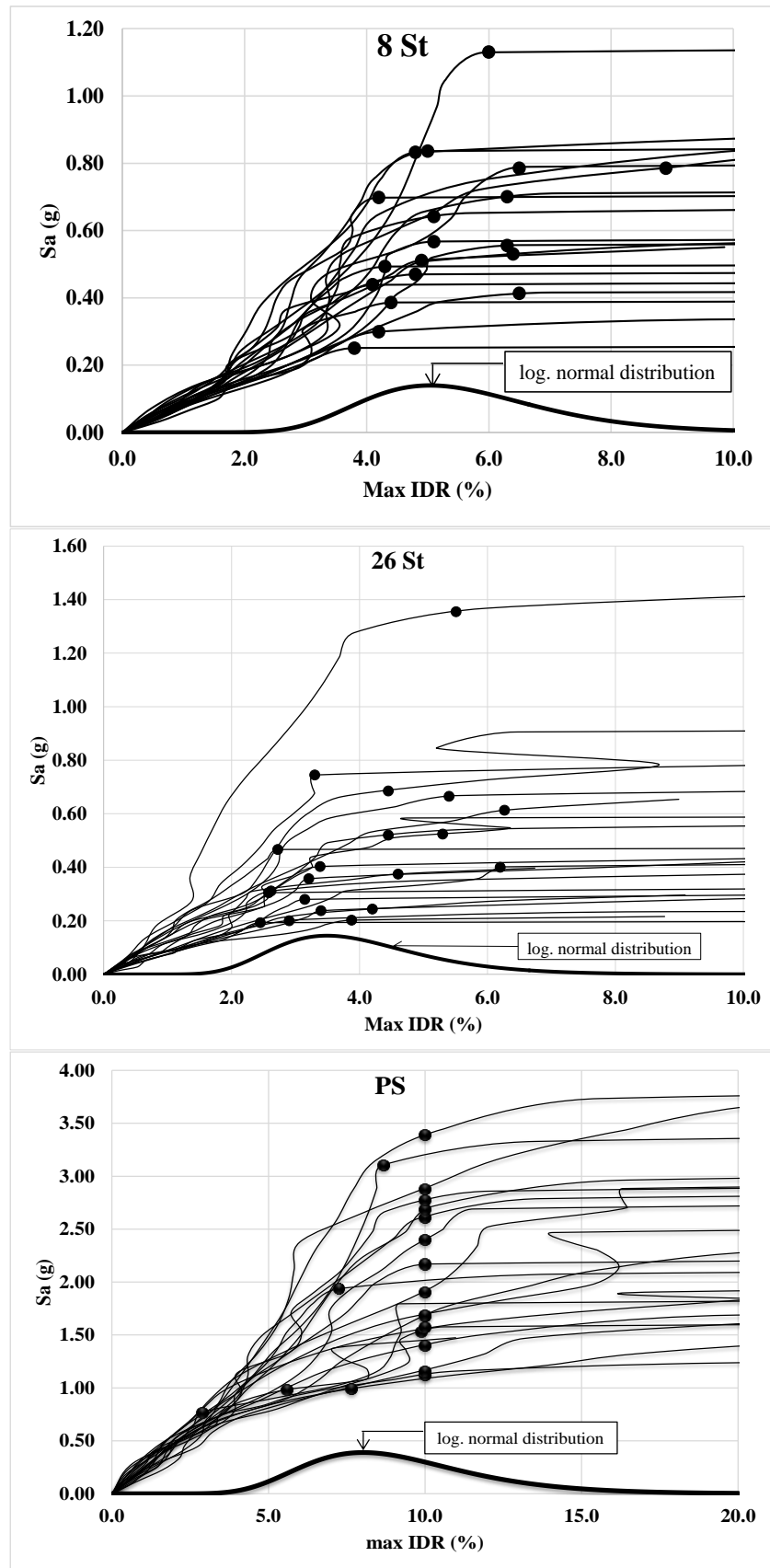


Figure 5.17: CP limit states for three representative buildings using 20 far-field records

5.5.6 Selection of Limit States

The performance criteria adopted in the present study takes into consideration the results presented in previous sections as well as those recommended by the code provisions and previous experimental and analytical studies presented in Chapter 2, as follows:

- For the pre-code frame and wall structures, the IO limit states are determined from the IDA curves based on the 16 percentile of the IDR at the first indication of non-linear response (Vamvatsikos & Cornell, 2002a).
- The IDA results indicated a significantly higher limit states compared with previous studies. Hence, the CP limit state of pre-code frames is determined based on the first crushing in confined concrete and 10% strength reduction of ultimate capacity, which are obtained from THA and IPA, respectively (Mwafy & Elnashai, 2001; Park, 1988). The strain corresponding to the crushing of confined concrete is obtained as per Mander et al. (1988).
- For the pre-code wall structures, the CP performance limit state is determined from THA based on the 16 percentile of the IDR at the first indication of crushing in the confined concrete of shear walls. The THA results are considered since this analysis is more reliable compared with IPA for high-rise structures.
- For emergency facilities, the IDA results indicated significantly higher limit states compared with previous studies (Dymiotis et al., 1999; Ghobarah et al., 1999a). Therefore, the IO limit state is selected based on the conclusions of design provisions and a previous study that covered a wide range of well-designed structure with different characteristics (ASCE/SEI-41, 2013; Ashri & Mwafy, 2014).

- The CP limit state is determined according to the statistical analysis of several previous test results (Dymiotis et al., 1999).
- Finally, the LS performance level is generally considered 50% of the CP value (ASCE/SEI-41, 2013).

Table 5.5 summarizes the literature review and results of the present study, which are used to select different limit states. All of the selected performance criteria are consistent with the results obtained from the current study, previous experimental studies (e.g. Dymiotis et al., 1999; Ghobarah et al., 1998; Wood, 1991); previous analytical studies (Ghobarah et al., 1999a; Liel et al., 2010; Ramamoorthy et al., 2008), and the code provisions (ASCE/SEI-41, 2013).

Table 5.5: Summary of IDRs corresponding to different limit states

Selection Approach		Reference Structure								
		Pre-code Frames			Pre-code Walls			Emergency Facilities		
		Limit State - Interstory Drift Ratios, IDRs (%)								
		IO	LS*	CP	IO	LS*	CP	IO	LS*	CP
ASCE-41, 2007		0.50	1.00	2.00				1.00	2.00	4.00
Experimental studies	Ghobarah, 1998	1.00	2.00	3.28						
	Wood, 1991 - 16%						1.36			
	Wood, 1991 - 50%						1.88			
	Wood, 1991 - 84%						2.60			
	Dymiotis et.al., 1999 - 16%									1.90
	Dymiotis et.al., 1999 - 50%									4.00
	Dymiotis et.al., 1999 - 84%									6.70
Analytical studies	Ghobarah et.al., 1999	0.70	1.10	2.50				0.40	1.80	3.00
	Ramamoorthy et.al., 2008 - 16 %	0.33		0.56						
	Ramamoorthy et.al., 2008 - 50 %	0.50		0.98						
	Ramamoorthy et.al., 2008 - 84 %	0.75		1.71						
	Liel et.al., 2010 - 16 %			3.26						
	Liel et.al., 2010 - 50 %			4.17						
	Liel et.al., 2010 - 84 %			5.34						
Current study	IPA, first yield and crushing	0.67		3.74	0.33		1.59	0.85		3.67
	IPA, 10% strength reduction			2.96						
	THA - 16%	0.40		2.96	0.32		1.78	0.77		2.91
	THA - 50%	0.48		3.38	0.39		2.27	0.98		3.16
	THA - 84%	0.57		4.00	0.48		2.89	1.24		3.44
	IDA - 16%	0.39		4.13	0.34		2.83	0.65		6.49
	IDA - 50%	0.57		5.43	0.62		3.83	1.00		8.79
	IDA - 84%	0.84		7.14	1.13		5.18	1.54		11.9
Selected Limit State		0.39	1.48	2.96	0.34	0.89	1.78	1.00	2.00	4.00

IO: Immediate Occupancy, LS: Life Safety, CP: Collapse Prevention

IPA: Inelastic Pushover Analysis, THA: Time History Analysis, IDA: Incremental Dynamic Analysis

* LS limit state is considered 50% of the CP counterpart

5.6 Derivation of Fragility Relationships using IDA

The fragility curve is a plot of the PGA along the horizontal axis versus the probability of exceedance along the vertical axis. Fragility curves account for the uncertainty and variability related to capacity and demand. These relationships are substantial for the assessment of monetary losses and taking seismic retrofit decisions. The possible approaches for deriving fragility curves were discussed in Chapter 2. It was concluded that generating damage data using inelastic multi-degree-of-freedom simulations is the most accurate and cost-effective option. Hence, this approach is adopted in the current study. In terms of time and effort, this option is computationally demanding since a large number of analyses are required in order to represent the ground motion uncertainty.

Fragility curves can be directly incorporated with seismic hazard maps and inventory data using earthquake loss estimation software to provide a tool for formulating risk reduction policies. The following six constituents are needed for deriving fragility relationships:

- (i) Selection and design of reference structures;
- (ii) Developing of analytical models and selection of analysis procedure;
- (iii) Uncertainty modeling and selection of input ground motions;
- (iv) Selection of performance criteria;
- (v) Selection of an approach for deriving fragility functions; and
- (vi) Selection of scaling approach.

The first five components were already covered in detail in Chapters 2 to 5. Several intensity measures were used and employed in previous studies such as the design PGA, Spectral Acceleration (S_a), and Spectral Displacement (S_d). The input ground motions are scaled in the present study using their PGA, which is selected as the input ground motion intensity for deriving vulnerability relationships. Scaling

earthquake records using their PGAs in the inelastic simulations relates the seismic forces directly to the input accelerations. This simple scaling approach agrees with the method adopted by design codes, and therefore used in several previous studies (ASCE-7, 2010; Kwon & Elnashai, 2006; Mwafy et al., 2014a; Mwafy, 2012b)

To account for the input ground motion uncertainty, forty natural ground motions (20 far-field and 20 near-source) were selected in the present study to represent the most critical seismic scenarios in the study region, as explained in Chapter 4. For the derivation of vulnerability relationships using IDAs, the nine analytical models of the reference structures are combined with the forty input ground motions. Each input ground motion is scaled to different intensity (PGA) levels. The inelastic response history analyses are carried out for the nine reference structures up to the fulfillment of the IO, LS and CP performance levels discussed earlier. A PGA scaling increment of 0.08g, which corresponds to half the design earthquake and 0.32g, which corresponds to twice the design PGA, are selected for far-field and near-source records, respectively. To attain all limit states, more than fourteen analyses are conducted for each building-input ground motion in each of the two seismic scenarios, starting from a PGA of 0.08g and ending with a PGA of 1.20g for far-field records, and from 0.32g to 4.8g for near-source records.

A large number of IDAs are performed to develop the fragility functions of the nine reference structures. The developments of plastic hinges and concrete crushing in various structural elements are traced. In addition, monitoring global response parameters such as IDR, top displacement and base shear is conducted in order to provide more understanding into the level of structural damage. As shown in Figure 5.18, 280 response points (PGA versus IDR) are plotted for each of the nine buildings from each seismic scenarios. Response results recorded far beyond collapse were excluded in the regression analysis and the development of fragility curves.

Regression analyses were performed for IDA results to develop fragility relationships.

Figure 5.18 shows the statistical distributions employed to estimate the probability of exceeding each of the selected limit states at different ground motion intensity levels. The vulnerability curves are generated by plotting the probability values versus PGAs. The fragility relationships of the reference structure are shown in Figure 5.19. The results show that the steepness of the fragilities decreases as the limit state changes from IO to CP. For pre-seismic code buildings, the probability of exceeding different limit states is higher for low-rise frame buildings. This indicates that earthquakes have less impact on high-rise wall structures. This statement is confirmed under the effect of both severe distant and moderate close events. This is attributable to the efficiency of shear walls in controlling drift and to the lower contribution of the fundamental mode of vibration to seismic response with an increase in the building height.

The vulnerability curves generally reflect the differences between the fragilities obtained from the two seismic scenarios (far-field and near-source) employed in the present study. Under the effect of the far-field ground motions, the slopes are sharper and the probability of exceeding various limit states is much higher compared with near-source events. This is more pronounced in the pre-code frame structures. The seismic response of the pre-code high-rise buildings (i.e. 18, 26 and 40 stories) is acceptable at the design PGA when subjected to the near-source records, as shown in Figure 5.19 (f, h and j). The results confirm that the earthquake scenario has a significant influence on the seismic risk of multi-story buildings. These findings support the observations discussed above about the higher vulnerability of the pre-code buildings to severe distant earthquakes compared with moderate close events. The low impact of short-period records on seismic

performance is noticeable for all reference buildings, and it follows the findings of previous analytical studies (e.g. Mwafy, 2012b). At the design PGA level, the four emergency facilities show satisfactory seismic performance under all seismic scenarios, with a higher impact from far-field records.

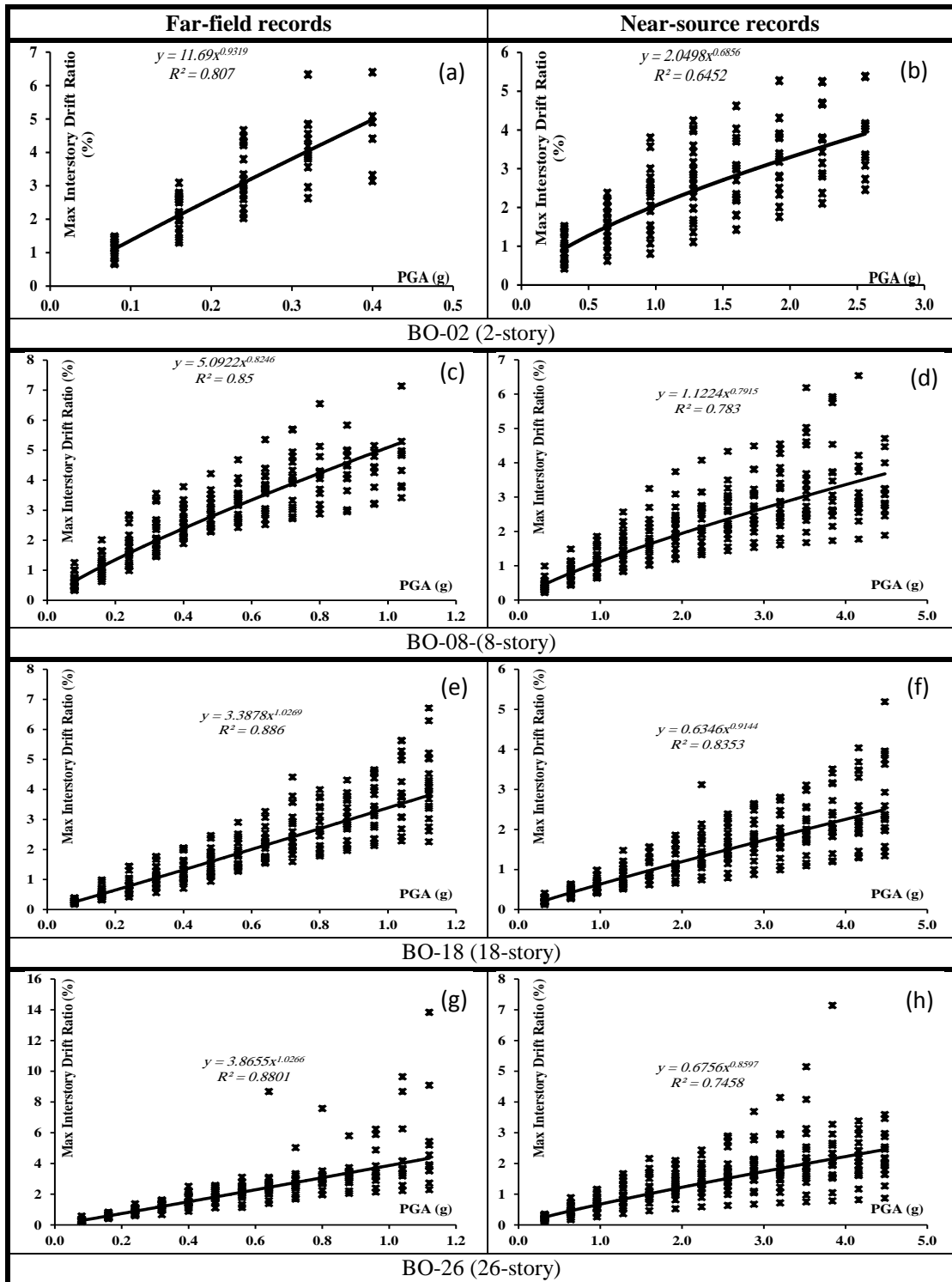


Figure 5.18: IDA results of the nine reference structures obtained from forty input ground motions along with the power law equations

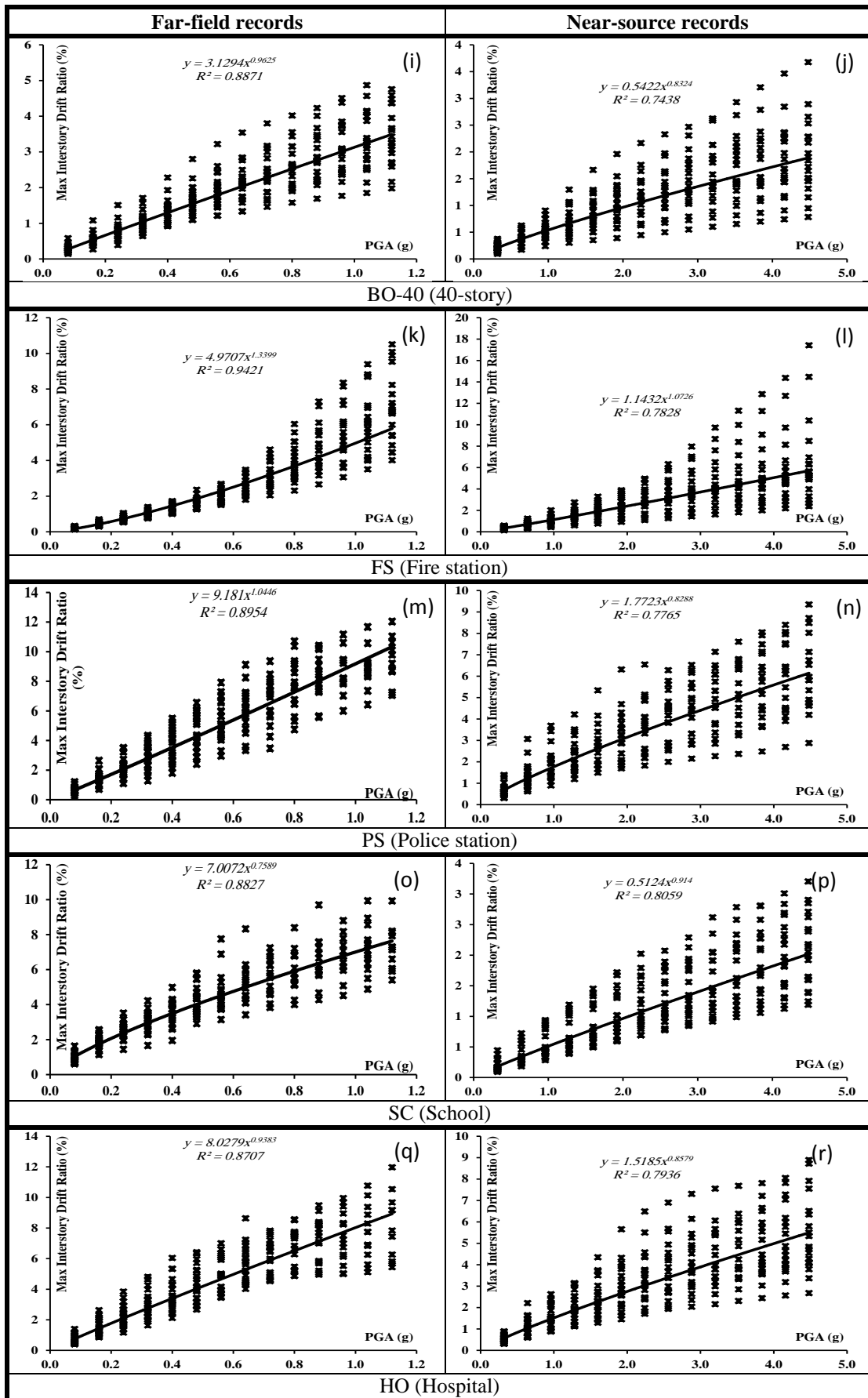


Figure 5.18 (cont'd): IDA results of the nine reference structures obtained from forty input ground motions along with the power law equations

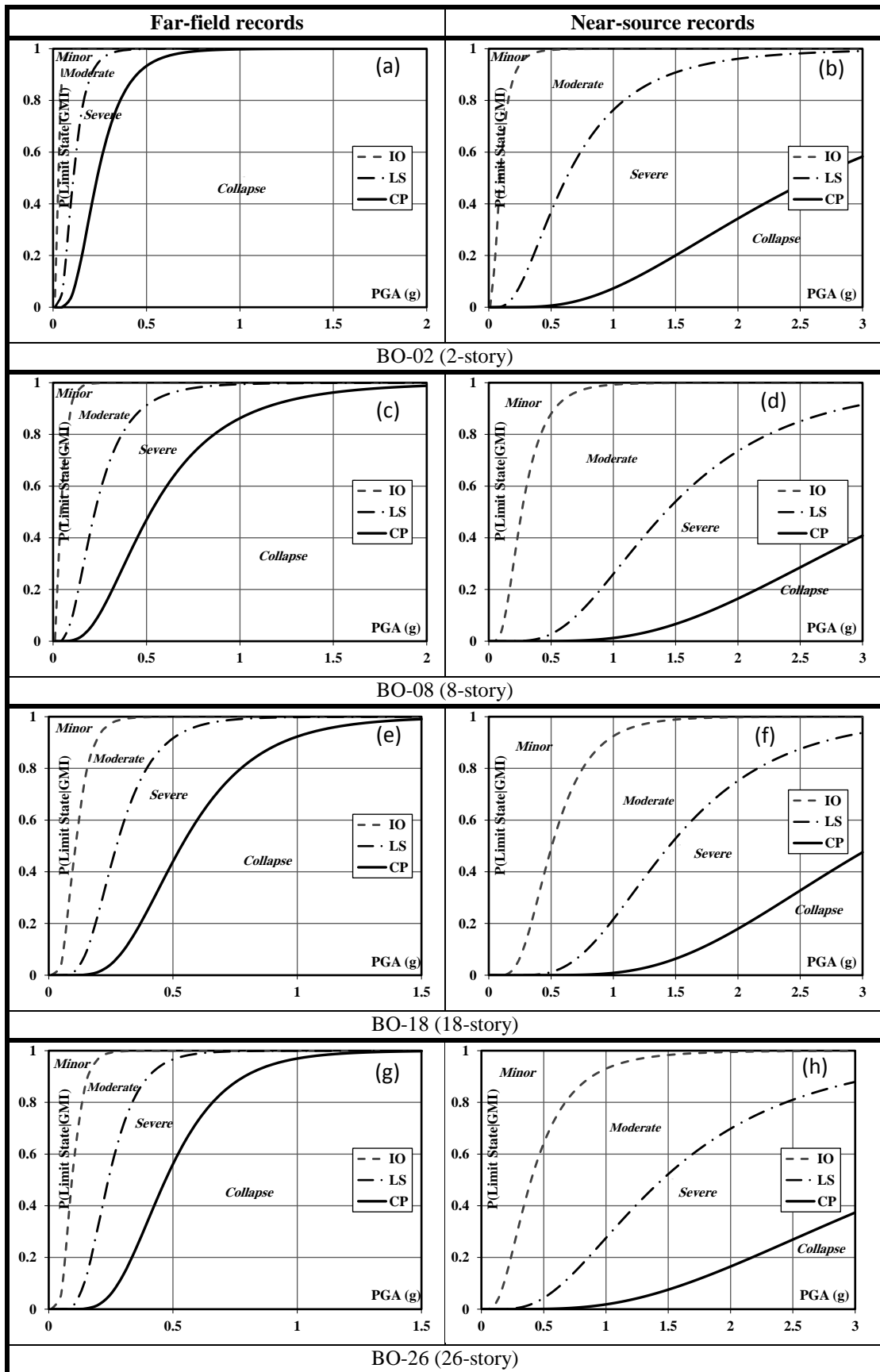


Figure 5.19: Fragility relationships of the nine reference structures obtained from IDAs

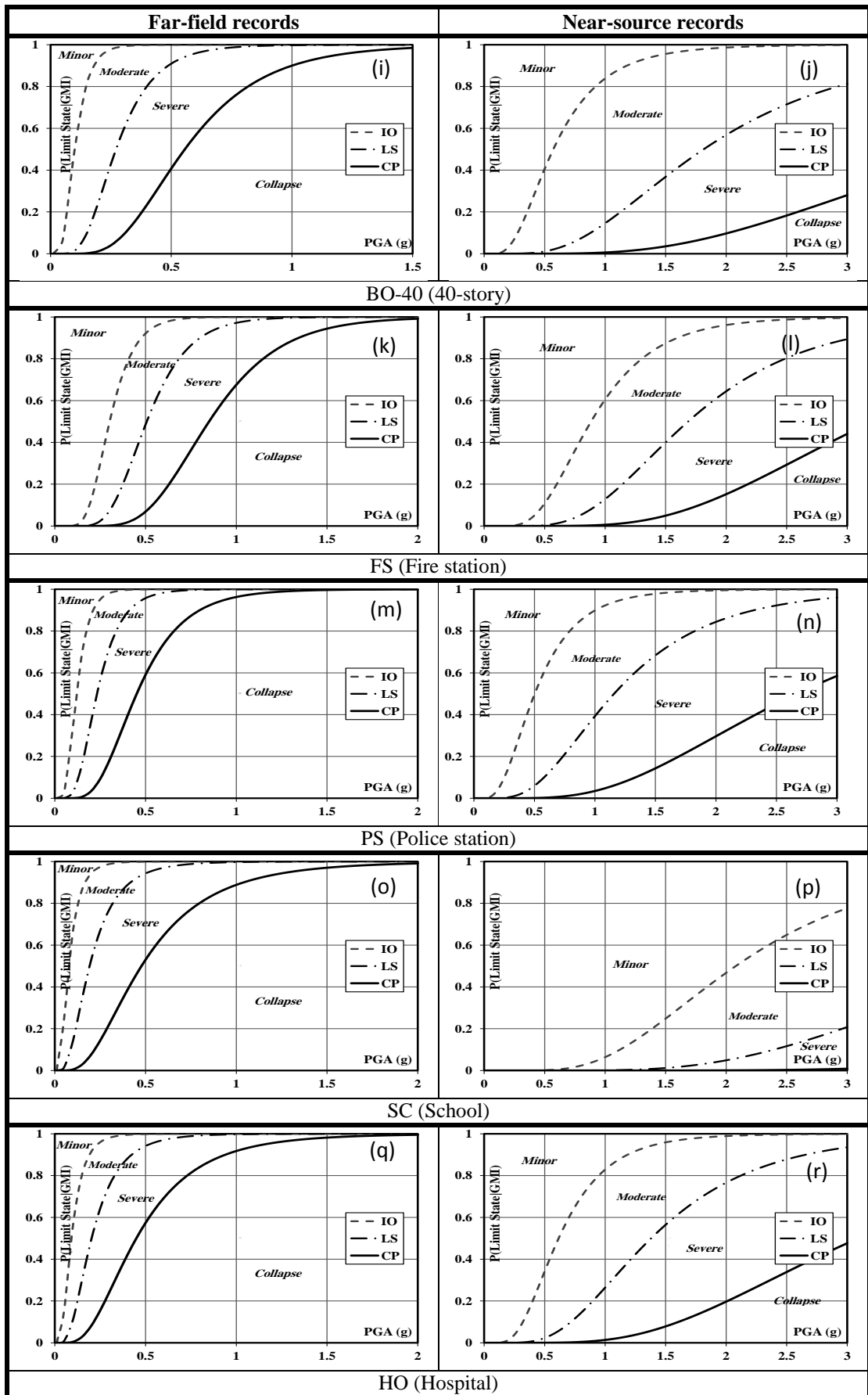


Figure 5.19 (cont'd): Fragility relationships of the nine reference structures obtained from IDAs

To provide more representative results from the derived fragility curves, limit state probabilities are estimated at the design and twice the design PGAs for far-field earthquake records, and at twice and four times the design for near-source records (Figure 5.20 and Figure 5.21). Two main observations are evident: pre-code structures are significantly more vulnerable compared with emergency facilities. Moreover, far-field records have much higher impact on the reference structures over the near-source records. The large increase in the probabilities of various limit states is also clear when the PGAs are doubled (i.e. twice and four times the design intensities for far-field and short-period records, respectively). The results presented in Figure 5.19 and Figure 5.20 reflect the need for seismic rehabilitation of pre-code structures to prevent collapse. Also, in spite of the good performance of modern code designed emergency buildings, and taking into consideration their important role during and after an earthquake, it is preferable to perform a precautionary retrofit for such facilities to minimize seismic losses.

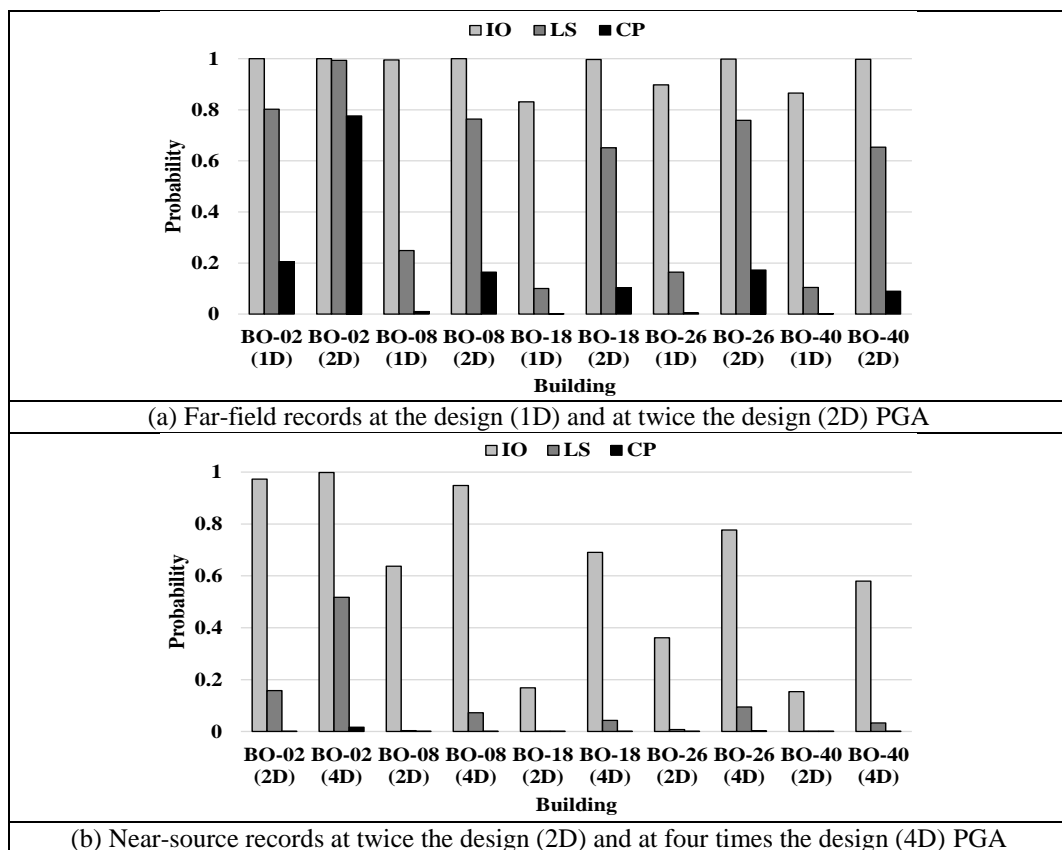


Figure 5.20: Limit state exceedance probabilities of the pre-code reference buildings

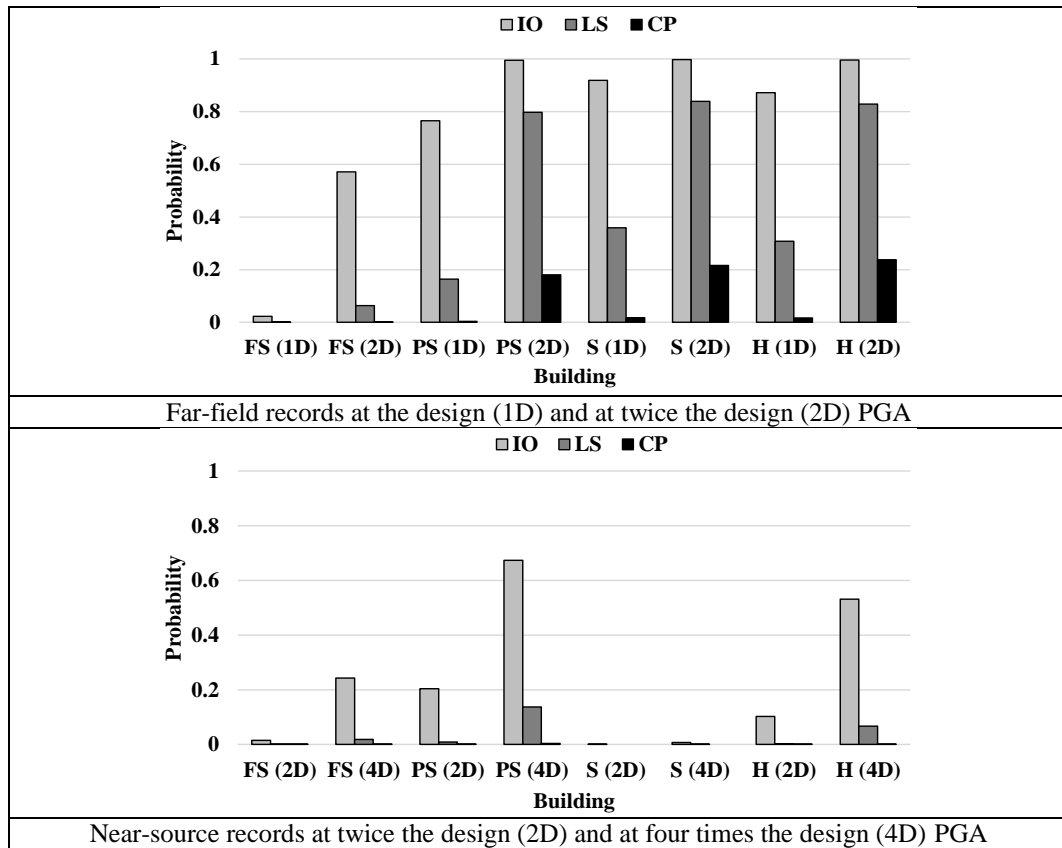


Figure 5.21: Limit state exceedance probabilities of the emergency facilities reference buildings

As discussed in Chapter 2, simulation-based fragility curves can be generated either using simplified methods such as the inelastic pushover analysis or by employing a more comprehensive methods such as the incremental dynamic analysis. The latter approach is adopted in the current study due to its ability to account for several sources of uncertainty such as the variability in ground motions and modeling approaches. A number of previous seismic vulnerability assessment studies were directed towards deriving fragility curves based on a simplified approach (e.g. Bilgin, 2013; Borzi et al., 2008; Giovinazzi et al., 2006; Kappos & Panagopoulos, 2010; Moharram et al., 2008; Polese et al., 2008; Rossetto & Elnashai, 2005).

For instance, Borzi et al. (2008) presented a simplified pushover-based method for the development of vulnerability curves for gravity load designed RC frame buildings. The definition of whether or not a building survives a limit

condition was based on displacements, which were correlated with building damage. It was emphasized in the above-mentioned study that further research is still required before the methodology is applicable to full-scale loss assessment applications. Figure 5.22 shows a sample fragility curves for two structures that are comparable to those investigated in the present study, namely BO-02 and BO-08.

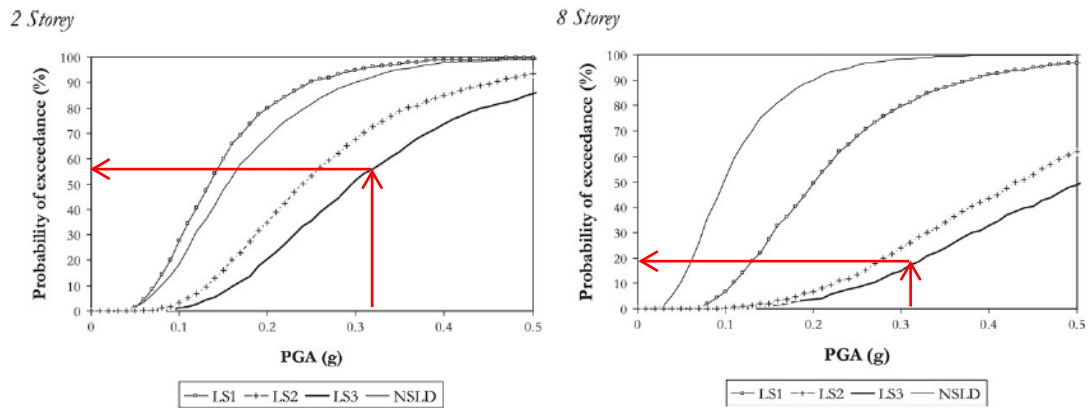


Figure 5.22: Developed fragility curves for comparable 2 and 8-story frame pre-code structures (Borzi et al., 2008)

The study of Borzi et al. (2008) was selected to provide a simple comparison between the fragility curves developed using simplified approaches with those developed using the detailed modeling and analysis techniques adopted in the present study due to the common formats of the fragilities of the two studies. It was shown in Figure 5.22 that at a PGA of 0.32g the probability of exceeding the CP limit state is 0.55 and 0.19 for the 2 and the 8-story buildings, respectively. The results of the present study confirm that for the far-field records the probability of exceeding the CP limit state at a PGA of 0.32g is 0.79 and 0.17 for the 2 and 8-story buildings, respectively. On the other hand, for the near-source input ground motions, the probability of exceeding the CP limit state at a PGA of 0.32g were marginal for the 2 and 8-story buildings, as shown in figures 5.19 and 5.20. It is clear that the Borzi et al. (2008) results are consistent with the findings of the present study in terms of the

higher vulnerability of low-rise structures. Moreover, the probabilities of exceeding the CP limit state from the above-mentioned study were between the values obtained in the present study from the far-field and near-source seismic scenarios. The comparison clearly shows the advantages of the detailed modeling and analysis approaches implemented in the present study, which account for several sources of uncertainty as well as the impact of different seismic scenarios on fragilities.

5.7 Concluding Remarks

The nine reference structures were subjected to a series of Eigenvalue analyses, IPAs and IDAs to assess their seismic performance. These analyses were performed using detailed fiber-based numerical models to predict the inelastic seismic demands of the reference buildings. In total, over 5000 inelastic multi-step analyses of nine multi-degree-of-freedom systems were performed. Additional analyses were performed to assess the vulnerability of the structures that proved to have unsatisfactory performance, and hence were retrofitted using different mitigation techniques.

The response of the nine reference structures at different limit states was investigated thoroughly using IPA under lateral load patterns recommended by the design provisions and previous studies. The lateral capacities, IDRs, plastic hinges and shear capacities were observed and investigated. For emergency facilities, the first indication of steel yielding was observed in horizontal members followed by vertical members. This is in agreement with the strong-column weak-beam code concept of having energy dissipation concentrated in horizontal elements. Pre-code structures lack this concept, especially the low-rise ones, and hence resulted in poor performance. Mapping of plastic hinges for the nine reference structures showed

significantly better performance for the emergency facilities over the pre-code structures, which was reflected on the total number of plastic hinges particularly in vertical elements.

It was noted from the IDA results that the use of diverse input ground motions produced a marginally different maximum IDRs in the same scenario, while produced significantly different IDRs when comparing the two earthquake scenarios with each other. Significantly higher IRDs were recorded in the pre-code structures due to their poor performance and the lack of sufficient seismic detailing. This caused the spread of plastic hinges in horizontal and vertical elements, leading to the formation of story mechanisms. In order to derive the fragility relationships of the reference structures, three limit states were selected and defined based on extensive inelastic analysis results as well as values recommended in previous analytical and experimental studies and code provisions. The IDA results were utilized to derive a wide range of fragility relationships under two seismic scenarios.

The limit state exceedance probabilities were evaluated in order to provide insights into the safety margins of the reference structures. Far-field records represented the worst case scenario compared to near source events. Pre-code structures were significantly more vulnerable compared with emergency facilities. A large increase in the limit states exceedance probabilities was observed when the design input ground motion was doubled. The results reflected the need of seismic rehabilitation for pre-code structures to reduce the probability of collapse, and for certain emergency facilities to improve their seismic performance and ensure their continuous service following a strong earthquake.

CHAPTER 6: PERFORMANCE ASSESSMENT OF RETROFITTED STRUCTURES

6.1 Introduction

It was shown in Chapter 5 that the performance of existing pre-seismic code RC frame and wall buildings in the UAE may not meet the recommended objectives, particularly for low-rise structures under far-field seismic events. Moreover, emergency facilities showed certain levels of damage associated with far-field events at twice the design intensity value that will require precautionary retrofit to minimize their seismic losses and ensure their continuous performance during and after earthquakes. Several retrofit strategies are available to enhance the main parameters related to the seismic performance of buildings, namely strength, stiffness and ductility. In order to achieve the desired strength of structures, certain targets have to be met. Selected reference structures with inadequate response are retrofitted in the current study to achieve the desired seismic performance. A number of steps should therefore be followed to meet this objective, including (Figure 6.1):

- (i) Set and define the new target design objective;
- (ii) Obtain most conservative spectral acceleration values from code spectrum and relevant seismic scenarios;
- (iii) Select a suitable retrofit technique, apply new seismic loads and redesign; and
- (iv) Verify the retrofitted structure.

In this study, four retrofit techniques are considered, namely, (i) FRP wrapping of columns; (ii) RC jacketing of columns; (iii) adding BRBs to RC frames and (iv) adding EUSP to shear walls and core walls.

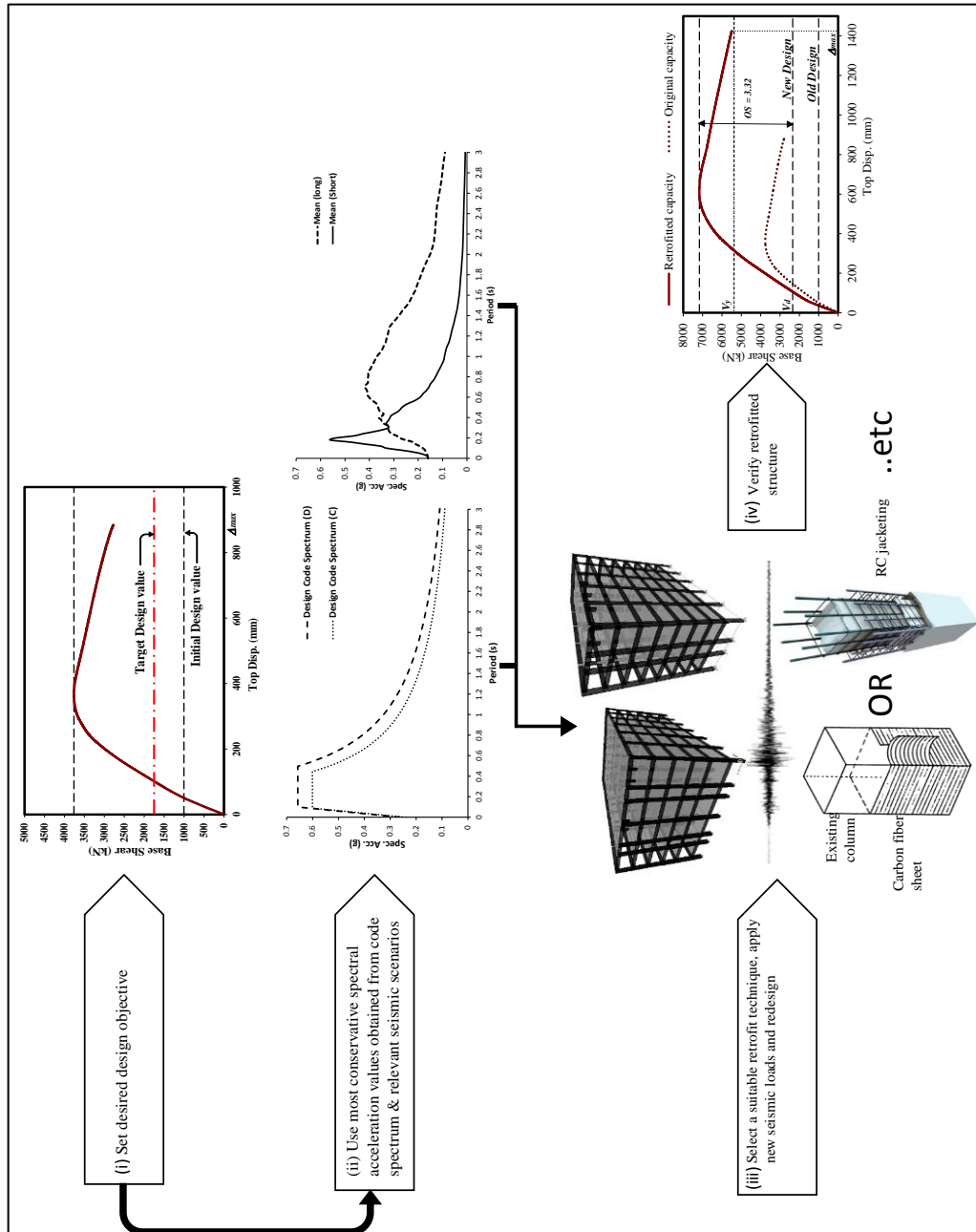


Figure 6.1: Proposed retrofit approach

6.2 Design of Strengthening Techniques

Different retrofit techniques were designed in order to obtain the desired target response. Because of their impact in providing lateral stability and gravity load resistance, the major focus for determining a realistic retrofit approach is mainly dependent on vertical members. FEMA-547 (2006) discussed two retrofit techniques among others, namely RC jacketing and FRP wrapping of columns, which are applicable to the deficiencies in global strength and stiffness. The RC jacketing approach is applicable to strength and stiffness deficiencies, and to the lack of strong column-weak-beam detailing. FRP wrapping of columns primarily improves shear strength and confinement. Two other retrofit techniques were recommended in previous studies and hence considered in the present study, namely adding BRB and EUSP to frames and shear walls, respectively (Di Sarno & Manfredi, 2010; Fahnestock et al., 2007; Taghdi et al., 2000; Tremblay et al., 2004). The above mentioned techniques were applied for the reference buildings depending on their efficiency and suitability.

6.2.1 RC Jacketing

Enlarging the existing column cross-section with a new RC jacket is an effective retrofit technique, yet a conventional one. The surface of the existing concrete should be roughened, then dowels are drilled into the existing concrete to achieve the required composite action. After installing transverse and longitudinal reinforcing steel around the existing column, the concrete jackets are constructed using cast-in-place concrete. Figure 6.2 shows a typical retrofit of rectangular columns. Some of the drawbacks of this retrofit method include the need for formwork and the difficulties in casting and vibrating due to access limitations at the

top of the column. Besides, major disturbance to occupants and the close of the buildings in some cases represent additional shortcomings for this technique.

Upgrading a deficient concrete column using this conventional method enhances the lateral resistance of moment resisting frames because of the increase in the column-to-beam strength ratio. In the current study, RC jacketing is applied to the 2, 8-story and hospital buildings. The design of the RC jackets is dependent upon the required strength. For the 2 and 8-story buildings, all columns are enlarged to achieve the required strength as per the code recommendations (ASCE-7, 2010). On the other hand, only internal columns are enlarged in the case of the hospital building to achieve this value since this emergency facility was already designed to seismic code provisions. The precautionary retrofit of the reference hospital is intended to improve its seismic performance to ensure its continuous operation. Table 6.1 depicts the design summary of RC jacketing for three reference structures, while Figure 6.3 to Figure 6.5 illustrate the retrofitted column cross-sections.

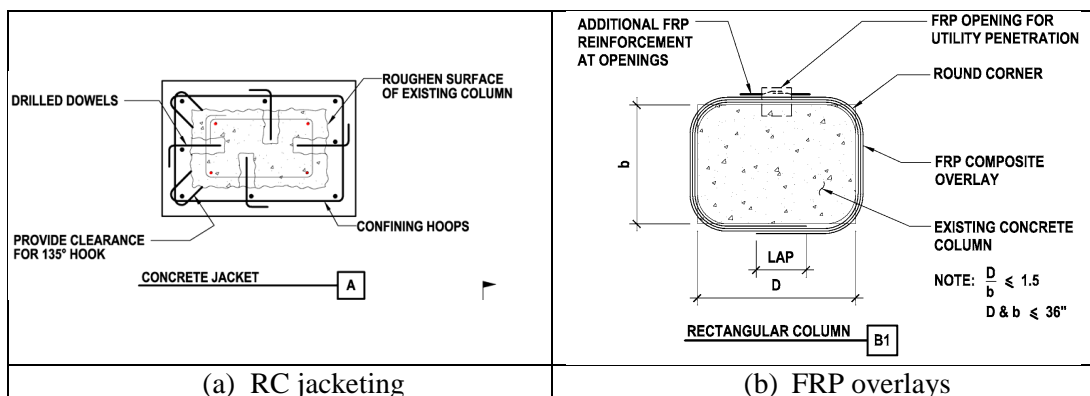
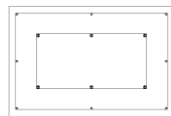


Figure 6.2: Typical retrofit of rectangular columns (FEMA-547, 2006)

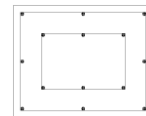
Table 6.1: Design summary of RC jacketing for three reference structures

New column section			C1N	C2N	C3N	
Building	2-story (all stories)	Jacket thickness (mm)	100	100	---	
		VL. reinforcement	8#8@260	8#12@230	---	
	8-story	Ground-4 th story	Jacket thickness (mm)	100	100	100
			VL. Reinforcement	20#16@200	14#12@220	12#10@250
		5 th -8 th story	Jacket thickness (mm)	100	100	---
			VL. Reinforcement	16#10@250	14#10@250	---
	Hospital	Ground-3 rd story	Jacket thickness (mm)	---	100	---
			VL. reinforcement	---	16#10@250	---
		4 th -6 th story	Jacket thickness (mm)	---	100	---
			VL. reinforcement	---	10#10@250	---

*Confining hoops of #10@200mm are used

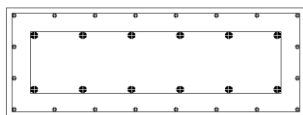


C1N at the foundation level

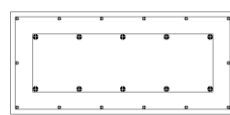


C2N at the foundation level

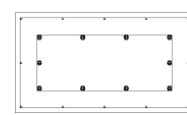
Figure 6.3: Retrofitted RC columns of the 2-story building



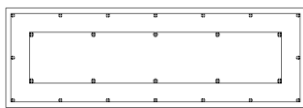
C1N at the foundation level



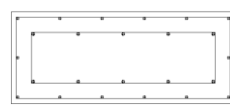
C2N at the foundation level



C3N at the foundation level

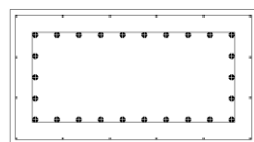


C1N at floor 5

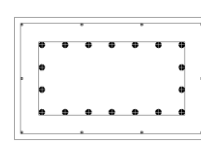


C2N at floor 5

Figure 6.4: Retrofitted RC columns of the 8-story building



C2N at the foundation level



C2N at floor 2

Figure 6.5: Retrofitted RC columns of the hospital

6.2.2 FRP Wrapping

FRP overlays are better than concrete jacketing in terms of disruption and construction time although they are relatively expensive. Existing columns cross-sections are wrapped with unidirectional fibers. These fibers are oriented horizontally. The wrapping of the FRP sheets prevents lateral buckling for

longitudinal bars and also improves concrete compression behavior as they increase the confinement, which increases strength and stiffness of the column, but not to the limit of concrete jacketing (FEMA-547, 2006; Mwafy & Elkholy, 2012). An additional retrofit approach, in which the existing column cross-section is wrapped with FRP overlays, is considered in the present study. High strength FRP overlays are used in this retrofit technique based on a review of previous experimental and analytical studies covering FRP with different characteristics (e.g. Lam & Teng, 2003; Wei & Wu, 2012). The selected FRP overlays have a thickness of 0.33mm/layer, elastic modulus of 257 GPa and tensile strength of 4519 MPa. In the present study, FRP wrapping is applied to the 2-story pre-code building, police station and school, in which the FRP wrapping criteria recommended by design codes is fulfilled (FEMA-547, 2006). This retrofit technique is not recommended by seismic design provisions for medium-rise frame buildings and high-rise wall structures, which have large columns and wall cross-sections with high aspect ratio. The number of retrofitted columns and FRP overlays is dependent upon the target lateral strength of the building. In the 2-story pre-code building, all columns are wrapped with 3 overlays, while only internal columns are wrapped with 2 and 3 overlays in the case of the police station and school, respectively.

6.2.3 Buckling Restrained Braces

The design of BRBs (Figure 6.6) is based upon results from qualifying cyclic tests in accordance with the procedures and acceptance criteria (AISC, 2010). Qualifying test results are based upon one of the following:

- a) Tests that are conducted specifically for the project,

- b) Tests reported in research or documented tests performed for other projects, which is the case considered in the current study (Figure 6.6).

The steel core (yielding steel bar) shall be designed to resist the entire axial force of the brace. The brace design axial strength, ϕP_{ysc} (LRFD), and the brace allowable axial strength, P_{ysc}/Ω (ASD), in tension and compression, in accordance with the limit state of yielding, shall be determined as follows:

$$P_{ysc} = F_{ysc} A_{sc} \quad (6.1)$$

where;

A_{sc} = cross-sectional area of the yielding segment of the steel core,

F_{ysc} = specified minimum yield stress of the steel core, or actual yield stress of the steel core as determined from a coupon test,

$\phi = 0.90$ (LRFD)

$\Omega = 1.67$ (ASD)

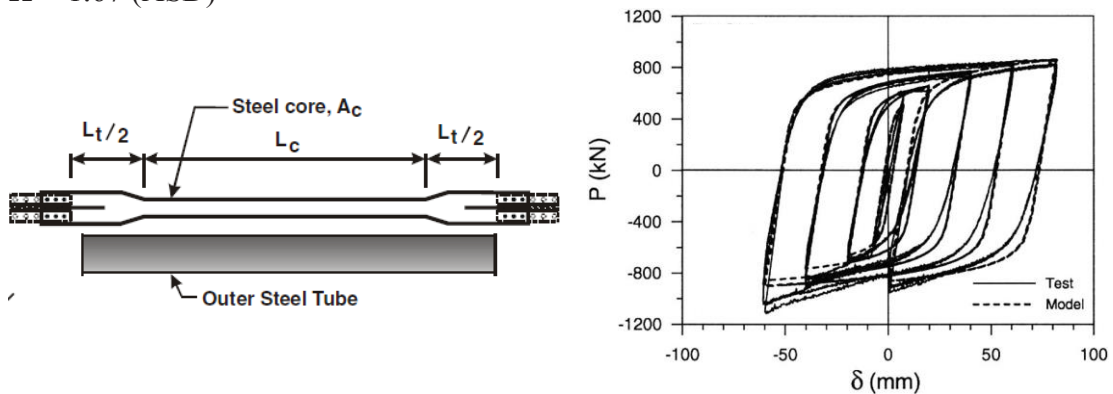


Figure 6.6: Typical BRB specimen (left) (Tremblay et al., 2004), adopted BRB test result (right) (Tremblay et al., 2008)

In the present study, the BRB retrofit technique was applied to the 8-story pre-code building. The BRBs are added to the middle bays of the external frames, as discussed hereafter. The axial force of the brace is obtained from the 3D design model (refer to Figure 3.14 and Figure 3.17). According to equation 6.1, the required

steel core area to resist the entire axial force in the brace is 2200mm^2 . Based on a brief literature review of previous experimental studies, the test results reported in the study of Tremblay et al. (2008) were adopted. Figure 6.6 show the load-deformation cyclic test of a BRB sub-assembly. Finally, the core encasement and the filling material vary according to the manufacturer, and hence they are not specified herein.

6.2.4 Steel Plates

Two possible ways of achieving an increase in strength without affecting stiffness of the walls are by the addition of External Unbonded Reinforcing Bars (EURB) or EUSP. When loaded horizontally, the wall will undergo vertical elongation (due to rotation and cracking) which will axially extend the external rebars or steel plates. In the EUSP scheme considered in the current study, steel plates are bolted to the wall by anchor bolts and steel angles. The level of strength increase can be controlled by the area (Elnashai & Pinho, 1998; Taghdi et al., 2000). In the present study, steel plates were designed using the 3D ETABS models (CSI, 2011), in the form of an additional steel area at the ends of the shear and core walls (Figure 6.7).

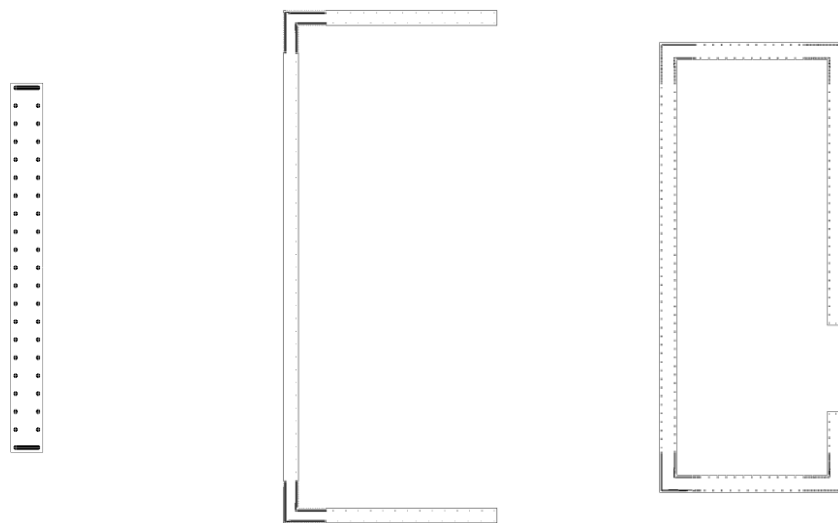


Figure 6.7: Retrofitted RC cross-sections of the wall buildings

6.3 Modeling of Strengthening Techniques

The above-mentioned retrofit techniques were implemented to the fiber models of the reference buildings using the ZEUS-NL (Elnashai et al., 2012). The detailed modeling approach of each of the techniques, namely RC jacketing, FRP wrapping, the installment of BRBs and EUSP is described below.

6.3.1 RC Jacketing

An RC jacket with a rectangular cross-section from the ZEUS-NL library is used to model the retrofitted RC columns in the 2-story and 8-story pre-code buildings and the hospital. Section height, section width and external and internal stirrup widths are needed to define this section, as shown in Figure 6.8. A steel yield strength of 460 MPa was used, while the original concrete strength of the reference structures was used to obtain the required composite action.

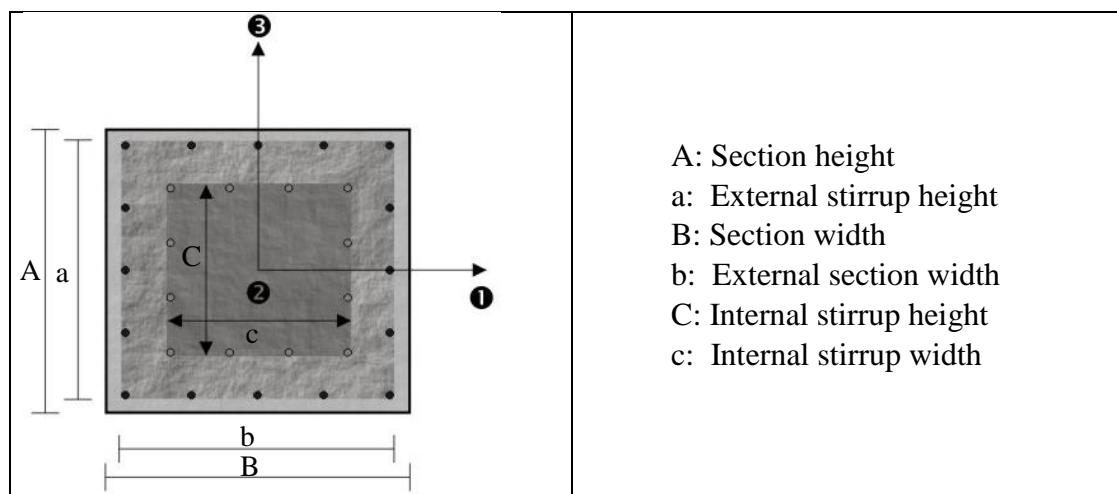


Figure 6.8: RC jacket with a rectangular section (Elnashai et al., 2012)

6.3.2 FRP Wrapping

A trilinear FRP model is used for the modeling of FRP overlays with initial stiffness of 257 GPa and tensile strength of 4519 MPa. The FRP overlays are added

to the original concrete sections with the required thickness obtained in design. The constitutive relationship of the FRP material is illustrated in Figure 6.9.

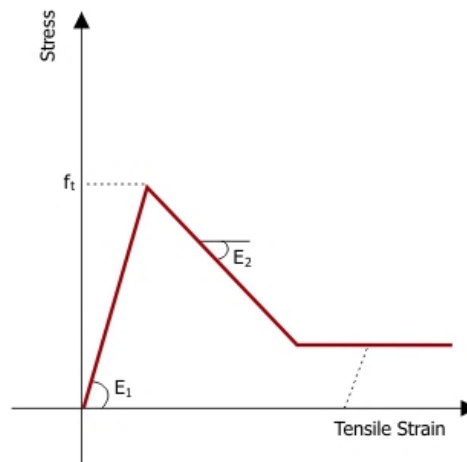


Figure 6.9: Trilinear FRP model (Elnashai et al., 2012)

6.3.3 Buckling Restrained Braces

Using the test results shown previously in Figure 6.6, different parameters are extracted in order to accurately model the BRB behavior. Joint element with trilinear asymmetric elasto-plastic curve is used to model the BRB (Figure 6.10). Ten parameters are required by ZEUS-NL to model the BRB, including different stiffness and displacement values which describe the tension-compression response. Table 6.2 summarizes the required parameters.

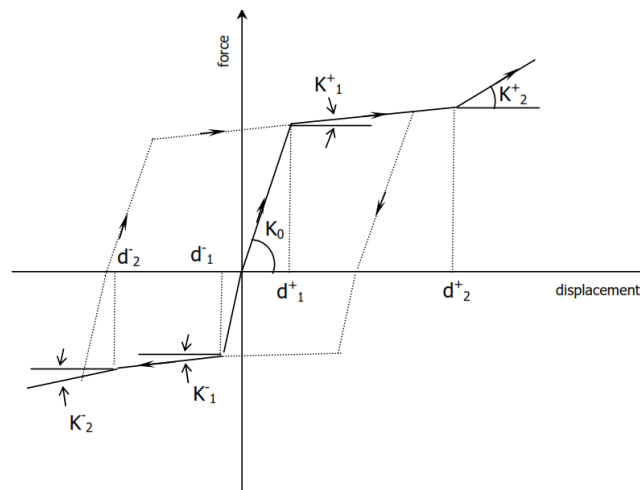


Figure 6.10: Trilinear asymmetric elasto-plastic curve (Elnashai et al., 2012)

Table 6.2: Parameters used for modeling the BRB trilinear asymmetric joint element

Parameter	Description	Value
K_0^+	Initial stiffness (positive displacement region)	80000 N/mm
d_1^+	Positive displacement where the stiffness changes from K_0^+ to K_1^+	10 mm
K_1^+	Stiffness of second branch (positive displacement region)	571 N/mm
d_2^+	Positive displacement where the stiffness changes from K_1^+ to K_2^+	70 mm
K_2^+	Stiffness of third branch (positive displacement region)	0 N/mm
K_0^-	Initial stiffness (negative displacement region)	80000 N/mm
d_1^-	Negative displacement where the stiffness changes from K_0^- to K_1^-	-11 mm
K_1^-	Stiffness of second branch (negative displacement region)	4898 N/mm
d_2^-	Negative displacement where the stiffness changes from K_1^- to K_2^-	-49 mm
K_2^-	Stiffness of third branch (negative displacement region)	0 N/mm

The member representing the BRB brace is divided into two segments connected at the middle with the BRB joint element described above. The BRB joint element has six Degrees of Freedom (DOFs). The axial DOF is utilized to model the hysteresis behavior of the BRB, while the other five DOFs are restrained. The ends of the BRB brace member have pin connection with concrete beam-column connections, as described in Figure 6.11.

The BRB modeling verification is carried out for the 8-story pre-code building using IPA and THA simulations. The BRB response at three story levels (ground, middle and top stories) was obtained. Figure 6.12 shows sample results at the three aforementioned levels. Moreover, the BRB response is also monitored using THA at two ground motion intensities, namely the design and 5 times the design PGA. Figure 6.13 illustrates the hysteresis behavior of the BRB during THA. The results validate the adopted modeling approach of the BRB using test results shown in Figure 6.6.

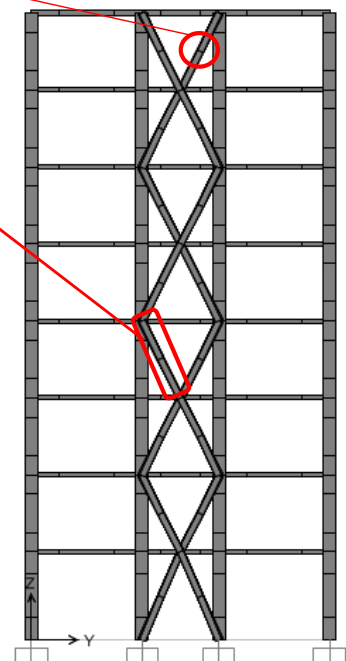
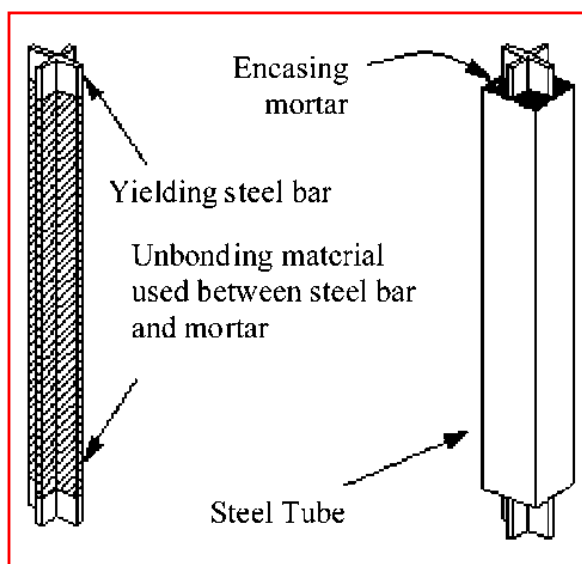
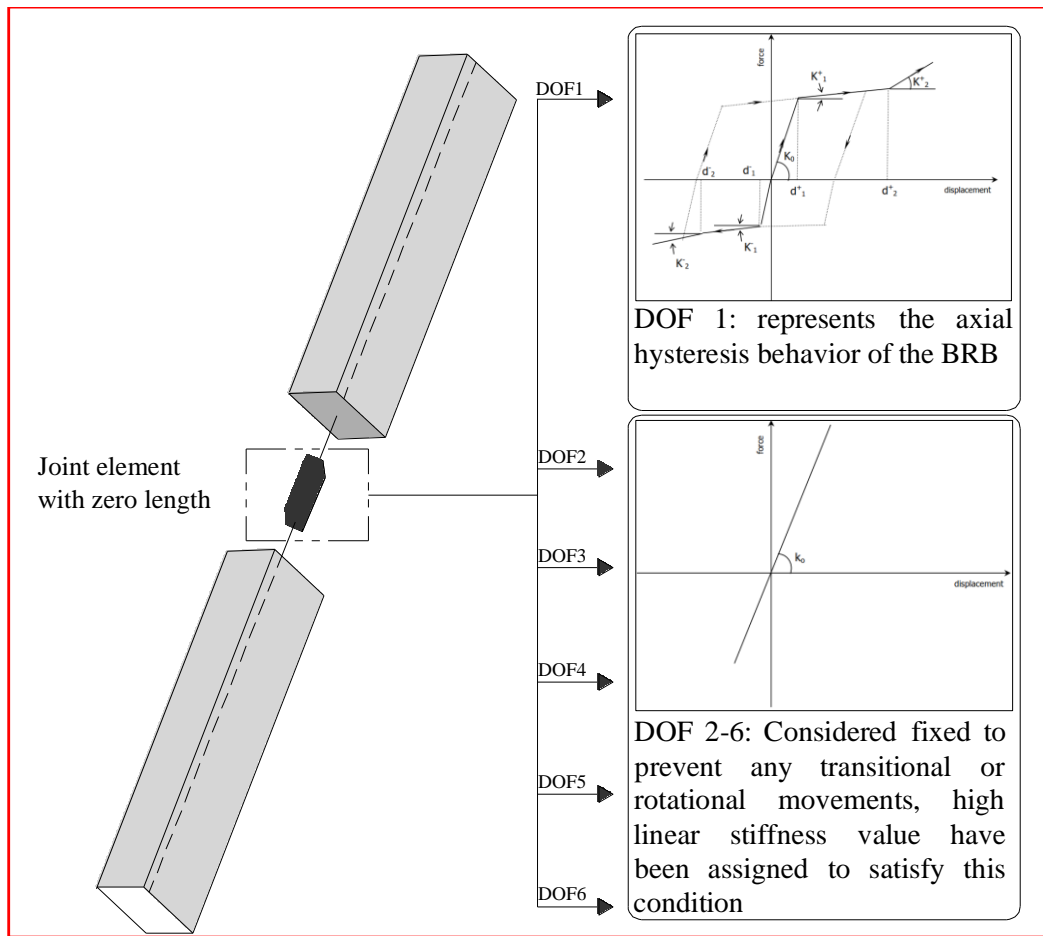


Figure 6.11: BRB modeling concept

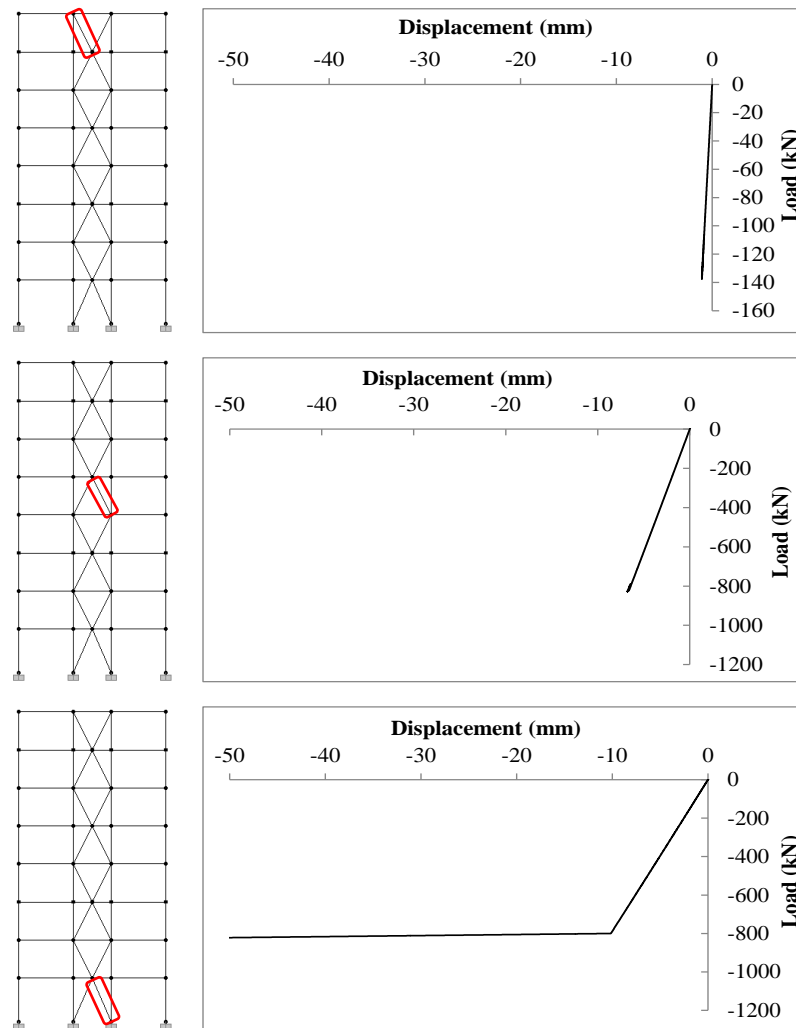


Figure 6.12: BRB load-displacement relationships obtained from IPA at three different story levels

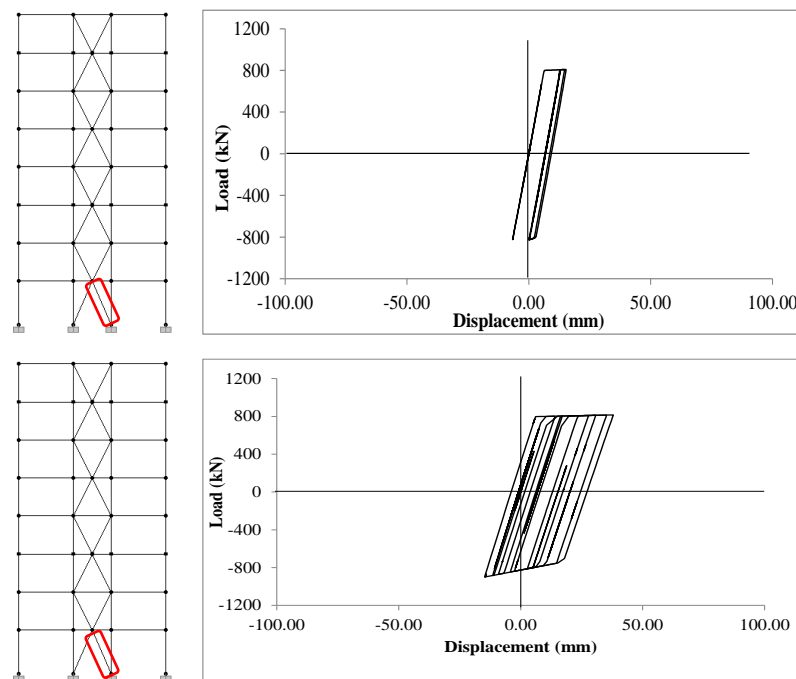


Figure 6.13: BRB load-displacement relationships at the design PGA (top) and five times the design (bottom) PGA

6.3.4 Steel Plates

The steel plates obtained from the design are modeled in ZEUS-NL using steel reinforcement having the same yield strength and area. The added steel area is represented at the ends of the shear and core walls. The yield strength of the steel plates is 240 MPa.

6.4 Impact of Retrofit on Lateral Capacity

The four different retrofit techniques were implemented in the ZEUS-NL models of the reference structures as discussed earlier. Pushover analysis was performed for each system after implementing the rehabilitation approach. Pre-code frame structures (BO-02 and BO-08) were provided with two retrofit alternatives, while one retrofit technique was employed for other buildings. Table 6.3 summarizes the IPA results for the eight retrofitted structures. For the 2-story building, RC jacketing of columns results in higher stiffness and strength over the FRP retrofit approach due to increasing cross-section sizes, as shown in Figure 6.14 (a). For the 8-story building, the BRBs produce higher stiffness and strength over the RC jacketing, but results in reduced ductility due to the sudden failure in such retrofit technique when it reaches its ultimate axial capacity, as shown in Figure 6.14 (b). Both RC jacketing and FRP wrapping of columns significantly enhance the ductility for the 2 and 8-story pre-code structures. As shown in Figure 6.14 (c-e), adding EUSP to the shear walls of the pre-code wall structures has a marginal impact on stiffness, while it increases the strength to the required design level (i.e. $V_d * \Omega_0$).

For the emergency facilities, FRP wrapping of columns has a very minor effect on the initial stiffness, as shown in Figure 6.14 (f and g). For the hospital

building, RC jacketing of internal columns improved both the initial stiffness and ultimate strength, as shown in Figure 6.14 (h). All of the retrofit techniques produce the required strength according to the applied design loads. The higher impact of rehabilitation approaches are observed in the pre-code buildings over emergency facilities, especially the pre-code frames, since they were only designed to resist gravity and wind loads.

Table 6.3: Summary of IPA results for existing and retrofitted structures

Building	Original design load (kN)		New seismic design load (kN)	Lateral load increase (%)	Original strength (kN)	Strength of alternative # 1 (kN)	Strength of alternative # 2 (kN)
	Wind	EQ					
BO-02	110	---	655	495	605	1450 (FRP)	2048 (RCJ)
BO-08	968	---	2341	142	3763	7167 (RCJ)	8786 (BRB)
BO-18	1966	---	10852	452	24951	38162 (EUSP)	---
BO-26	2879	---	12298	327	19912	37896 (EUSP)	---
BO-40	6707	---	23117	245	45898	62226 (EUSP)	---
PS	429	3358	3790	13	10788	13177 (FRP)	---
SC	632	1902	2795	47	5936	6445 (FRP)	---
HO	1422	6670	9801	47	16978	19649 (RCJ)	---

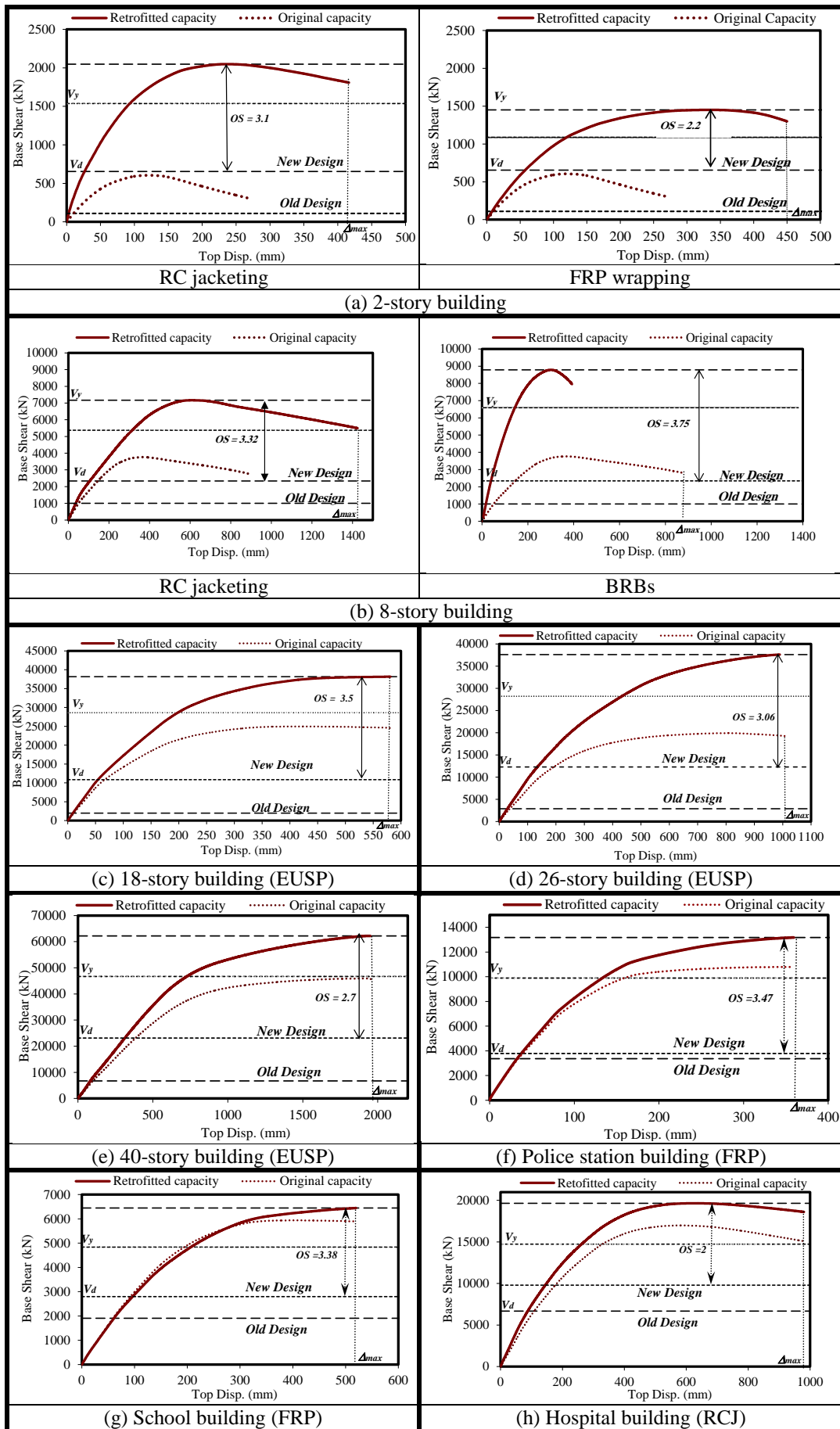


Figure 6.14: The capacity curves for existing and retrofitted structures

6.5 Impact of Retrofit on Seismic Performance

The same procedures employed in Chapter 5 for deriving the fragility curves of the reference structures are used herein to generate new fragility relationships for the retrofitted structures. IDAs were performed using the selected wide range of input ground motions and then regression analyses were conducted. Fragility curves were derived and limit state exceedance probabilities generated. As mentioned earlier, only long-period earthquake records were employed in this task since they represent the most significant seismic scenario. Figure 6.15 depicts the regression analysis results for the 280 IDAs undertaken for each retrofitted structure.

Fragility curves were generated and plotted for each building separately as shown in Figure 6.16. In order to observe the performance enhancement, the fragility curves of both the original and retrofitted structures were plotted in Figure 6.17. For the 2-story pre-code structure, both of the implemented retrofit techniques (RC jacketing and FRP wrapping of columns) improve the seismic performance differently. The seismic performance improvements are noticeable in both approaches but with a higher extent in the RC jacketing technique over the FRP wrapping approach. For the 8-story structure, nearly the same performance improvement is observed for the employed techniques, namely the RC jacketing of columns and the BRBs. On the other hand, slight enhancement in the seismic performance is achieved after adding steel plates to the shear walls of the pre-code wall structures. Comparable marginal improvements are observed in the police station and school buildings with the FRP wrapping of internal columns. Finally, slopes of the fragilities become less steep for the 6-story hospital after the RC jacketing of internal columns compared with the original structure, as shown in Figure 6.17.

A better comparison of the seismic performance of the original and retrofitted structures is achieved by comparing between the limit state exceedance probabilities of existing and retrofitted structures. Figure 6.18 depicts the IO, LS and CP limit state exceedance probabilities before and after employing different rehabilitation techniques for the eight retrofitted structures. The impact of different retrofit techniques on the limit state exceedance probabilities varies among the different limit states. For the pre-code frame structures, the highest reduction in the limit state exceedance probabilities is observed for the RC jacketing and BRB approaches. The observed high improvement in the seismic performance of the pre-code frame structures is attributed to their original poor performance unlike the pre-code wall structures and emergency facilities.

The enhancement achieved in the seismic performance of the reference structures using the selected retrofit approaches confirms the success of such retrofit techniques to upgrade the seismic performance to reach the target levels and reduce the earthquake losses in the study area. The pre-code frame structures come as top priority when implementing earthquake mitigation programs due to their wide spreading and high vulnerability in the study area (refer to Figure 3.2).

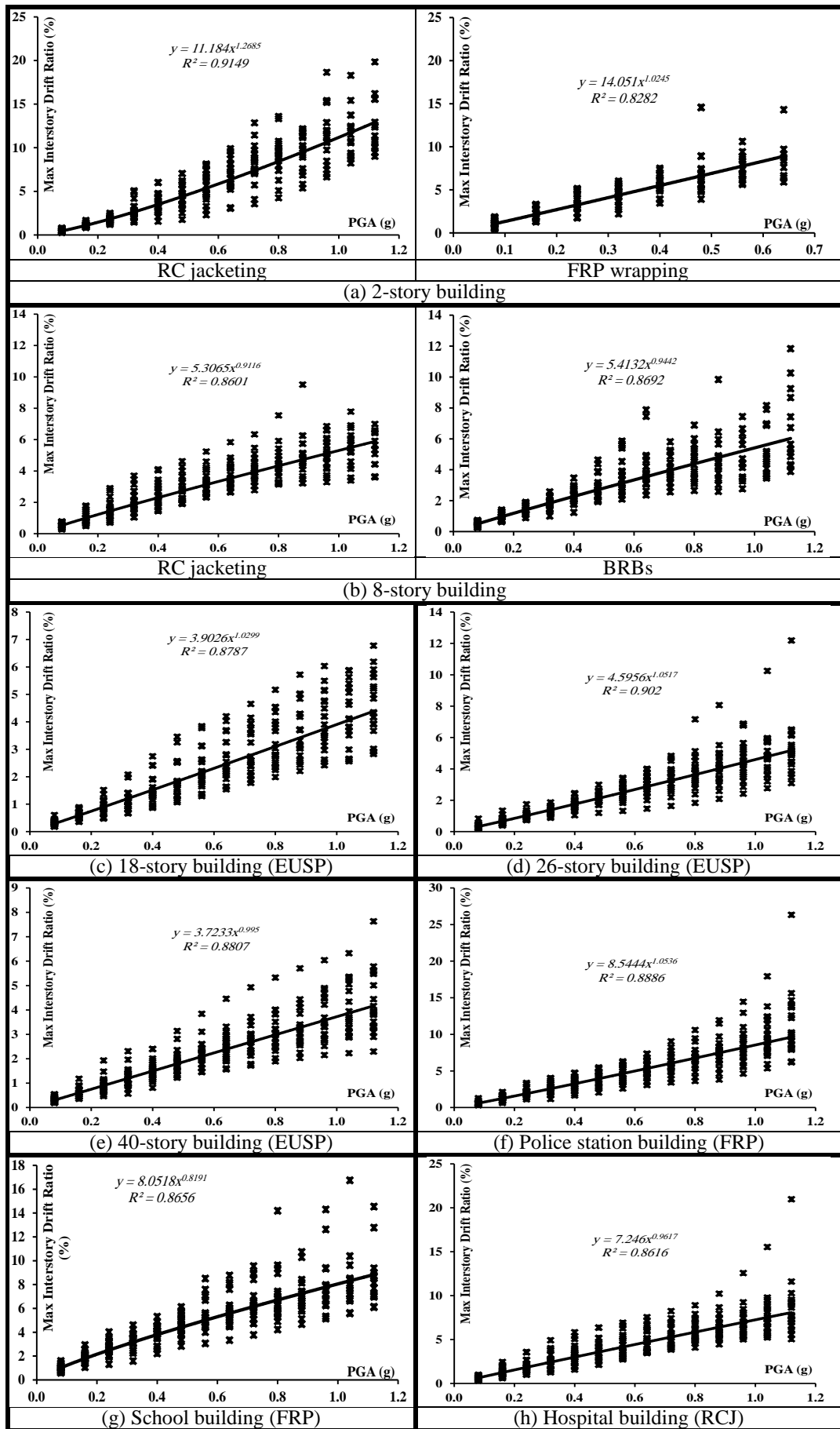


Figure 6.15: Regression analysis of retrofitted structures using 20 long period records

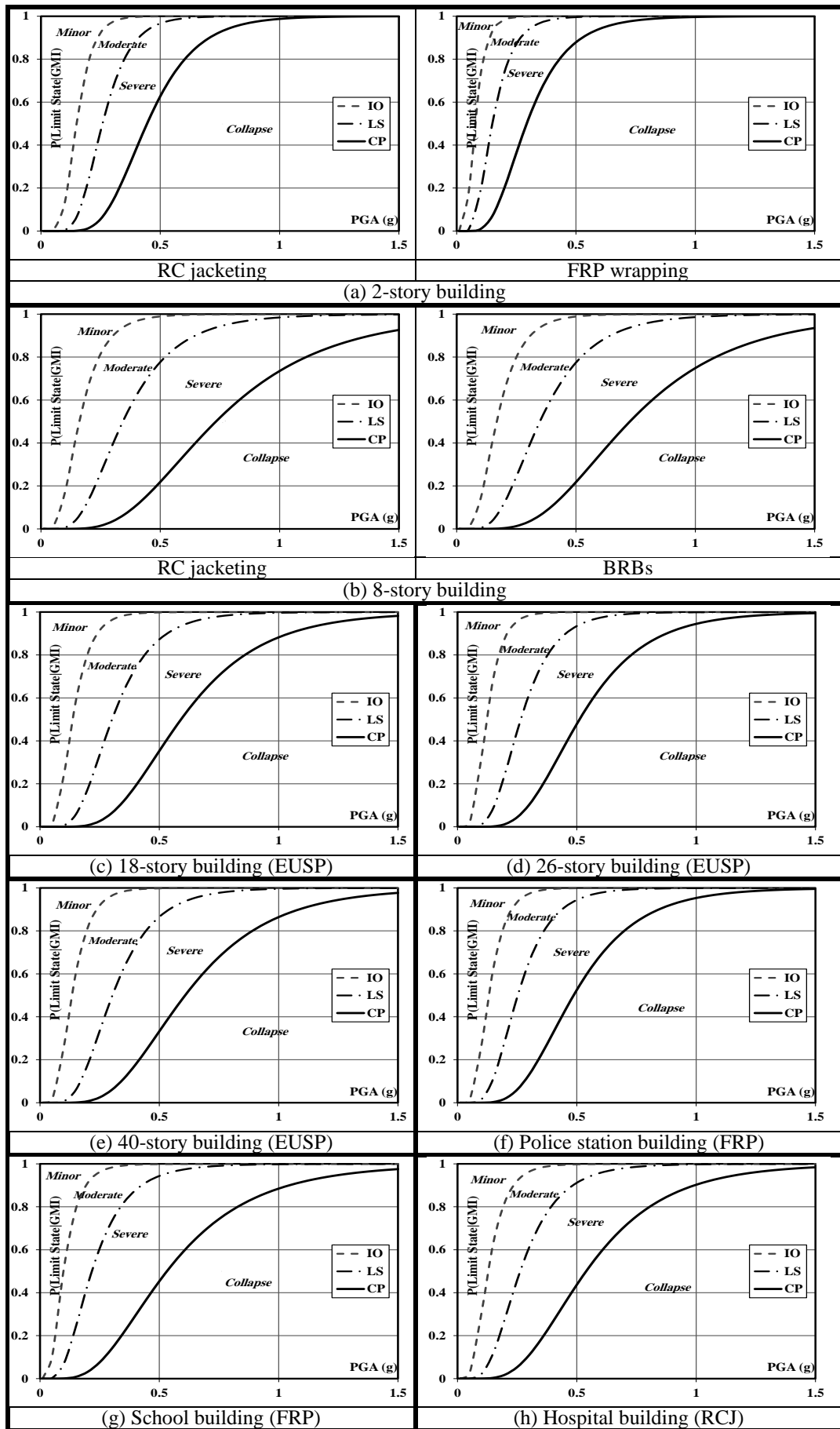


Figure 6.16: Fragility curves of retrofitted structures using 20 long period records

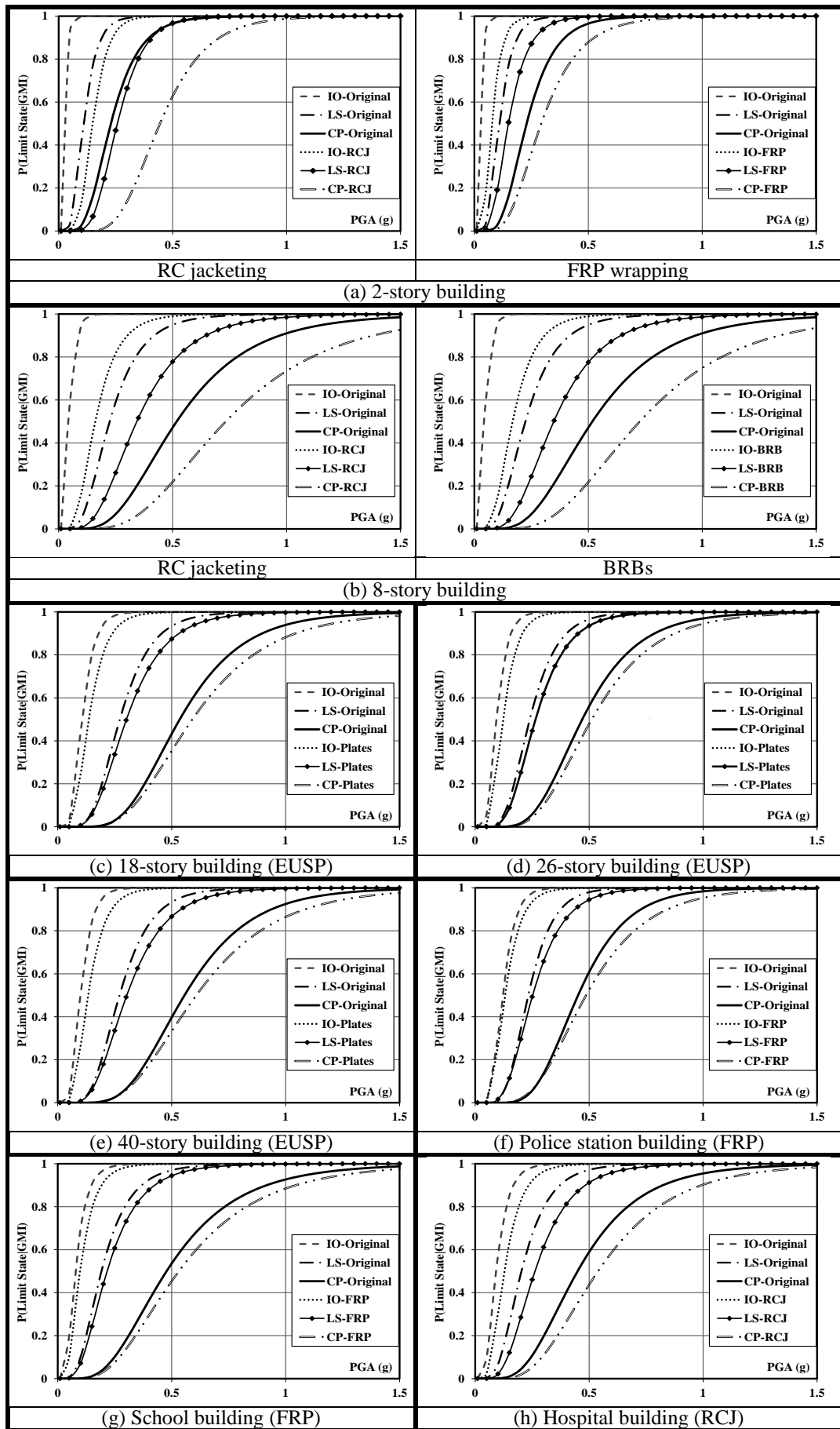


Figure 6.17: Fragility curves before and after retrofit using 20 long period records

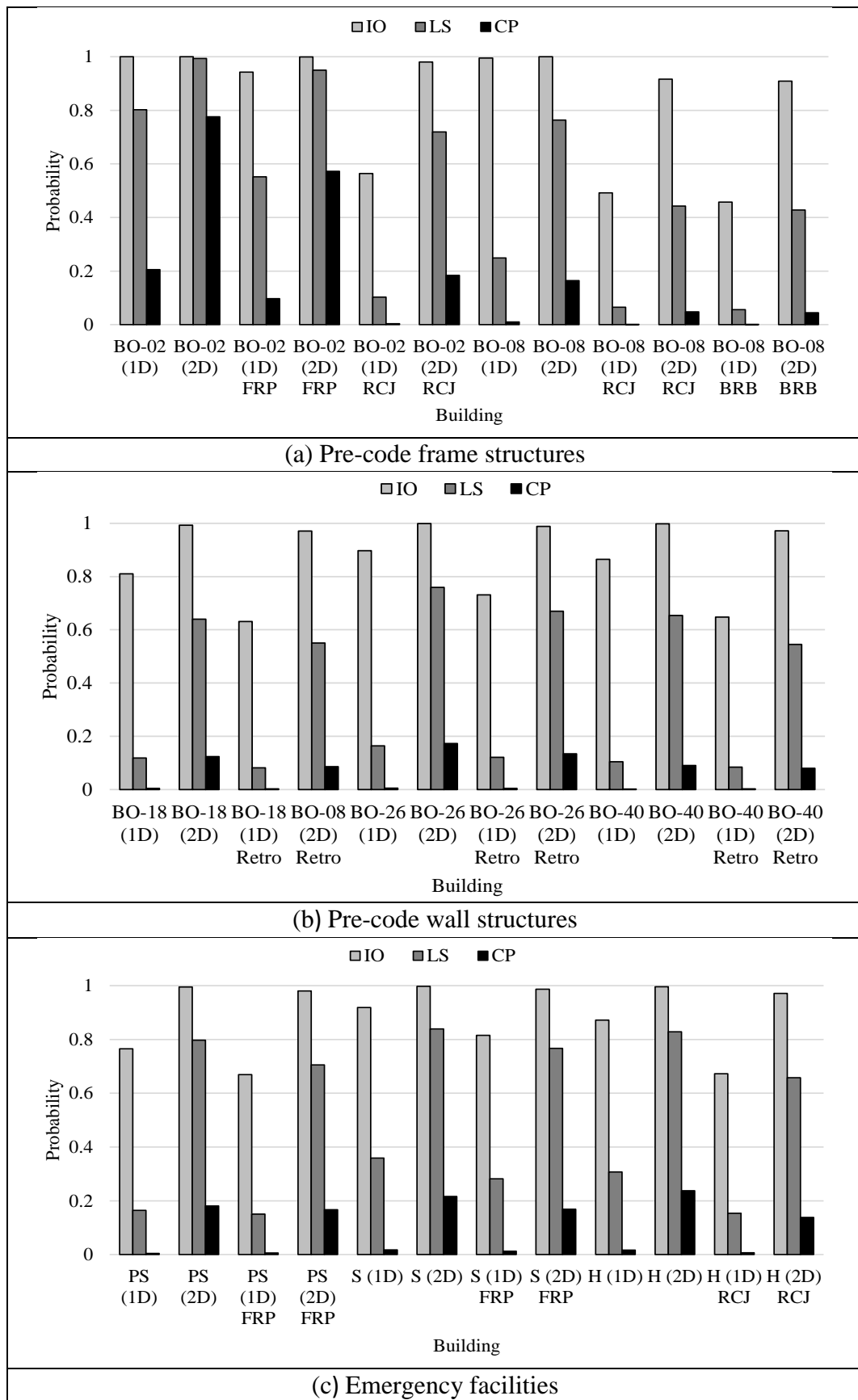


Figure 6.18: Limit state exceedance probabilities of the eight buildings before and after retrofit

6.6 Concluding Remarks

The reference structures that did not meet the code recommended objectives were retrofitted in the current study to achieve the desired seismic performance. A number of steps were followed to upgrade the buildings, including: (i) set and define the new target design objective; (ii) obtain most conservative spectral acceleration values from code spectrum and relevant seismic scenarios; (iii) select a suitable retrofit technique, apply new seismic loads and redesign, and finally (iv) verify the performance of the retrofitted structure. Four retrofit techniques were considered, namely FRP wrapping of columns, RC jacketing of columns, adding BRBs to RC frames and installing EUSP to shear walls and core walls.

RC jacketing was applied to the 2 and 8-story pre-code structures as well as hospital building. In the 2 and 8-story buildings, all columns were enlarged, while only internal columns were retrofitted in the case of the hospital building. FRP overlays were applied to the 2-story pre-code structure as well as to the police station and school buildings. In the 2-story pre-code building, all columns were wrapped with 3 FRP overlays, while only internal columns were wrapped with 2 and 3 in overlays in the case of the police station and school buildings, respectively, to achieve the target performance levels. The experimentally verified RC jacket rectangular section and FRP model from ZEUS-NL library were employed to model the RC jacketing and FRP wrapping retrofit techniques.

The design and modeling of BRBs was based on results obtained from previous cyclic tests. The BRB retrofit technique was implemented in the external frames of the 8-story pre-code building. The member representing the BRB brace is divided into two segments connected at the middle with asymmetric joint element.

Pushover and dynamic response simulations proved the effectiveness of the BRB modeling approach. The EUSP retrofit approach was implemented to the pre-code wall structures due to its effectiveness and applicability.

The IPA results of the 2-story pre-code building indicated that the RC jacketing of columns result in higher stiffness and strength compared with the FRP technique. In the 8-story building, although the BRB approach produced higher stiffness and strength than the RC jacketing of columns, it had an unfavorable impact on ductility due to sudden failure when it reaches its ultimate axial capacity. For the pre-code wall structures, EUSP had a marginal impact on stiffness, while it enhanced the strength to the target level. FRP wrapping of internal columns had minor effect on the stiffness of the police station and school buildings. For the hospital building, RC jacketing of internal columns improved both the initial stiffness and ultimate strength. The highest impacts on the lateral capacity were observed in the pre-code buildings over emergency facilities, especially the pre-code frames, since they were only designed to resist gravity and wind loads.

The derived fragility relationships of the retrofitted 2-story pre-code structure using RC jacketing and FRP wrapping of columns improved the seismic performance to a higher extent for the former technique. For the 8-story structure, nearly the same performance improvement was observed from both the RC jacketing of columns and BRBs. On the other hand, slight enhancement in the seismic performance was achieved after adding steel plates to the shear walls of the pre-code wall structures. Comparable marginal improvements were observed in the police station and school buildings with the FRP wrapping of internal columns. The fragility slopes decreased for the 6-story hospital after the RC jacketing of internal columns compared to the original structure.

The impact of different retrofit techniques on the limit states exceedance probabilities varied among the different limit states. For the pre-code frame structures, the highest reduction in the limit state exceedance probabilities was observed for the RC jacketing and BRBs approaches. The observed high improvement in the seismic performance of the pre-code frame structures was attributed to their original poor performance unlike the pre-code wall structures and emergency facilities. The achieved enhancement in the seismic performance of the reference structures using the selected retrofit approaches confirmed the success of such rehabilitation approaches to upgrade the seismic performance to reach the target levels and reduce the earthquake losses in the study area.

CHAPTER 7: CONCLUSIONS AND RECOMMENDATIONS

7.1 Synopsis

The number of buildings in the existing inventory that may be at risk because of insufficient seismic design provisions cannot be underestimated. A crucial role in the recovery period following an earthquake is also played by emergency facilities. Hence, this study focused on the probabilistic seismic vulnerability assessment of a diverse range of reference buildings representing substandard and emergency structures in a highly populated and seismically active area in the UAE. The following main tasks were undertaken to achieve the objectives of the present study:

Selection, Design and Modeling of Reference Buildings

Five pre-seismic code buildings and four emergency facilities were selected based on an on ground survey to represent the architectural layouts commonly adopted for buildings in the UAE. An iterative design process was adopted by targeting a D/C ratio as close as possible to unity to ensure both safety and cost-effectiveness. The material properties and design provisions implemented at the construction time of the pre-seismic code buildings were taken into account. Lateral actions from wind loads were considered in the design of pre-code buildings, while those from seismic forces were accounted for in the design of the modern emergency facilities. Detailed two and three-dimensional fiber-based idealizations for wall and frame structures, respectively, were developed using a verified inelastic analysis platform to assess the seismic response of the buildings using IPAs and IDAs. The fiber-based models developed were verified by comparing their dynamic

characteristics with those obtained from the 3D design models and with those reported in other studies.

Forty far-field and near-source earthquake records were carefully chosen based on the conclusions of previous studies to represent the study area and account for the uncertainty in ground motions. These scenario-based earthquake records consisted of 20 long-period earthquakes of magnitude 6.93 to 7.64 with epicentral distances of 91 km to 161 km as well as 20 short-period earthquakes of magnitude 5.14 to 6.04 with epicentral distances of 6 km to 30 km.

Vulnerability Assessment of Reference structures

The nine reference structures were subjected to a series of Eigenvalue analyses, IPAs and IDAs to assess their dynamic characteristics, lateral capacities and seismic performance. Over 5000 inelastic multi-step analyses of nine multi-degree-of-freedom fiber-based numerical models were performed. The lateral capacities, IDRs, plastic hinge distributions and shear response were monitored and compared. Three limit states were defined based on extensive IPA and IDA results as well as the values recommended in previous analytical and experimental studies and code provisions. The IDA results were utilized to derive a wide range of fragility relationships of the pre-code buildings and emergency facilities in the UAE under two earthquake scenarios. The limit state exceedance probabilities were compared for different buildings and seismic scenarios to provide insights into the vulnerability of the building inventory and the need for seismic hazard mitigation.

Vulnerability Assessment of Retrofitted Structures

About 3000 additional inelastic analyses were performed to assess the vulnerability of the reference structures that proved to have unsatisfactory performance, and hence retrofitted using different mitigation techniques. The procedure followed to upgrade the buildings involves defining a new target design objective, obtaining the most conservative spectral acceleration parameters, selection and design of a suitable retrofit technique, and finally verifying the retrofitted structures using IPA and IDA. Four retrofit techniques were considered, namely FRP wrapping of columns, RC jacketing of columns, adding BRBs to RC frames and installing EUSP for shear walls and core walls. Fragility curves were derived and limit states exceedance probabilities were generated to arrive at conclusions regarding the effectiveness of the adopted mitigation actions.

7.2 Summary of Conclusions

The most important observations and conclusions from the present study are summarized below:

Design and Modeling Verification of Reference Buildings

Although the pre-seismic code structures, especially multi-story buildings, were designed to resist gravity and wind loads only, large cross sections were produced for vertical elements due to the low material strength used at the construction time. These large cross sections added additional mass and stiffness to pre-code buildings. In addition to the lack of efficient reinforcement and detailing, such mass attracted high inertia forces and increased the vulnerability of this class of structures. Wind loads of pre-code low-rise structures were considerably lower than

their high-rise counterparts. This reduced the lateral capacity of the former buildings, and hence increased their vulnerability. The design results also confirmed the significance of considering the lateral loads in the design of floor slabs, which may sometimes be ignored by practicing engineers.

Despite the different modeling approaches of the nine reference structures for design and vulnerability assessment, the observed discrepancies between the dynamic characteristics obtained from the 3D finite element models and the detailed fiber-based idealizations were insignificant. These minor differences were due to employing the actual/mean material strength values in the latter models rather than the nominal/characteristic values used in the design, in addition to the effective representation of reinforcing steel.

Vulnerability Assessment of Pre-code Buildings and Emergency Facilities

For emergency facilities, the first indication of steel yielding was observed in horizontal members, which was followed by vertical members. This is in agreement with the strong-column weak-beam concept of having energy dissipated mainly in horizontal elements. Pre-code structures lacked this concept, especially the low-rise building, due to their inefficient lateral force design under wind loads. Mapping the number and sequence of plastic hinges of the nine reference structures, particularly in vertical elements, showed significantly better performance for the emergency facilities over the pre-code structures.

The use of input ground motions representing the same earthquake scenario produced marginally different maximum IDRs, unlike when comparing the seismic demands from two different seismic scenarios. Far-field records had much higher impact on the reference structures over the near-source records. High IDRs were

recorded in the pre-code frame structures at moderate-to-high ground motion intensity levels due to their inefficient LFRSs. This increased the spread of plastic hinges in horizontal and vertical elements, leading to the formation of story mechanisms. The limit state exceedance probabilities provided insights into the relative safety margins of different structures. At the design PGA, pre-code structures were significantly more vulnerable compared with emergency facilities. A large increase in the exceedance probabilities of various limit states was clear when the PGAs were doubled. The results reflected the urgent need of seismic retrofit for all pre-code structures to reduce their seismic losses and for certain emergency facilities to improve their seismic performance and ensure their continued service following a strong earthquake.

Seismic Vulnerability Assessment of Retrofitted Structures

Pushover analysis results confirmed that the RC jacketing of columns effectively increased both the initial stiffness and ultimate strength when compared with the FRP wrapping technique. The BRB retrofit approach, although produced higher stiffness and strength than the RC jacketing of columns, had an unfavorable impact on ductility due to the premature failure when it reaches its ultimate axial capacity. The EUSP retrofit technique had a marginal impact on stiffness, while it enhanced the strength to the target level.

The seismic performance of the retrofitted buildings from the derived fragility relationships using IDAs was consistent with that from IPA results. Lower vulnerability was observed when the columns of the 2-story pre-code structure were retrofitted with RC jacketing compared with that of FRP wrapping. For the 8-story structure, the improvements in seismic performance using RC jacketing of columns

and BRBs were comparable. Marginal enhancements in seismic performance were achieved when implementing the EUSP retrofit technique to the pre-code wall structures. Comparable improvements were observed in the police station and school buildings with the FRP wrapping of internal columns. The fragilities decreased when the 6-story hospital was retrofitted using RC jacketing of internal columns. The observable improvements in the seismic performance of the pre-code frame structures were attributed to their original poor performance unlike the pre-code wall buildings and emergency facilities. The reduced vulnerability of the retrofitted structures confirmed the effectiveness of the selected retrofit approaches for mitigation of earthquake losses in the study area.

7.3 Recommendations for Future Research

Based on the findings and conclusions of the present study, the following recommendations are proposed for future studies:

1. A detailed study is urgently needed to compile all information related to the building and infrastructure inventories in the UAE from different municipalities and government agencies in a unified database to be used in developing a comprehensive loss estimation system for the UAE.
2. A comprehensive shear assessment study using a wide range of reference structures with different systems and diverse input ground motions is urgently needed to arrive at a final decision regarding the significance or otherwise of shear as a controlling failure criterion in seismic loss estimation.
3. A further study is required to assess the impacts of the combined horizontal and vertical components of ground motion on local response and limit state criteria, particularly shear response, and hence on the fragilities.

4. In order to represent the study area more comprehensively, it is recommended to investigate the vulnerability of all other classes of structures represented in the building inventory such as industrial structures, government facilities and infrastructure.
5. More research is needed to cover other retrofit alternatives along with a comprehensive feasibility study to arrive at the most efficient and cost-effective mitigation approaches for mitigating earthquake losses in the UAE.

REFERENCES

- Abdalla, J. A., & Al-Homoud, A. S. (2004). Seismic hazard assessment of United Arab Emirates and its surroundings. *Journal of earthquake engineering*, 8(6), 817-837.
- Abdelnaby, A. E., Frankie, T. M., Elnashai, A. S., (...), & Chang, C.-M. (2014). Numerical and hybrid analysis of a curved bridge and methods of numerical model calibration. *Engineering structures*, 70, 234-245.
- Abu-Dagga, K., Barakat, S., & Shanableh, A. (2010). *Seismic fragility assessment of model buildings in Sharjah, United Arab Emirates*. Paper presented at the International Conference on Computing in Civil and Building Engineering, The University of Nottingham, UK, June 30-July 2 2010.
- ACI-318. (1963). Building Code Requirements for Structural Concrete and Commentary: American Concrete Institute, Detroit, Michigan.
- ACI-318. (2011). Building Code Requirements for Structural Concrete and Commentary: American Concrete Institute, Detroit, Michigan.
- ADIBC. (2013). Abu Dhabi International building code, . *Abu Dhabi, UAE*.
- AISC. (2010). Seismic Provisions for Structural Steel Buildings,(ANSI/AISC 341-10): American Institute of Steel Construction, Chicago, IL.
- Al-Haddad, M., Siddiqi, G., Al-Zaid, (...), & Turkelli, N. (1994). A basis for evaluation of seismic hazard and design criteria for Saudi Arabia. *Earthquake Spectra*, 10(2), 231-258.
- Al Marzooqi, Y., Abou Elenean, K., Megahed, A., (...), & Al Khatibi, E. (2008). Source parameters of March 10 and September 13, 2007, United Arab Emirates earthquakes. *Tectonophysics*, 460(1), 237-247.
- Al Shamsi, G. A. (2013). *Seismic Risk Assessment of Buildings in Dubai, United Arab Emirates*. (Master thesis), American University of Sharjah.
- Al Waile, W., Mwafy, A. M., Pilakoutas, K., & Guadagnini, M. (2014). *Framework for Developing Fragility Relations of High-Rise RC Wall buildings based on verified Modelling Approach*. Paper presented at the European Conference on Earthquake Engineering and Seismology (2ECEES), Istanbul, Turkey, 24-28 August 2014.
- Aldama-Bustos, G., Bommer, J., Fenton, C., & Stafford, P. (2009). Probabilistic seismic hazard analysis for rock sites in the cities of Abu Dhabi, Dubai and Ra's Al Khaymah, United Arab Emirates. *Georisk*, 3(1), 1-29.

- Ali, A. (1994). Wind regime of the Arabian Gulf. *The Gulf War and the Environment*, 31-48.
- Ambraseys, N., Smit, P., Douglas, J., (...), & Costa, G. (2004). Internet site for European strong-motion data. *Bollettino di Geofisica Teorica ed Applicata*, 45(3), 113-129.
- Arya, C., Clarke, J., Kay, E., & O'Regan, P. (2002). TR 55: Design guidance for strengthening concrete structures using fibre composite materials: a review. *Engineering structures*, 24(7), 889-900.
- ASCE-7. (2010). Minimum Design Loads for Buildings and Other Structures, ASCE Standard ASCE/SEI 7-10 (Vol. 7). American Society of Civil Engineers, Reston, VA.
- ASCE/SEI-41. (2013). Seismic Evaluation and Retrofit of Existing Buildings (ASCE/SEI 41-13) *American Society of Civil Engineers, Reston, VA.*
- ASCE/SEI. (2007). Seismic Rehabilitation of Existing Buildings (ASCE/SEI 41-06) *American Society of Civil Engineers, Reston, VA, US.*
- Ashri, A., & Mwafy, A. M. (2014). *3D vulnerability functions for contemporary buildings with varying structural systems and heights*. Paper presented at the European Conference on Earthquake Engineering and Seismology (2ECEES), Istanbul, Turkey, 24-28 August 2014.
- Bilgin, H. (2013). Fragility-based assessment of public buildings in Turkey. *Engineering structures*, 56, 1283-1294.
- Borzi, B., Pinho, R., & Crowley, H. (2008). Simplified pushover-based vulnerability analysis for large-scale assessment of RC buildings. *Engineering structures*, 30(3), 804-820.
- Bruneau, M., & Reinhorn, A. (2007). Exploring the concept of seismic resilience for acute care facilities. *Earthquake Spectra*, 23(1), 41-62.
- Bruno, S., Decanini, L., & Mollaioli, F. (2000). *Seismic Performance of pre-code reinforced concrete buildings*. Paper presented at the Proc. 12th WCEE, Auckland, New Zeland, 30 January - 4 February 2000.
- BS8110. (1986). Structural use of concrete *BS8110*: British Standard Institution, London, UK.
- CSA. (1994). *Standard, C. S. A. (1994). Design of Concrete Structures (A23. 3-94)*. . Canadian Standards Association, Rexdale, Ontario, Canada.

- CSI. (2011). ETABS - Integrated building design software: Computers and Structures, Inc., Berkeley, California.
- Di Ludovico, M., Prota, A., Manfredi, G., & Cosenza, E. (2008). Seismic strengthening of an under-designed RC structure with FRP. *Earthquake engineering & structural dynamics*, 37(1), 141-162.
- Di Sarno, L., & Manfredi, G. (2010). Seismic retrofitting with buckling restrained braces: application to an existing non-ductile RC framed building. *Soil Dynamics and Earthquake Engineering*, 30(11), 1279-1297.
- Dymiotis, C., Kappos, A. J., & Chryssanthopoulos, M. K. (1999). Seismic reliability of RC frames with uncertain drift and member capacity. *Journal of Structural Engineering*, 125(9), 1038-1047.
- Elnashai, A., & Mwafy, A. (2002). Overstrength and force reduction factors of multistorey reinforced-concrete buildings. *The structural design of tall buildings*, 11(5), 329-351.
- Elnashai, A., & Pinho, R. (1998). Repair and retrofitting of RC walls using selective techniques. *Journal of earthquake engineering*, 2(4), 525-568.
- Elnashai, A. S., Cleveland, L. J., Jefferson, T., & Harrald, J. (2009). Impact of New Madrid Seismic Zone Earthquakes on the Central USA, Vol. 1 and 2. *illinois digital environment for access to learning and scholarship*.
- Elnashai, A. S., Papanikolaou, V., & Lee, D. (2012). Zeus-NL - A System for Inelastic Analysis of Structures - User Manual Mid-America Earthquake Center, University of Illinois at Urbana-Champaign, Urbana, IL.
- Eurocode. (2004). Eurocode 8: Design of structures for earthquake resistance. *Part, 1*, 1998-1991.
- Fahnestock, L. A., Ricles, J. M., & Sause, R. (2007). Experimental evaluation of a large-scale buckling-restrained braced frame. *Journal of Structural Engineering*, 133(9), 1205-1214.
- FEMA-356. (2000). *Commentary for the seismic rehabilitation of buildings*, Federal Emergency Management Agency, (Vol. 356). Washington, US.
- FEMA-547. (2006). *Techniques for the Seismic Rehabilitation of Existing Buildings*, Federal Emergency Management Agency, . Washington, US: FEMA.
- FEMA. (2009). *NEHRP Recommended Seismic Provisions for New Buildings and Other Structures: FEMA P-750/2009 Edition*. Washington, US.

- Ghobarah, A., Abou-Elfath, H., & Biddah, A. (1999a). Response-based damage assessment of structures. *Earthquake engineering & structural dynamics*, 28(1), 79-104.
- Ghobarah, A., Aly, N., & El-Attar, M. (1998). Seismic reliability assessment of existing reinforced concrete buildings. *Journal of earthquake engineering*, 2(4), 569-592.
- Ghobarah, A., Aziz, T., & Abou-Elfath, H. (1999b). Softening effects on the seismic response of non-ductile concrete frames. *Journal of earthquake engineering*, 3(1), 59-81.
- Ghobarah, A., & Galal, K. (2004). Seismic rehabilitation of short rectangular RC columns. *Journal of earthquake engineering*, 8(1), 45-68.
- Giovinazzi, S., Pampanin, S., & Lagomarsino, S. (2006). Alternative Retrofit Strategies For Pre'70 RC Buildings: Vulnerability Models and Damage Scenarios.
- Haselton, C. B., Liel, A. B., Deierlein, G. G., Dean, B. S., & Chou, J. H. (2010). Seismic collapse safety of reinforced concrete buildings. I: Assessment of ductile moment frames. *Journal of Structural Engineering*, 137(4), 481-491.
- Hubert, W. E., Hull, A. N., Morford, D. R., & Englebretson, R. E. (1983). Forecaster Handbook for the Middle East/Arabian Sea: DTIC Document.
- Hussain, N. (2012). *Seismic Performance and Economics of High-rise Buildings under Seismic and Wind Loads*. (Master thesis), United Arab Emirates University, UAE.
- IBC. (2000). International building code. *International Code Council, Inc. Country Club Hills, IL*.
- IBC. (2003). International building code. *International Code Council, Inc. Country Club Hills, IL*.
- Jamali, F., Aghda, S. F., & Aliyari, A. (2006). *Evaluation of seismic sources for hazard assessment in the Fujairah Emirate (UAE)*. Paper presented at the The 10th IAEG International Congress, Nottingham, United Kingdom, 6th to 10th September 2006.
- Jeong, S.-H., & Elnashai, A. S. (2005). Analytical assessment of an irregular RC frame for full-scale 3D Pseudo-dynamic testing part I: analytical model verification. *Journal of earthquake engineering*, 9(1), 95-128.

- Jeong, S.-H., Mwafy, A. M., & Elnashai, A. S. (2012). Probabilistic seismic performance assessment of code-compliant multi-story RC buildings. *Engineering structures*, 34, 527-537.
- Kappos, A. J., & Panagopoulos, G. (2010). Fragility curves for reinforced concrete buildings in Greece. *Structure and Infrastructure Engineering*, 6(1-2), 39-53.
- Khan, Z., El-Emam, M., Irfan, M., & Abdalla, J. (2013). Probabilistic seismic hazard analysis and spectral accelerations for United Arab Emirates. *Natural hazards*, 67(2), 569-589.
- Kircher, C. A., Whitman, R. V., & Holmes, W. T. (2006). HAZUS earthquake loss estimation methods. *Natural Hazards Review*, 7(2), 45-59.
- Kwon, O.-S., & Elnashai, A. (2006). The effect of material and ground motion uncertainty on the seismic vulnerability curves of RC structure. *Engineering structures*, 28(2), 289-303.
- Lam, L., & Teng, J. (2003). Design-oriented stress-strain model for FRP-confined concrete. *Construction and Building Materials*, 17(6), 471-489.
- Liel, A. B. (2008). *Assessing the collapse risk of California's existing reinforced concrete frame structures: Metrics for seismic safety decisions*. Stanford University.
- Liel, A. B., Haselton, C. B., & Deierlein, G. G. (2010). Seismic collapse safety of reinforced concrete buildings. II: Comparative assessment of nonductile and ductile moment frames. *Journal of Structural Engineering*, 137(4), 492-502.
- Malkawi, A. I. H., Barakat, S., Shanableh, A., (...), & Altoubat, S. (2007). *Seismic Hazard Assessment and Mitigation of Earthquake Risk in the United Arab Emirates: Technical Report, A Collaboration Project on Capacity Building in Seismology Between the University of Sharjah and Jordan University of Science and Technology*.
- Mander, J. B., Priestley, M. J., & Park, R. (1988). Theoretical stress-strain model for confined concrete. *Journal of Structural Engineering*, 114(8), 1804-1826.
- Moehle, J. P. (2000). *State of research on seismic retrofit of concrete building structures in the US*. Paper presented at the US-Japan symposium and workshop on seismic retrofit of concrete structures, Pacific Earthquake Engineering Research Center, University of California, Berkeley.
- Moharram, A., Elghazouli, A., & Bommer, J. (2008). Scenario-based earthquake loss estimation for the city of Cairo, Egypt. *Georisk*, 2(2), 92-112.

- Mwafy, A. (2012a). Analytically derived fragility relationships for the modern high-rise buildings in the UAE. *The Structural Design of Tall and Special Buildings*, 21(11), 824-843.
- Mwafy, A., & Elkholy, S. (2012). *Comparative Vulnerability Assessment of Retrofit Techniques for Pre-Code RC Structures*. Paper presented at the The 15th World Conference on Earthquake Engineering.
- Mwafy, A., & Elnashai, A. (2001). Static pushover versus dynamic collapse analysis of RC buildings. *Engineering structures*, 23(5), 407-424.
- Mwafy, A., Hussain, N., & El-Sawy, K. (2014a). Seismic performance and cost-effectiveness of high-rise buildings with increasing concrete strength. *The Structural Design of Tall and Special Buildings*, 10.1002/tal.1165.
- Mwafy, A. M. (2012b). *Classification and idealization of the building stock in the UAE for earthquake loss estimation*. Paper presented at the 15th World Conference on Earthquake Engineering.
- Mwafy, A. M. (2013). Seismic Vulnerability Assessment of the Building Stock in Highly Populated Areas in the UAE, Final UAEU-NRF Research Project Report: United Arab Emirates University, Al Ain, UAE.
- Mwafy, A. M., Elnashai, A. S., Sigbjornsson, R., & Salama, A. (2006). Significance of severe distant and moderate close earthquakes on design and behavior of tall buildings. *The Structural Design of Tall and Special Buildings*, 15(4), 391-416. doi: 10.1002/tal.300
- Mwafy, A. M., Khalifa, S., & EL-Arris, B. (2014b). *Relative Safety Margins of Code-Conforming Vertically Irregular High-Rise Buildings*. Paper presented at the European Conference on Earthquake Engineering and Seismology(2ECEES), Istanbul, Turkey, 24-28 August 2014.
- NBCC. (2005). *National Building Code of Canada*. National Research Council, Ottawa, Canada: The National Research Council of Canada.
- NCMS. (2014). National Center for Meteorology and Seismology, Abu Dhabi, UAE <http://www.ncms.ae/>. Retrieved 20 August, 2014
- Park, R. (1988). *Ductility evaluation from laboratory and analytical testing*. Paper presented at the 9th World Conference on Earthquake Engineering, Tokyo-Kyoto, Japan.
- Park, Y. J., Reinhorn, A. M., & Kunnath, S. K. (1987). IDARC: Inelastic damage analysis of reinforced concrete frame-shear-wall structures.

- Pasucci, V., Free, M., & Lubkowski, Z. (2008). *Seismic hazard and seismic design requirements for the Arabian Peninsula region*. Paper presented at the The 14th World Conference on Earthquake Engineering.
- PEER. (2013). PEER NGA database, <http://peer.berkeley.edu/nga>. Retrieved 01 October, 2013
- Polese, M., Verderame, G. M., Mariniello, C., Iervolino, I., & Manfredi, G. (2008). Vulnerability analysis for gravity load designed RC buildings in Naples–Italy. *Journal of earthquake engineering*, 12(S2), 234-245.
- Priestley, M. N., Verma, R., & Xiao, Y. (1994). Seismic shear strength of reinforced concrete columns. *Journal of Structural Engineering*, 120(8), 2310-2329.
- Ramamoorthy, S. K., Gardoni, P., & Bracci, J. M. (2006). Probabilistic demand models and fragility curves for reinforced concrete frames. *Journal of Structural Engineering*, 132(10), 1563-1572.
- Ramamoorthy, S. K., Gardoni, P., & Bracci, J. M. (2008). Seismic fragility and confidence bounds for gravity load designed reinforced concrete frames of varying height. *Journal of Structural Engineering*, 134(4), 639-650.
- Ray-Chaudhuri, S., & Shinozuka, M. (2010). Enhancement of seismic sustainability of critical facilities through system analysis. *Probabilistic Engineering Mechanics*, 25(2), 235-244.
- Reches, Z. e., & Schubert, G. (1987). Models of post-Miocene deformation of the Arabian Plate. *Tectonics*, 6(6), 707-725.
- Rodgers, A., Fowler, A.-R., Al-Amri, A., & Al-Enezi, A. (2006). The March 11, 2002 Masafi, United Arab Emirates earthquake: insights into the seismotectonics of the northern Oman Mountains. *Tectonophysics*, 415(1), 57-64.
- Rossetto, T., & Elnashai, A. (2005). A new analytical procedure for the derivation of displacement-based vulnerability curves for populations of RC structures. *Engineering structures*, 27(3), 397-409.
- Saadatmanesh, H., Ehsani, M. R., & Jin, L. (1997). Repair of earthquake-damaged RC columns with FRP wraps. *ACI structural journal*, 94(2).
- SEAOC. (1999). Recommended lateral force requirements and commentary, Seventh Edition *Seismology Committee Structural Engineers Association of California, Sacramento, CA*.

- Shama, A. A. (2011). Site specific probabilistic seismic hazard analysis at Dubai Creek on the west coast of UAE. *Earthquake Engineering and Engineering Vibration*, 10(1), 143-152.
- Sigbjornsson, R., & Elnashai, A. (2006). Hazard assessment of Dubai, United Arab Emirates, for close and distant earthquakes. *Journal of earthquake engineering*, 10(5), 749-773.
- Taghdi, M., Bruneau, M., & Saatcioglu, M. (2000). Seismic retrofitting of low-rise masonry and concrete walls using steel strips. *Journal of Structural Engineering*, 126(9), 1017-1025.
- Tremblay, R., Lacerte, M., & Christopoulos, C. (2008). Seismic response of multistory buildings with self-centering energy dissipative steel braces. *Journal of Structural Engineering*, 134(1), 108-120.
- Tremblay, R., Poncet, L., Bolduc, P., Neville, R., & DeVall, R. (2004). *Testing and design of buckling restrained braces for Canadian application*. Paper presented at the Proceedings of the 13th World Conference on Earthquake Engineering.
- UBC. (1967). Uniform Building Code. International Council of Building Officials, Whittier, CA.
- UBC. (1997). Uniform Building Code, Vol. 2. International Council of Building Officials, Whittier, CA.
- USGS. (2014). United States Geological Survey, USA, <http://www.usgs.gov/>. Retrieved 20 August, 2014
- Vamvatsikos, D., & Cornell, C. A. (2002a). Incremental dynamic analysis. *Earthquake engineering & structural dynamics*, 31(3), 491-514.
- Vamvatsikos, D., & Cornell, C. A. (2002b). *The incremental dynamic analysis and its application to performance-based earthquake engineering*. Paper presented at the Proceedings of the 12th European Conference on Earthquake Engineering, London, UK, 9-13 September 2002.
- Vernant, P., Nilforoushan, F., Hatzfeld, D., (...), & Bayer, R. (2004). Present-day crustal deformation and plate kinematics in the Middle East constrained by GPS measurements in Iran and northern Oman. *Geophysical Journal International*, 157(1), 381-398.
- Vita-Finzi, C. (2001). Neotectonics at the Arabian plate margins. *Journal of Structural Geology*, 23(2), 521-530.

- Wei, Y.-Y., & Wu, Y.-F. (2012). Unified stress–strain model of concrete for FRP-confined columns. *Construction and Building Materials*, 26(1), 381-392.
- Wen, Y., Ellingwood, B., & Bracci, J. M. (2004). Vulnerability function framework for consequence-based engineering, MAE Center Project DS-4 Report. *illinois digital environment for access to learning and scholarship*.
- Wood, S. L. (1991). Performance of reinforced concrete buildings during the 1985 Chile earthquake: implications for the design of structural walls. *Earthquake Spectra*, 7(4), 607-638.
- Yamamoto, Y., & Baker, J. W. (2013). Stochastic model for earthquake ground motion using wavelet packets. *Bulletin of the Seismological Society of America*, 103(6), 3044-3056.
- Ye, L., Zhang, K., Zhao, S., & Feng, P. (2003). Experimental study on seismic strengthening of RC columns with wrapped CFRP sheets. *Construction and Building Materials*, 17(6), 499-506.

APPENDIX A: SAMPLE IDA RESULTS

Table A.1: Incremental dynamic analysis results showing inter-story drift ratios of reference buildings at different PGA levels for 20 far-field records

File Name	Earthquake	PGA	Story Drift (%)								
			BO-02	BO-08	BO-18	BO-26	BO-40	FS	PS	SC	HO
bu.crv	Bucharest	0.08	1.04	0.99	0.37	0.25	0.26	0.15	0.68	0.90	1.10
		0.16	2.13	1.65	0.71	0.50	0.50	0.36	1.33	1.81	2.11
		0.24	---	1.94	0.98	0.78	0.77	0.59	1.66	2.29	2.92
		0.32	---	2.57	1.27	1.09	1.08	0.84	2.37	3.12	3.27
		0.40	---	3.18	1.65	1.46	1.41	1.09	2.92	4.26	4.26
		0.48	---	3.68	2.06	1.85	1.69	1.38	3.55	5.45	5.26
		0.56	---	4.08	2.43	2.18	1.94	1.72	4.70	6.89	6.21
		0.64	---	4.38	2.77	2.44	2.12	2.14	6.20	9.92	7.05
		0.72	---	4.61	3.08	2.63	2.25	2.63	8.16	---	7.83
		0.80	---	4.79	3.39	2.73	2.56	3.22	---	---	8.51
		0.88	---	4.97	3.69	2.77	2.85	3.91	---	---	9.12
		0.96	---	5.15	3.98	2.90	3.10	4.70	---	---	9.67
		1.04	---	5.29	4.26	3.19	3.39	5.60	---	---	---
1.12	---	5.95	4.53	3.54	3.67	6.63	---	---	---		
hmi.crv	Hector Mine-Indio	0.08	1.24	0.44	0.20	0.24	0.34	0.17	0.44	1.01	0.52
		0.16	1.96	1.08	0.33	0.41	0.57	0.35	1.07	1.77	1.09
		0.24	3.80	1.66	0.61	0.62	0.80	0.56	1.72	2.18	1.93
		0.32	---	1.72	1.07	1.20	0.95	0.79	3.19	2.48	2.76
		0.40	---	2.11	1.23	1.44	1.13	1.04	3.91	2.88	3.23
		0.48	---	2.31	1.14	1.83	1.32	1.32	3.93	3.44	3.15
		0.56	---	2.43	1.43	2.13	1.48	1.65	4.45	4.78	3.73
		0.64	---	2.53	1.68	2.36	1.58	2.05	5.23	6.04	4.27
		0.72	---	2.72	1.82	2.51	1.68	2.55	5.96	6.77	4.63
		0.80	---	3.19	1.85	2.66	1.96	3.10	6.73	6.80	4.87
		0.88	---	3.65	2.68	2.89	2.19	3.74	7.47	6.67	5.21
		0.96	---	3.77	4.53	3.14	2.36	4.56	7.98	6.77	5.53
		1.04	---	3.76	5.29	---	2.50	5.37	8.56	7.11	5.62
1.12	---	4.17	4.30	---	2.59	6.00	---	7.30	5.82		
tap90.crv	Hector Mine- Mecca	0.08	1.13	0.72	0.29	0.29	0.30	0.21	0.54	0.85	1.02
		0.16	1.97	1.40	0.61	0.64	0.48	0.48	1.50	1.94	1.93
		0.24	3.18	1.90	0.79	1.04	0.75	0.79	2.71	2.61	2.69
		0.32	---	2.45	0.97	1.44	1.08	1.08	3.24	3.42	3.35
		0.40	---	2.94	1.34	1.81	1.41	1.38	4.18	3.74	4.27
		0.48	---	3.41	1.91	2.31	1.72	1.84	5.87	3.79	5.20
		0.56	---	3.89	2.52	3.10	2.02	2.40	7.92	4.25	6.06
		0.64	---	4.40	3.07	8.68	2.27	3.09	---	4.33	6.88
		0.72	---	4.94	3.57	---	2.46	4.01	---	4.78	7.71
		0.80	---	---	3.99	---	2.59	5.04	---	5.48	8.58
		0.88	---	---	4.31	---	2.69	6.12	---	6.22	9.49
		0.96	---	---	4.59	---	2.80	7.35	---	7.06	---
		1.04	---	---	5.62	---	2.92	8.68	---	8.56	---
1.12	---	---	6.71	---	3.06	9.89	---	---	---		
ev.crv	Loma Prieta-Emeryville	0.08	1.46	0.46	0.29	0.26	0.30	0.20	0.63	1.62	0.63
		0.16	2.51	0.85	0.48	0.54	0.58	0.45	1.50	2.37	1.24
		0.24	3.34	1.20	0.65	0.84	0.90	0.71	2.45	2.87	1.73
		0.32	4.55	1.81	0.86	1.12	1.21	1.00	3.58	3.22	2.20
		0.40	---	2.47	1.04	1.46	1.42	1.33	4.48	3.72	3.02
		0.48	---	3.04	1.12	1.83	1.56	1.73	5.12	4.33	3.98
		0.56	---	3.51	1.32	2.04	1.66	2.12	5.94	4.87	5.02
		0.64	---	3.85	1.67	2.22	1.75	2.51	6.62	5.29	6.00
		0.72	---	4.11	2.07	2.50	1.87	3.10	7.13	5.57	6.87
		0.80	---	4.31	2.46	2.78	2.11	3.82	7.54	5.76	7.59
		0.88	---	4.48	2.84	3.52	2.34	4.59	7.88	5.88	8.18
		0.96	---	4.80	3.20	4.88	2.56	5.35	8.20	5.97	9.42
		1.04	---	4.98	3.50	6.25	2.77	6.06	8.46	6.02	---
1.12	---	5.07	3.69	9.09	2.97	6.71	8.66	6.06	---		

Table A.1 (cont'd): Incremental dynamic analysis results showing inter-story drift ratios of reference buildings at different PGA levels for 20 far-field records

ggb.crv	Loma Prieta-ggb	0.08	1.12	0.41	0.23	0.23	0.24	0.14	0.65	1.03	0.51
		0.16	2.68	0.77	0.40	0.45	0.45	0.34	1.36	1.85	1.04
		0.24	4.30	1.12	0.54	0.72	0.64	0.55	2.15	2.70	1.57
		0.32	4.19	1.46	0.76	0.99	0.87	0.78	2.63	3.36	2.02
		0.40	6.40	1.89	1.00	1.25	1.14	1.04	3.35	3.76	2.41
		0.48	---	2.28	1.23	1.51	1.45	1.34	4.21	3.87	2.87
		0.56	---	2.63	1.42	1.77	1.75	1.70	5.11	3.73	3.44
		0.64	---	2.98	1.54	2.07	2.05	2.15	6.16	4.12	4.02
		0.72	---	3.33	1.60	2.39	2.33	2.71	7.39	4.65	4.59
		0.80	---	3.70	1.78	2.74	2.60	3.38	9.17	5.17	5.14
		0.88	---	4.07	2.05	3.09	2.84	4.18	12.09	5.67	5.69
		0.96	---	4.45	2.35	3.38	3.06	5.09	15.31	6.17	6.25
		1.04	---	4.83	2.69	3.60	3.26	6.11	16.20	6.66	6.84
		1.12	---	5.21	3.02	3.81	3.43	7.22	15.50	7.14	7.44
lpa.crv	Loma Prieta-Alameda	0.08	0.68	0.77	0.39	0.37	0.23	0.33	0.47	0.79	1.00
		0.16	2.00	1.20	0.64	0.56	0.45	0.70	0.93	1.79	1.72
		0.24	4.22	1.93	0.82	0.72	0.68	1.05	1.37	2.60	2.41
		0.32	---	2.68	1.14	0.99	0.94	1.39	1.85	3.19	3.51
		0.40	---	3.21	1.48	1.36	1.25	1.72	2.41	4.29	4.66
		0.48	---	3.39	1.85	1.73	1.56	2.14	3.18	5.48	5.72
		0.56	---	3.34	2.22	2.03	1.86	2.69	4.23	6.71	6.61
		0.64	---	3.56	2.38	2.35	2.13	3.28	5.64	7.91	7.24
		0.72	---	4.32	2.40	2.74	2.37	3.94	7.64	9.02	7.58
		0.80	---	5.13	2.67	3.12	2.59	4.65	---	---	7.67
		0.88	---	5.84	3.07	3.50	2.78	5.40	---	---	7.49
		0.96	---	8.94	3.45	3.85	2.95	6.18	---	---	6.99
		1.04	---	---	3.78	4.17	3.10	6.95	---	---	6.91
		1.12	---	---	4.10	5.43	3.24	7.71	---	---	7.84
lpo.crv	Loma Prieta-Oakland	0.08	0.73	0.35	0.18	0.23	0.20	0.16	0.61	0.71	0.47
		0.16	1.71	0.78	0.32	0.52	0.37	0.38	1.47	1.45	0.98
		0.24	2.15	1.40	0.50	0.86	0.53	0.61	2.31	1.99	1.63
		0.32	2.96	2.02	0.70	1.18	0.71	0.85	2.86	2.33	2.41
		0.40	4.90	2.56	0.92	1.45	0.92	1.10	3.00	2.69	3.26
		0.48	---	3.04	1.18	1.69	1.09	1.35	3.54	3.27	4.11
		0.56	---	3.43	1.49	1.89	1.21	1.75	4.05	3.88	4.97
		0.64	---	3.72	1.75	2.00	1.33	2.21	4.51	4.50	5.84
		0.72	---	3.91	2.09	1.98	1.46	2.53	4.98	5.05	6.73
		0.80	---	4.05	2.61	1.96	1.58	2.94	5.32	5.51	7.59
		0.88	---	4.18	3.06	2.06	1.69	3.37	5.58	5.96	8.40
		0.96	---	4.26	3.35	2.15	1.77	3.63	6.00	6.38	8.95
		1.04	---	4.33	3.50	2.23	1.85	4.20	6.43	6.81	9.38
		1.12	---	4.37	3.45	2.30	1.98	4.85	7.25	7.28	9.68
lpb.crv	Loma Prieta-Berkeley LBL	0.08	0.93	0.33	0.18	0.23	0.18	0.21	0.80	0.62	0.41
		0.16	1.60	0.70	0.33	0.48	0.36	0.50	1.59	1.34	0.86
		0.24	2.04	1.12	0.42	0.69	0.54	0.79	2.35	1.94	1.35
		0.32	2.63	1.58	0.56	1.01	0.74	1.05	3.32	2.28	1.89
		0.40	3.15	2.08	0.71	1.38	0.97	1.30	4.05	2.61	2.48
		0.48	3.63	2.53	0.94	1.75	1.21	1.72	4.34	2.92	3.12
		0.56	4.22	2.86	1.27	2.16	1.44	2.25	4.35	3.14	3.76
		0.64	6.70	3.05	1.58	2.57	1.66	2.85	4.77	3.42	4.41
		0.72	---	3.10	1.84	2.92	1.86	3.51	5.62	3.84	4.99
		0.80	---	3.03	2.04	3.20	2.05	4.20	6.48	4.25	5.47
		0.88	---	2.95	2.15	3.40	2.22	4.91	7.35	4.66	5.85
		0.96	---	3.23	2.13	6.22	2.38	5.59	8.19	5.08	6.12
		1.04	---	3.81	2.42	9.65	2.53	6.21	9.01	5.50	6.26
		1.12	---	4.44	2.75	---	2.67	6.75	9.81	5.92	6.27

Table A.1 (cont'd): Incremental dynamic analysis results showing inter-story drift ratios of reference buildings at different PGA levels for 20 far-field records

ch.crv	Chi-Chi-ILA013	0.08	1.40	0.68	0.39	0.38	0.39	0.31	0.77	1.34	1.12
		0.16	3.09	1.62	0.69	0.65	0.72	0.60	1.74	2.52	2.16
		0.24	4.34	2.85	1.31	1.16	0.97	0.94	2.29	3.51	3.45
		0.32	---	3.56	1.77	1.63	1.39	1.23	3.51	4.21	4.81
		0.40	---	3.09	1.98	1.83	1.64	1.54	5.48	4.98	6.04
		0.48	---	3.38	1.79	2.16	2.01	1.78	6.54	5.75	6.33
		0.56	---	4.68	2.34	2.44	2.42	2.20	7.28	6.83	6.34
		0.64	---	5.35	2.26	2.67	2.77	2.71	8.25	8.10	6.08
		0.72	---	5.68	4.41	3.01	3.11	3.33	9.37	9.35	6.98
		0.80	---	6.55	8.36	3.30	3.55	4.03	---	---	7.68
		0.88	---	---	---	3.30	4.01	4.95	---	---	8.29
		0.96	---	---	---	---	4.38	5.96	---	---	---
		1.04	---	---	---	---	4.57	7.08	---	---	---
		1.12	---	---	---	---	4.59	8.23	---	---	---
tap32.crv	Chi-Chi-ILA030	0.08	1.33	0.48	0.22	0.31	0.34	0.25	1.04	1.23	0.57
		0.16	2.14	0.99	0.40	0.46	0.61	0.59	1.59	1.88	1.25
		0.24	2.61	1.49	0.54	0.93	0.82	0.94	2.41	2.46	1.78
		0.32	3.56	2.07	0.72	1.40	0.99	1.29	3.54	3.24	2.46
		0.40	---	2.69	1.08	1.75	1.29	1.59	4.14	3.50	3.59
		0.48	---	3.22	1.49	2.32	1.62	1.81	4.01	3.75	4.83
		0.56	---	3.54	1.83	2.76	1.86	2.15	5.66	3.75	5.92
		0.64	---	4.15	2.04	3.02	2.05	2.67	6.06	4.94	6.57
		0.72	---	---	2.23	3.21	2.26	3.18	5.73	5.81	7.20
		0.80	---	---	2.45	7.58	2.63	3.68	6.47	6.79	7.76
		0.88	---	---	2.75	---	3.11	4.15	7.28	7.58	7.94
		0.96	---	---	3.12	---	3.56	4.58	7.84	8.17	---
		1.04	---	---	3.51	---	3.99	5.01	8.33	8.94	---
		1.12	---	---	4.05	---	4.36	5.42	8.75	9.93	---
tap05.crv	Chi-Chi-TAP005	0.08	1.41	0.76	0.29	0.35	0.3	0.19	0.67	1.11	0.86
		0.16	2.62	1.65	0.53	0.67	0.57	0.43	2.64	2.22	2.01
		0.24	2.99	2.17	1.05	1.05	0.84	0.70	3.47	2.73	3.19
		0.32	4.85	2.59	1.67	1.35	1.12	0.99	4.19	3.05	3.98
		0.40	---	2.74	1.99	2.20	1.45	1.35	4.86	3.32	4.31
		0.48	---	2.89	1.93	2.52	1.81	1.81	5.49	3.59	4.67
		0.56	---	3.28	2.00	2.82	2.10	2.46	5.98	4.46	4.97
		0.64	---	3.62	2.17	3.10	2.18	3.36	6.49	5.56	5.24
		0.72	---	3.89	2.40	3.33	2.21	4.61	7.18	6.61	5.99
		0.80	---	4.16	2.62	3.52	2.47	6.04	7.71	7.21	6.66
		0.88	---	5.01	2.92	5.81	2.73	7.30	8.48	7.55	7.09
		0.96	---	---	3.34	---	3.03	8.15	---	7.79	7.24
		1.04	---	---	3.75	---	3.32	8.83	---	9.94	7.75
		1.12	---	---	4.23	---	3.61	9.54	---	---	9.18
tap10.crv	Chi-Chi-TAP010	0.08	1.48	1.25	0.31	0.39	0.33	0.18	0.59	1.08	1.40
		0.16	2.21	2.01	0.99	0.73	0.59	0.42	2.08	1.96	2.63
		0.24	---	2.81	1.45	1.10	0.82	0.68	3.50	2.45	3.85
		0.32	---	3.35	1.76	1.39	1.15	0.96	4.33	2.89	4.65
		0.40	---	3.79	2.05	2.17	1.49	1.30	5.24	3.92	5.34
		0.48	---	4.22	2.47	2.41	1.76	1.72	5.99	5.80	5.96
		0.56	---	6.17	2.91	2.57	2.04	2.31	6.57	7.75	7.00
		0.64	---	---	3.27	2.74	2.31	3.10	7.17	8.33	8.63
		0.72	---	---	3.58	2.92	2.53	4.19	7.95	6.98	---
		0.80	---	---	3.77	3.21	2.95	5.57	9.36	---	---
		0.88	---	---	3.63	3.73	3.43	7.04	---	---	---
		0.96	---	---	4.66	5.89	3.85	8.36	---	---	---
		1.04	---	---	5.11	8.68	4.15	9.39	---	---	---
		1.12	---	---	5.02	5.20	4.48	---	---	---	---

Table A.1 (cont'd): Incremental dynamic analysis results showing inter-story drift ratios of reference buildings at different PGA levels for 20 far-field records

tap21.crv	Chi-Chi-TAP021	0.08	0.89	1.02	0.38	0.26	0.30	0.18	0.47	0.82	1.19
		0.16	2.79	1.63	0.92	0.55	0.55	0.39	0.99	1.62	2.29
		0.24	---	1.78	1.44	0.98	0.85	0.63	1.74	2.33	2.88
		0.32	---	2.03	1.44	1.60	1.20	0.90	2.92	2.84	2.94
		0.40	---	2.27	1.59	2.01	1.50	1.20	4.42	3.13	3.49
		0.48	---	2.69	1.72	2.22	1.86	1.58	5.67	4.71	3.88
		0.56	---	3.22	1.93	2.26	2.16	2.06	7.03	8.40	4.16
		0.64	---	3.68	2.37	2.62	2.50	2.70	9.12	---	4.92
		0.72	---	4.01	2.93	5.03	2.82	3.49	---	---	5.85
		0.80	---	4.25	3.44	---	3.16	4.47	---	---	6.84
		0.88	---	4.80	3.79	---	3.48	5.68	---	---	7.68
		0.96	---	---	4.38	---	3.74	7.11	---	---	8.33
		1.04	---	---	5.64	---	4.11	8.72	---	---	8.88
		1.12	---	---	6.29	---	4.76	---	---	---	9.17
tap95.crv	Chi-Chi-TAP095	0.08	1.15	0.45	0.28	0.30	0.24	0.26	0.59	0.67	0.61
		0.16	2.59	1.07	0.46	0.69	0.42	0.54	1.30	1.83	1.31
		0.24	4.46	1.55	0.80	0.91	0.58	0.81	1.89	2.93	1.92
		0.32	3.82	1.89	1.02	1.31	0.80	1.07	2.60	3.53	2.58
		0.40	4.41	2.61	1.37	1.43	1.09	1.34	3.17	4.13	2.96
		0.48	---	3.11	1.68	1.68	1.40	1.73	3.87	4.40	3.87
		0.56	---	3.50	1.94	2.20	1.72	2.14	4.96	4.45	4.88
		0.64	---	3.85	2.22	2.52	1.97	2.55	6.26	4.51	5.78
		0.72	---	4.11	2.59	2.74	2.16	2.94	7.71	4.62	6.51
		0.80	---	4.28	2.92	2.99	2.32	3.30	9.19	5.17	7.32
		0.88	---	4.52	2.84	3.26	2.44	3.63	---	5.74	8.32
		0.96	---	4.94	2.81	3.25	2.51	3.87	---	6.16	---
		1.04	---	7.14	3.09	4.15	2.57	4.07	---	6.36	---
		1.12	---	---	3.37	4.56	2.71	4.46	---	6.60	---
mat.crv	Manjil-Tonekabun	0.08	1.19	0.61	0.30	0.23	0.24	0.29	0.63	1.09	0.73
		0.16	2.58	1.09	0.51	0.52	0.44	0.60	1.44	2.04	1.54
		0.24	3.03	1.56	0.79	0.60	0.65	0.92	1.85	2.76	2.16
		0.32	4.83	1.73	0.98	0.67	0.91	1.22	1.98	3.38	2.79
		0.40	---	2.13	1.04	0.89	1.28	1.49	2.60	4.04	3.15
		0.48	---	2.42	1.25	1.11	1.62	1.66	2.88	4.34	3.40
		0.56	---	2.59	1.53	1.14	1.93	1.87	5.08	3.80	3.99
		0.64	---	2.70	1.78	1.40	2.20	2.35	7.22	4.52	4.45
		0.72	---	2.79	1.98	1.69	2.45	2.98	8.46	4.58	4.75
		0.80	---	2.88	2.13	2.23	2.66	3.72	8.88	5.12	4.89
		0.88	---	3.01	2.30	2.75	2.86	4.54	9.04	6.00	4.95
		0.96	---	3.20	2.36	3.11	3.03	5.36	9.24	6.77	5.04
		1.04	---	3.42	2.29	3.35	3.17	6.19	9.14	7.39	5.36
		1.12	---	3.65	2.26	3.52	3.27	7.06	9.19	7.94	5.68
maa.crv	Manjil-Abhar	0.08	0.67	0.48	0.23	0.57	0.23	0.16	0.57	0.70	0.41
		0.16	1.38	1.27	0.34	0.83	0.41	0.35	0.95	1.14	1.31
		0.24	2.33	2.58	0.78	1.38	0.62	0.54	1.44	1.44	2.24
		0.32	4.41	3.30	1.42	1.35	0.80	0.75	1.63	1.66	4.26
		0.40	---	3.34	2.05	1.52	0.97	1.00	1.82	1.95	5.33
		0.48	---	3.53	2.38	1.71	1.11	1.26	2.42	3.37	6.42
		0.56	---	3.57	2.22	1.91	1.22	1.50	2.97	4.55	6.62
		0.64	---	3.76	2.55	2.20	1.34	1.80	3.34	5.16	6.44
		0.72	---	5.70	2.86	2.54	1.63	2.05	3.47	5.65	6.78
		0.80	---	---	3.12	2.87	1.90	2.31	4.75	5.56	6.28
		0.88	---	---	3.40	3.18	2.16	2.66	5.65	6.90	7.00
		0.96	---	---	4.07	3.45	2.42	3.06	7.02	8.80	7.52
		1.04	---	---	4.98	3.68	2.81	3.50	8.94	---	---
		1.12	---	---	5.04	3.92	3.17	4.01	---	---	---

Table A.1 (cont'd): Incremental dynamic analysis results showing inter-story drift ratios of reference buildings at different PGA levels for 20 far-field records

iza.crv	Izmit-Ambarli	0.08	1.44	0.49	0.29	0.27	0.36	0.19	1.19	1.30	0.56
		0.16	2.74	0.87	0.45	0.81	0.62	0.48	2.05	2.29	1.17
		0.24	3.21	1.16	0.68	1.05	0.92	0.80	3.24	3.14	1.70
		0.32	3.93	1.51	0.82	1.34	1.16	1.15	3.80	3.80	2.19
		0.40	5.08	2.14	0.99	1.83	1.47	1.66	4.64	4.06	2.61
		0.48	---	2.83	1.10	1.89	2.00	2.35	5.28	4.49	2.95
		0.56	---	3.16	1.38	2.37	2.45	2.61	5.65	5.29	3.90
		0.64	---	3.82	1.72	2.59	2.84	3.47	5.82	5.94	5.16
		0.72	---	---	2.13	2.48	3.17	4.36	6.01	6.28	6.44
		0.80	---	---	6.01	2.94	3.44	5.07	7.93	6.09	7.48
		0.88	---	---	6.86	3.38	3.67	5.58	---	5.99	8.17
		0.96	---	---	2.74	12.10	3.77	6.08	---	6.78	8.23
		1.04	---	---	3.07	4.03	3.87	6.44	---	7.51	8.30
		1.12	---	---	3.86	4.11	3.95	6.84	---	8.20	---
izz.crv	Izmit-Zeytinburnu	0.08	0.69	0.35	0.24	0.23	0.15	0.20	0.28	0.71	0.45
		0.16	1.31	0.63	0.42	0.46	0.27	0.45	0.73	1.73	0.89
		0.24	2.71	0.99	0.52	0.66	0.39	0.70	1.11	2.56	1.17
		0.32	3.88	1.47	0.73	0.94	0.64	0.94	1.30	2.76	1.64
		0.40	3.32	2.05	0.91	1.08	0.96	1.15	2.17	3.24	2.12
		0.48	---	2.48	1.21	1.12	1.27	1.36	2.88	3.71	2.67
		0.56	---	2.76	1.54	1.31	1.53	1.63	3.28	3.98	3.52
		0.64	---	2.90	1.69	1.58	1.73	1.97	3.58	4.10	4.56
		0.72	---	3.02	1.84	1.81	1.88	2.36	4.26	4.04	5.10
		0.80	---	3.56	1.88	2.00	1.98	2.75	5.58	4.01	5.25
		0.88	---	4.05	1.97	2.21	2.07	3.16	8.10	4.29	5.07
		0.96	---	4.42	2.21	2.38	2.16	3.58	8.14	4.53	4.99
		1.04	---	4.89	2.43	2.57	2.14	3.99	7.36	4.88	5.12
		1.12	---	9.86	2.61	2.72	2.16	4.44	7.08	5.41	5.44
kob.crv	Kocaeli- Bursa	0.08	1.39	0.59	0.32	0.32	0.58	0.19	0.48	1.22	0.71
		0.16	2.68	1.32	0.49	0.70	1.08	0.46	1.49	2.56	1.42
		0.24	4.66	1.99	0.81	1.09	1.51	0.70	2.29	3.14	2.50
		0.32	---	2.36	1.19	1.56	1.71	0.92	3.69	3.48	3.30
		0.40	---	2.46	1.30	2.52	2.28	1.13	5.06	3.98	4.00
		0.48	---	2.85	1.52	2.58	2.80	1.33	6.07	4.93	4.44
		0.56	---	3.44	1.83	---	3.22	1.73	6.67	5.54	4.85
		0.64	---	4.12	2.29	---	3.54	2.19	7.02	6.27	5.64
		0.72	---	---	3.78	---	3.80	2.65	6.96	7.24	6.73
		0.80	---	---	3.73	---	4.02	3.07	7.58	8.40	7.44
		0.88	---	---	3.89	---	4.23	3.95	8.62	9.70	8.24
		0.96	---	---	4.55	---	4.51	4.85	9.45	---	9.96
		1.04	---	---	3.89	---	4.87	5.76	---	---	---
		1.12	---	---	5.21	---	---	6.73	---	---	---
koh.crv	Kocaeli-Hava Alani	0.08	0.99	0.47	0.26	0.22	0.45	0.13	0.78	0.64	0.56
		0.16	2.09	1.27	0.45	0.47	0.81	0.29	1.61	1.34	1.31
		0.24	2.92	1.62	0.78	1.14	1.16	0.54	2.16	2.22	2.36
		0.32	6.33	1.84	1.08	1.46	1.56	0.81	2.32	3.50	2.83
		0.40	---	2.20	1.15	2.15	1.93	1.07	2.68	4.06	3.07
		0.48	---	2.54	1.43	2.45	2.26	1.32	3.57	3.73	3.43
		0.56	---	2.69	1.78	108.16	2.60	1.59	5.13	4.36	3.93
		0.64	---	3.71	2.12	16.41	2.84	2.05	6.23	5.42	4.34
		0.72	---	4.81	2.24	21.35	3.00	2.57	7.36	6.24	4.53
		0.80	---	---	2.69	3.38	3.15	3.04	8.60	6.86	5.26
		0.88	---	---	3.26	3.70	3.33	3.39	9.46	7.23	5.78
		0.96	---	---	3.83	4.20	3.72	3.86	9.40	7.40	6.74
		1.04	---	---	3.73	9.35	4.00	4.60	9.25	7.69	7.74
		1.12	---	---	3.97	---	4.38	5.37	---	8.11	---

Table A.2: Incremental dynamic analysis results showing inter-story drift ratios of reference buildings at different PGA levels for 20 near-source records

File Name	Earthquake	PGA	Story Drift (%)								
			BO-02	BO-08	BO-18	BO-26	BO-40	FS	PS	SC	HO
co394.crv	Coalinga-04(394)	0.32	0.93	0.36	0.20	0.23	0.19	0.38	0.62	0.16	0.48
		0.64	2.01	0.73	0.31	0.43	0.35	0.79	1.30	0.30	1.00
		0.96	2.59	1.14	0.46	0.57	0.51	1.14	1.97	0.42	1.50
		1.28	2.48	1.45	0.68	0.73	0.65	1.43	2.50	0.53	1.95
		1.60	3.08	1.72	0.90	0.90	0.81	1.88	2.75	0.64	2.31
		1.92	3.90	1.94	1.14	1.08	0.96	2.34	2.87	0.75	2.70
		2.24	4.67	2.10	1.40	1.31	1.09	2.74	3.48	0.87	3.08
		2.56	5.38	2.23	1.56	1.54	1.20	3.09	4.52	0.98	3.39
		2.88	---	2.34	1.63	1.78	1.29	3.43	5.45	1.10	3.62
		3.20	---	2.44	1.68	1.99	1.35	3.76	6.09	1.22	3.79
		3.52	---	2.52	1.75	2.18	1.39	4.10	6.33	1.33	3.90
		3.84	---	2.60	1.83	2.33	1.42	4.42	6.28	1.44	3.99
		4.16	---	2.67	1.90	2.42	1.44	4.74	6.10	1.55	4.05
		4.48	---	2.82	1.97	2.47	1.46	5.05	5.82	1.65	4.11
co395.crv	Coalinga-04(395)	0.32	0.43	0.22	0.12	0.11	0.10	0.15	0.33	0.12	0.31
		0.64	0.63	0.43	0.28	0.17	0.17	0.31	0.62	0.24	0.60
		0.96	0.81	0.64	0.41	0.26	0.24	0.45	0.90	0.34	0.89
		1.28	1.11	0.85	0.51	0.37	0.30	0.61	1.20	0.44	1.17
		1.60	1.43	1.03	0.62	0.46	0.35	0.77	1.50	0.53	1.42
		1.92	1.76	1.18	0.72	0.53	0.39	0.93	1.69	0.61	1.64
		2.24	2.11	1.32	0.82	0.59	0.45	1.10	1.83	0.69	1.82
		2.56	2.46	1.43	0.91	0.63	0.50	1.27	2.00	0.77	1.94
		2.88	2.82	1.53	1.00	0.68	0.55	1.45	2.15	0.85	2.04
		3.20	3.18	1.61	1.08	0.72	0.60	1.63	2.27	0.92	2.16
		3.52	3.54	1.67	1.16	0.75	0.65	1.82	2.37	0.99	2.31
		3.84	3.91	1.73	1.22	0.78	0.70	2.01	2.49	1.06	2.44
		4.16	4.43	1.78	1.29	0.82	0.74	2.20	2.69	1.12	2.57
		4.48	5.18	1.89	1.34	0.87	0.78	2.40	2.88	1.19	2.68
co405.crv	Coalinga-04(405)	0.32	0.94	0.41	0.21	0.29	0.19	0.35	0.63	0.15	0.56
		0.64	1.59	0.89	0.38	0.44	0.28	0.69	1.20	0.32	1.10
		0.96	2.03	1.20	0.55	0.53	0.41	1.01	2.17	0.46	1.49
		1.28	2.28	1.43	0.60	0.73	0.52	1.37	2.83	0.61	1.92
		1.60	2.34	1.66	0.73	0.99	0.63	1.86	2.69	0.76	2.29
		1.92	2.50	1.85	0.90	1.46	0.73	2.36	3.80	0.91	2.59
		2.24	2.81	2.02	1.13	1.74	0.88	2.75	4.85	1.08	2.83
		2.56	3.09	2.17	1.43	1.73	1.03	3.04	5.62	1.22	3.00
		2.88	3.44	2.31	1.68	1.67	1.18	3.25	6.16	1.35	3.20
		3.20	3.64	2.54	1.78	1.78	1.30	3.37	6.37	1.46	3.46
		3.52	3.85	2.73	1.89	1.89	1.42	3.46	6.42	1.58	3.79
		3.84	4.31	2.88	2.02	1.94	1.53	4.01	6.44	1.70	4.29
		4.16	---	2.99	2.17	1.94	1.63	4.61	6.45	1.81	4.87
		4.48	---	3.09	2.37	2.01	1.72	5.28	6.53	1.92	5.35
cl.crv	Coyote Lake	0.32	1.17	0.99	0.28	0.32	0.19	0.53	0.78	0.18	0.87
		0.64	2.19	1.49	0.64	0.62	0.38	1.04	1.70	0.35	2.21
		0.96	2.45	1.76	0.99	0.85	0.63	1.42	2.12	0.50	2.62
		1.28	3.98	2.17	1.13	0.97	0.87	1.96	2.52	0.65	2.84
		1.60	---	2.35	1.57	1.09	1.09	2.59	2.75	0.82	3.51
		1.92	---	2.24	1.78	1.27	1.22	3.20	3.23	1.01	3.93
		2.24	---	2.67	3.12	1.38	1.26	3.75	3.69	1.28	4.57
		2.56	---	3.26	2.28	1.58	1.38	4.25	3.82	1.54	5.55
		2.88	---	3.80	2.65	2.05	1.60	4.71	4.06	1.75	6.14
		3.20	---	4.27	2.48	2.17	1.80	5.12	4.53	1.91	6.07
		3.52	---	4.87	2.27	2.09	2.03	5.48	5.15	2.06	5.96
		3.84	---	5.92	2.43	2.04	2.26	5.81	5.74	2.11	5.97
		4.16	---	---	2.60	1.94	2.24	6.09	7.48	2.17	6.19
		4.48	---	---	2.93	1.96	2.66	6.35	---	2.18	6.35

Table A.2 (cont'd): Incremental dynamic analysis results showing inter-story drift ratios of reference buildings at different PGA levels for 20 near-source records

fri.crv	Friuli (aftershock)	0.32	0.52	0.30	0.21	0.13	0.13	0.21	0.42	0.11	0.32
		0.64	0.84	0.53	0.31	0.25	0.23	0.46	0.85	0.23	0.61
		0.96	1.08	0.70	0.44	0.38	0.33	0.71	1.24	0.34	0.89
		1.28	1.37	0.93	0.55	0.61	0.42	0.95	1.56	0.45	1.21
		1.60	1.80	1.17	0.71	0.83	0.51	1.20	1.84	0.57	1.50
		1.92	2.34	1.36	0.89	0.98	0.57	1.45	1.98	0.68	1.77
		2.24	2.87	1.56	1.04	1.07	0.63	1.69	2.17	0.80	1.98
		2.56	3.36	1.78	1.14	1.10	0.68	1.95	2.60	0.91	2.30
		2.88	3.80	1.98	1.21	1.10	0.72	2.20	3.01	1.03	2.64
		3.20	4.23	2.17	1.28	1.06	0.77	2.44	3.37	1.14	3.00
		3.52	4.63	2.32	1.35	0.97	0.82	2.64	3.73	1.26	3.33
		3.84	5.06	2.45	1.40	1.05	0.86	2.76	4.08	1.37	3.66
		4.16	6.28	2.55	1.46	1.17	0.91	2.90	4.41	1.48	3.99
		4.48	8.16	2.62	1.58	1.27	0.95	2.97	4.76	1.59	4.28
HOL.crv	Hollister-04	0.32	1.07	0.48	0.41	0.27	0.26	0.42	0.70	0.29	0.63
		0.64	2.16	0.93	0.58	0.58	0.50	0.86	1.42	0.55	1.25
		0.96	3.00	1.33	0.73	0.92	0.75	1.42	2.08	0.79	1.86
		1.28	4.03	1.64	0.90	1.28	1.02	2.08	2.54	1.01	2.37
		1.60	4.03	2.01	1.17	1.64	1.29	2.78	2.93	1.22	2.74
		1.92	5.27	2.32	1.47	1.98	1.54	3.41	3.57	1.41	3.04
		2.24	---	2.59	1.80	2.28	1.76	3.95	4.06	1.65	3.60
		2.56	---	2.84	2.15	2.54	1.93	4.84	4.45	1.89	4.21
		2.88	---	3.08	2.48	2.77	2.05	5.72	4.92	2.13	4.79
		3.20	---	3.30	2.80	2.97	2.13	6.50	5.74	2.35	5.38
		3.52	---	3.51	3.11	3.14	2.18	7.16	6.59	2.58	5.96
		3.84	---	3.71	3.41	3.28	2.20	7.70	7.49	2.80	6.51
		4.16	---	3.91	3.69	3.38	2.20	8.14	8.40	3.01	7.04
		4.48	---	4.47	3.96	3.47	2.18	8.49	9.35	3.20	7.56
la.crv	Lazio Abr. Y	0.32	1.51	0.70	0.32	0.34	0.27	0.46	1.03	0.29	0.89
		0.64	2.17	1.14	0.58	0.64	0.57	0.90	1.79	0.55	1.61
		0.96	3.57	1.58	0.80	0.88	0.90	1.32	3.43	0.82	2.36
		1.28	4.24	1.89	1.04	1.45	1.30	1.88	4.22	1.10	3.12
		1.60	---	2.13	1.30	1.69	1.66	2.74	5.34	1.37	3.68
		1.92	---	2.42	1.63	2.00	1.96	3.75	6.31	1.72	4.07
		2.24	---	2.70	1.83	2.44	2.17	4.56	6.55	2.02	4.36
		2.56	---	2.87	2.07	2.73	2.33	5.73	6.28	2.07	4.56
		2.88	---	3.04	2.24	2.88	2.47	7.02	6.28	2.29	4.53
		3.20	---	3.87	2.36	2.93	2.59	8.67	6.51	2.62	4.80
		3.52	---	6.19	2.54	2.97	2.69	9.99	6.80	2.78	5.16
		3.84	---	---	3.17	2.96	2.79	---	7.14	2.81	5.55
		4.16	---	---	3.30	2.95	2.85	---	7.96	2.84	5.98
		4.48	---	---	3.63	2.98	2.89	---	8.71	2.90	6.51
liv.crv	Livemore-02	0.32	0.93	0.36	0.20	0.23	0.19	0.38	0.62	0.16	0.48
		0.64	2.01	0.73	0.31	0.43	0.35	0.79	1.30	0.30	1.00
		0.96	2.59	1.14	0.46	0.57	0.51	1.14	1.97	0.42	1.50
		1.28	2.48	1.45	0.68	0.73	0.66	1.43	2.50	0.53	1.95
		1.60	3.08	1.72	0.90	0.90	0.81	1.88	2.75	0.64	2.31
		1.92	3.89	1.94	1.14	1.08	0.96	2.34	2.87	0.75	2.70
		2.24	4.67	2.10	1.40	1.31	1.09	2.74	3.48	0.87	3.08
		2.56	5.38	2.23	1.56	1.54	1.20	3.09	4.52	0.98	3.39
		2.88	---	2.34	1.63	1.79	1.29	3.43	5.45	1.10	3.62
		3.20	---	2.44	1.69	1.99	1.35	3.76	6.09	1.22	3.79
		3.52	---	2.52	1.75	2.19	1.39	4.10	6.33	1.33	3.90
		3.84	---	2.60	1.83	2.33	1.42	4.42	6.28	1.44	3.99
		4.16	---	2.67	1.90	2.42	1.44	4.74	6.10	1.55	4.05
		4.48	---	2.82	1.97	2.47	1.46	5.05	5.82	1.65	4.11

Table A.2 (cont'd): Incremental dynamic analysis results showing inter-story drift ratios of reference buildings at different PGA levels for 20 near-source records

ml2.crv	Mammoth Lake-02	0.32	0.65	0.31	0.17	0.21	0.16	0.19	0.46	0.11	0.35
		0.64	1.14	0.58	0.31	0.41	0.29	0.39	0.89	0.22	0.69
		0.96	1.42	0.81	0.46	0.62	0.39	0.60	1.32	0.32	1.01
		1.28	1.67	1.03	0.64	0.83	0.46	0.80	1.73	0.41	1.35
		1.60	2.21	1.28	0.82	1.03	0.58	1.00	2.10	0.50	1.68
		1.92	2.81	1.50	1.00	1.21	0.70	1.27	2.39	0.59	2.03
		2.24	3.44	1.71	1.18	1.37	0.83	1.58	2.61	0.69	2.38
		2.56	4.11	1.91	1.36	1.50	0.95	1.89	2.76	0.78	2.73
		2.88	4.81	2.09	1.54	1.63	1.07	2.19	2.84	0.87	3.08
		3.20	5.53	2.26	1.70	1.75	1.18	2.47	2.85	0.96	3.45
		3.52	6.25	2.43	1.87	1.86	1.28	2.72	3.24	1.04	3.79
		3.84	---	2.58	2.03	1.97	1.36	2.94	3.68	1.12	4.13
		4.16	---	2.79	2.18	2.06	1.44	3.14	4.14	1.18	4.44
		4.48	---	3.07	2.32	2.15	1.51	3.30	4.63	1.24	4.73
ml6.crv	Mammoth Lake-06	0.32	0.54	0.26	0.16	0.16	0.14	0.25	0.31	0.09	0.33
		0.64	1.26	0.47	0.27	0.24	0.22	0.42	0.70	0.18	0.64
		0.96	1.53	0.65	0.41	0.37	0.31	0.63	1.09	0.28	0.91
		1.28	1.98	0.83	0.56	0.55	0.41	0.83	1.42	0.39	1.13
		1.60	2.19	1.01	0.63	0.71	0.50	1.01	1.66	0.49	1.30
		1.92	2.78	1.20	0.66	0.82	0.58	1.16	1.81	0.60	1.46
		2.24	3.15	1.39	0.74	0.89	0.66	1.29	2.19	0.70	1.71
		2.56	3.30	1.55	0.79	0.99	0.73	1.48	2.53	0.80	2.04
		2.88	3.54	1.68	0.87	1.05	0.79	1.72	2.80	0.90	2.35
		3.20	4.15	1.80	0.99	1.23	0.89	1.93	3.08	1.00	2.62
		3.52	4.85	1.98	1.09	1.39	0.99	2.13	3.35	1.10	2.85
		3.84	5.55	2.15	1.19	1.52	1.08	2.32	3.63	1.20	3.03
		4.16	6.21	2.30	1.32	1.68	1.18	2.48	3.91	1.29	3.19
		4.48	---	2.45	1.44	1.80	1.31	2.68	4.19	1.38	3.37
mon.crv	Montenegro (aftershock)	0.32	0.83	0.53	0.31	0.29	0.22	0.53	0.53	0.13	0.77
		0.64	1.60	1.05	0.62	0.58	0.40	0.92	1.00	0.27	1.64
		0.96	2.38	1.31	0.71	0.77	0.58	1.28	1.49	0.39	2.23
		1.28	2.97	1.71	0.96	0.96	0.79	1.74	1.97	0.53	2.54
		1.60	3.71	2.23	1.28	1.23	1.00	2.16	2.43	0.66	2.60
		1.92	3.80	2.71	1.63	1.40	1.23	2.46	2.91	0.81	3.06
		2.24	4.70	3.15	1.98	1.57	1.45	2.65	3.33	0.96	3.70
		2.56	---	3.50	2.32	1.82	1.63	2.93	3.85	1.11	4.31
		2.88	---	3.82	2.58	2.09	1.78	3.43	4.47	1.26	4.91
		3.20	---	4.40	2.73	2.29	1.87	3.91	4.94	1.42	5.67
		3.52	---	5.03	2.98	2.46	1.93	4.37	5.18	1.58	6.38
		3.84	---	5.75	3.15	2.59	1.97	4.82	5.33	1.74	7.22
		4.16	---	6.54	3.49	2.68	1.98	5.24	6.27	1.90	8.05
		4.48	---	9.51	3.75	2.87	1.98	5.65	7.13	2.05	8.89
nor.crv	Northridge-06	0.32	0.60	0.38	0.18	0.21	0.16	0.36	0.53	0.14	0.53
		0.64	1.03	0.73	0.30	0.45	0.30	0.64	0.96	0.28	0.99
		0.96	1.29	1.04	0.43	0.71	0.44	0.99	1.34	0.42	1.45
		1.28	1.59	1.28	0.63	0.93	0.57	1.37	1.64	0.56	1.81
		1.60	1.80	1.50	0.87	1.08	0.68	1.75	1.87	0.68	2.03
		1.92	2.01	1.71	1.13	1.20	0.79	2.10	2.09	0.80	2.18
		2.24	2.37	1.90	1.40	1.30	0.89	2.40	2.48	0.91	2.47
		2.56	2.73	2.07	1.64	1.37	0.97	2.64	2.90	1.02	2.74
		2.88	3.10	2.23	1.86	1.46	1.03	2.86	3.32	1.13	2.99
		3.20	3.49	2.37	2.04	1.51	1.07	3.04	3.75	1.22	3.21
		3.52	3.89	2.49	2.21	1.59	1.11	3.20	4.17	1.33	3.39
		3.84	4.36	2.60	2.36	1.63	1.13	3.29	4.60	1.42	3.55
		4.16	4.88	2.69	2.48	1.62	1.15	3.61	4.99	1.52	3.69
		4.48	5.39	2.77	2.59	1.64	1.15	3.97	5.34	1.61	3.79

Table A.2 (cont'd): Incremental dynamic analysis results showing inter-story drift ratios of reference buildings at different PGA levels for 20 near-source records

um.crv	Umbria Ma.	0.32	1.45	0.58	0.26	0.31	0.38	0.58	1.39	0.44	0.74
		0.64	1.83	1.06	0.54	0.66	0.63	1.24	3.07	0.72	1.48
		0.96	2.29	1.53	0.85	1.16	0.83	2.01	3.69	0.94	2.12
		1.28	3.43	1.98	1.21	1.57	1.07	2.74	3.42	1.13	2.51
		1.60	4.62	2.70	1.55	1.84	1.25	3.29	4.16	1.33	3.02
		1.92	---	3.09	1.86	1.82	1.38	3.88	4.70	1.51	4.33
		2.24	---	3.14	2.14	1.97	1.47	4.96	5.06	1.67	5.50
		2.56	---	3.05	2.39	2.90	1.60	5.95	5.36	1.81	5.68
		2.88	---	3.06	2.62	2.11	1.88	6.82	5.69	1.94	5.45
		3.20	---	3.69	2.81	2.23	2.13	7.62	6.07	2.05	5.49
		3.52	---	4.61	2.98	4.08	2.30	8.39	6.72	2.20	6.09
		3.84	---	8.84	3.51	---	2.38	9.08	7.05	2.37	6.65
		4.16	---	---	4.04	---	2.36	9.74	7.54	2.66	7.28
		4.48	---	---	5.19	---	2.28	---	8.48	2.85	8.73
wn589.crv	Whittier Narrows-01(589)	0.32	1.34	0.46	0.26	0.32	0.30	0.38	1.29	0.23	0.66
		0.64	1.87	1.01	0.44	0.72	0.55	0.88	2.43	0.46	1.48
		0.96	2.65	1.59	0.61	1.06	0.68	1.44	2.96	0.67	2.37
		1.28	2.85	2.29	1.12	1.34	0.79	1.91	3.25	0.90	3.08
		1.60	2.99	2.24	1.43	1.51	1.05	2.41	3.78	1.12	3.74
		1.92	3.82	2.48	1.62	1.60	1.25	2.89	4.06	1.33	3.81
		2.24	5.24	2.76	1.74	1.65	1.43	3.77	4.90	1.53	4.40
		2.56	---	2.96	1.82	1.76	1.64	4.69	5.78	1.73	4.94
		2.88	---	3.12	1.90	1.86	1.77	5.39	6.53	1.90	5.27
		3.20	---	3.25	1.95	2.05	1.86	5.83	7.14	2.05	5.47
		3.52	---	3.35	1.96	2.08	1.86	6.10	7.61	2.18	5.59
		3.84	---	3.74	2.04	2.18	1.87	6.37	7.91	2.27	5.72
		4.16	---	4.22	2.11	2.17	1.87	6.67	8.07	2.34	5.77
		4.48	---	4.71	2.24	2.19	1.90	6.95	8.03	2.39	5.79
wn601.crv	Whittier Narrows-01(601)	0.32	0.99	0.45	0.28	0.22	0.25	0.42	0.57	0.14	0.57
		0.64	1.88	0.85	0.50	0.38	0.42	0.85	1.21	0.29	1.02
		0.96	2.04	1.20	0.67	0.55	0.56	1.30	1.91	0.46	1.47
		1.28	2.59	1.47	0.77	0.75	0.67	1.80	2.43	0.65	1.87
		1.60	3.01	1.67	0.91	1.00	0.78	2.34	3.07	0.83	2.22
		1.92	3.39	1.92	1.02	1.17	0.90	2.87	3.56	1.02	2.82
		2.24	3.78	2.03	1.16	1.32	1.02	3.34	3.90	1.20	3.32
		2.56	4.16	2.04	1.29	1.43	1.13	3.75	4.16	1.38	3.67
		2.88	4.46	2.45	1.42	1.47	1.25	4.08	4.40	1.56	3.88
		3.20	4.71	2.83	1.54	1.46	1.36	4.41	4.65	1.73	3.96
		3.52	4.78	3.18	1.72	1.51	1.45	4.74	4.91	1.91	3.80
		3.84	5.39	3.47	1.92	1.55	1.52	5.04	5.17	2.08	3.85
		4.16	---	3.74	2.22	1.61	1.68	5.64	5.48	2.25	4.20
		4.48	---	4.00	2.38	1.65	1.84	6.28	5.97	2.43	4.55
wn619.crv	Whittier Narrows-01(619)	0.32	0.69	0.37	0.20	0.23	0.15	0.27	0.63	0.14	0.49
		0.64	1.38	0.80	0.36	0.40	0.30	0.58	1.23	0.27	1.01
		0.96	2.45	1.28	0.57	0.66	0.44	0.90	1.54	0.41	1.58
		1.28	2.77	1.74	0.74	0.84	0.56	1.22	1.70	0.55	2.21
		1.60	2.26	2.11	0.87	0.98	0.73	1.58	1.84	0.68	2.72
		1.92	3.19	2.35	1.16	1.08	0.93	1.90	1.99	0.81	3.20
		2.24	3.80	2.52	1.46	1.16	1.18	2.39	2.42	0.93	3.58
		2.56	4.10	2.63	1.70	1.28	1.44	2.92	2.88	1.06	3.89
		2.88	4.87	2.68	1.83	1.45	1.70	3.47	3.31	1.20	4.12
		3.20	---	2.65	1.84	1.68	1.93	3.99	3.81	1.35	4.46
		3.52	---	2.60	1.94	1.92	2.09	4.48	4.20	1.50	4.87
		3.84	---	2.63	1.97	2.18	2.20	4.91	4.40	1.66	5.17
		4.16	---	2.90	1.99	2.42	2.26	5.26	4.52	1.83	5.45
		4.48	---	3.23	1.98	2.54	2.29	5.53	4.75	2.00	5.50

Table A.2 (cont'd): Incremental dynamic analysis results showing inter-story drift ratios of reference buildings at different PGA levels for 20 near-source records

wn626.crv	Whittier Narrows-01(626)	0.32	0.69	0.30	0.17	0.19	0.20	0.33	0.57	0.15	0.42
		0.64	1.56	0.59	0.28	0.34	0.37	0.64	1.08	0.29	0.81
		0.96	1.92	0.92	0.42	0.56	0.53	0.96	1.56	0.42	1.16
		1.28	1.98	1.20	0.55	0.76	0.67	1.33	2.09	0.54	1.51
		1.60	2.71	1.45	0.74	0.90	0.81	1.74	2.71	0.65	1.81
		1.92	3.31	1.69	0.93	1.03	0.95	2.14	3.27	0.75	2.12
		2.24	3.76	1.92	1.11	1.19	1.08	2.64	3.78	0.83	2.41
		2.56	4.03	2.10	1.27	1.38	1.19	3.16	4.18	0.92	2.68
		2.88	4.12	2.25	1.42	1.57	1.29	3.66	4.40	1.00	2.96
		3.20	4.05	2.39	1.56	1.74	1.36	4.10	4.52	1.09	3.20
		3.52	4.67	2.50	1.68	1.85	1.42	4.53	4.53	1.17	3.42
		3.84	5.26	2.60	1.82	1.94	1.46	4.94	4.45	1.25	3.60
		4.16	---	2.85	1.94	2.06	1.49	5.25	4.44	1.31	3.78
		4.48	---	3.24	2.05	2.01	1.52	5.62	4.90	1.40	4.06
wn629.crv	Whittier Narrows-01(629)	0.32	1.36	0.36	0.32	0.20	0.29	0.32	0.81	0.31	0.46
		0.64	1.87	0.69	0.51	0.45	0.41	0.67	1.57	0.61	0.96
		0.96	2.77	1.07	0.68	0.80	0.58	1.04	2.29	0.91	1.41
		1.28	3.59	1.43	0.96	1.20	0.79	1.51	3.52	1.19	1.89
		1.60	---	1.80	1.21	1.72	0.98	2.11	3.40	1.45	2.31
		1.92	---	2.25	1.39	1.69	1.13	2.81	4.31	1.67	6.20
		2.24	---	2.67	1.64	1.82	1.19	3.42	5.14	1.79	3.48
		2.56	---	3.00	1.91	2.84	1.34	3.83	4.81	1.83	3.76
		2.88	---	3.23	2.14	3.69	1.47	4.03	4.64	1.85	14.03
		3.20	---	3.41	2.37	4.15	1.58	4.14	5.32	1.92	10.04
		3.52	---	3.69	2.58	5.15	1.76	4.14	6.52	2.10	12.41
		3.84	---	4.54	2.73	7.14	2.07	4.13	8.05	2.28	6.67
		4.16	---	---	3.47	---	2.34	4.59	---	2.46	---
		4.48	---	---	3.90	---	2.53	5.25	---	2.62	---
wn639.crv	Whittier Narrows-01(639)	0.32	0.97	0.29	0.22	0.17	0.23	0.31	0.75	0.18	0.41
		0.64	1.62	0.59	0.46	0.40	0.40	0.68	1.54	0.32	0.79
		0.96	2.49	0.96	0.64	0.67	0.57	1.06	2.15	0.46	1.21
		1.28	3.16	1.35	0.78	0.99	0.73	1.52	2.55	0.60	1.65
		1.60	3.79	1.73	0.90	1.26	0.89	2.01	2.92	0.74	2.08
		1.92	4.31	2.07	1.08	1.49	1.03	2.53	3.53	0.87	2.56
		2.24	5.25	2.36	1.27	1.66	1.16	3.01	4.10	1.01	3.01
		2.56	---	2.58	1.48	1.75	1.27	3.47	4.58	1.16	3.40
		2.88	---	2.75	1.70	1.76	1.37	3.85	4.98	1.31	3.72
		3.20	---	2.88	1.88	1.71	1.44	4.09	5.32	1.46	4.00
		3.52	---	2.98	2.01	1.67	1.46	4.15	5.67	1.63	4.25
		3.84	---	3.06	2.16	1.56	1.45	4.12	6.00	1.80	4.47
		4.16	---	3.13	2.22	1.75	1.53	4.46	6.38	1.97	4.64
		4.48	---	3.25	2.27	1.92	1.65	4.89	6.75	2.14	4.84
wn645.crv	Whittier Narrows-01(645)	0.32	1.39	0.50	0.30	0.35	0.34	0.49	1.35	0.38	0.59
		0.64	2.37	1.12	0.52	0.89	0.59	1.02	2.87	0.66	1.35
		0.96	3.80	1.86	0.98	1.14	0.83	1.70	3.11	0.87	2.13
		1.28	---	2.57	1.48	1.67	1.05	2.44	3.87	1.05	3.14
		1.60	---	3.25	2.12	2.16	1.23	2.97	5.64	1.19	4.35
		1.92	---	3.74	2.72	2.10	1.36	3.59	7.44	1.30	5.66
		2.24	---	4.08	3.04	2.02	1.64	4.84	8.97	1.43	6.49
		2.56	---	4.33	3.14	1.99	1.97	6.31	---	1.57	6.90
		2.88	---	4.49	3.32	2.14	2.31	7.97	---	1.77	7.31
		3.20	---	4.55	3.41	2.33	2.62	9.74	---	2.04	7.55
		3.52	---	4.52	3.48	2.54	2.93	---	---	2.34	7.69
		3.84	---	5.87	3.28	2.66	3.21	---	---	2.58	7.81
		4.16	---	---	3.31	3.14	3.47	---	---	2.69	7.82
		4.48	---	---	3.53	3.59	3.68	---	---	2.71	7.92

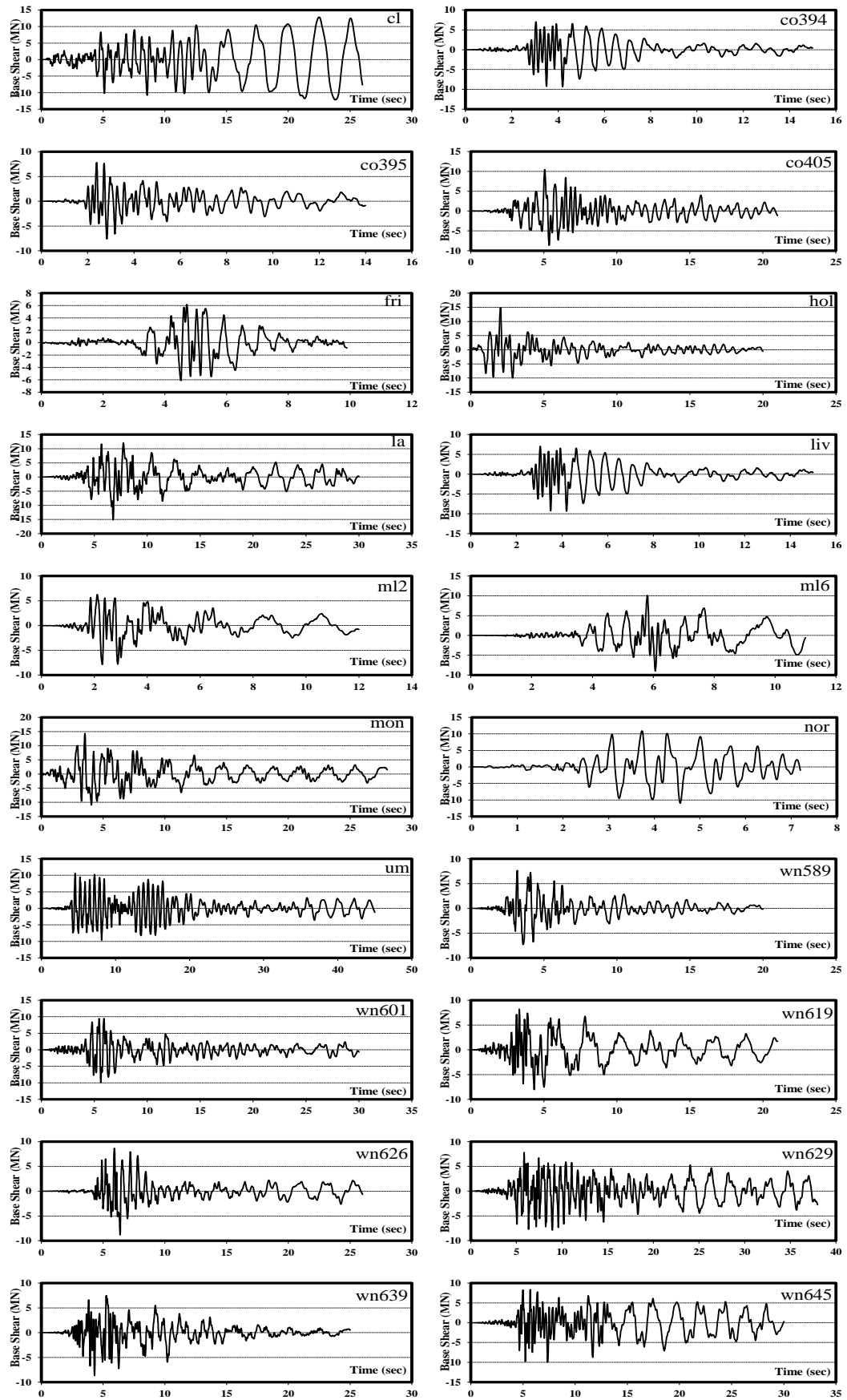


Figure A.1: Base shear response histories of the 8-story building under twenty short-period records scaled to twice the design (0.32g) earthquake intensity

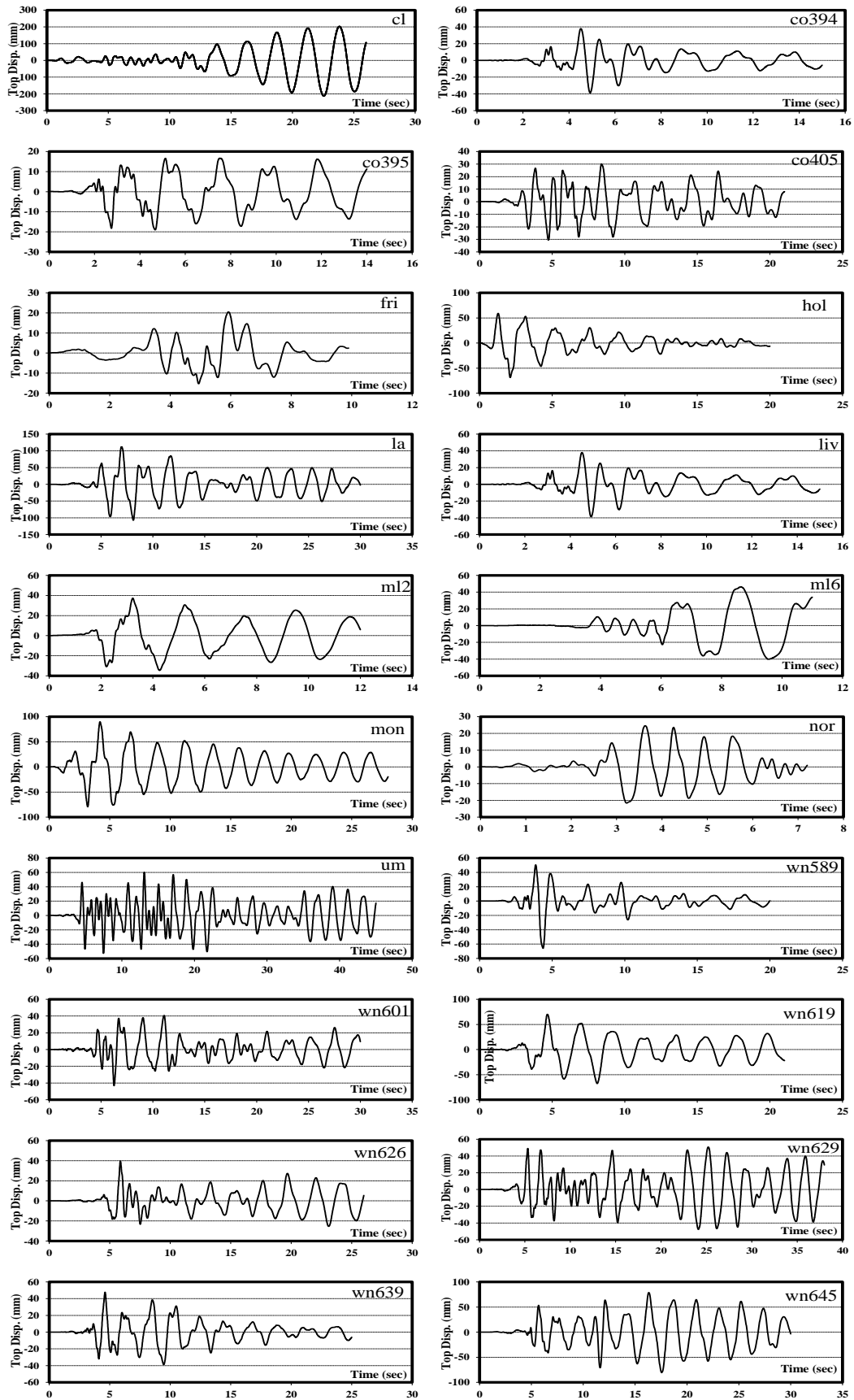


Figure A.2: Top displacement response histories of the 8-story building under twenty short-period records scaled to twice the design (0.32g) earthquake intensity

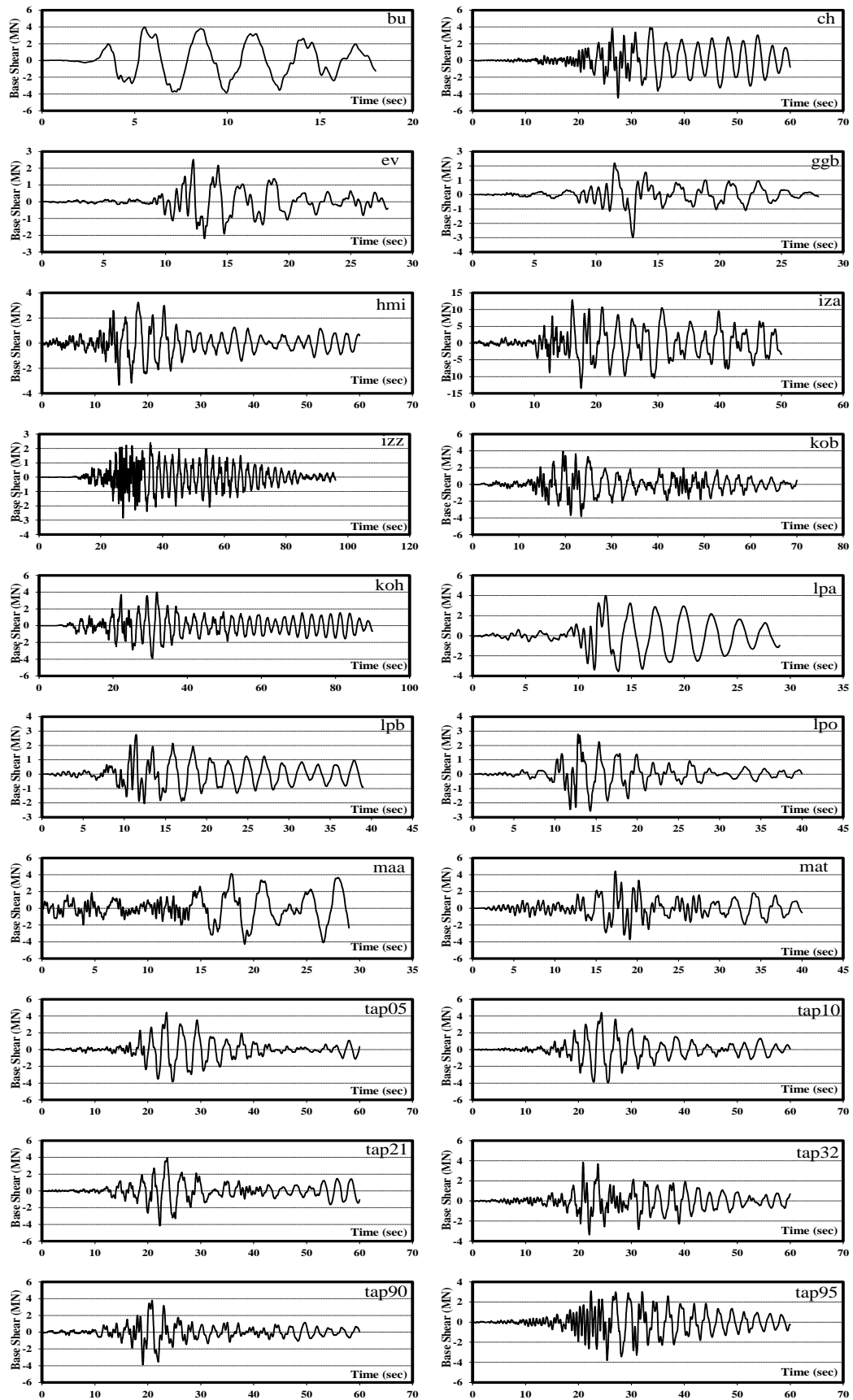


Figure A.3: Base shear response histories of the 8-story building under twenty long-period records scaled to the design (0.16g) earthquake intensity

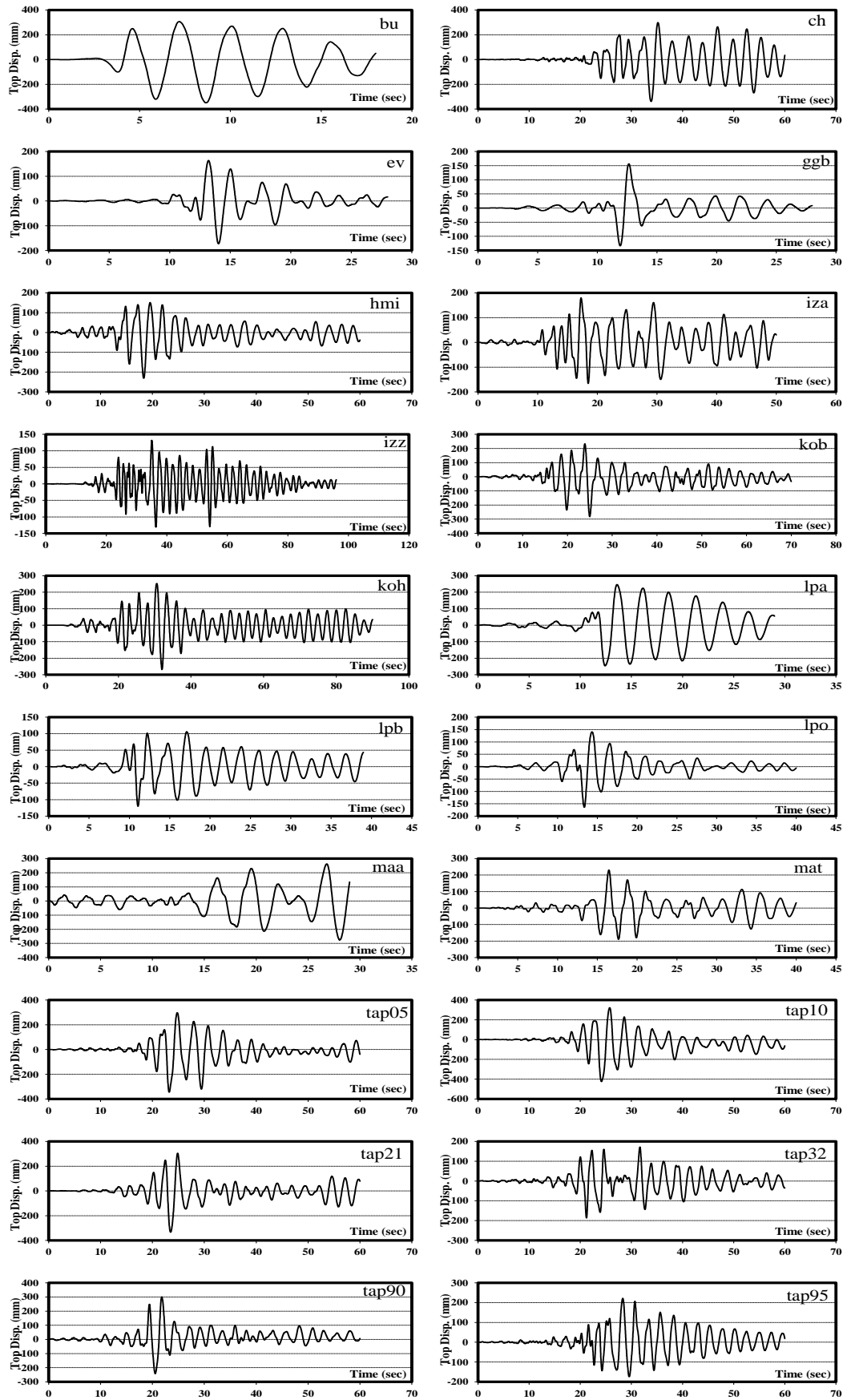


Figure A.4: Top displacement response histories of the 8-story building under twenty long-period records scaled to the design (0.16g) earthquake intensity

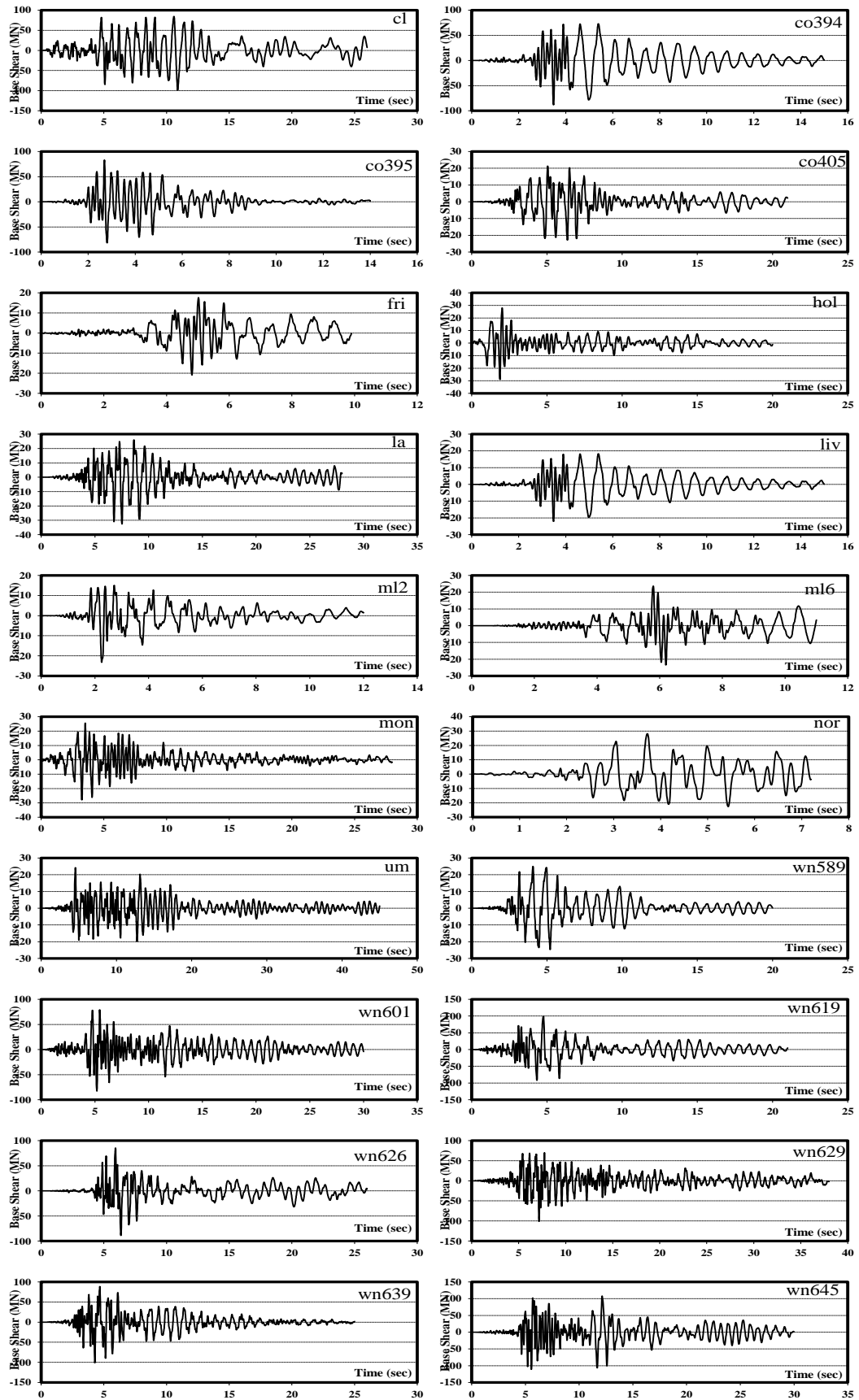


Figure A.5: Base shear response histories of the 26-story building under twenty short-period records scaled to twice the design (0.32g) earthquake intensity

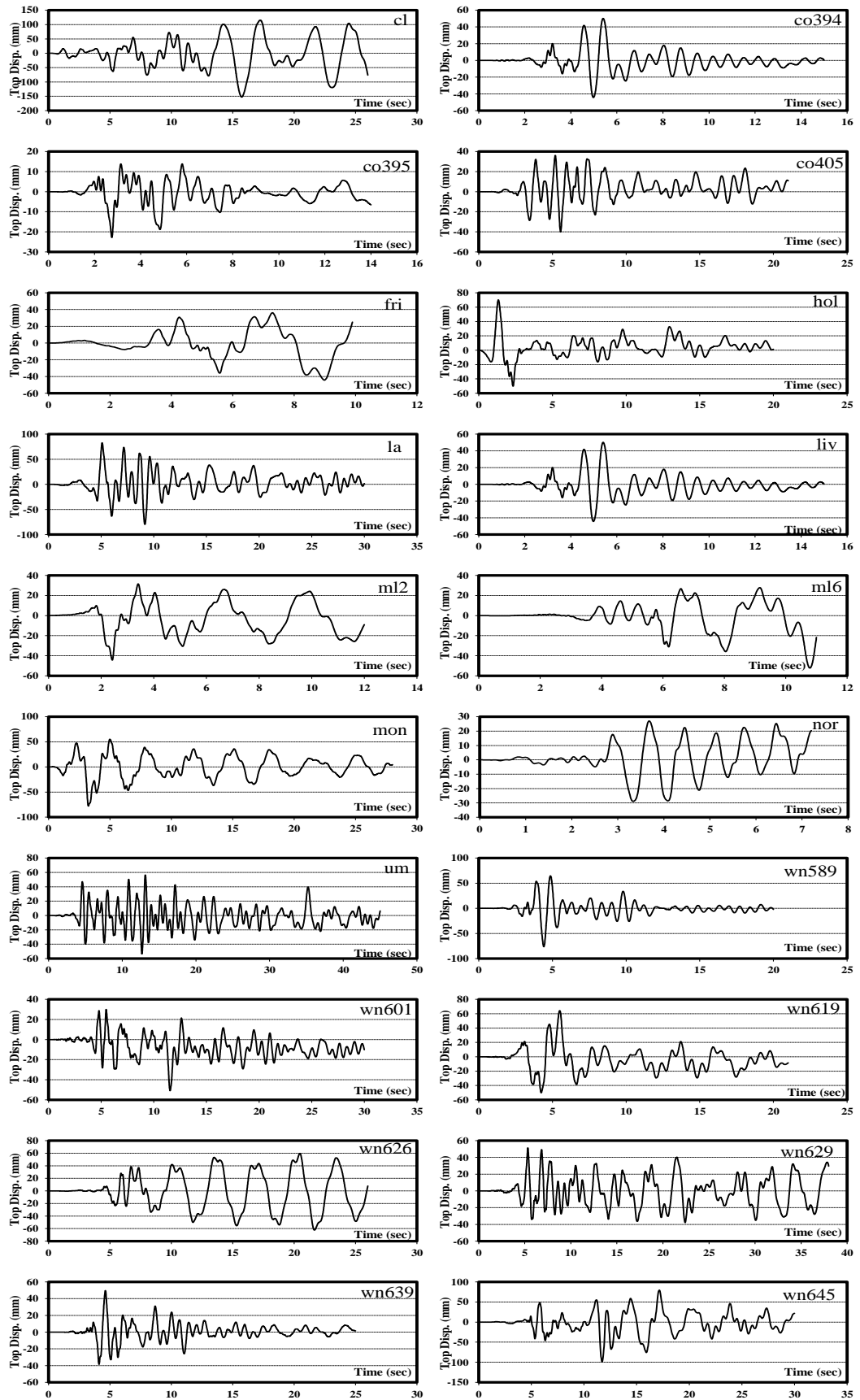


Figure A.6: Top displacement response histories of the 26-story building under twenty short-period records scaled to twice the design (0.32g) earthquake intensity

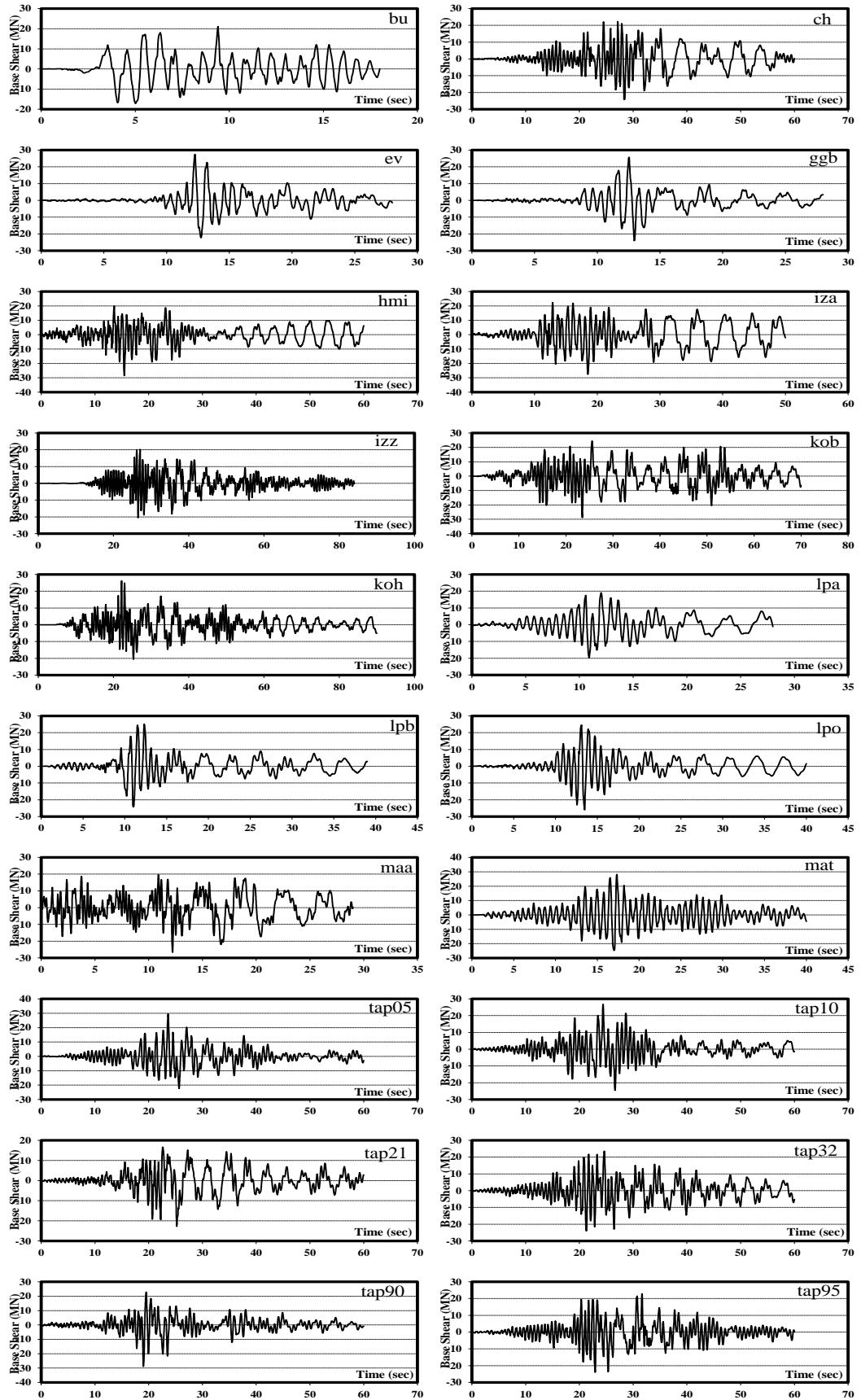


Figure A.7: Base shear response histories of the 26-story building under twenty long-period records scaled to the design (0.16g) earthquake intensity

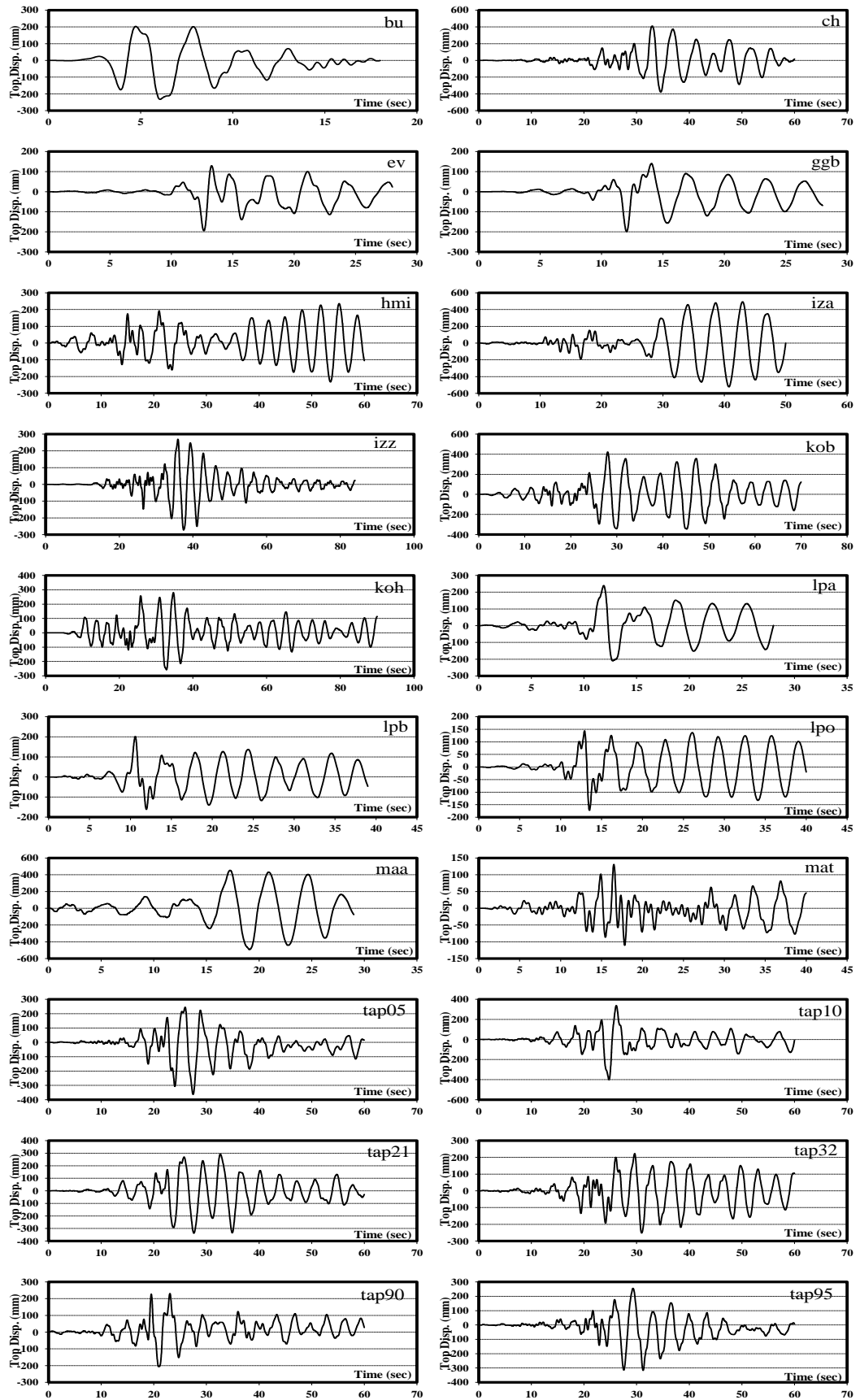


Figure A.8: Top displacement response histories of the 26-story building under twenty long-period records scaled to the design (0.16g) earthquake intensity

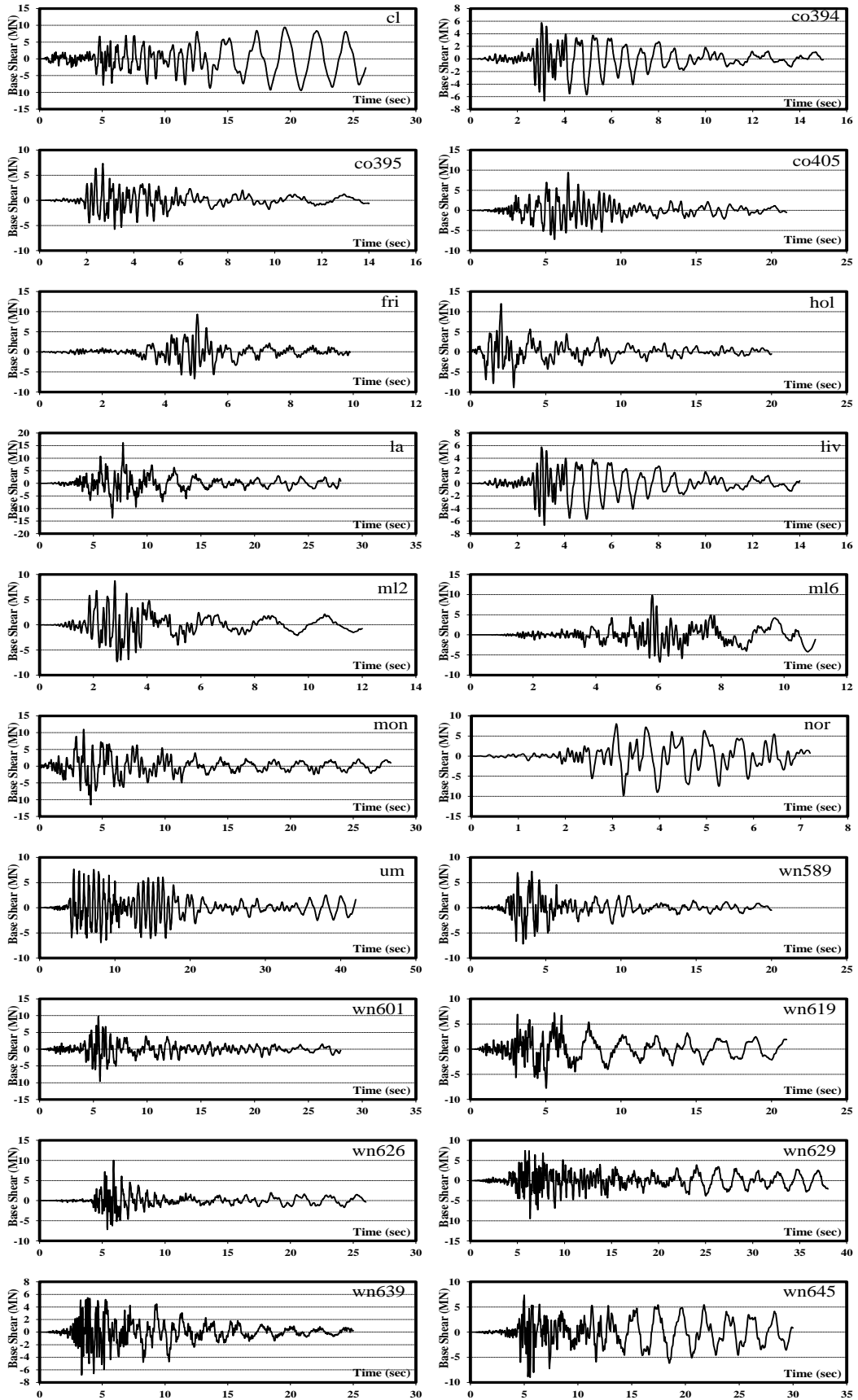


Figure A.9: Base shear response histories of the hospital building under twenty short-period records scaled to twice the design (0.32g) earthquake intensity

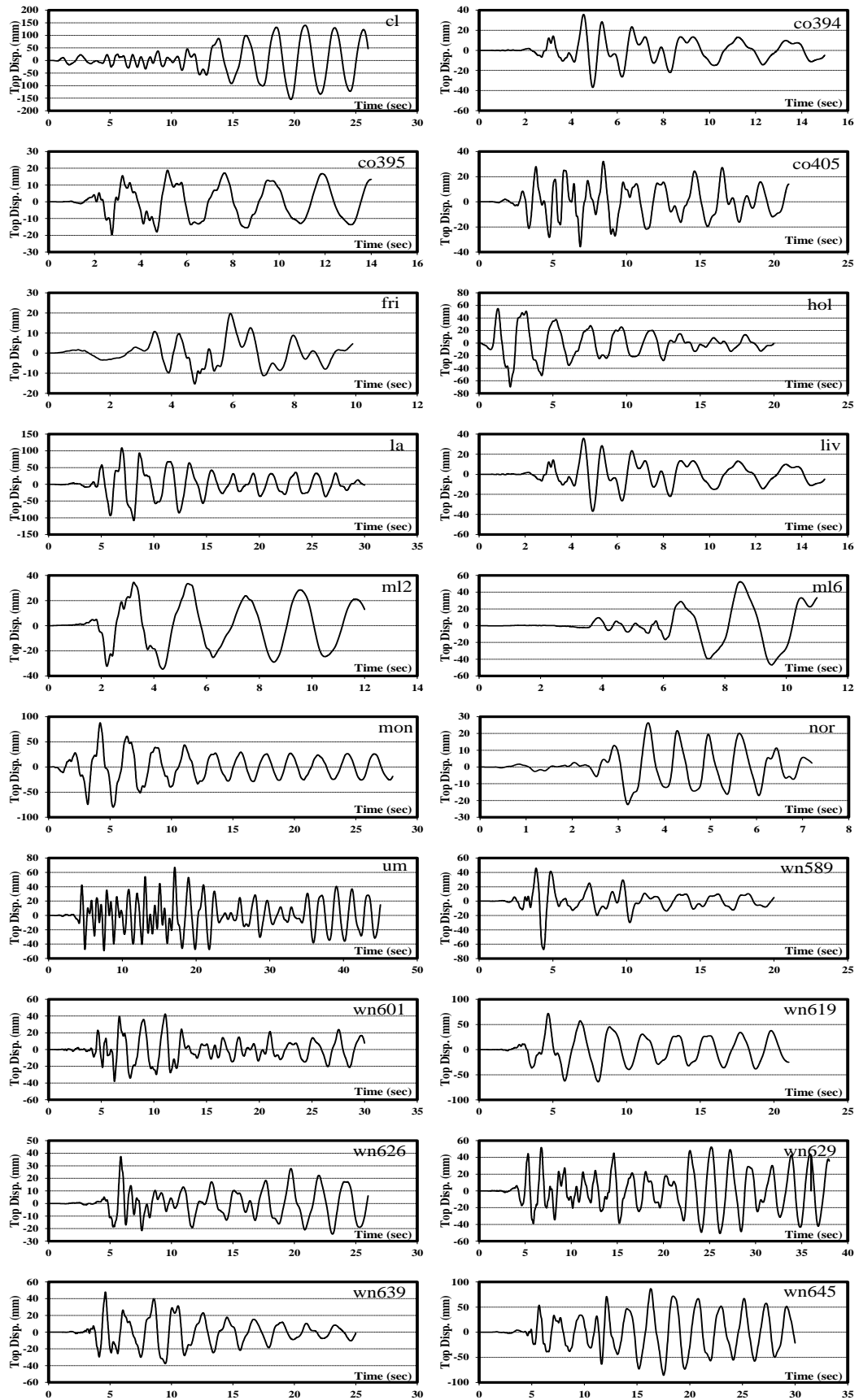


Figure A.10: Top displacement response histories of the hospital building under twenty short-period records scaled to twice the design (0.32g) earthquake intensity

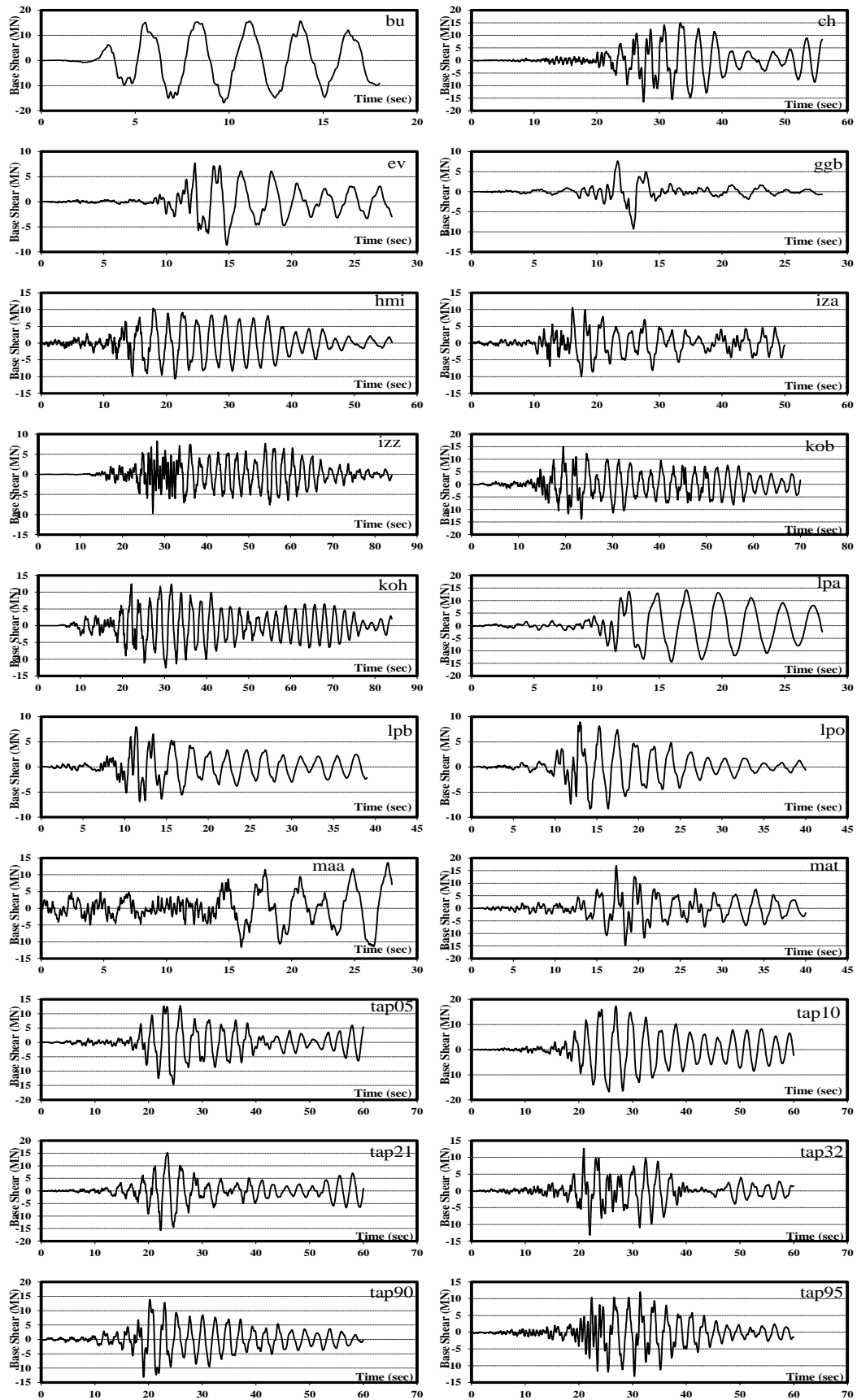


Figure A.11: Base shear response histories of the hospital building under twenty long-period records scaled to the design (0.16g) earthquake intensity

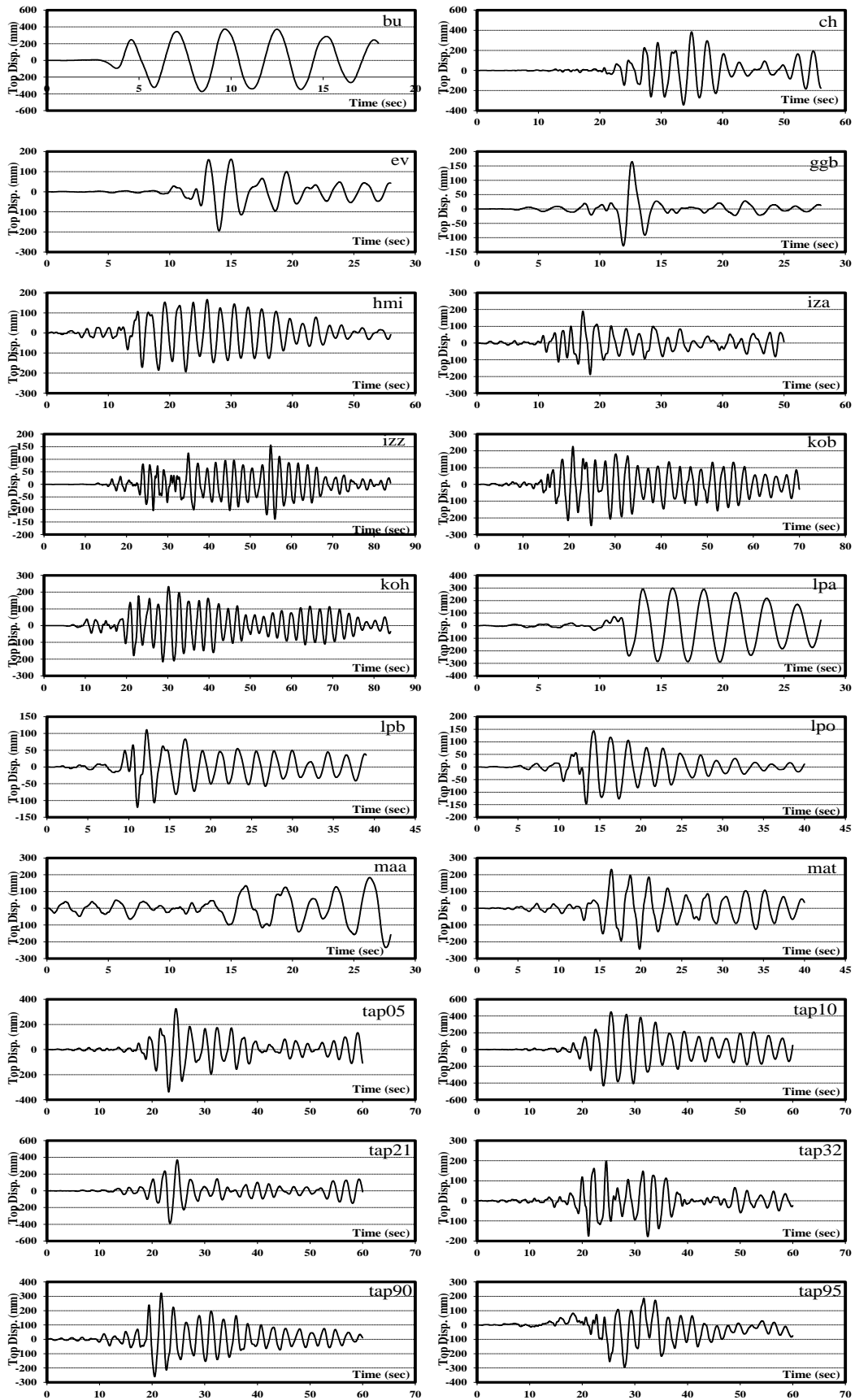


Figure A.12: Top displacement response histories of the hospital building under twenty long-period records scaled to the design (0.16g) earthquake intensity